



GSI

REPORT 97-07
Juli 1997

**Conceptual Design Study
of the GSI
Electron - Nucleon Collider**

Budker Institute for Nuclear Physics
630090 Novosibirsk, Russian Federation

June 18, 1997



Gesellschaft für Schwerionenforschung mbH
Planckstraße 1 • D-64291 Darmstadt • Germany
Postfach 11 05 52 • D-64220 Darmstadt • Germany

**Conceptual Design Study
of the GSI
Electron – Nucleon Collider**

Budker Institute for Nuclear Physics
630090 Novosibirsk, Russian Federation

June 18, 1997

Foreword

This report is a summary of work, which was carried out for the working group "Accelerator studies" on the long term perspectives of the Gesellschaft für Schwerionenforschung mbH (Darmstadt, Germany) by the Budker Institute for Nuclear Physics of the Siberian Branch of RAS (Novosibirsk), during the period covering March 1996 till March 1997. It describes a feasibility study for the future electron-nucleon collider with the luminosity 10^{33} 1/[cm²s] per nucleon in the energy range $\sqrt{s} = 10 \div 30$ GeV/u. The participants to this report are listed below:

N.S. Dikansky, A.A Didenko, Yu.I. Eidelman, I.K. Kuksanov, P.V. Logachev, A.V. Malinin, P.I. Nemyitov, V.V. Parkhomchuk, D.V. Pestrikov, V.I. Ptitsin, R.A. Salimov, B.A. Skarbo, A.N. Skrinsky, M.E. Weis, V.E. Yakimenko.

Contents

1	Introduction	4
1.1	Zones for Experiments	4
2	Design Concepts of the ENC	7
2.1	Limitations on the Luminosity Performance	7
2.1.1	Beam-beam instability	7
2.1.2	Space charge effect	10
2.1.3	Synchrotron radiation losses	12
2.1.4	Collective instabilities	15
2.1.5	Beam loading of the RF-system	18
2.1.6	Beam cooling and intrabeam scattering	18
2.2	Luminosity Lifetime	22
2.2.1	Radiative recombination lifetime	24
2.2.2	Lifetime of electron beam	24
2.3	Parameter Sets	26
3	Beam-Beam Instability	32
3.1	Linear Effects	34
3.1.1	Beam-beam instability of short bunches	35
3.1.2	Hour-glass effect	36
3.1.3	Flip-flop phenomenon	39
3.2	Nonlinearity of the Beam-Beam Force	42
3.2.1	Effect of the beam cooling	45
3.2.2	Long bunches	49
3.2.3	Coherent beam-beam instability	50
3.3	Ion Space Charge and the Beam-Beam Instability	51
3.3.1	Ion tune shifts	52
3.3.2	Simulations	56
3.3.3	Working point for ion ring	59
3.4	Parasitic Crossings	61
3.5	Conclusion	63

4	Cooling of Ion Bunches	65
4.1	Stochastic Cooling of High Energy Ion Beams	65
4.1.1	Theoretical limit for the cooling time	65
4.1.2	Numerical example for ENC operation	66
4.2	Electron Cooling for the Electron-Ion Collider	66
4.2.1	Cooling force	67
4.2.2	Experimental background	69
4.3	Effect of the Magnetic Field on Cooling	74
4.3.1	Drift of the cooling electrons due to ion space charge	74
4.3.2	Effect of the magnetic field on the cooling force	75
4.4	Cooling Rates	75
4.4.1	Magnetized electron cooling	78
4.4.2	Magnetized momentum cooling	79
5	Intrabeam Scattering	83
5.1	Bunch Entropy Growth Rate	85
5.2	Equilibrium Emittances	88
5.3	Space Charge Effect	91
5.4	Touschek Lifetimes	94
6	Conventional Collective Effects	98
6.1	Single-Bunch Effects	98
6.1.1	Head-tail instability	98
6.1.2	Mode-coupling instability	102
6.1.3	Longitudinal single-bunch effects	105
6.2	Multi-Bunch Effects	110
6.3	Instabilities Due To Captured Ions	113
7	Lattice Design	117
7.1	Arc Lattices	118
7.2	Main Interaction Region	121
7.3	Cooling Region Straight Section	126
7.4	Synchronization of Ion and Electron Revolution Frequencies	126
8	Polarization Control	133
8.1	Electron Bunches	133
8.2	Ion Bunches	137
8.2.1	Acceleration of the polarized beam	138
8.2.2	Longitudinal polarization	139
9	Injection Chain	141
9.1	General Description	141
9.2	Electron Linac	145
9.2.1	General scheme of the electron linac	145

9.2.2	RF module	147
9.2.3	Beam diagnostic.	147
9.2.4	RF control system.	148
9.2.5	A rough cost estimation.	148
9.3	The Full-Energy ENC Filling-up Scenario	148
10	Basic Technical Systems	150
10.1	Main Interaction Region Magnets	150
10.2	RF-systems	150
10.3	Technical Design Study of the Cooling Device	151
10.3.1	Cooling region solenoid	151
10.3.2	High voltage accelerator	153
11	First Cost Estimations	159
12	Time Schedule	161
A		163
A.1	To the Calculation of the Luminosity	163
B		165
B.1	Calculation of the Beam-Beam Kick	165
B.2	Coulomb Tune Shifts	168
C		170
C.1	IBS Diffusion Coefficients	170
C.2	Calculation of $G(s)$	174
C.3	IBS Integrals	175

Chapter 1

Introduction

In this report we present a feasibility study for the construction of the Electron – Nucleon Collider (ENC), which could provide the luminosity of electron-nucleon collisions $L = 10^{33}$ 1/[cm²s] in the range of the center of mass energies $\sqrt{s} = 10 \div 30$ GeV/u. The envisaged operational modes of such a collider should enable the collisions of electron against the bare ion bunches from protons till U₂₃₈⁹². Two interaction points should be foreseen in the collider. Colliding bunches should have at the interaction points the longitudinal polarization.

In order to avoid huge beam currents, so challenging value of the luminosity must be reached using the most of the modern beam handling techniques. In this report we especially examine the limitations on the luminosity performance, which are specific namely for electron – ion colliders. More detailed technical study is left for the future designing of such a collider. This task will be partially simplified by the fact that many requirements for ENC are similar, or close to those, which are specific for the future electron – positron factories (see, for example, in Ref [1, 2]). For that reason, we assume that relevant technical solutions, which will be developed for B (or, C- τ) factories, can be used in the future design of ENC.

Initial data for the estimations in this report were chosen as close as possible to these from Ref.[3].

1.1 Zones for Experiments

As we mentioned, ENC is planed to have two interaction regions (IR). The requirements to the main interaction region are well defined. It must contain the detector solenoid ($\int Bdl = 5$ Tm, similar to TOPAZ [4]) surrounded by two spectrometer dipoles ($\int Bdl = 1.7$ Tm, see also in Fig.1.1). Optical requirements for the second interaction region are not well defined yet, except for an assumption that the β -function at this interaction point can be large. Since a collider with different optical properties are more difficult in operation, in present design study we assume that optical properties are identical in both IR. The studies of the more realistic cases are left for the future design.

The optical scheme of the main interaction region should provide the observations of both the large angle ($\theta > 10^\circ$) and the small angle ($\theta < 3^\circ$) collisions. For that reason, the optical elements in the main IR should be placed inside the cones between $3^\circ < \theta < 10^\circ$ (see in Fig.1.1). Since transverse dimensions in such a cone increase

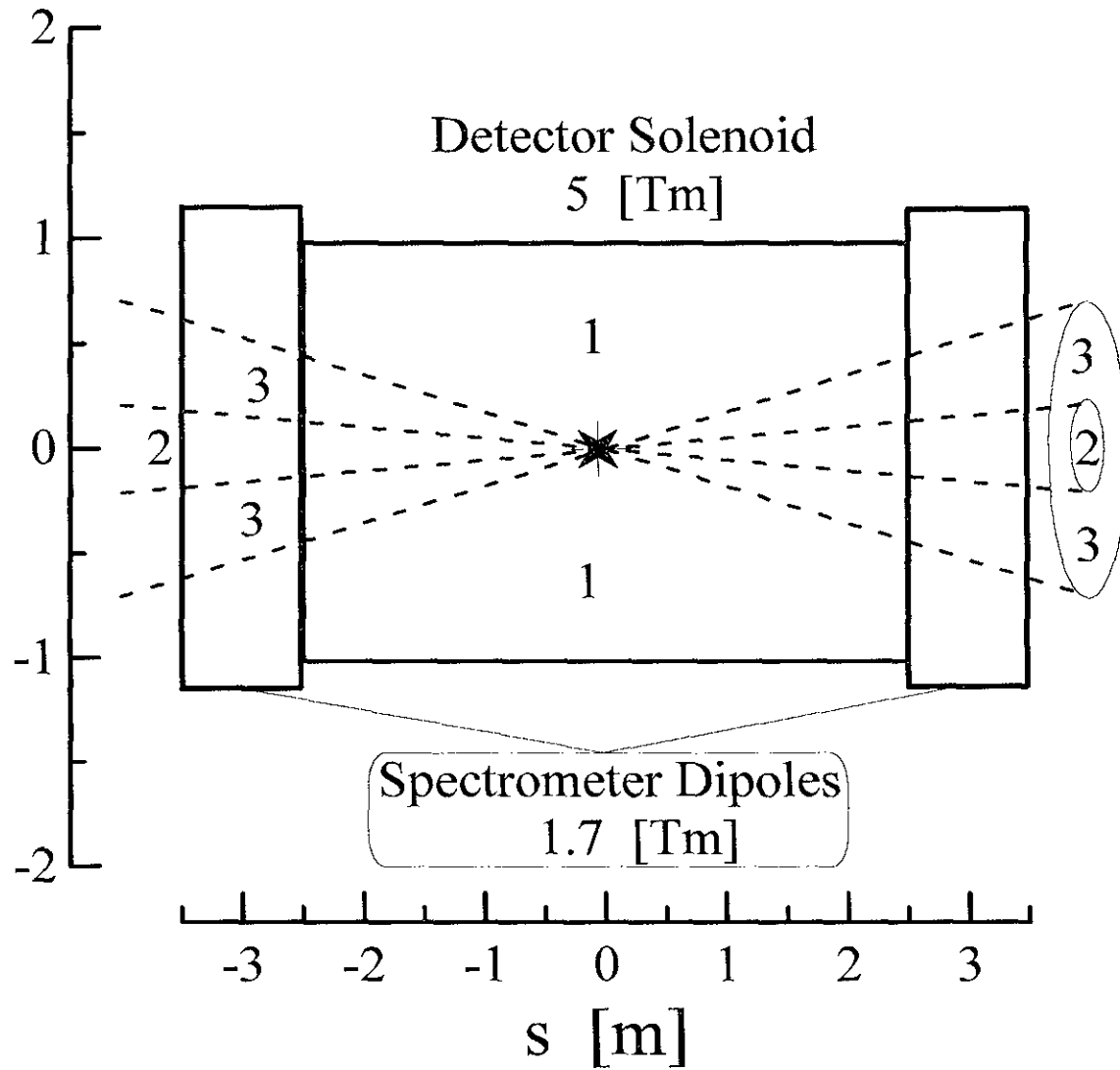


Figure 1.1: Schematic layout of the main interaction region. Transverse dimensions are measured in meters, 1 - large collision angle zones, 2 - small collision angle zones, 3 - equipment zones.

along the path, these requirements may pose additional limitations on the designing of the necessary optical magnets (see in Table 1.1).

Table 1.1: Inner and outer radii in the $3^\circ \div 10^\circ$ cones along the particle path.

Distance from IP	m	1	2.5	3.5
Inner radius	cm	5.2	13	18.3
Outer radius	cm	17.4	43.6	61

Chapter 2

Design Concepts of the ENC

The luminosity of nucleon-electron collisions for the bunches with the rms length σ_s and round cross sections reads (see, for example, in Appendix A.1)

$$L = L_0 F(\sigma_s/\beta), \quad (2.1)$$

Here, L_0 is the luminosity of the short colliding bunches ($\sigma_s \ll \beta$):

$$L_0 = A f_b \frac{N_i N_e}{2\pi \beta \epsilon_i (1 + \chi)}, \quad \chi = \frac{\epsilon_e}{\epsilon_i}, \quad (2.2)$$

while

$$F(\zeta) = \frac{2}{\sqrt{\pi}} \int_0^\infty \frac{ds e^{-s^2}}{1 + \zeta^2 s^2}, \quad \zeta = \frac{\sigma_s}{\beta}, \quad (2.3)$$

– is the form-factor, describing the "hour-glass" reduction of the luminosity due to the finite bunch lengths, suffixes i and e mark the values related to ion and electron bunches, N_i and N_e are the numbers of particles in bunches, $\epsilon_{i,e}$ are their emittances, β is the value of the β -function at the interaction point, A is the atomic number of the ion. As is shown in Fig.2.1, the luminosity is a decreasing function of the bunch length. For that reason, the bunch length (σ_s) should not considerably exceed the value of the β -function at the interaction point.

The design goal is to find the parameter sets of ENC, which enable in the electron-proton till electron-U₂₃₈⁹² operational modes the luminosity $L = 10^{33}$ 1/[cm²s] per nucleon.

2.1 Limitations on the Luminosity Performance

2.1.1 Beam-beam instability

Let us first examine the limitations on the luminosity performance due to the beam-beam instability of the colliding bunches. This manifold phenomenon will be discussed in more detail in Chapter 3. Here, we use the fact that the strengths of these

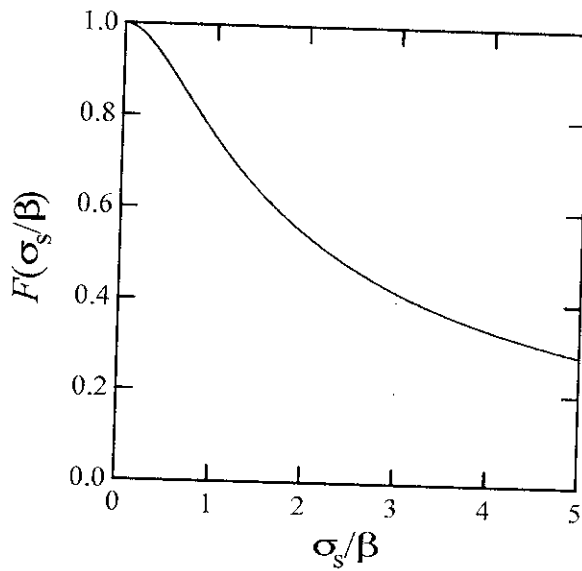


Figure 2.1: Dependence of the luminosity on the bunch length. This graph shows that for $\sigma_s/\beta = 1$ the luminosity reduction factor is about 25% as compared to the luminosity for collisions of the short bunches ($\sigma_s \ll \beta$). For $\sigma_s/\beta = 2$ this factor increases till approximately 45%.

instabilities can be described in terms of the threshold values of the beam-beam parameters. For the case of ENC, the beam-beam parameters for electron and ion bunches of the round cross section read

$$\xi_e = \frac{N_i Z r_e}{4\pi\gamma_e\epsilon_i}, \quad r_e = \frac{e^2}{m_e c^2}, \quad (2.4)$$

and

$$\xi_i = \frac{N_e Z r_p}{4\pi A \gamma_i \epsilon_e}, \quad r_p = \frac{e^2}{m_p c^2}. \quad (2.5)$$

Here, we take that velocities of the colliding particles almost coincide with the speed of light ($v_{i,e} \approx c$), Ze is the charge of an ion and m_p is the proton mass. If we express the luminosity in terms of the energy of the colliding particles in their center of mass reference system (\sqrt{s})

$$\begin{aligned} s &= (m_p c^2)^2 + (m_e c^2)^2 + 2E_e(E_i + \sqrt{E_i^2 - m_p^2 c^4}) \\ &\simeq 4E_e E_i, \quad \gamma_i, \gamma_e \gg 1, \end{aligned} \quad (2.6)$$

where E_i and E_e are the energies of the ion and electron respectively, we may replace γ_e in Eq.(2.4) by $\gamma_e \simeq s/(4m_e m_p c^4 \gamma_i)$ to find

$$\xi_e = \frac{N_i Z r_p}{\pi \gamma_s^2 \epsilon_i} \gamma_i, \quad \gamma_s = \frac{\sqrt{s}}{m_p c^2}. \quad (2.7)$$

Assuming that the threshold value of ξ_e is better understood and taking as a base the value $\xi_e = 0.05$, which is common, for instance, for B-factories [1], we stand for N_i/ϵ_i in Eq.(2.1) its expression from Eq.(2.4), or from Eq.(2.7)

$$\frac{N_i}{\epsilon_i} = \frac{4\pi\xi_e\gamma_e}{Zr_e} = \frac{\pi\xi_e\gamma_s^2}{Zr_p\gamma_i}.$$

That results in

$$L = \left(\frac{A}{Z}\right) f_b N_e \frac{2\xi_e\gamma_e}{\beta r_e(1+\chi)} F(\zeta), \quad (2.8)$$

or

$$L \simeq f_b N_e \left(\frac{A}{Z}\right) F(\zeta) \frac{\xi_e \gamma_s^2}{2\beta r_p(1+\chi)\gamma_i}. \quad (2.9)$$

These expressions show that the luminosity increases with an increase in γ_e , or s , but for given s and N_e it decrease with an increase in γ_i .

2.1.2 Space charge effect

The calculated values of the ion bunch densities should not contradict to a requirement that the so-called Laslett tune shift for ion bunches

$$\Delta\nu_L \simeq \frac{Z^2}{A} \cdot \frac{N_i r_p}{4\pi\gamma_i^3 \epsilon_i} \cdot \frac{\Pi}{\sigma_s \sqrt{2\pi}} \quad (2.10)$$

must not exceed some threshold value. For a conventional ion storage ring this threshold depends on the modulations of β -functions and generally can be increased, if the modulations are not very deep and if the superperiodicity of the ring is high enough.

As was pointed out in Refs [6], for the reasons, which will be discussed in the Chapter 3, for ENC with a strong cooling of ion bunches, the emittances of electron and ion bunches must be set to be equal ($\chi = 1$). In [7] it was also shown that in the case of ENC with two interaction points, this threshold value must be some safe fraction of ξ_i . The reason is that, if $\Delta\nu_L > 2\xi_i$ (two interaction points) and provided that $\chi \simeq 1$, the incoherent oscillations of ions become unstable, when ion betatron tunes occur above the resonant values ($\nu_{bet} \geq n/m$, n and m are integers), whereas the incoherent oscillations in electron bunch and the dipole coherent oscillations of ions become unstable, when $\nu_{bet} \leq n/m$. The requirement that $\xi_i > \Delta\nu_L$ eliminates such a contradiction in the stability conditions for coherent and incoherent oscillations of the ion bunch. We also note that even in the case, when the stability of coherent oscillations of ion bunch is provided using some additional damping, a contradiction in the stability conditions for incoherent oscillations in ion and electron bunches results in a strong difference in their β -functions due to self-consistent beam-beam interaction [5].

Taking as a possible threshold value $\Delta\nu_L \simeq \xi_i$ (two interaction points), we find that in the space charge dominance region the ratio N_i/ϵ_i should not exceed its threshold value

$$\left(\frac{N_i}{\epsilon_i}\right)_{th} = \frac{A}{Z^2} \frac{4\pi\xi_i \gamma_i^3 \sigma_s \sqrt{2\pi}}{r_p \Pi} \quad (2.11)$$

Correspondingly, in this region the luminosity varies according to

$$L = \left(\frac{A}{Z}\right)^2 f_b N_e F(\zeta) \frac{\xi_i \gamma_i^3 \sigma_s \sqrt{2\pi}}{\beta r_p \Pi}, \quad \Delta\nu_L \geq \xi_e. \quad (2.12)$$

This equation and Eq.(2.9) show that for a given value of \sqrt{s} the luminosity of ENC as a function of the ion energy has a maximum (see in Fig.2.2), which occurs when $\Delta\nu_L(\gamma_i) = \xi_e(\gamma_i)$ ¹:

¹More generally, when $\Delta\nu_L(\gamma_i) = \mathcal{R}\xi_e(\gamma_i)$, where $\mathcal{R} \leq 1$. In this case, we write

$$(\gamma_i)_{max} = \left(\frac{ZQ}{A\mathcal{R}}\right)^{1/4} \sqrt{\frac{\gamma_s}{2}}, \quad Q = \frac{\Pi}{\sigma_s \sqrt{2\pi}},$$

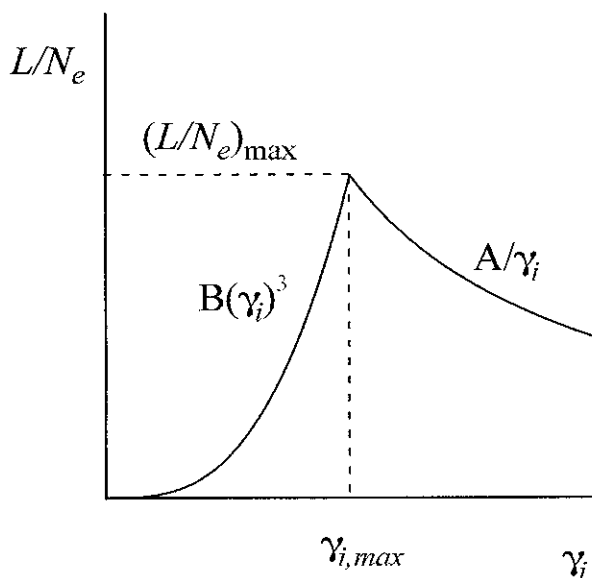


Figure 2.2: Schematic dependence of the specific luminosity (L/N_e) on γ_i . The maximum corresponds to the ion energy, when $\Delta\nu_L(\gamma_i) = \xi_e(\gamma_i)$.

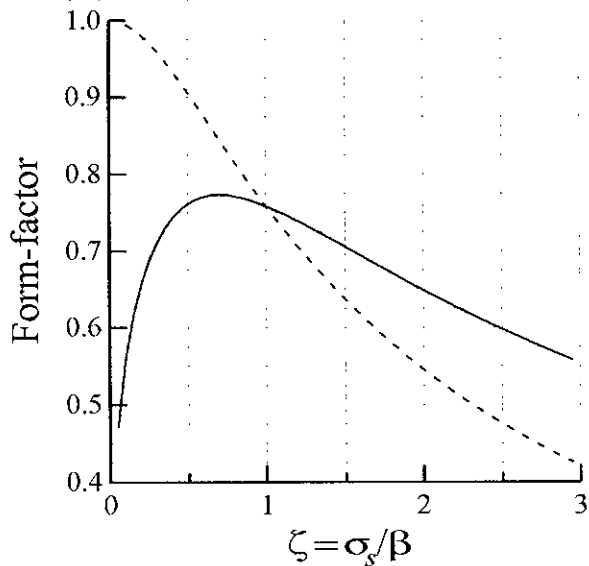


Figure 2.3: Dependences of the hour glass luminosity reduction form-factors on the bunch length. Solid curve shows $\zeta^{1/4}F(\zeta)$, dashed curve: $F(\zeta)$.

$$\gamma_e = \frac{A m_p \sigma_s \sqrt{2\pi}}{Z m_e \Pi} \gamma_i^3, \quad (2.13)$$

or

$$(\gamma_i)_{\max} \simeq \left\{ \frac{Z\Pi}{4A\sigma_s\sqrt{2\pi}} \right\}^{1/4} \sqrt{\gamma_s}, \quad \gamma_s = \frac{\sqrt{s}}{m_p c^2}. \quad (2.14)$$

The transporting of particles with such energies demand the following magnetic rigidities of the ion and electron storage rings:

$$(BR)_i = 3.126 \times \left(\frac{A}{Z} \right)^{3/4} \left(\frac{\Pi}{\sigma_s \sqrt{2\pi}} \right)^{1/4} \sqrt{\frac{\gamma_s}{2}}, \quad [\text{Tm}] \quad (2.15)$$

$$(BR)_e = 3.126 \times \left(\frac{A}{Z} \right)^{1/4} \left(\frac{\Pi}{\sigma_s \sqrt{2\pi}} \right)^{-1/4} \left(\frac{\gamma_s}{2} \right)^{3/2} \quad [\text{Tm}]. \quad (2.16)$$

These equations show (see also in Fig.2.4) that the required rigidities for electron-proton mode of ENC are in the range $(BR)_i \leq 100$ Tm, while the electron-ion modes demand the rigidities in the range $(BR)_i = 100 \div 200$ Tm.

Substituting $(\gamma_i)_{\max}$ from Eq.(2.14) in, for example, Eq.(2.12), we find for the maximum value of the specific luminosity (L/N_e) the following expression

$$\left(\frac{L}{N_e} \right)_{\max} \simeq f_b F(\zeta) \left(\frac{A}{Z} \right)^{5/4} \left(\frac{\sigma_s \sqrt{2\pi}}{\Pi} \right)^{1/4} \frac{\xi(\gamma_s/2)^{3/2}}{\beta r_p}. \quad (2.17)$$

An inspection of Fig.2.3 indicates a broad maximum in the dependence of the maximum specific luminosity in Eq.(2.17) on the bunch length (ζ) at $\zeta \simeq 0.75$. Since $(\gamma_e)_{\max} \propto \sigma_s^{1/4}$ and $(\gamma_i)_{\max} \propto 1/\sigma_s^{1/4}$, it makes not a big sense to choose ζ far from $\zeta = 1$. According to Eq.(2.17) and provided that the ion bunch cooling ensures $(\xi_i)_{th} = (\xi_e)_{th} = \xi$, the higher luminosity performance is more feasible for higher \sqrt{s} (see also in Fig.2.5). If, for some reasons, the electron and ion energies deviate from the optimum values, the specific luminosity of ENC decreases. This dependence is more sharp in the region, where $\gamma_i \leq (\gamma_i)_{\max}$ and hence, $(L/N_e) \propto \gamma_i^3$.

2.1.3 Synchrotron radiation losses

For optimum specific luminosity higher \sqrt{s} generally correspond to higher electron energies (see also in Fig.2.6). Moving along the closed orbit the electrons lose their

and

$$(\gamma_c)_{\max} = \frac{m_p}{m_e} \left(\frac{AR}{ZQ} \right)^{1/4} \left(\frac{\gamma_s}{2} \right)^{3/2},$$

so that position of the optimum does not indicates a strong dependence on an exact value of \mathcal{R}

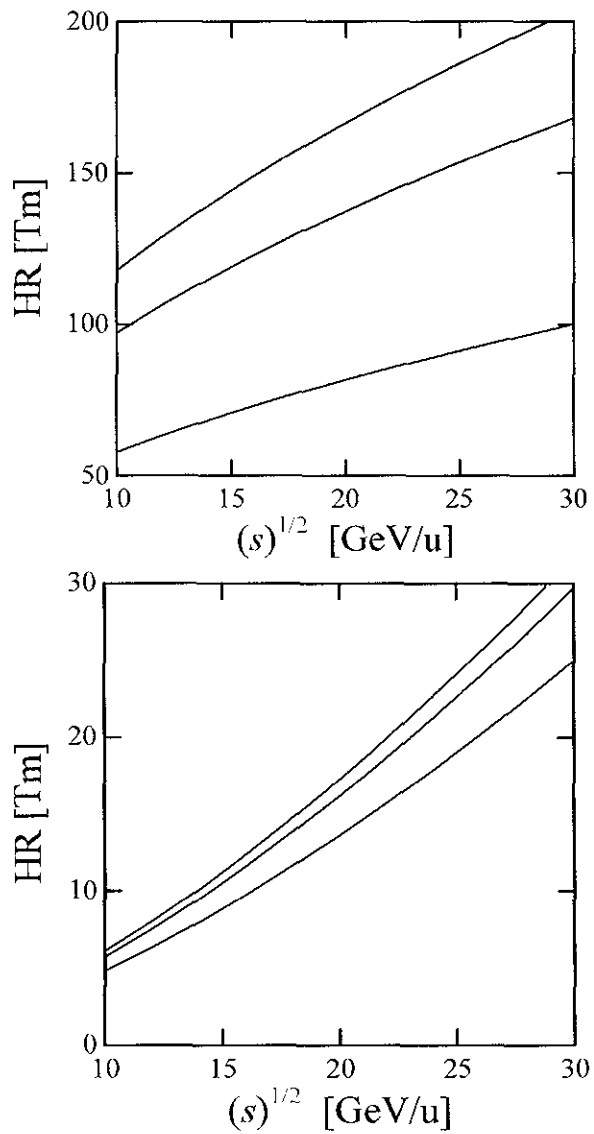


Figure 2.4: Dependences of the magnetic rigidities of the ion (left figure) and electron (right figure) storage rings of ENC on the center of mass energy. The rigidities were calculated for particle energies corresponding to the maximum specific luminosity; in both figures from top to bottom the lines correspond to the electron - U_{238}^{92} , electron - deuteron and electron - proton operational modes.

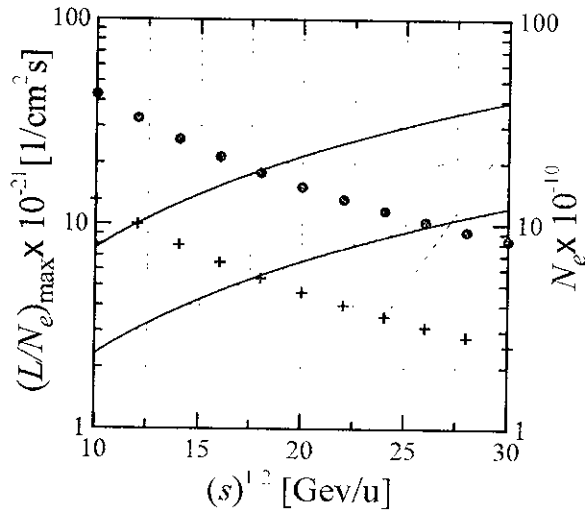


Figure 2.5: Dependence of the maximum value of the specific luminosity on \sqrt{s} (solid lines; upper curve – U_{238}^{92} , lower curve – protons). Full dots show the numbers of particles in electron bunches required to achieve the luminosity $L = 10^{33} \text{ 1/(cm}^2\text{s)}$; full crosses – same for electron- U_{238}^{92} collider.

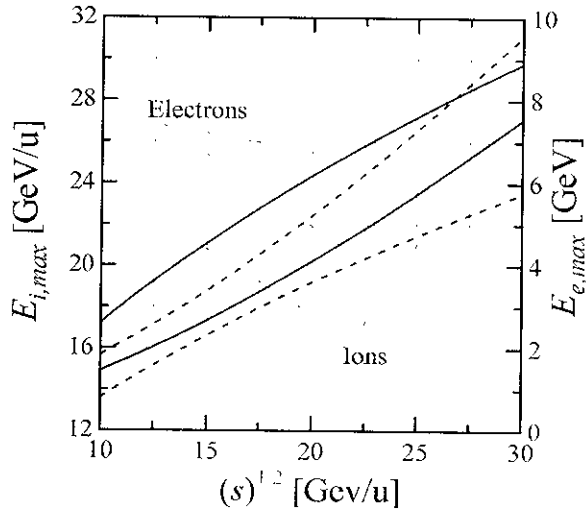


Figure 2.6: Dependences of the ion (left axes) and electron (right axes) energies, corresponding to the maximum specific luminosity (L/N_e) and to a given \sqrt{s} , on \sqrt{s} . Solid lines: electron-proton collider, dashed lines: electron- U_{238}^{92} collider.

energy due to the so-called synchrotron radiation. If the orbit consists of the sectors with the constant curvature radius R , the electron energy loss per turn reads

$$\Delta E_c [\text{MeV}] \simeq 0.09 \frac{(E_e [\text{GeV}])^4}{R [\text{m}]} \quad (2.18)$$

These energy losses must be compensated by the RF-system of the ring. The required power of the accelerating RF-system of the ring

$$P \simeq 0.09 \frac{(E_e [\text{GeV}])^4}{R [\text{m}]} f_b N_e \quad (2.19)$$

should not exceed some reasonable value. Substituting in Eqs (2.18) and (2.19)

$$(E_e)_{\text{max}} = m_p c^2 \left(\frac{A \sigma_s \sqrt{2\pi}}{Z \Pi} \right)^{1/4} \left(\frac{\gamma_s}{2} \right)^{3/2},$$

and calculating N_e using Eq.(2.17) and $L = 10^{33} \text{ 1}/(\text{cm}^2\text{s})$, we find that in the energy range $10\text{MeV}/u \leq \sqrt{s} \leq 30\text{MeV}/u$ and for all ions till U_{238}^{92} the synchrotron radiation power although reaches the range of several MW, still is in a reasonable region (see in Fig.2.7). Both this value and the electron energy loss per turn increase for higher energies. However, even if we demand the RF-voltage as twice as higher than E_e , the required power of the RF-system remains within 10 MW, which is typical for a factory-type collider. Hence, the energy losses of electrons do not pose a strong limit on the luminosity performance in ENC.

2.1.4 Collective instabilities

One more limitation on the intensity of electron bunches may occur due to their collective interactions with surrounding electrodes, which can result in various instabilities of the bunch coherent oscillations. Postponing a detailed discussion of these phenomena to the Chapter 6, we shall mention here only several limitations. Specific features of possible instabilities depend on the memory in the system, or on the frequency bandwidth of electrodes. The interaction with electrodes, which remember the induced fields during the time intervals exceeding the bunch to bunch period, results in the so-called multi-bunch instabilities. In the multi-bunch collider these instabilities must be damped using relevant feedback system anyway.

In this subsection we shall estimate the limitations on the bunch intensity due to interaction with a wideband system, which can cause the so-called single-bunch instabilities of the transverse oscillations of the bunch. These can be the so-called head-tail instability and the instability due to the coupling of the synchro-betatron modes of the bunch. The increments of the head-tail instabilities are proportional to the lattice chromaticity, which must be carefully compensated to provide stability of both coherent and incoherent oscillations.

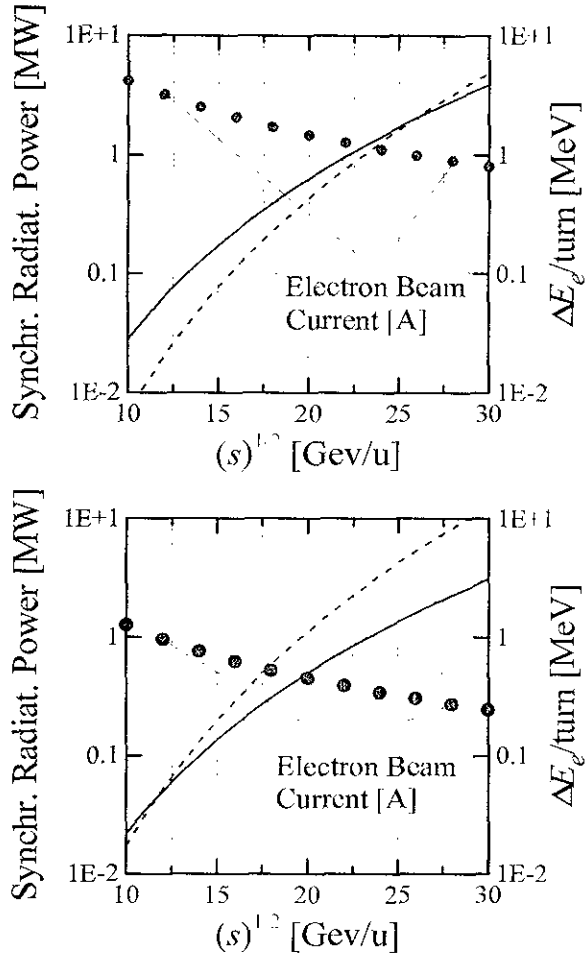


Figure 2.7: Dependence of the synchrotron radiation power (solid line), electron energy loss per turn (dashed line) and of the electron beam current (full dots), required to reach the luminosity 10^{33} $1/(\text{cm}^2\text{s})$ per nucleon, for electron-proton (left) and electron-U₂₃₈⁹² (right) colliders.

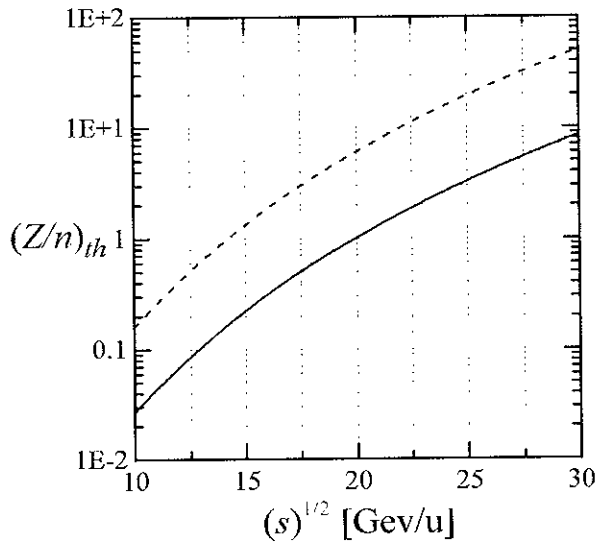


Figure 2.8: Dependence of the threshold value of the wideband coupling impedance on \sqrt{s} . Solid curve: electron - proton collider, dashed curve: electron - U_{238}^{92} collider. Electron and ion energies correspond to the maximum value of the specific luminosity, the number of particles in electron bunch is chosen to fit the requirement $L = 10^{33} \text{ 1/(cm}^2\text{s)}$, the RF-voltage as twice as exceeds the electron energy loss per turn, $l_{\perp} = 3 \text{ cm}$.

The synchro-betatron mode coupling instability occurs due to merging of the frequencies of the (dipole) betatron coherent mode and its nearest synchro-betatron sideband. For a given N_e , the threshold value of the coupling impedance of the vacuum chamber can be estimated using

$$(Z/n)_{th} = \nu_s \frac{2\pi E_c}{N e^2 \omega_0} \frac{l_1^2 \sigma_s}{R_0^3}, \quad \omega_0 = 2\pi f_b/n_b. \quad (2.20)$$

Here, ν_s is the tune of the synchrotron oscillations. An inspection of the dependence of the threshold value of the pipe impedance on \sqrt{s} (see in Fig.2.8) shows that without special efforts the mode coupling instability can limit the luminosity performance in the electron-proton collider for $\sqrt{s} \leq 17.5$ GeV/u and in electron-U₂₃₈⁹² collider for $\sqrt{s} \leq 12.5$ GeV/u.

2.1.5 Beam loading of the RF-system

One more limitation on the lower required value of the RF-voltage can be caused by the so-called beam loading of accelerating cavities (see, for example, in Ref.[1]). A beam, passing an accelerating cavity, leaves there the wake-field disturbing the accelerating field. The resulting field corresponds to the detuning of the cavity down the resonant frequency (in our case, $f_k = f_b$) by the amount (see in Ref. [14] for more detail)

$$\Delta f_k \simeq -f_b \frac{I_t(Z_k/Q_k)}{2V}. \quad (2.21)$$

Here, $I_t = f_b Z e N$ is the beam current, Z_k is the shunt impedance of the fundamental mode of the accelerating cavity, Q_k is its quality factor. In order to maintain the desired accelerating voltage the resonant frequency of cavity must be shifted up by the amount of Δf_k . Here, Z_k is the shunt impedance of the fundamental mode of the accelerating cavity and Q_k is its quality factor, $I_t = Z e N_{i,e} f_b$ (for electrons $Z = 1$). An inspection of the results, shown in Fig.2.9, indicates that without special efforts the loading of the fundamental mode of the accelerating cavity by the electron beam can limit the luminosity performance ($\Delta f_k/f_0 \leq 0.1$) in electron-proton collider starting from $\sqrt{s} \leq 17.5$ GeV and in electron-U₂₃₈⁹² collider starting from $\sqrt{s} \leq 13$ GeV.

2.1.6 Beam cooling and intrabeam scattering

The desired value of the luminosity 10^{33} [cm⁻²s⁻¹] can be achieved only in the case when N_e , ξ_e and f_b are high enough. In particular, the threshold value of ξ_i must essentially exceed the values, which are typical for conventional schemes of hadron colliders ($\xi_{i,conv} \sim 0.001$). That is possible only in the case, when the ion bunches are cooled, so that the cooling enable suppressions of the higher order beam-beam resonances. Assuming that the fast electron cooling can be employed to cool the ion

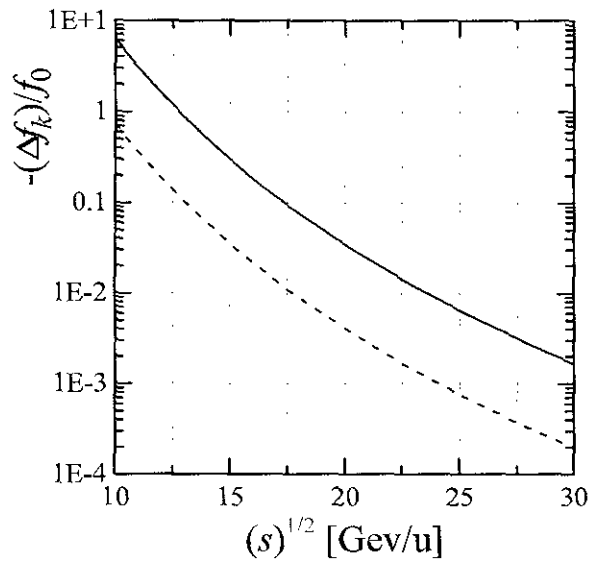


Figure 2.9: Dependence of the detuning of the RF-fundamental mode due to its loading by the electron beam on \sqrt{s} . Solid curve: electron - proton collider, dashed curve: electron - U_{238}^{92} collider. Electron and ion energies correspond to the maximum value of the specific luminosity, the number of particles in electron bunch is chosen to fit the requirement $L = 10^{33}$ 1/(cm²s), the RF-voltage as twice as exceeds the electron energy loss per turn.

bunches and that the ion bunches have about equal betatron emittances as well as equal and constant β -functions along the cooling region, we write

$$\lambda_{\perp} = \frac{\Lambda_0}{2\sqrt{2\pi}} \Phi_x(z), \quad \lambda_{\parallel} = \frac{2\Lambda_0}{\sqrt{2\pi}} \frac{\Phi(z)}{z}. \quad (2.22)$$

Here,

$$\Lambda_0 = \frac{Z^2}{A} \frac{4\pi n_e e^4 L_c}{\gamma^5 m M c^3 (\epsilon/\beta_c)^{3/2} \Pi} l$$

estimates the betatron cooling rate of the monochromatic bunch ($\delta = 0$), while the form factors

$$\Phi_x(z) = \begin{cases} \frac{1+2z^2}{(1-z^2)^{5/2}} \arcsin \sqrt{1-z^2} - \frac{3z}{(1-z^2)^2}, & z \leq 1, \\ \frac{1+2z^2}{(z^2-1)^{5/2}} \ln [z + \sqrt{z^2-1}] - \frac{3z}{(z^2-1)^2}, & z \geq 1, \end{cases}$$

and

$$\Phi(z) = \begin{cases} \frac{2+z^2}{(1-z^2)^2} - \frac{3z \arcsin(\sqrt{1-z^2})}{(1-z^2)^{5/2}}, & z \leq 1, \\ \frac{2+z^2}{(z^2-1)^2} - \frac{3z \ln(z + \sqrt{z^2-1})}{(z^2-1)^{5/2}}, & z \geq 1. \end{cases}$$

describe dependences of the cooling decrements on the bunch momentum spread [$z = (\delta/\gamma)\sqrt{\beta_c/\epsilon}$], n_e is the density of the cooling electron beam, suffix c marks the values in the cooling region, l is the length of the cooling region.

The lower limit on the rate of electron cooling poses the intrabeam scattering (IBS) in ion bunches (see, for example in Refs [8], [9] and [10]). Here, we follow Refs [8] and [9] and evaluate the IBS lifetime as the sum of the partial emittances growth rates

$$\Lambda = \frac{1}{\epsilon_x} \frac{d\epsilon_x}{dt} + \frac{1}{\epsilon_z} \frac{d\epsilon_z}{dt} + \frac{1}{\delta^2} \frac{d\delta^2}{dt}.$$

Ion bunches reach the equilibrium due to cooling, if their parameters satisfy an inequality

$$\lambda_x + \lambda_z + \lambda_{\parallel} \simeq 2\lambda_{\perp} + \lambda_{\parallel} > \Lambda.$$

Straightforward calculations, based on the Landau kinetic equation (see, for example in Chapter 5 and in Appendix C, section C.1), show that for a FODO-like lattices the main contributions to Λ can be estimated using the smoothed focusing

approximation, when one takes $D_x \rightarrow R_0/\nu_x^2$, $\beta \rightarrow R_0/\nu_x$ ($\Pi = 2\pi R_0$) and when Λ is determined by the following expressions

$$\Lambda = \frac{K_{IBS}}{\epsilon_x \epsilon_z \sigma_s \delta} G(a), \quad K_{IBS} = \frac{N_i (Z^2/A)^2 r_p^2 c L_{IBS}}{2\pi \gamma^4}, \quad (2.23)$$

$$G(a) = \frac{2+a}{\sqrt{a-1}} \arcsin \left(\sqrt{\frac{a-1}{a}} \right) - 3, \quad a = \frac{\gamma^2 D_x^2}{\beta_{av}^2} + \frac{\gamma^2 \epsilon}{\beta_{av} \delta^2} > 1.$$

For small synchrotron oscillations in the bunched beam ($\sigma_s \ll \Pi/n_b$) the bunch length and the bunch momentum spread are related via

$$\delta = \frac{\sigma_s}{\Pi} \sqrt{\frac{2\pi n_b Z e V}{E_i |\alpha_p|}},$$

which determines the required acting accelerating voltage in ion ring (V). The entering in these equation values N_i and ϵ can be expressed in terms of N_e using the relationships $\Delta\nu_L = \xi_i$ and

$$\epsilon = \frac{Z}{A} \frac{N_e r_p}{4\pi \gamma_i \xi_i}. \quad (2.24)$$

That results in

$$N_i = \frac{N_e \gamma_s}{2\sqrt{AZ}} \left(\frac{\sigma_s \sqrt{2\pi}}{\Pi} \right)^{1/2} \propto \frac{Z^{3/4}}{A^{7/4}}, \quad (2.25)$$

and

$$\epsilon = \left(\frac{Z}{A} \right)^{3/4} \frac{N_e r_p}{4\pi \xi} \left(\frac{\sigma_s \sqrt{2\pi}}{\Pi} \right)^{1/4} \sqrt{\frac{2}{\gamma_s}} \propto \left(\frac{Z}{A} \right)^2. \quad (2.26)$$

Since the density of the cooling electron beam in the cooling region must exceed the density of the ion bunch, using these formulae we can also find

$$n_{e,min} = \frac{N_i}{2\pi \beta_c \epsilon \sqrt{2\pi} \sigma_s} = \frac{A^{1/4}}{Z^{5/4}} \frac{\xi \gamma_s^{3/2}}{2\sqrt{\pi} r_p \beta_c} \left(\frac{\sqrt{2\pi}}{\sigma_s \Pi} \right)^{1/4} \quad (2.27)$$

This expression shows that the ion beam density and required density of the cooling beam increase with γ_s proportional to the maximum specific luminosity. The bunch emittances of the cooled bunches for various \sqrt{s} are shown in Fig. 2.10. These data enable evaluation of the cooling times and of the IBS growth rates (Fig. 2.11).

In the colliding beam operational mode the equilibrium bunch emittances are strongly affected by the beam-beam and probably by the space charge (for ion bunches) instabilities. For that reason, the calculation of the equilibria parameters, which take into account a balance between the beam cooling and IBS does not make big sense. For a single beam operation, the estimations of such equilibria do not approach any extraordinary regions of bunch parameters (see in Ref.[9]).

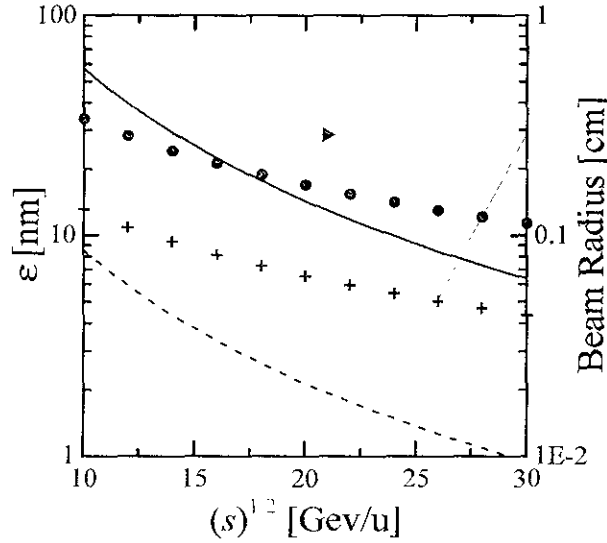


Figure 2.10: Dependence of the ion beam emittance (left axes) and of the rms ion beam radius (right axes) on \sqrt{s} . Solid curve and full dots: electron - proton collider, dashed curve and full crosses: electron - U_{238}^{92} collider. Electron and ion energies correspond to the maximum value of the specific luminosity, the number of particles in electron bunch is chosen to fit the requirement $L = 10^{33} \text{ 1/(cm}^2\text{s)}$.

2.2 Luminosity Lifetime

As far as the colliding bunches are cooled, the luminosity lifetime is determined by the particle losses from bunches. We write

$$\frac{dL}{dt} = \frac{f_b}{4\pi\beta\epsilon} \left(N_i \frac{dN_e}{dt} + N_e \frac{dN_i}{dt} \right),$$

or

$$\frac{dL}{dt} = -\frac{L}{\tau}, \quad \frac{1}{\tau} = \frac{1}{\tau_e} + \frac{1}{\tau_i}. \quad (2.28)$$

Here, τ_e and τ_i are the lifetimes of electron and ion bunches

$$\frac{1}{\tau_e} = -\frac{d \ln N_e}{dt}, \quad \frac{1}{\tau_i} = -\frac{d \ln N_i}{dt}.$$

If T is the run time, the average value of the luminosity during the run

$$\langle L \rangle = \frac{1}{T} \int_0^T L(t) dt = L_0 \frac{1 - \exp(-T/\tau)}{(T/\tau)}$$

will be smaller than its peak value (L_0 ; see also in Fig. 2.12) In particular, after the lifetime τ the luminosity depression is about 40% (Fig.2.12).

Below we discuss several examples, which are most specific for ENC operations and which give main contributions in the bunches lifetimes.

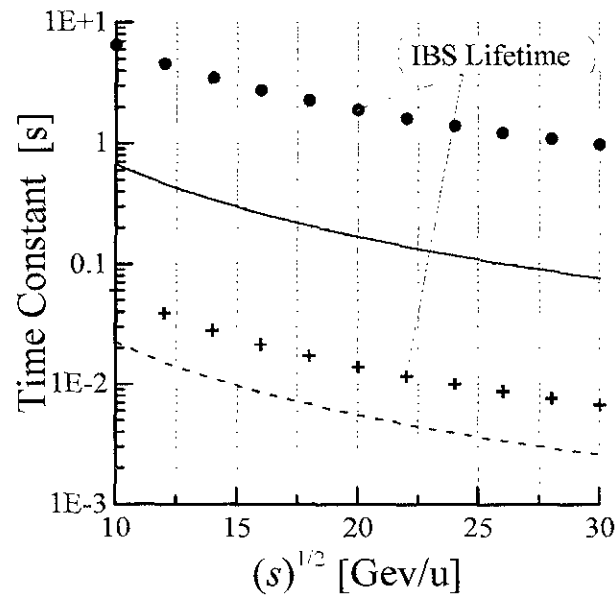


Figure 2.11: Dependence of the cooling time and IBS growth rate (symbols) on \sqrt{s} . Solid curve and full dots: electron - proton collider, dashed curve and full crosses: electron - U_{238}^{92} collider. Electron and ion energies correspond to the maximum value of the specific luminosity, the number of particles in electron bunch is chosen to fit the requirement $L = 10^{33} \text{ 1/(cm}^2\text{s)}$, the density of the cooling electron beam is taken $2n_{e,min}$.

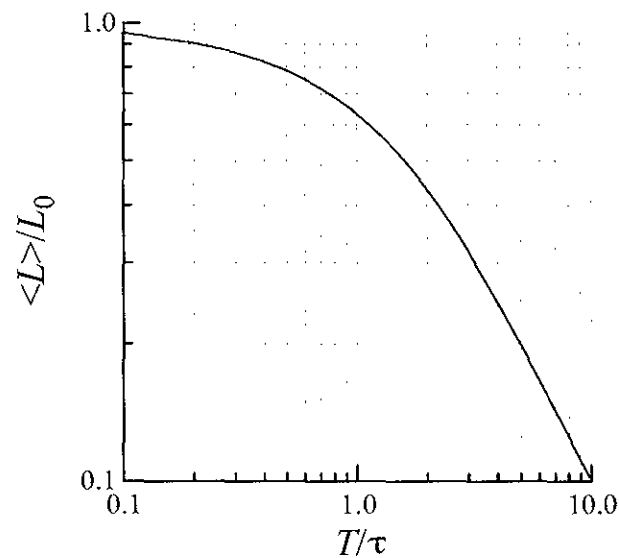


Figure 2.12: Dependence of the average luminosity ($\langle L \rangle / L_0$) on the run period T .

2.2.1 Radiative recombination lifetime

When passing the cooling device the ions can be lost due to their recombination with the cooling electrons. Since the capture of an electron occurs due to collisions with small impact parameters, for the parameters of ENC the leading contribution to the recombination rate gives the radiative recombination. For the conditions, specific for the cooling devices, the recombination coefficient was calculated in Ref. [11]. In the beams rest frame system it reads

$$C_{rec} \simeq 32Zr_e^2cq \left[\ln q + b_0 + \frac{b_1}{q^{3/2}} + \frac{b_2}{q^{4/3}} + \frac{b_3 - b_4 \ln q}{2q^2} \right]. \quad (2.29)$$

Here, $q = Z\alpha/(v/c)$, $\alpha \simeq 1/137$, v is the relative velocity of the colliding particles,

$$b_0 = 1.143, \quad b_1 = 0.33, \quad b_2 = 0.039, \\ b_3 = 0.068, \quad b_4 = 0.046.$$

The life time was calculated using

$$\tau_{rec} = \frac{\gamma_i^2}{n_e C_{rec}} \cdot \frac{\Pi}{l}, \quad (2.30)$$

l is the length of the cooling section.

In the case of ENC, the recombination will take place in strong magnetic field, while the bunch densities of electron and especially light ion beams will be very high (on the cooling section $n > 10^{10}$ 1/cm³). It is not very clear will the described radiative recombination process still dominate, or the recombination coefficient will be modified due to effect of the magnetic field and/or due to high (phase space) densities of the cooled bunches. For example, the measurements at NAP-M [12] indicated much faster decrease in the recombination coefficient with an increase in the velocities of the Larmor circles that with an increase in the electron Larmor velocities. The growth of the recombination coefficient with an increase in the magnetic field was also observed at ESR [13]. The nature of these phenomena is not clear yet. For that reason, additional studies of the recombination in very cold ion beams on the cooling section are very desirable.

2.2.2 Lifetime of electron beam

The life time of electrons was estimated assuming that most important are the losses of electrons due to their collision with ions at the interaction points. The dominating process is the bremsstrahlung of electrons on the counter moving ions, when the energy of the radiated photons exceeds the energy aperture of the ring. If the cross section of this process is σ , the rate of such loss reads

$$\frac{dN_e}{dt} = \frac{\sigma_R L}{A n_b}, \quad (2.31)$$

which yields the lifetime of an electron bunch

$$\frac{1}{\tau_{br}} = \frac{1}{N_e} \frac{dN_e}{dt} = \frac{\sigma_R}{An_b} \left(\frac{L}{N_e} \right). \quad (2.32)$$

Here,

$$\sigma_R \simeq \frac{Z^2 \alpha r_e^2}{25.7} \left\{ \ln(4\gamma_i^2 \gamma_e^2) \left(-\ln[\Delta E_a/E_e] - \frac{1}{2} \right) + \frac{1}{2} \ln^2(\Delta E_a/E_e) \right\}, \quad (2.33)$$

while $\Delta E_a/E_e$ is the relative energy aperture of the electron ring. This limitation is the most severe for heavy ion collider modes of ENC. As is seen from the Tables 2.2 – 2.4, the shortest lifetime of electron bunches is expected for the electron-U₂₃₈⁹² mode of ENC, where it varies from 1600 to about 500 seconds.

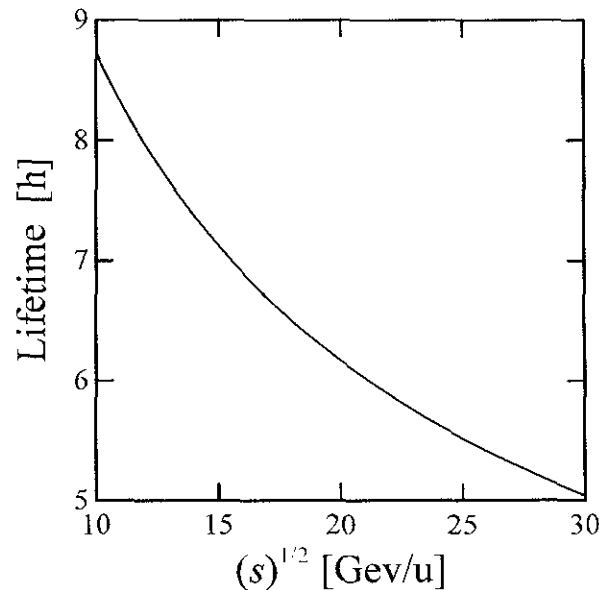


Figure 2.13: Dependence of the lifetime of electron beam due to elastic single scattering of electrons on the bare uranium ions on \sqrt{s} .

These numbers can be compared, for example, to the lifetimes of electron bunches due to elastic single scattering of electrons on uranium ions (Fig.2.13), when typical lifetimes are in the 6 – 9 hours region. The last process can be, however, important populating tails in the transverse distribution of electrons (see in Fig.2.14). In the tail regions the particles are strongly affected by the beam-beam resonances, which may transport them to larger oscillation amplitudes.

Rough estimation of the tail population can be obtained multiplying the production rate of the particles with amplitudes exceeding some amount of σ_{\perp} ($C_A = \sqrt{\epsilon_A/\epsilon}$) by the synchrotron radiation damping time. For the optimum luminosity conditions

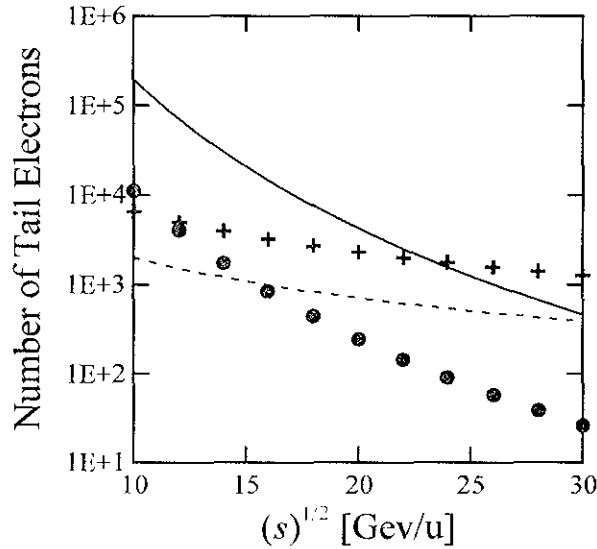


Figure 2.14: Dependence of the tail population on \sqrt{s} . Solid and dashed lines describe the electron- U_{238}^{92} mode; characters describe the electron-proton mode. Dashed line and full crosses give a Gaussian tail population.

relevant production rate reads

$$\left(\frac{dN_e}{dt}\right)_A \simeq 128 \frac{Z^2}{A} f_0 F(\zeta) \frac{\pi^2 \xi^2}{C_A \gamma_s}, \quad f_0 = \frac{f_b}{n_b}. \quad (2.34)$$

As is seen from Fig.2.14, this effect is not important for the electron-proton mode, where for most energies the tail population in electron bunches is determined by the fluctuations of the synchrotron radiation of electrons. On the contrary, for electron- U_{238}^{92} mode the contribution of the Coulomb collisions to the tail population dominate (see in Fig.2.14).

The evaluation of the beam lifetime due to common effects of the Coulomb scattering and beam-beam instability demands tedious simulations. For the case of ENC, that should also take into account the space charge of the ion beam so that the codes, which were developed for the electron-positron colliders, very likely will not work.

2.3 Parameter Sets

Described facts and equations were used for the calculations of the parameter sets enabling the luminosity of electron-nucleon collisions $L = 10^{33}$ 1/[cm²s] in the energy range

$$10 \text{ [GeV/u]} \leq \sqrt{s} \leq 30 \text{ [GeV/u]}$$

In our estimations we considered as limiting cases the electron-proton, electron-deuteron and electron- U_{238}^{92} operational modes of ENC. General parameters of ion

Table 2.1: General parameter list

Closed orbit perimeter	1 km
Collision frequency	60 MHz
$\chi = \epsilon_e/\epsilon_i$	1
Curvature radius in bending magnets	60 m
β -function at IP	10 cm
Rms bunch length	10 cm
β_{av}	12 m
$D_{x,av}$	1.6 m
Momentum compaction factor	0.006
β -function in cooling section	200 m
Length of the cooling region	50 m
Cathode temperature	0.1 eV
Longitudinal magnetic field in cooling region	0.5 T
$\xi_e = \xi_i$	0.05

and electron rings of ENC for these estimations are listed in the Table 2.1. The assumed perimeters of the rings are more relevant to the electron-proton mode with 30 GeV protons ($BR = 100$ Tm). As is seen from Fig.2.4, if we demand the maximum specific luminosity, such a magnetic rigidity of the ion ring can enable the operation of ENC in the electron-ion mode with $A/Z = 2$ only at low energies ($\sqrt{s} \simeq 10$ GeV/u). Wider ion energy ranges are possible, if the ion energy is shifted down the energy, corresponding to the maximum specific luminosity. However, in such a case, the suppression of the specific luminosity ($L/N_e \propto \gamma_i^3$) and the requirement to maintain the designed luminosity demands higher electron beam currents and higher energies of electrons. On its turn, those result in the increase of the necessary power of the RF-system of the electron ring.

According to Fig.2.4 in the desired interval of the center of mass energies more relevant magnetic rigidity of the ion ring is $BR = 200$ Tm. For the case, when the magnetic system of the ion ring of ENC is performed using the normal-conducting elements, the perimeters of the closed orbit must be enlarged till approximately 2 km. A limitation, for some reasons, of the perimeters of the ENC rings by the values $\simeq 1$ km, will make necessary to use for the magnetic system of the ion ring the super-conducting elements.

The results of the calculations (see in Tables 2.2 and 2.4) show that in the considered limiting cases the high luminosity performance in ENC although is feasible, but encounters various problems. For example, in the electron-proton operational mode of ENC (see in the Table 2.2) huge cooling beam densities big cooling beam currents are required to ensure short enough cooling times of ion bunches. For electron-positron colliders ξ_{th} varies proportionally to $\lambda_e^{1/2}$ (or, even $\lambda_e^{1/3}$). Even if we adopt

this scaling rule for ENC, the cooling times of proton bunches still are too long to ensure $\xi_i \simeq 0.05$. More reliable requirement for the cooling times will be figured out during future studies. A comparison of the Tables 2.2 and 2.3 shows that shorter cooling times can be achieved in the electron-deuteron mode due to $(\lambda_c)_{opt} \propto (A/Z)^{7/2}$

The colliding electron bunch intensities, which are necessary to ensure $L = 10^{33}$ 1/[cm²s], are rather high. That will result in embarrassments due to collective interactions of these bunches with surrounding electrodes requiring a serious R&D study of the necessary damping feedback systems. Again, the electron-deuteron mode meets less problems.

In the electron-U₂₃₈⁹² operational mode the main limitation on the luminosity performance occurs due to short lifetime of electron and uranium bunches (see in the Table 2.4). Since $(L/N_e)_{max} \propto (A/Z)^{5/4}$ and $\sigma_R \propto Z^2$, the lifetime of electrons due to their bremsstrahlung on the bare ions varies according to

$$\tau_{br} \propto \frac{1}{A^{1/4}Z^{3/4}} \propto \frac{1}{Z}.$$

This problem is specific for electron-heavy ion modes of ENC. Scaling the electron beam lifetime from U₂₃₈⁹² (500 s) to lighter ions we find that it approaches to one hour only for $Z \simeq 15$. For all intermediate cases, it is short enough to demand the preparation of electron bunches in additional booster synchrotron prior to their injection in ENC.

The radiative recombination lifetime of bare uranium bunches can be made longer using artificial excitation of the Larmor motion of electrons prior they enter the cooling region. The radius of the Larmor circle, corresponding to the cathode temperature 0.1 eV is $r_L = 1.5 \mu\text{m}$, while the minimum value from the maximal impact parameters of adiabatic collisions varies in the range $260 \mu\text{m} - 90 \mu\text{m}$. An increase in the electron Larmor velocities by a factor, for example, 3 decreases the value of the Coulomb logarithm for about 20%, while the lifetime increases 3 times.

Table 2.2: Parameter set for an electron-proton collider, calculated assuming that $(\Delta\nu_L)_{th} = \xi_i$; RF-voltage in the proton ring 50 kV, and $\xi_i = 0.05$.

\sqrt{s} [GeV]	10	20	30
Specific Luminosity ($\times 10^{-21}$) [$1/\text{cm}^2\text{s}$]	2.3	6.5	12
$N_i \times 10^{-10}$	3.6	2.6	2.1
Proton Beam Current [A]	0.35	0.25	0.2
Proton Energy [Gev]	17.21	24.34	29.81
Emittans [nm]	57	14	6.3
Momentum Spread $\times 10^5$	7.1	5	4
Z/n [Ohm]	1.8	3.3	4.5
$\Delta f_{load}/f_0$	0.14	0.1	0.1
IBS Growth Time [s]	6.4	1.6	0.7
Cooling Time [s]	0.13	0.03	0.02
Betatron Cooling Time [s]	3.3	0.8	0.4
Longitudinal Cooling Time [s]	0.14	0.036	0.02
Density of Cooling Beam ($\times 10^{-10}$) [$1/\text{cm}^3$]	0.4	1.15	2.1
Current of Cooling Beam [A]	14	9.9	8
Rms Beam Radius [cm]	0.34	0.1	0.11
Current Density of Cooling Beam [A/cm^2]	19	55	101
Radiat. Recombination Lifetime [h]	87	61	50
$N_e \times 10^{-10}$	43.3	15.3	8.3
Electron Beam Current [A]	4.	1.5	0.8
Electron Energy [GeV]	1.45	4.1	7.5
Emittance [nm]	57	14	6.4
Synchr. Radiat. Energy Loss per Turn [MeV]	0.007	0.43	4.9
RF-Power [MW]	0.028	0.63	4
Z/n [Ohm]	0.027	1.0	8.5
$\Delta f_{load}/f_0$	6.2	0.034	0.0016
Bremsstrahlung Lifetime [h]	50	22	15

Table 2.3: Parameter set for an electron-deuteron collider calculated assuming that $(\Delta\nu_L)_{th} = \xi_i$; RF-voltage in the ion ring 12 kV, and $\xi_i = 0.05$.

\sqrt{s} [GeV]	10	20	30
Specific Luminosity ($\times 10^{-21}$) [$1/\text{cm}^2\text{s}$]	5.5	15.5	28.5
$N_i \times 10^{-10}$	1.1	0.77	0.63
Ion Beam Current [mA]	104	74	60.
Ion Energy [GeV/u]	14.47	20.47	25.07
Emittans [mm]	14.3	3.6	1.6
Momentum Spread $\times 10^5$	3	2.1	1.7
Z/n [Ohm]	7	13.7	19.4
$\Delta f_{load}/f_0$	0.2	0.13	0.12
IBS Growth Time [s]	1.13	0.28	0.12
Cooling Time [s]	0.012	0.003	0.001
Betatron Cooling Time [s]	0.3	0.07	0.03
Longitudinal Cooling Time [s]	0.013	0.003	0.001
Density of Cooling Beam ($\times 10^{-10}$) [$1/\text{cm}^3$]	0.5	1.4	2.5
Current of Cooling Beam [A]	4.2	3	2.4
Rms Beam Radius [cm]	0.17	0.085	0.056
Current Density of Cooling Beam [A/cm^2]	23	65	120
Radiat. Recombination Lifetime [h]	52	36	30
$N_e \times 10^{-10}$	18.21	6.439	3.5
Electron Beam Current [A]	1.75	0.62	0.34
Electron Energy [GeV]	1.73	4.9	8.98
Emittance [mm]	14	3.6	1.6
Synchr. Radiat. Energy Loss per Turn [MeV]	0.013	0.86	9.7
RF-Power [MW]	0.023	0.53	3.3
Z/n [Ohm]	0.1	3.7	31.3
$\Delta f_{load}/f_0$	1.3	0.007	0.0003
Bremsstrahlung Lifetime [h]	44	20	14

Table 2.4: Parameter set for an electron- U_{238}^{92} collider calculated assuming that $(\Delta\nu_L)_{th} = \xi_i$; RF-voltage in the ion ring 7 kV, and $\xi_i = 0.05$.

\sqrt{s} [GeV]	10	20	30
Specific Luminosity ($\times 10^{-21}$) [$1/\text{cm}^2\text{s}$]	7.6	21.4	39.4
$N_i \times 10^{-7}$	7.5	5.32	4.35
Ion Beam Current [mA]	66.5	47	38.4
Ion Energy [Gev/u]	13.57	19.19	23.51
Emittans [nm]	8.6	2.1	1
Momentum Spread $\times 10^5$	2.1	1.5	1.3
Z/n [Ohm]	11.5	23	33
$\Delta f_{load}/f_0 \times 10^3$	3	2	2
IBS Growth Time [ms]	6	2	0.7
Cooling Time [ms]	4	1	0.5
Betatron Cooling Time [ms]	120	30	13
Longitudinal Cooling Time [ms]	5	4	0.6
Density of Cooling Beam ($\times 10^{-7}$) [$1/\text{cm}^3$]	5.6	15.8	29.
Current of Cooling Beam [mA]	28.8	20.4	16.6
Rms Beam Radius [cm]	0.13	0.065	0.044
Current Density of Cooling Beam [A/cm^2]	0.27	0.76	1.4
Radiat. Recombination Lifetime [s]	786	556	434
$N_e \times 10^{-10}$	13.2	4.7	2.5
Electron Beam Current [A]	1.3	0.45	0.24
Electron Energy [GeV]	1.8	5.2	9.6
Emittance [nm]	8.56	2.14	0.95
Synchr. Radiat. Energy Loss per Turn [MeV]	0.017	1.1	12.6
RF-Power [MW]	0.022	0.5	3.0
Z/n [Ohm]	0.16	6.	51
$\Delta f_{load}/f_0$	0.73	0.004	0.0002
Bremsstrahlung Lifetime [s]	1672	766	520

Chapter 3

Beam-Beam Instability

The motion of a particle passing the interaction region is perturbed by the space charge fields of the counter-moving bunch – the so-called beam-beam interaction. If the bunches move in identical rings the collisions occur with the rotation period divided by the number of interaction points (IP). For that reason, such a perturbation results in numerous resonant phenomena. Their strengths and relevant increases in the particle oscillations amplitude depend on the values of the particle oscillation tunes. That a manifold phenomenon may result in the instability of both coherent and incoherent oscillations of colliding bunches, limiting the value of the collider luminosity (see, for example in Fig.3.1).

Due to nonlinear dependence of the beam-beam kick on the particle offsets (see, for example, in Fig.3.2), the interactions of colliding bunches result in numerous nonlinear effects: in the dependence of the tunes on the particle oscillations amplitudes and in the excitation of various nonlinear resonances. Dependences of particle tunes on amplitudes result in the spreading of the bunch image in the working space of tunes (ν_x , ν_z and ν_s) over some area – the so-called footprint of the bunch and in the saturation of the particle amplitude blow-ups.

Although, a detailed description of the beam-beam instability in a particular ring is very complicated, there are several parameters, describing the most crucial features of this instability. One of those is the so-called beam-beam parameter (ξ), which describes the amplitude of the perturbing kicks and which is equal numerically to the tune shift of linear oscillations of particles per one interaction point. Expecting similar behavior of colliding bunches in similar conditions we may design new colliders scaling the results, obtained studying this instability on previous rings.

When designing a high luminosity electron-nucleon collider, where the particle energies are not very high, the choice of a good working point should take into account the instabilities of ion bunches due to their space charge. The intensities of electron bunches are not limited due to space charge effect. Then, a joint requirement of the stability of colliding bunches against the beam-beam and space charge instability demands an employment of asymmetric lattices. The tunes in the electron ring can be chosen slightly above integer resonances (the case of two interaction points).

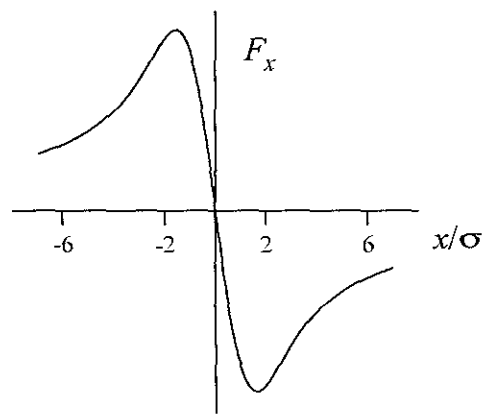
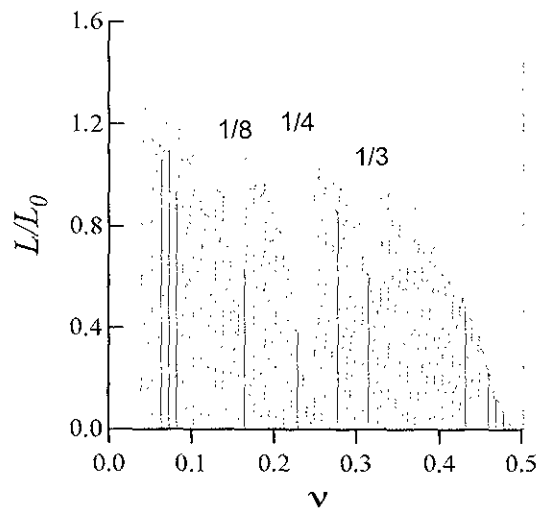


Figure 3.1: An example of the dependence of the luminosity on the tune. Relativistic e^+e^- bunches, which have round cross sections ($\sigma_x = \sigma_z$), one IP, equal betatron tunes, synchrotron radiation damping $\simeq 1000$ rotation periods, $\xi = 0.1$, L_0 is the luminosity without beam-beam perturbations.

Figure 3.2: Dependence of the beam-beam kick on transverse offset of a particle. The strong bunch has a round cross section and a Gaussian distribution in transverse coordinates.

In the ion ring the total tune shift for linear betatron oscillations is equal to the difference between the Laslett tune shift ($\Delta\nu_L$) and the tune shift due to the beam-beam interaction (for two IP $\Delta\nu_{bb} = 2\xi$, where ξ is the beam-beam parameter)

$$\Delta\nu_t = 2\xi - \Delta\nu_L$$

In the case, when the Laslett tune shift exceeds the beam-beam one ($\Delta\nu_L \gg \Delta\nu_{bb}$), the stopbands of the beam-beam and of the space charge resonances occur above the resonances of the unperturbed lattice (in the simplest case, above $\nu = n/m$, where n and m are integers). Hence, the ion tunes should be chosen slightly below integers. Indeed, the ratio between $\Delta\nu_L$ and $\Delta\nu_{bb}$ depends on the beam intensities and sizes. For that reason, a good position of the working points in ion ring will depend on the operational mode employed.

In general, two main approaches are used to study the limitations due to beam-beam interactions of bunches. These are the so-called weak-strong bunch approximation and the so-called strong-strong bunch approximation. The weak-strong bunch approach is based on the tracking of the motion of a particle (or of some ensemble of particles; weak bunch) neglecting the perturbation of the strong beam by the weak one. This method is a most widely used for designs and yields numerous useful predictions concerning the single particle beam-beam dynamics.

3.1 Linear Effects

The effect of the resonance perturbations due to beam-beam interactions is usually studied within the framework of the so-called weak-strong bunch approximation. It implies a study of oscillations of a particle from the weak bunch in a given field of the counter-moving strong bunch. So that a selfconsistent behaviour of the colliding bunches is ignored. The simplest predictions concerning the stability of the particle oscillations can be obtained in the linear approximation in the particle transverse offsets. If a particle moves in the interaction region with the average velocity c , and the strong bunch - with the velocity $-c$, each time passing IP a particle feels the kicks, which in the linear approximation in the particle offsets and for a Gaussian density of the counter-moving bunch are described by the following equations (see in Appendix B.1)

$$\frac{dp_z}{ds} = -\frac{4N_2Ze^2}{c\sigma_z(\sigma_x + \sigma_z)}\lambda(s+ct)z, \quad (3.1)$$

$$\frac{dp_x}{ds} = -\frac{4N_2Ze^2}{c\sigma_x(\sigma_x + \sigma_z)}\lambda(s+ct)x.$$

Here, N_2 is the number of particles in the counter-moving bunch, σ_x and σ_z are its r.m.s. horizontal and vertical sizes, $Ze^2 = -e_1e_2$ are the charges of particles, c is

the speed of light and s is the path along the closed orbit. The linear density in the bunch $\lambda(s)$ is supposed to be a periodic function of s , which repeats with the period of the collisions.

3.1.1 Beam-beam instability of short bunches

Between the final quadrupoles the unperturbed β -functions vary according to

$$\beta_z(s) = \beta_z + \frac{s^2}{\beta_z}, \quad \beta_x(s) = \beta_x + \frac{s^2}{\beta_x}$$

Then, if the rms bunch length is small as compared to $\min(\beta_z, \beta_x)$ [$\sigma_s \ll \min(\beta_z, \beta_x)$], we can replace $\lambda(s)$ by the periodic δ -function. Using a linear mapping between IPs (with the betatron phase advances $\mu_{(x,z)0}$), we obtain new tunes

$$\cos \mu_z = \cos \mu_{z0} - 2\pi\xi_z \sin \mu_{z0}, \quad (3.2)$$

and new β -functions

$$\beta_z = \beta_{z0} \frac{\sin \mu_{z0}}{\sin \mu_z}. \quad (3.3)$$

Here, we introduced the so-called beam-beam parameter for vertical oscillations

$$\xi_z = \frac{N_2 Z e^2 \beta_z}{2\pi p c \sigma_z (\sigma_x + \sigma_z)}. \quad (3.4)$$

Similar parameter

$$\xi_x = \frac{N_2 Z e^2 \beta_x}{2\pi p c \sigma_x (\sigma_x + \sigma_z)} \quad (3.5)$$

describes the beam-beam kicks for the horizontal oscillations. For a ring with two interaction regions we have $\mu = \pi\nu$. In a linear approximation in ξ_z Eqs (3.2) and (3.3) yield

$$\Delta\nu_z \simeq 2\xi_z, \quad \frac{\Delta\beta_z}{\beta_{z0}} \simeq -2\pi\xi_z \cot \mu_{z0}. \quad (3.6)$$

The oscillations are stable provided that $|\cos \mu_z| \leq 1$, or (for two IP)

$$\xi_z \leq \xi_{th} = \frac{1}{2\pi} \cot \left(\frac{\pi\nu_{z0}}{2} \right), \quad 0 \leq \nu_{z0} \leq 1. \quad (3.7)$$

The stability diagram for (see in Fig.3.3) indicates the stop-bands below the resonances $\nu = n$. Above the resonances the width of the stability diagram dramatically increases. Such a position of the stop-band relative the resonance value of the tune occurs due to the positive sign of the tune shift for particles with $e_1 e_2 < 0$ (a true resonance condition reads $\nu_{z0} + \Delta\nu_z = n$). For the same reason, above the resonance the value of the β -function in the IP can be substantially smaller than the unperturbed value (see in Fig.3.4). As far as the luminosity of the collider is proportional

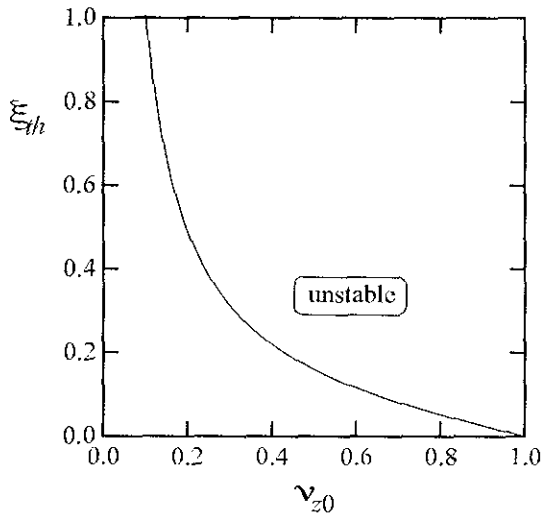


Figure 3.3: The stability diagram for linear betatron oscillations. Two interaction points.

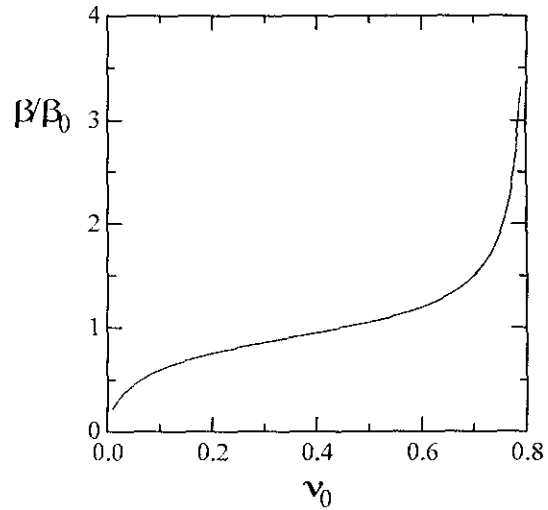


Figure 3.4: Dependence of the β -function on the tune of unperturbed betatron oscillations. Two interaction points; $\xi = 0.05$.

to $1/\sigma_x\sigma_z \propto 1/\sqrt{\beta_x\beta_z}$, we may expect relevant increase in the luminosity in such a region. The value of β -function increases, when ν_0 approaches the lower border of the stop-band. In this region of the tunes the luminosity drops. The described behavior of the stability diagram and of the dependences of β -functions on the tunes make more preferable the choice of the working point in (ν_x, ν_z) when these tunes only slightly exceed the integers.

The tune shifts for colliding beams with a round cross section are obtained, if we substitute in Eqs (3.4) and (3.5) $\sigma_x = \sigma_z = \sigma$. In that case, we write

$$\xi_z = \frac{N_2 Z e^2 \beta_z}{4\pi p c \sigma^2} = \frac{N_2 Z e^2}{4\pi p c \epsilon_z}, \quad (3.8)$$

where $\epsilon_z = \sigma^2/\beta_z$ is the vertical bunch emittance.

Similarly, for horizontal oscillations we have

$$\xi_x = \frac{N_2 Z e^2}{4\pi p c \epsilon_x}. \quad (3.9)$$

Hence, the values of the beam-beam parameters for the vertical and horizontal oscillations will be equal ($\xi_x = \xi_z$), if $\epsilon_x = \epsilon_z$.

3.1.2 Hour-glass effect

If the colliding bunches are not short as compared to the value of the β -function at the interaction point, the calculations related to the beam-beam instability must take into account that in the interaction region the low- β insertion makes a waist in the bunch shape. That results in the so-called hour-glass effect.

Betatron Oscillations

In the hour-glass region the calculations of betatron tune shifts must take into account longitudinal distributions of particles in the bunches. It means that simple expressions for the beam-beam tune shifts can be obtained using the perturbation theory. For long colliding bunches apart from assuming $\xi \ll 1$, it also demands an assumption that the so-called disruption parameter is small:

$$\mathcal{D} = 4\pi\xi \frac{\sigma_s}{\beta} < 1.$$

Then, the tune shifts can be obtained averaging the equations for the phase variables. For two IP simple calculations result in

$$\Delta\nu_z = 2 \frac{N_2 Z e^2}{2\pi p c} \int_0^{\Pi/2} ds \frac{2\beta_z(s)\lambda(2s)}{\sigma_z(s)[\sigma_x(s) + \sigma_z(s)]}. \quad (3.10)$$

The integral in this equation is essentially simplified, if β -functions of the colliding bunches are identical and if $\beta_x(s) = \beta_z(s) = \beta(s)$. In such a case, we write

$$\frac{\beta_z(s)}{\sigma_z(s)[\sigma_x(s) + \sigma_z(s)]} = \frac{\beta(s)}{\beta(s)[\sqrt{\epsilon_z} + \sqrt{\epsilon_x}]\sqrt{\epsilon_z}} = \frac{1}{[\sqrt{\epsilon_z} + \sqrt{\epsilon_x}]\sqrt{\epsilon_z}}$$

so that Eq.(3.10) is reduced to the following

$$\begin{aligned} \Delta\nu_z &= 2 \frac{N_2 Z e^2}{2\pi p c [\sqrt{\epsilon_z} + \sqrt{\epsilon_x}] \sqrt{\epsilon_z}} 2 \int_0^{\Pi/2} ds \lambda(2s) \\ &= 2 \frac{N_2 Z e^2}{2\pi p c [\sqrt{\epsilon_z} + \sqrt{\epsilon_x}] \sqrt{\epsilon_z}} = 2\xi_z. \end{aligned} \quad (3.11)$$

If also the vertical and horizontal emittances of the strong bunch are equal ($\epsilon_x = \epsilon_z = \epsilon$), the colliding bunches will have at the interaction point a round cross sections, while the tune shifts of the vertical and horizontal oscillations become equal

$$\Delta\nu_x = \Delta\nu_z = 2\xi = 2 \frac{N_2 Z e^2}{4\pi p c \epsilon} \quad (3.12)$$

Note, that in both cases the tune shifts of betatron oscillations do not depend on the bunch lengths. If we repeat the calculations for a particle, executing the synchrotron oscillations ($s = ct + a_s \cos(\psi_s)$, $\dot{\psi}_s = \omega_0 \nu_s$), the tune shift in Eqs (3.11) and (3.12) will not depend on the amplitude of the synchrotron oscillations either. In other words, for colliding bunches with the round envelopes or with the round cross sections the synchrotron motion does not increase the dimension of betatron resonances in the space of oscillation amplitudes.

For flat colliding bunches ($\sigma_x \gg \sigma_z$ and $\beta_x \gg \beta_z$) more typical is the region, where $\sigma_s \simeq \beta_z \ll \beta_x$ and, therefore

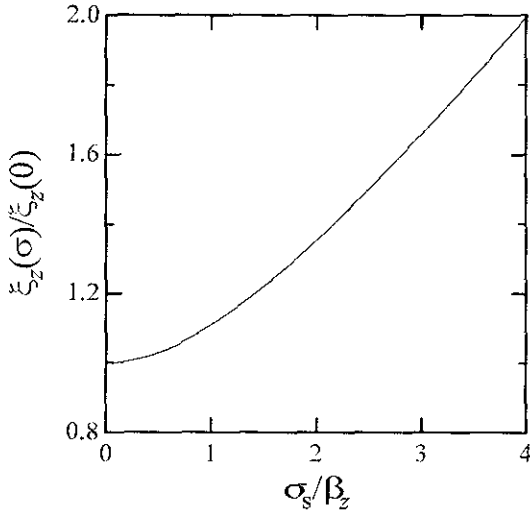


Figure 3.5: Dependence of the beam-beam parameter for vertical oscillations on the bunch length. The linear density in the counter-moving bunch is a Gaussian function: $\lambda(s) = \exp[-s^2/(2\sigma_s^2)]/\sigma_s\sqrt{2\pi}$.

$$\begin{aligned} \Delta\nu_z &= 2 \frac{N_2 Z e^2 \beta_z}{2\pi p c \sigma_z \sigma_x} 2 \int_0^{11/2} ds \lambda(2s) \sqrt{1 + \frac{s^2}{\beta_z}} \\ &\simeq 2 \frac{N_2 Z e^2 \beta_z}{2\pi p c \sigma_z \sigma_x} 2 \int_{-\infty}^{\infty} ds \lambda(2s) \sqrt{1 + \frac{s^2}{\beta_z}} = 2\xi_z(\sigma_s). \end{aligned} \quad (3.13)$$

In this case, the tune shift of vertical betatron oscillations substantially increase in the region, where $\sigma_s \gg \beta_z$ (see in Fig.3.5). For off-synchronous particles one also should expect an increase in $\Delta\nu_z$ with an increase in amplitudes of the synchrotron oscillations. Apart from the blow-up of the width of the beam footprint in the vertical direction, this fact results in the increase of the dimension of betatron resonances and, hence, in more freedom for particles to leave the bunch core, traveling along these resonances.

The described dependences of betatron tune shifts on the bunch length show that the round cross section geometry of colliding bunches generally simplifies the particle dynamics in the colliding bunches.

Synchrotron Oscillations

The longitudinal modulation of the potential drop of the counter-moving bunch due to the bunch waist results in the energy kick, when particles pass the interaction region. On its turn, such kicks yield the tune shifts of synchrotron oscillations due to beam-beam interaction. Simple calculations using equations in Appendix B.1 (see also in Ref.[15]) result in the following expression for the tune shift of linear synchrotron oscillations

$$\Delta\nu_s \simeq - \frac{N Z e^2 \alpha_p R_0}{4\pi p c \nu_s \beta^2} \simeq -\xi \frac{\epsilon}{\beta^2} \left(\frac{\alpha_p R_0}{\nu_s} \right). \quad (3.14)$$

Here, α_p is the momentum compaction factor of the ring, ν_s is the tune of synchrotron oscillations. For the discussed parameters of ENC (U_{238}^{92} -ion bunch: $\beta = 10$ cm, $\alpha_p \simeq 0.02$, $\nu_s \simeq 0.001$, $\Pi = 1000$ m, $\epsilon = 2 \times 10^{-7}$ cm) Eq.(3.14) yields

$$\left(\frac{\Delta\nu_s}{\nu_s}\right)_i \simeq -0.6\xi_i.$$

For the electron ring the value of ν_s can be taken about 50 times higher so that even taking into account larger emittances, the hour-glass tune shift for synchrotron oscillations in electron ring will be correspondingly smaller.

Finally, we note that in both cases distortions of the RF-potential well due to interactions of bunches with surrounding electrodes may give the contributions comparable to the described here beam-beam tune shifts of the synchrotron oscillations. A comprehensive study of the perturbations of synchrotron oscillations of colliding bunches demands more careful simulations.

3.1.3 Flip-flop phenomenon

Numerous limitations on the luminosity performance can be set up by self-consistent variations of the bunches parameters due to their beam-beam interactions. In general, this is a very complicated problem. However, useful predictions can be done in the cases, when the limiting phenomenons are described in the linear approximation on a particular perturbation. An example of such a problem presents an analysis of the coherent stability of colliding bunches (see, for instance, in Ref[10]). When solving these problems, we usually assume the parameters of unperturbed bunches and of the ring lattices to be given.

Another scope of problems, related to the self-consistent behavior of colliding bunches, was pointed out a while ago in Refs [16] and [17], where the self-consistent emittances of colliding bunches were calculated within the framework of a simplified model. That model assumed Gaussian distributions in the colliding bunches and a linear dependence of the beam-beam kicks on the particles offsets. Though giving a limiting view on the problem, the model predicted qualitatively correctly the previously observed spontaneous breaking of the symmetry of colliding bunches due to their beam-beam interactions (the so-called flip-flop effect). Namely, it was found out that collisions of bunches with equal unperturbed beam sizes, betatron tunes and betatron functions at the interaction point may result in a sudden blow up of the transverse beam size of one bunch and corresponding shrink of the size of its counter-moving partner.

This phenomenon can be described using Eq.(3.3), written in the following form (see, for example, in Ref.[16])

$$\beta_{\pm} = \beta_{0\pm} \frac{\sin \mu_{0\pm}}{\sin \mu_{\pm}}. \quad (3.15)$$

For a ring with two interaction regions we have $\mu = \pi\nu$. The oscillations are stable provided that $|\cos \mu_{\pm}| \leq 1$, or (for two IP)

$$\xi_{\pm} \leq \xi_{th} = \frac{1}{2\pi} \cot\left(\frac{\pi\nu_{0\pm}}{2}\right), \quad 0 \leq \nu_{0\pm} \leq 1. \quad (3.16)$$

Here, the indexes \pm mark the ion and electron bunches, $\beta_{0\pm}$ is the unperturbed β -function at IP.

Defining

$$x = \frac{\beta_0}{\beta_+}, \quad y = \frac{\beta_0}{\beta_-}$$

we write

$$x = \frac{\sin(\mu_+)}{\sin(\mu_{0+})}, \quad y = \frac{\sin(\mu_-)}{\sin(\mu_{0-})} \quad (3.17)$$

and

$$\xi_+ = y \frac{N_- Z e^2}{4\pi(p c)_{+} \epsilon_-} = y \xi_+^{(0)}, \quad \xi_- = x \xi_-^{(0)}.$$

where

$$\xi_+ = \frac{N_- Z e^2 \beta_0}{4\pi(p c)_{+} \sigma_-^2} = \frac{\beta_0}{\beta_-} \frac{N_- Z e^2}{4\pi(p c)_{+} \epsilon_-}. \quad (3.18)$$

Similar parameter

$$\xi_- = \frac{\beta_0}{\beta_+} \frac{N_+ Z e^2}{4\pi(p c)_{-} \epsilon_+}. \quad (3.19)$$

describes the beam-beam kicks for central particles in the counter-moving bunch.

Using Eq.(3.15), we find ($B_{\pm} = 2\pi\xi_{\pm}^{(0)}$)

$$\begin{aligned} x^2 &= 1 - B_+^2 y^2 + 2B_+ y \cot(\mu_{0+}) \\ y^2 &= 1 - B_-^2 x^2 + 2B_- x \cot(\mu_{0-}) \end{aligned} \quad (3.20)$$

that in the case of the strong-strong interactions, the β -functions of the colliding bunches are not independent, but must be found as the roots of Eqs (3.20).

For the case of symmetrical collisions

$$B_+ = B_- = B, \quad \mu_{0+} = \mu_{0-} = \mu_0,$$

we write

$$\begin{aligned}x^2 &= 1 - B^2 y^2 + 2B y \cot(\mu_0) \\y^2 &= 1 - B^2 x^2 + 2B x \cot(\mu_0).\end{aligned}\quad (3.21)$$

The β -functions of bunches present those roots of Eqs (3.21), which satisfy the stability conditions

$$0 \leq x \leq \frac{\cot(\mu_0/2)}{B}, \quad 0 \leq y \leq \frac{\cot(\mu_0/2)}{B}. \quad (3.22)$$

Simple calculations show that Eqs (3.21) may have both symmetrical ($x = y$) and non symmetrical ($x \neq y$) solutions. The roots, corresponding to the symmetrical case ($x = y$) read

$$y = \frac{B \cos(\mu_0) + \sqrt{B^2 + \sin^2(\mu_0)}}{(1 + B^2) \sin(\mu_0)}. \quad (3.23)$$

These solutions exist for all μ_0 (see in Fig.3.6). Asymmetric solutions exist only in

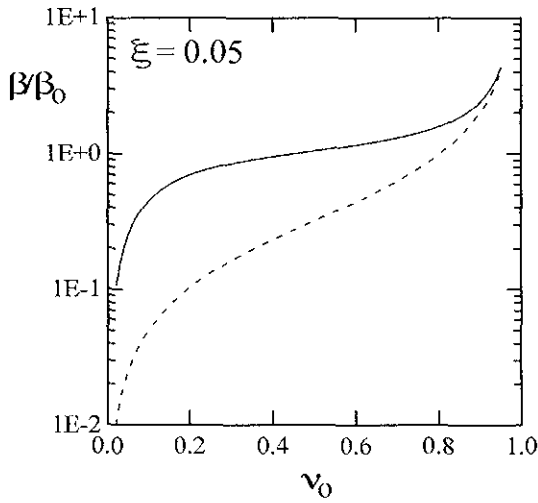


Figure 3.6: Dependence of the self-consistent β -functions on the unperturbed tune. Symmetrical roots. Dashed curve shows the stability limit $\beta/\beta_0 = B \tan(\mu_0/2)$.

the regions, where

$$A = -\frac{2B \cot(\mu_0)}{1 - B^2} > 0. \quad (3.24)$$

These roots read

$$y = \frac{1}{2} \left[A + \sqrt{\frac{A^2(B^2 - 3) + 4}{1 + B^2}} \right], \quad x = \frac{1}{2} \left[A - \sqrt{\frac{A^2(B^2 - 3) + 4}{1 + B^2}} \right]. \quad (3.25)$$

These roots correspond to the flip-flop case, when transverse size of one bunch ($\sqrt{\epsilon\beta}$) becomes essentially larger than that of its counter-moving partner (see in Fig.3.7). Note, that in the region $\cos(\mu_0) > 0$ such solutions appear only in the case,

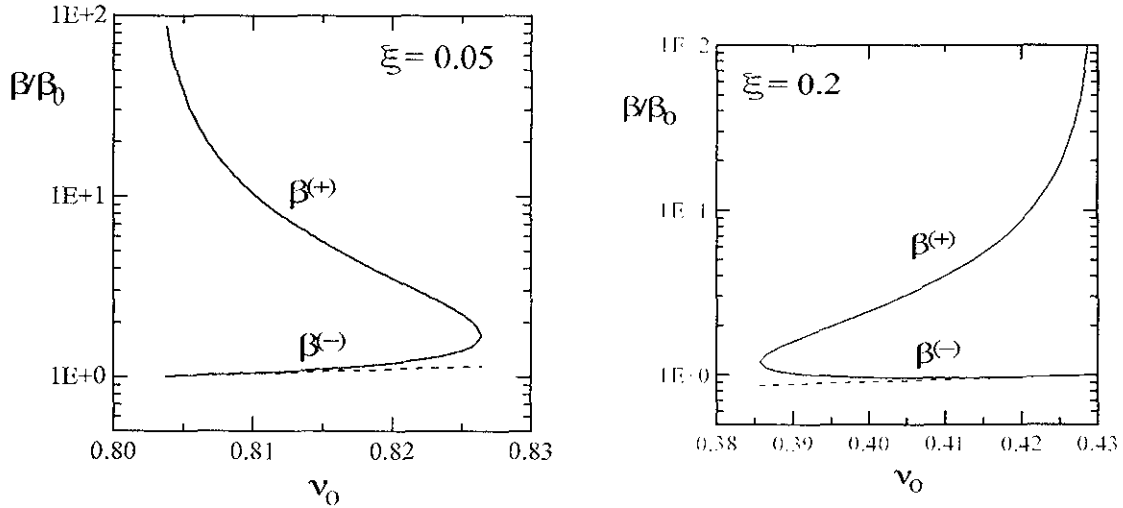


Figure 3.7: Dependences of the β -functions on the unperturbed tune. Flip-flop solutions. Dashed curve shows the stability limit $\beta/\beta_0 = B \tan(\mu_0/2)$.

when the beam-beam parameter is unrealistically large (right picture in Fig.3.7). Note also, that in realistic region ($B < 1$) and in linear approximation the stable flip-flop solutions occupy relatively narrow band in tunes (see in Fig.3.8).

An inspection of the solutions of Eqs(3.20) shows that initial asymmetry in unperturbed tunes ($\nu_{0\pm}$) and β -functions ($\beta_{0\pm}$) does not cure the instability very much. In such a case, the flip-flop effect may take place in the region

$$\frac{\cot(\mu_{0+}/2)}{B} < \frac{1}{\sin \mu_{0-}}, \quad \frac{1}{\sin(\mu_{0+})} > \frac{\cot(\mu_{0-}/2)}{B}.$$

Typical behaviour of the non flip-flop solutions is shown in Fig.3.9.

Although our calculations were performed in the linear approximation in the particle offsets, we may expect (and that is observed in collider operations) similar breaking of the symmetry of colliding bunches, if the non-linear beam-beam kicks are taken into account in a self-consistent way. In such a case, the flip-flop phenomenon can be expected near the lower borders of the stopbands of the non-linear beam-beam resonances. For the case of ENC, such a possibility demands more careful study.

3.2 Nonlinearity of the Beam-Beam Force

Nonlinear dependences of the beam-beam forces on the particle offsets result in numerous limitations on the luminosity performance. First, it produced the nonlinear dependence of the particle tune shifts ($\Delta\nu$) on the amplitudes of the particle oscillations. Since the force is a decaying function of the particle coordinates, for ENC the

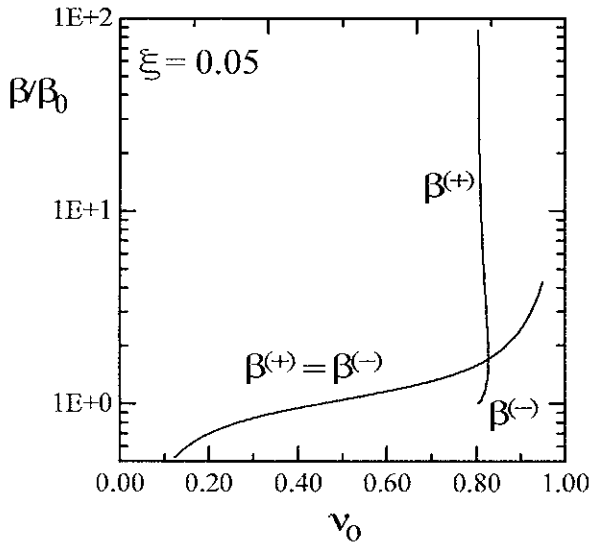


Figure 3.8: Dependences of the self-consistent (symmetrical and flip-flop) β -functions on the unperturbed tune.

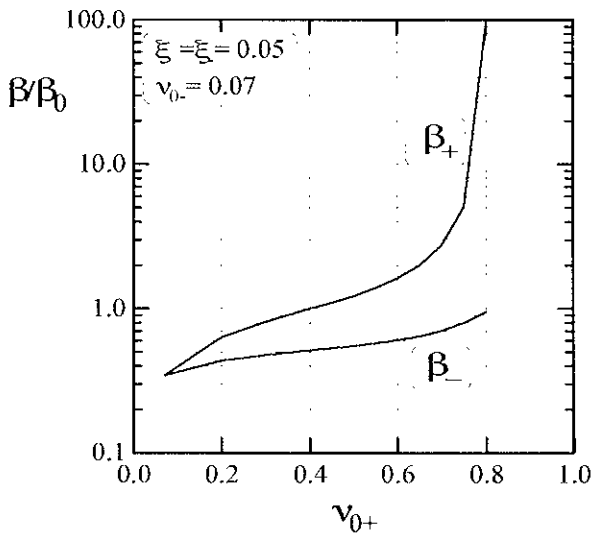


Figure 3.9: An example of the dependence of self-consistent β -functions on unperturbed tune in the ion ring.

tune shifts are spreaded within the range

$$0 \leq \Delta\nu \leq \xi.$$

It means that the bunch forms a surface in the space of the tunes. A projection of this surface on some plane (ν_x, ν_z) , (ν_x, ν_s) , or (ν_z, ν_s) is usually called as a footprint of the bunch. An example of such a footprint is shown in Fig.3.10. The symmetrical

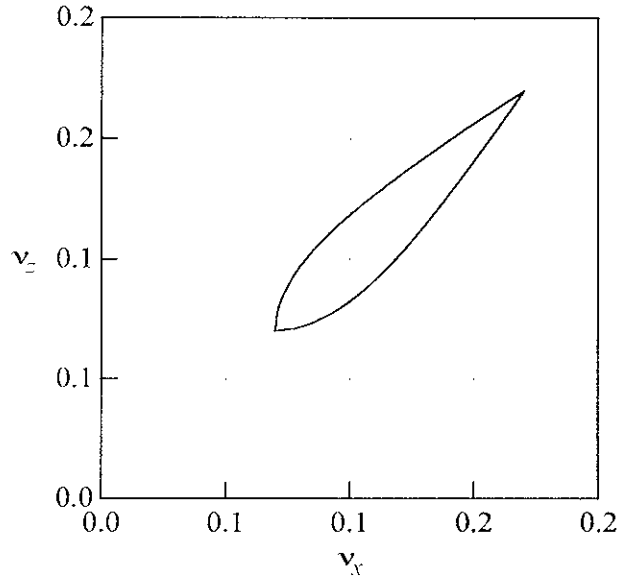


Figure 3.10: An example of the footprint of the sort bunch ($\sigma_s \ll \beta$); round cross sections, $\xi = 0.1$

shape of the footprint is specific for bunches with the round cross section.

Apart from producing the tune shifts, the beam-beam interaction generates numerous nonlinear resonances, when

$$m_x\nu_x + m_z\nu_z + m_s\nu_s = n. \quad (3.26)$$

Since for the counter-charged particles the beam-beam tune shift is positive, one-dimensional beam-beam resonances occur below the resonance tunes ($\nu_\alpha = m_\alpha/n$, where m_α and n are integers, $\alpha = x, z, s$). Due to the dependence of these tune shifts on the amplitudes of oscillations of particles the resonant conditions define some surfaces in the space of amplitudes of particle oscillations so that the particles, which are trapped in the resonance, can travel along those surfaces, increasing the beam size, or decreasing the beam lifetime.

The strengths of these resonances is determined by the harmonics of the Hamiltonian of the interaction of a particle with the field of the counter-moving bunch. For the head-on collisions, the deflecting beam-beam forces are the odd functions of the displacements of a particle from the bunch center. It means that only even harmonics

of the interaction Hamiltonian in phases of the particle oscillations will contribute in the beam-beam perturbation ($m_\alpha = 2k_\alpha$). The bunch separation at the IP breaks up this symmetry exciting new families of the beam-beam resonances. Such a separation can occur, for example, if the bunches execute at IP coherent oscillations.

If β -functions of the electron and ion rings in the interaction region are equal, then, for short colliding bunches ($\sigma_s \ll \beta$) with a round cross section both betatron tune shifts and the strengths of the beam-beam resonances do not depend on β -function at IP. In this case, the perturbation of the betatron oscillations of a particle is described by the potential $\delta_T(s)U(r_+^2/\sigma_+^2)$ (for the counter moving bunch suffixes (+) and (-) change their places). Writing

$$x = \sqrt{\beta_+ J_x} \cos(\phi_x), \quad z = \sqrt{\beta_+ J_z} \cos(\phi_z),$$

and

$$\sigma_-^2 = \beta_- (\epsilon_x + \epsilon_z),$$

we find

$$\frac{r_+^2}{\sigma_-^2} = \frac{\beta_+ J_x \cos^2(\phi_x) + J_z \cos^2(\phi_z)}{\beta_- (\epsilon_x + \epsilon_z)}.$$

Hence, the perturbation does not depend on β provided that $\beta_+ = \beta_- = \beta$.

The beam-beam resonances make the phase space of the particles very non-uniform. For the lower order resonances such a non-symmetry occurs not necessarily in the close vicinity of the resonance. That can be traced inspecting dependences of the phase harmonics of the bunch distribution function in the phase space

$$\Delta N_m = \int_0^\infty dJ \int_0^{2\pi} \frac{d\psi}{2\pi} f(J, \psi) \exp(-im\psi).$$

on the unperturbed tunes (see in Fig.3.11). Visible decreases in amplitudes of the shown harmonics indicate decreasing in the strengths of relevant resonances.

3.2.1 Effect of the beam cooling

A possibility to reach in ENC the luminosity in the range of 10^{33} 1/[cm²s] per nucleon is strongly based on the employment of a strong cooling of the ion bunches. Mainly, such a cooling is necessary to ensure a possibility to reach as high as possible the threshold value of the beam-beam parameter for ion bunches. We remind the reader that in the case, when the bunch intensities are limited by the beam-beam interactions, the luminosity of a collider:

$$L = f_b A \frac{N_i N_e}{2\pi \beta^* [\epsilon_i + \epsilon_e]} \quad (3.27)$$

can be written in the following form

$$L = f_b \left(\frac{A}{Z}\right)^2 \frac{4\pi \xi_i \xi_e \gamma_i \gamma_e}{\beta^* \gamma_c r_p} \cdot \frac{2\epsilon_e \epsilon_i}{\epsilon_i + \epsilon_e}. \quad (3.28)$$

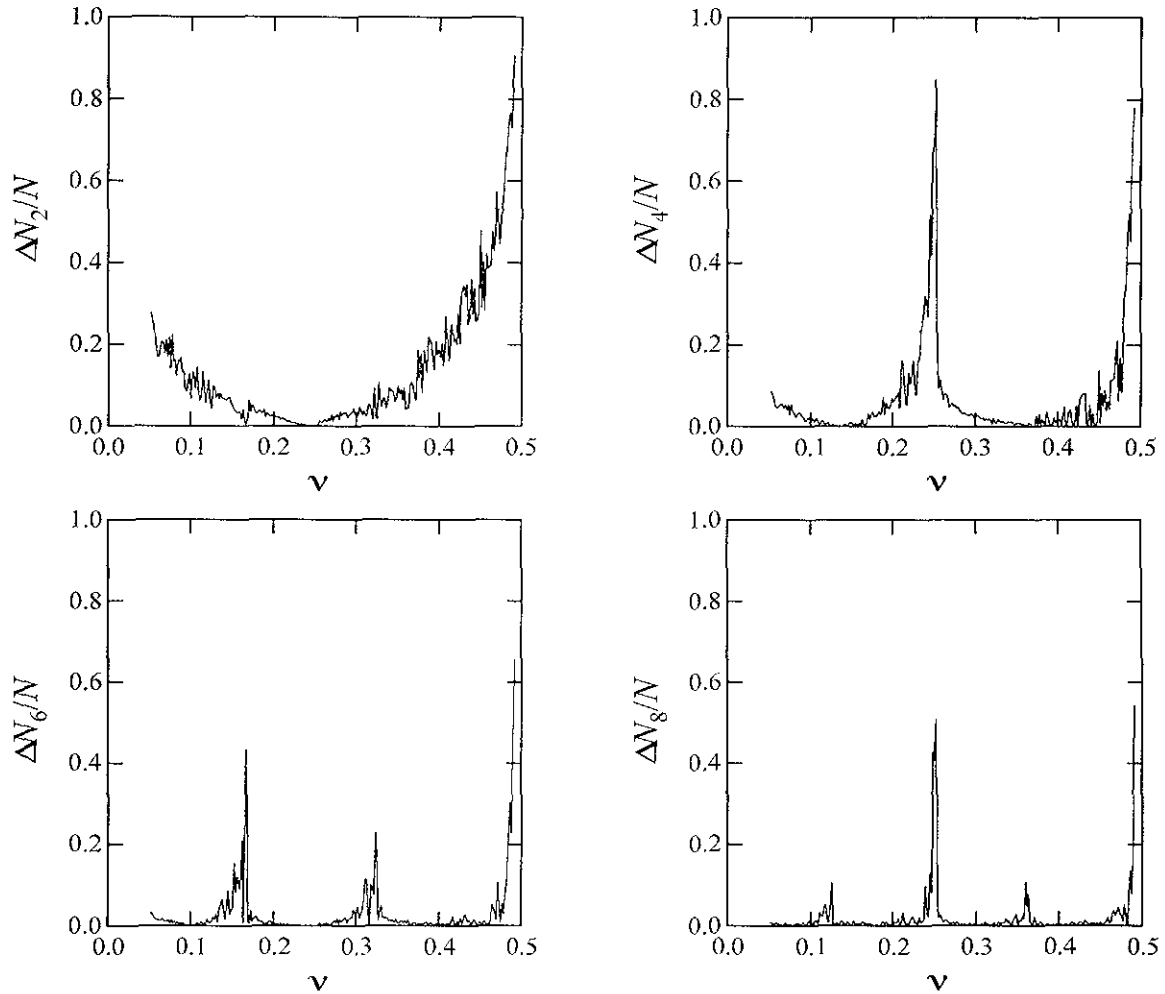


Figure 3.11: Dependence of amplitudes of the 2nd, 4th, 6th and 8th harmonics of the phase density (ΔN_m) on the betatron tune. Short colliding electron-positron bunches with a round cross section, one IP, $\xi = 0.1$. The data was calculated for the number of turns, corresponding to 5 synchrotron radiation damping times.

According to Eq.(3.28), for given bunch emittances, a strong decrease in the threshold value of ξ_i will result in a corresponding decrease in the luminosity of the collider. For example, in conventional hadron colliders, which do not use beam cooling, the typical threshold value of ξ is about 0.001, which is approximately two orders of magnitude less than that, achieved for e^+e^- colliders. In these conditions an essential increase in the luminosity of hadron colliders without the beam cooling can be done only by stacking of huge ion currents.

The beam-beam resonances of higher orders can be suppressed by the beam cooling. That is why the threshold values of ξ for electron-positron colliders essentially exceed those for hadron colliders. An exact evaluation of the necessary cooling rate is a very difficult task. In the case of electron cooling, it also is embarrassed due to nonlinear dependencies of the cooling rates on amplitudes of particle oscillations.

A rough criterion can be estimated comparing the power of the beam cooling (λa^2 , where a is an amplitude of oscillations) and the powers of the beam-beam resonances ($V_m(a)$). In the first approximation of the perturbation theory the amplitudes V_m are exactly equal to the absolute values of the harmonics of the beam-beam Hamiltonian in betatron phases and azimuth (θ), if θ is chosen as an independent variable. For that purpose, we note that for bunches with a round cross section the values V_m can be presented in the following form

$$V_m(a) = \frac{\xi \sigma^2}{k} Q_m(a/\sigma), \quad m = 2k, \quad (3.29)$$

where σ is the rms bunch radius. The cooling will suppress the resonances, if for some amplitudes holds the following condition

$$Q_m(a/\sigma) \leq \frac{\lambda}{\omega_0 \xi} \left(\frac{a}{\sigma} \right)^2 \quad (3.30)$$

An inspection of the Fig.3.12 shows that for the synchrotron radiation cooling this condition holds for resonances above 1/15 for amplitudes $a \leq 5\sigma$. In these calculations we accepted that the power of the electron cooling decays when the particle leaves the bunch core. The cooling decrements for small amplitudes ($a \ll \sigma$; λ_0) were taken the same, or $\lambda_0 = 100\lambda_{SR}$. As is seen, equivalent suppressions of the beam-beam resonances for ions occur, when the electron cooling decrements for small amplitudes 100 times exceeds that due to synchrotron radiation. This number is certainly too big for practical applications. Fortunately, the beam-beam resonances of long bunches can be significantly suppressed for high amplitudes of betatron oscillations and provided that the amplitudes of synchrotron oscillations are not very big (see, for example, in the next subsection).

We would say, however, that effect of the electron cooling on the beam-beam instability and especially on the threshold value of ξ must be more carefully studied in the future.

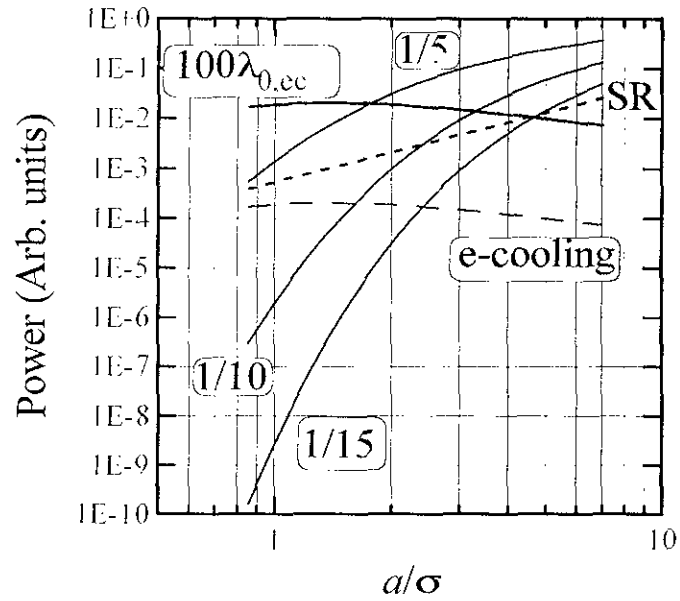


Figure 3.12: To comparison of the powers of the beam cooling and beam-beam resonances $\nu = 1/5$, $\nu = 1/10$ and $\nu = 1/15$. Dashed curve (small dashes) shows the power of the synchrotron radiation cooling (SR-cooling). Lower dashed curve (long dashes) shows the power of electron cooling with same cooling decrement for small amplitudes as the SR-cooling.

3.2.2 Long bunches

For long bunches ($\sigma_s \simeq \beta$) exist long intervals of phases of the betatron oscillations, when a particle crosses the interaction region at some angle ($\theta \sim a/\beta$). That results in two important effects:

- the suppressions of the strengths of at least some beam-beam resonances;
- in the excitations of the synchro-betatron beam-beam resonances.

The consequences of these effects are different for bunches with round and flat cross sections.

For bunches with identical β -functions and round cross sections at the interaction point the dependences of strengths of the beam-beam resonances (V) on amplitudes of betatron oscillations and on the amplitude of synchrotron oscillations as well as on the bunch length can be factored

$$V = \xi V_b(a_x, a_z) Y_{q, m_s}(a_s, \zeta), \quad 2q = |m_x + m_z|. \quad (3.31)$$

Here, a_x , a_z and a_s are amplitudes of the horizontal, vertical and synchrotron oscillations. In this equation the factor $Y_{q, m}$ describes the so-called phase averaging effect [18]. For short bunches ($\sigma_s \rightarrow 0$) of a round cross sections $Y_{q, m_s} = \delta_{m_s, 0}$, while for long colliding bunches $|Y_{q, m_s}| \leq 1$. A more close inspection of typical dependences of these factors on the bunch lengths and on the amplitudes of synchrotron oscillations of particles (see in Fig.3.13) shows that an increase in the length of the interaction region provided that $\sigma_s \simeq \beta$ substantially decreases the strengths of the beam-beam resonances of the core particles ($a_s \leq \sigma_s$) and almost does not affect the strengths for the particle in the bunch tails ($a_s \gg \sigma_s$). For that reason, the strength of the beam-beam instability for long bunches can be suppressed, if the diffusion processes, populating the longitudinal tails of the bunches, are suppressed.

If colliding bunches are flat, then usually the horizontal bunch size (σ_x) essentially exceeds vertical one (σ_z) and $\beta_x \gg \beta_z$. Such a bunch is a long one, if

$$\beta_z \simeq \sigma_s \ll \beta_x.$$

The resonances of horizontal oscillations are almost not affected by the phase averaging. The strengths of vertical betatron and synchro-betatron oscillations are strongly suppressed for small amplitudes of synchrotron oscillations. However, for large amplitudes of synchrotron oscillations ($a_s \gg \sigma_s$) the strengths of these resonances increase. So that the suppression of resonances for flat bunches requires stronger beam cooling.

All these features make as a more preferable designing of ENC to have a round cross section and the rms bunch length approximately equal to β -function at the IP. In such a case, the phase averaging gives "the averaged suppression coefficients" for resonances with $k \geq 8$ in the range $\simeq 0.1$. That makes feasible the high luminosity operations, provided that the cooling times for small amplitudes are in the millisecond region. For longer cooling times, we probably may use the e^+e^- scaling that $\xi_{th} \sim \lambda_0^{1/3}$.

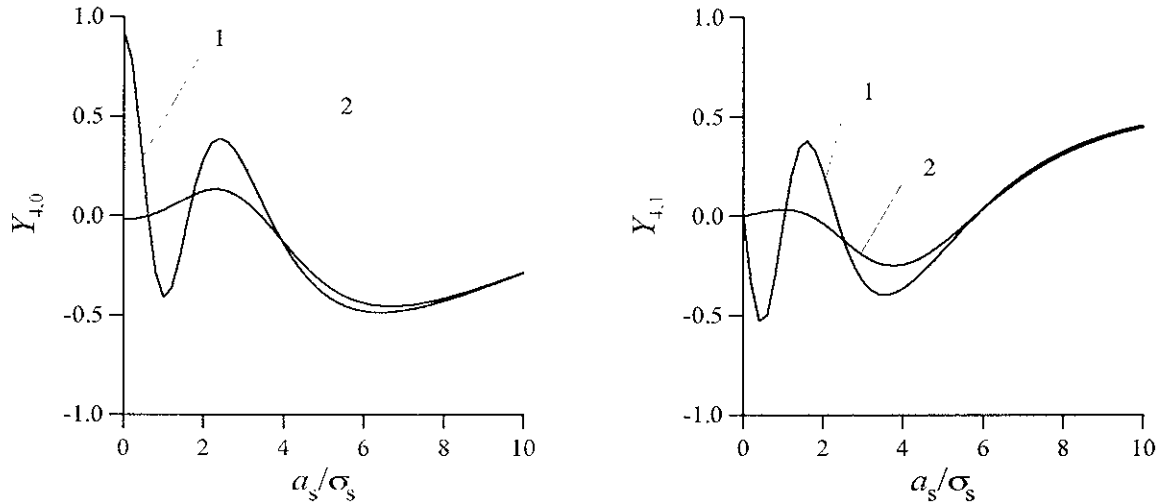


Figure 3.13: Dependence of the strengths of betatron ($\nu_b = 1/4$) and of the first synchrotron resonances ($8\nu_b \pm \nu_s = 2k$) on the amplitude of synchrotron oscillations; 1: $\zeta = 0.1$, 2: $\zeta = 1$.

3.2.3 Coherent beam-beam instability

The beam-beam effects produce a twofold influence on the stability of the coherent oscillations of colliding bunches. First, the dependence of the particle tunes on amplitudes results in the enlargement of the bunch frequency spreads. This increases the Landau damping of coherent oscillations and thus, increases the widths of the stability diagrams for cases, when the bunch interacts with surrounding electrodes. The widths of such stability diagrams correspond to the tune spreads about $0.17 \times \xi$ (see, for example in Ref.[10]).

The beam-beam interaction may produce a resonant instability of coherent oscillations of colliding bunches [19]. The coherent tune shift for this effect is about twice as large as the incoherent tune shift. As far as coherent beam-beam oscillations become unstable due to the mode-coupling instability, for short bunches they are not stabilized by the Landau damping due to the beam-beam tune spread (see, for example, Ref.[20], or Ref.[10]).

Most phenomena for incoherent and coherent beam-beam instabilities are very similar. If $\xi > 0$, the stopbands of one-dimensional coherent beam-beam resonances are found below the resonant tunes. For long bunches ($\sigma_s \simeq \beta$) the strengths of the coherent beam-beam resonances are suppressed for small amplitudes of coherent oscillations [21]. Dependences of relevant suppression factors on the bunch length are very similar to those, shown in Fig.3.13. Since the incoherent beam-beam tune shifts are not affected by the phase averaging, the phase averaging of coherent beam-beam resonances may open the possibility to suppress the instability of higher modes due to Landau damping.

The growth of the unstable coherent beam-beam oscillations is limited by a nonlinear dependence of the coherent tune shifts on the amplitudes of coherent oscillations (this nonlinearity also affects the spectra of these oscillations). However, the values of the stationary amplitudes are usually well outside the bunch radii. If, for example, for some particular coherent resonance ($\nu = n/m$, where n and m are integers) holds the condition $\xi \gg |\nu - n/m|$, then the amplitudes of the stationary coherent oscillations can be evaluated using

$$a_{st}^2 \propto \frac{\xi}{|\Delta|} \epsilon, \quad \Delta = \nu - \frac{n}{m} \leq 0.$$

An equivalent increase in the bunch effective cross section limits the luminosity similar to the instability of incoherent oscillations.

$$L \propto \frac{N^2}{\sigma^2 + a_{st}^2} \propto \frac{N^2 |\Delta|}{\xi \epsilon}.$$

3.3 Ion Space Charge and the Beam-Beam Instability

If the ion energies are not very high, due to deep cooling of ion bunches the perturbations of the ion motion due to their Coulomb repulsion may have as strong effect as the beam-beam perturbations due to the interaction with the counter-moving bunch. In general, both effects produce the (nonlinear) tune shifts of the unperturbed oscillations and the resonant perturbations of the ion phase space, creating there numerous buckets (or, the so-called islands). If ions populate these buckets (due to a scattering, or due to some other mechanism), the phase space density of the ion bunch dilutes resulting in a decrease in the luminosity. The nonlinearity of the force perturbing the ion motion depends on the bunch radii (the radius of the electron bunch in the case of the beam-beam interaction, and the radius of the ion bunch in the case of the space charge instability).

In conventional cases, when either beam-beam instability, or the space charge instability dominates, an increase in the bunch radii can substantially decrease the strengths of the leading nonlinear resonances. In the case of the presently discussed ENC ([8]), both kinds of perturbations may have comparable strengths especially for highly charged ions. Since the beam-beam interaction increases and the space charge repulsion decreases the betatron tunes of ions, depending on the bunch densities the common effect of these perturbation can produce both positive and negative tune shifts of the ion betatron oscillations. For that reason, some features of the beam-beam interactions and of the space charge instability in ENC may differ from that in conventional machines.

In this section we discuss the limitations on the luminosity performance in ENC due to common effects of the beam-beam and of the space charge interactions of ions. For the sake of simplicity, we assume that the bunches have round cross sections.

3.3.1 Ion tune shifts

Since we expect that the bunches blow up due to resonant perturbations, important issues are associated with the values and with the amplitude dependences of the tune shifts of the particle oscillations. In this section we calculate the tune shifts of betatron oscillations for synchronous particles. The unperturbed oscillations are described by the following formulae

$$\begin{aligned}
 x &= \sqrt{J_x \beta_x(s)} \cos(\psi_x + \chi_x(s)), & p_x &= p \frac{dx}{ds}, \\
 z &= \sqrt{J_z \beta_z(s)} \cos(\psi_z + \chi_z(s)), & p_z &= p \frac{dz}{ds}, \\
 \frac{d\psi_{x,z}}{ds} &= \frac{\nu_{x,z}}{R_0}, & \frac{d}{ds}[\chi_{x,z} + \psi_{x,z}] &= \frac{1}{\beta_{x,z}}.
 \end{aligned} \tag{3.32}$$

Here, we neglect the effects due to the lattice dispersion, $p = AM\gamma c$ is the momentum of the synchronous particle, $pJ_{x,z}/2, \psi_{x,z}$ are the action-phase variables of betatron oscillations and $2\pi R_0$ is the perimeter of the closed orbit. The charge distributions in the bunches, producing the perturbing fields are taken as Gaussian ones

$$\rho_e(\mathbf{r}, t) = -\frac{N_e e \lambda_e(s+ct)}{2\pi\sigma_e^2} \exp\left(-\frac{\mathbf{r}_\perp^2}{2\sigma_e^2}\right), \tag{3.33}$$

$$\rho_i(\mathbf{r}, t) = \frac{N_i Z e \lambda_i(s-ct)}{2\pi\sigma_i^2} \exp\left(-\frac{\mathbf{r}_\perp^2}{2\sigma_i^2}\right). \tag{3.34}$$

Here, suffixes i and e mark the ion and electron bunches, $\lambda_{i,e}(s)$ are relevant linear densities, $\sigma_{i,e}$ are rms bunch radii, Ze is the charge of an ion. The total force perturbing the ion motion is the sum of the contributions from the electron beam space charge ($\mathbf{F}^{(e)}$), acting at the interaction region, and from the ion bunch space charge ($\mathbf{F}^{(i)}$), acting along the closed orbit

$$\mathbf{F}^{(t)} = \mathbf{F}^{(e)} + \mathbf{F}^{(i)}. \tag{3.35}$$

For the charge distributions, given in Eqs (3.33) and (3.34), the calculations of $F^{(e,i)}$ result in the following expressions for the tune shift of, for example, horizontal betatron oscillations of the synchronous ion (two interaction points; see, for example in Ref.[10], or in Appendix B.2)

$$\Delta\nu_x(J_x, J_z) = 2\xi Q_x \left(\frac{J_x}{\epsilon_c}, \frac{J_z}{\epsilon_c} \right) - \Delta\nu_L Q_x \left(\frac{J_x}{\epsilon_i}, \frac{J_z}{\epsilon_i} \right). \tag{3.36}$$

Here,

$$\xi = \frac{N_e Z e^2}{4\pi p_i c \epsilon_e}. \tag{3.37}$$

is the beam-beam parameter due to space charge of the electron bunch,

$$\Delta\nu_L = \frac{N_i(Ze)^2\lambda_i(0)\Pi}{4\pi p_i c \gamma_i^2 \epsilon} \quad (3.38)$$

is the Laslett tune shift of the ion bunch,

$$Q_x(x, z) = \int_0^1 dt \exp\left(-t \frac{x+z}{4}\right) I_0\left(\frac{tz}{4}\right) \left[I_0\left(\frac{tx}{4}\right) - I_1\left(\frac{tx}{4}\right) \right], \quad (3.39)$$

and $I_m(x)$ is the Bessel function of the imaginary argument. The tune shift for vertical oscillations is obtained from Eqs (3.36) and (3.39) substituting $z \longleftrightarrow x$. Eqs (3.36) and (3.39) enable various calculations concerning the tune distributions in ion bunches. Simple expressions for the tune shifts are obtained for one-dimensional cases, when

$$Q_x(x, z=0) = \frac{1 - \exp(-x/4)I_0(x/4)}{x/4} \quad (3.40)$$

and

$$Q_x(x=0, z) = \exp(-z/4)[I_0(z/4) + I_1(z/4)]. \quad (3.41)$$

As it was expected, the common effect of the beam-beam interaction and of the space charge of the ion bunch results in a reduction of the tune shifts of betatron oscillations of ions. If $\Delta\nu_{bb} = 2\xi \neq \Delta\nu_L$, and the electron and ion radii are not equal, the dependencies of, for example, $\Delta\nu_x$ on the amplitudes of the horizontal ($\sqrt{J_x/\epsilon_i}$) and vertical ($\sqrt{J_z/\epsilon_i}$) oscillations are non-monotonous functions of their arguments (see in Fig.3.14). If the amplitudes of oscillations increase, the tune shift $\Delta\nu_x$ initially also increase and tends to zero after passing the maximum. According to Fig.3.14 and if the difference $2\xi - \Delta\nu_L$ is not very small, the position of this maximum occurs outside the ion bunch and slightly outside the electron bunch. For that reason and in the region, where $2\xi \geq \Delta\nu_L$, the resonant conditions

$$\Delta\nu_x(J_x, J_z) = \Delta_{m,n} = \frac{n}{m} - \nu_x, \quad (3.42)$$

where n and m are integers, are held for two sets of amplitudes. One set occurs close to bunch cores, while the other – well outside. In the case of collective resonances, that may cause a resonant coupling of the core and tail particles of the bunch.

If $2\xi < \Delta\nu_L$, the resonant condition in Eq.(3.42) yields unique roots, when $\Delta_{m,n} < 0$ and the doubled roots when $\Delta_{m,n} \geq 0$. The position of the stopbands of relevant beam-beam (or the space charge) resonances is correspondingly shifted from the found for the conventional case ($\Delta\nu_L = 0$, or $\xi = 0$).

The plotting of the footprints for the described cases (see in Fig.3.15) indicates an increase of the resonance spot area, when the difference in the bunch radii increases.

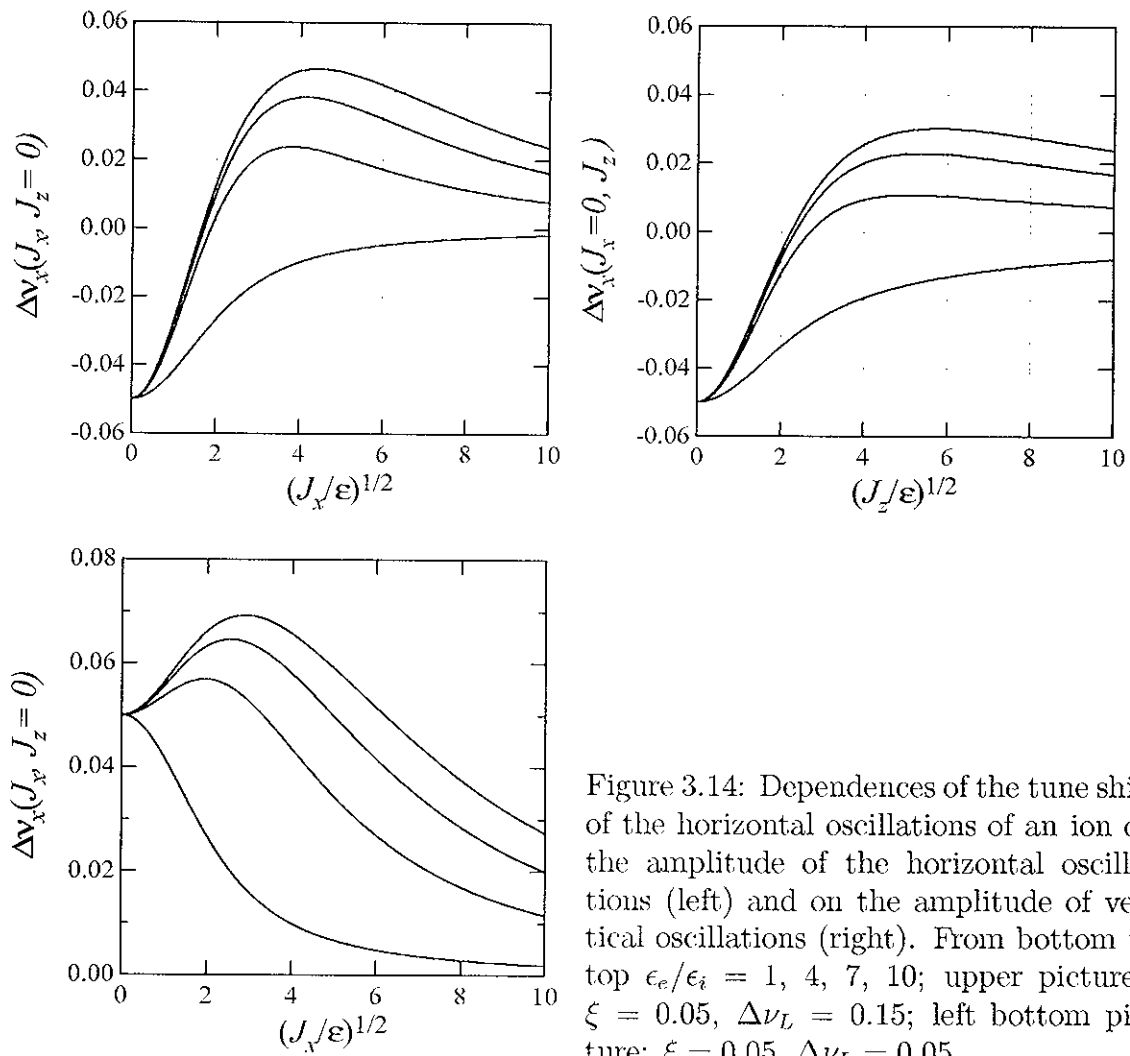


Figure 3.14: Dependences of the tune shift of the horizontal oscillations of an ion on the amplitude of the horizontal oscillations (left) and on the amplitude of vertical oscillations (right). From bottom to top $\epsilon_e/\epsilon_i = 1, 4, 7, 10$; upper pictures: $\xi = 0.05, \Delta\nu_L = 0.15$; left bottom picture: $\xi = 0.05, \Delta\nu_L = 0.05$.

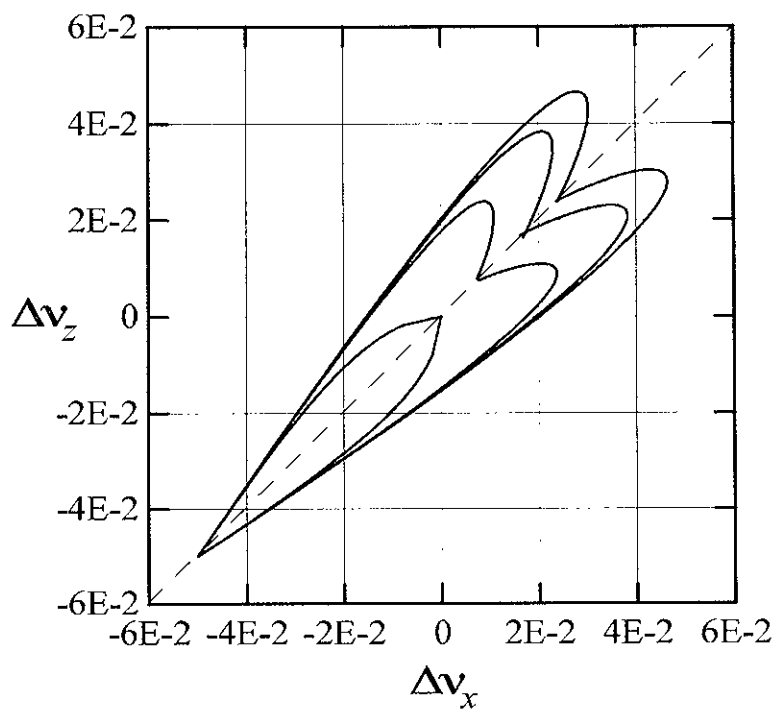


Figure 3.15: The footprints of ion bunches. From inside to outside $\epsilon_c/\epsilon_i = 1, 4, 7, 10$; $\xi = 0.05$, $\Delta\nu_L = 0.15$.

3.3.2 Simulations

Described properties of the tune shifts of the ion betatron oscillations may affect both the space charge and the beam-beam instabilities of the ion bunch. A comprehensive simulation of the beam-beam and of the ion space charge instabilities is a very hard task. However, it seems that, in general, the beam-beam interaction producing more sharp perturbations may result in more dangerous instabilities. In this section we use a simplified model to examine how the common action of the beam-beam and of the space charge fields affect, for example, the beam-beam instabilities of ion bunches. For these simulations we take the weak-strong beam model so that the motion of a test ion was traced. Twice a turn the test ion felt the beam-beam kick according to

$$\delta p_x = -p \frac{4\pi\xi}{\beta} \frac{x}{1 + (x/d)^2}. \quad (3.43)$$

Here, d is the electron bunch radius. Between the kicks the particle was transported using (see, for example, in Ref.[22])

$$\begin{pmatrix} x' \\ p'_x/p \end{pmatrix} = \sqrt{\Lambda} \begin{bmatrix} c(J/\epsilon) & \beta s(J/\epsilon) \\ -s(J/\epsilon)/\beta & c(J/\epsilon) \end{bmatrix} \begin{pmatrix} x \\ p_x/p \end{pmatrix} + \sqrt{1-\Lambda} \begin{pmatrix} \sqrt{\epsilon}\beta r_x \\ \sqrt{\epsilon/\beta} r_p \end{pmatrix}, \quad (3.44)$$

where the factor $\Lambda = \exp(-\lambda T_0/2)$ describes the damping of oscillations between the kicks, $r_{x,p}(k)$ are the independent Gaussian random number generators, providing the correct rms bunch sizes without beam-beam interaction ($\langle r_{x,p}^2 \rangle = 1$, $\langle r_{x,p} \rangle = 0$, $\langle r_x r_p \rangle = 0$),

$$c(J/\epsilon) = \cos(\pi[\nu_0 - \Delta\nu(J/\epsilon)]), \quad s(J/\epsilon) = \sin(\pi[\nu_0 - \Delta\nu(J/\epsilon)]),$$

ν_0 is the unperturbed tune and

$$\Delta\nu(x) = \frac{\Delta\nu_L}{1 + x + \sqrt{1+x}}, \quad x = \frac{J}{\epsilon}$$

is the space charge tune shift. The particle displacements x were measured in units of $\sqrt{\beta\epsilon}$, while the particle momentum – in units of $\sqrt{\epsilon/\beta}$. Initial conditions for these calculations were chosen at the origin ($x_{in} = 0$, $p_{x,in} = 0$). To simplify the calculations the cooling decrements were assumed to be independent of the amplitudes of oscillations.

The calculations with this simplified model show that in the case, when $\Delta\nu_L \geq 2\xi$ the safe region of the tunes of betatron oscillations is moved from the regions $\nu_0 > n$ (n is an integer) to the regions, where $\nu_0 < n$ (see in Figs 3.16 and 3.17). Note, that in such a case, the positions of the centers of the resonant buckets will depend both on the electron bunch and ion bunch currents. For the chosen ratio of $\Delta\nu_L$ and ξ a difference in the electron and ion bunch radii results in an additional blow up of the ion bunch, when $\nu_0 > n$ (see in Figs 3.16, 3.17 and 3.18). Figures 3.19 show that in the region $\nu_0 > n$ an instability occurs due to resonances of high order.

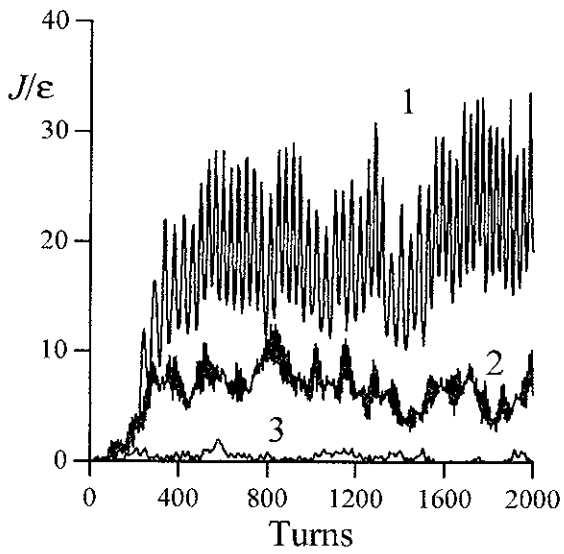


Figure 3.16: Dependences of the test ion action variable on the time (number of turns). $\xi = 0.05$, $\Delta\nu_L = 0.15$, $\nu_0 = 0.15$, $\Lambda = 0.001$; 1: $\epsilon_e/\epsilon_i = 10$, 2: $\epsilon_e/\epsilon_i = 1$, 3: $\epsilon_e/\epsilon_i = 1$ and $\Delta\nu_L = 0$.

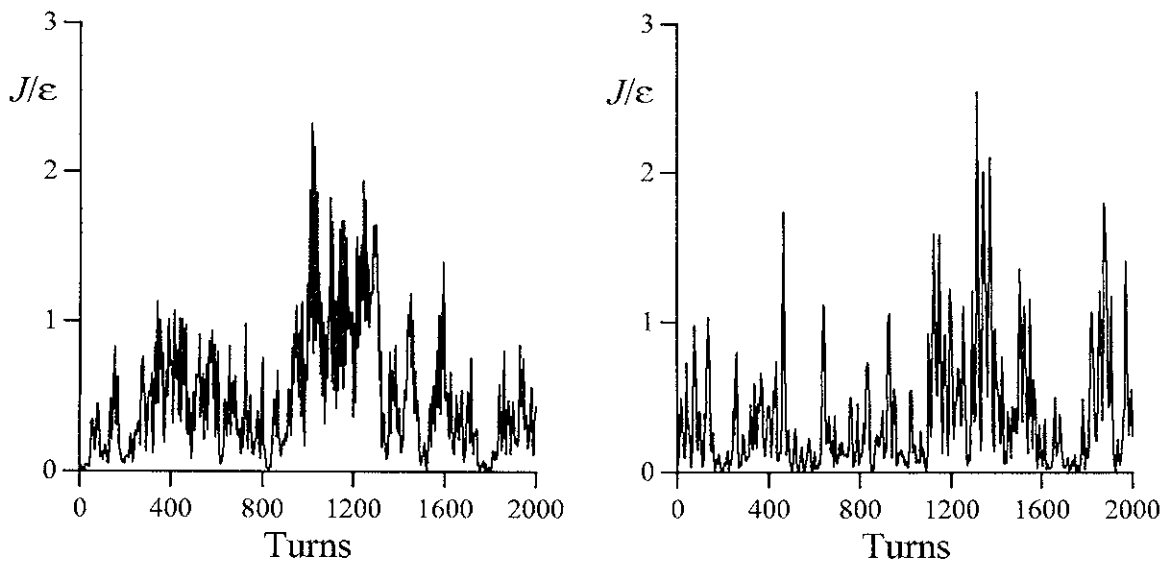


Figure 3.17: Dependences of the test ion action variable on the time (number of turns). $\xi = 0.05$, $\Delta\nu_L = 0.15$, $\nu_0 = 0.85$, $\Lambda = 0.001$; left: $\epsilon_e/\epsilon_i = 1$, right: $\epsilon_e/\epsilon_i = 10$.

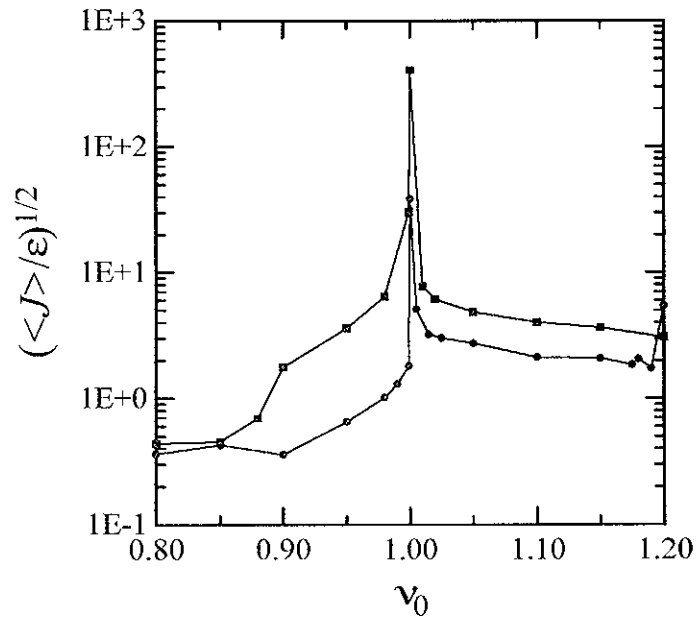


Figure 3.18: Dependences of the ion "bunch radius" ($\sigma = \sigma_0 \sqrt{\sum_{k=0}^N [x_k^2 + (\beta p_k/p)^2]}/N$, N is the number of turns, σ_0 is the unperturbed bunch radius) on the unperturbed tune (ν_0). Upper curve: $\epsilon_e/\epsilon_i = 10$, lower curve: $\epsilon_e/\epsilon_i = 1$; $\xi = 0.05$, $\Delta\nu_L = 0.15$, $\Lambda = 0.001$.

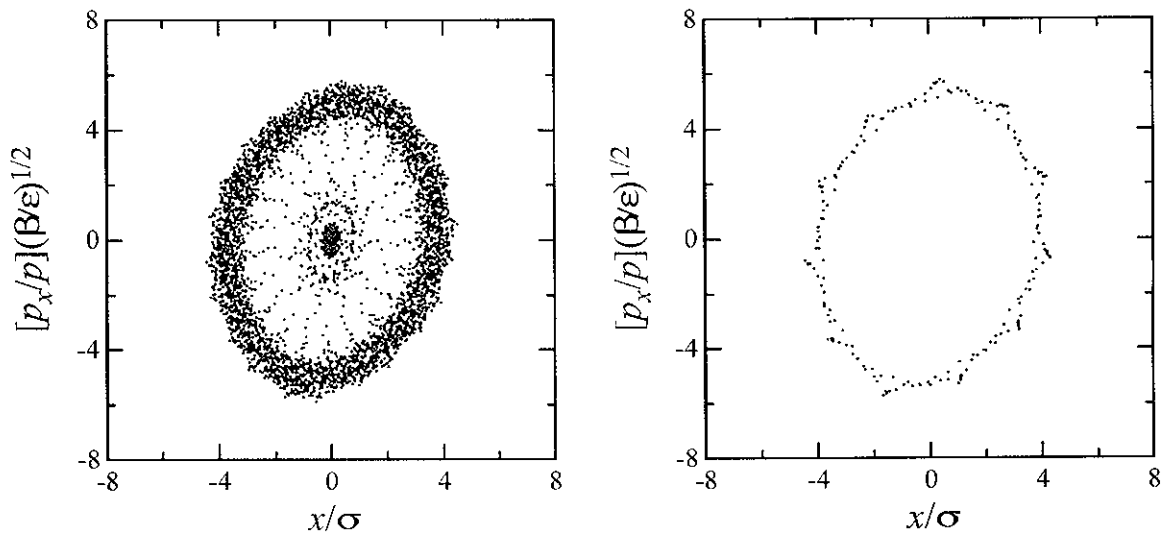


Figure 3.19: The phase portraits of an ion trajectory after the first 2000 turns in ENC (left) and its last 200 turns (right). $\xi = 0.05$, $\Delta\nu_L = 0.15$, $\nu_0 = 0.15$, $\Lambda = 0.001$; $\epsilon_e/\epsilon_i = 10$.

3.3.3 Working point for ion ring

The limitations due to both the beam-beam and the space charge instability are mainly caused by non-linear dependences of relevant deflecting forces on the particle offsets from the equilibrium position in the bunch. Non-linear behaviors of these forces result in the dependences of relevant tune shifts on the particle amplitudes of oscillations and in an excitations of various non-linear resonances, when the particle oscillations tunes approach resonant values.

In the discussed cases, the tune shifts due to beam-beam interaction, or due to ion space charge, are the decreasing (in absolute value) functions of the amplitudes. For instance, for the beam-beam interaction $\Delta\nu_b(a)$ has the following asymptotes (n_{IP} is the number of interaction points)

$$\Delta\nu_b \sim n_{IP}\xi \begin{cases} 1, & a \ll \sigma, \\ \sigma^2/a^2, & a \gg \sigma. \end{cases} \quad (3.45)$$

The resonant condition, for example,

$$\nu_b(a) = \nu_b + \Delta\nu_b(a_s) = n/m, \quad (3.46)$$

and Eq.(3.45) show that the positions of the resonances in the tune space relative to the lines $\nu_b = n/m$ depend on the sign of the tune shift of small oscillations. If, for example, $\Delta\nu_b(0)$ is positive, Eq.(3.46) holds only in the case, when $\nu_b < n/m$. So that the resonance stopband occurs below the resonance $\nu_b = n/m$. On the contrary, if $\Delta\nu_b(0)$ is negative, the stopbands of resonances n/m occur above the resonant value $\nu_b = n/m$. Such simple reasons become crucial for evaluation of the threshold value of the Laslett tune shift of ion bunches in the case of ENC.

For relativistic electron bunches the tune shifts of betatron oscillations are determined by the beam-beam interaction only. Since these tune shifts are positive (see in Fig.3.20), the stopbands for resonant perturbations of the electron bunches are placed above the resonances $\nu_b = n/m$. It means that the oscillations of electrons will be more stable, if the working point of the ring in ν -space is tuned as close as possible to $\nu_{x,z} \simeq 1$. In such a case, ν_b can be removed from strong lower order resonances like $\nu_b = 1, 1/2, 1/3, 1/4$, while the perturbations due to resonances of the higher order can be suppressed by the synchrotron radiation damping. A choice of the working point in the corner close to some integer is a common for electron-positron collider.

The values of the tune shifts for betatron oscillations of ions due to beam-beam interaction and due to space charge repulsion compensate each other (see in Fig.3.20):

$$\Delta\nu_i = n_{IP}\xi_i - \Delta\nu_L. \quad (3.47)$$

Depending on the ratio of the tune shift due to beam-beam interaction to $\Delta\nu_L$, the quantities $\Delta\nu_i$ can take both positive and negative values so that the Laslett tune shift compensates the beam-beam tune shift. Generally, due to different spectra of the beam-beam and ion beam space charge perturbations such a compensation does not takes place for the strengths of relevant non-linear resonances.

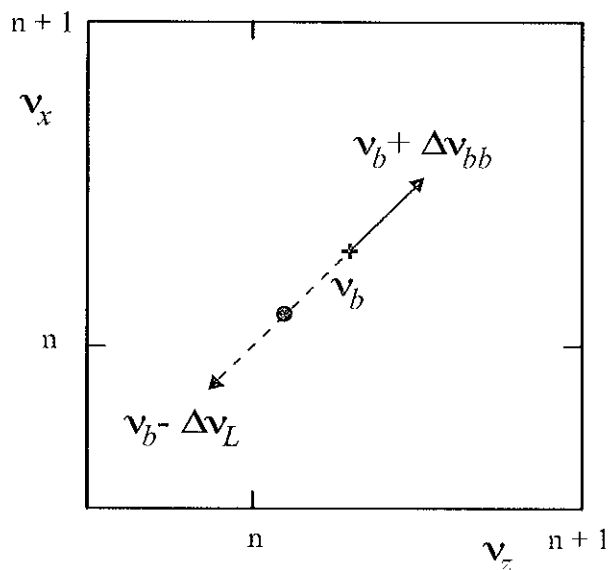


Figure 3.20: Schematic variation of the working point of betatron oscillations due to beam-beam interaction (solid line) and due to the space charge field (dashed line). Full cross shows the position of the unperturbed working point; full dot its position due to common effect of the beam-beam and space charge perturbations.

In the case, when $n_{IP}\xi > \Delta\nu_L$, the total tune shift $\Delta\nu_i > 0$. As was already discussed, in this case the most preferable is to place the working point slightly above integers. It occurs, if the value of $\Delta\nu_L$ is equal to some fraction of the beam-beam tune shift ($n_{IP}\xi_i$):

$$\Delta\nu_{L,ih} = Cn_{IP}\xi_i, \quad C < 1. \quad (3.48)$$

We also note, that since the particles oscillations are stabilized due the dependence of $\Delta\nu_i$ on a , the blow-up of the ion bunch emittances due to these perturbations will be smaller, if C does not approach 1.

Let us now consider the stability conditions of ion oscillations for the case, when

$$\Delta\nu_L > n_{IP}\xi. \quad (3.49)$$

Since $\Delta\nu_i$ is now negative, the stopbands of resonances of incoherent oscillations of ions are placed above the resonant values $\nu_b = n/m$. From this point of view, the most preferable become the working points, where the tunes ν_x and ν_z are placed in the corner below integers. Again, the higher order resonances must be suppressed by the ion beam cooling.

On the other hand, a correct choice of the working point must ensure the stability of both incoherent and coherent oscillations of ion bunches. As far as the space charge forces depend only on relative positions of ions in the bunch, they do not affect at least the dipole coherent oscillation of ion bunches. For that reason, the equations describing dipole beam-beam oscillations in ENC will not contain the Laslett tune shift of ions. Hence, the stability conditions of these coherent modes will have the same form like that for electron-positron bunches. Namely, independent of the value of the Laslett tune shift the stopband for the dipole coherent beam-beam oscillations always occurs below the integers. It means that in the case, when Eq.(3.49) holds, the stability conditions for dipole coherent beam-beam oscillations contradict to the stability conditions for incoherent ion oscillations. Since the instability of the dipole beam-beam mode is very strong, practically, such a contradiction means that the ion ring of ENC can never reach the region of the parameters, where the Laslett tune shift exceeds the beam-beam tune shift.

3.4 Parasitic Crossings

After a head-on collision at the main interaction point the colliding bunches must be separated in order to avoid the parasitic interactions at the neighbor interaction points. If the bunch-to-bunch distance is D , then two first parasitic interaction point (PIP) appear, when $\Delta s = \pm D/2$. Usually, the β -functions at these points are not small, so that the bunches must not overlap there. Provided that bunches are not shielded electromagnetically, their interaction at such parasitic crossings will contribute to the beam-beam perturbation and may result in additional limitations on the collider luminosity performance (see, for example, in Refs [2], or [1]). In the

case of ENC, the bunch-to-bunch distance is $D = 5$ m, so that two first parasitic crossing points occur at $D/2 = 2.5$ m, which is inside of the discussed detector.

Although the beam-beam interaction at parasitic crossings is a manifold phenomenon, its strength (and effect on the bunch dynamics) can be described qualitatively by the values of corresponding tune shifts. If, for example, the bunches are separated at PIP in the horizontal plane by the distance d , then simple calculations result in the following expressions for the linear tune shifts per one PIP (see, for example, in Ref.[2])

$$\begin{aligned}\Delta\nu_x &= -\frac{NZe^2\beta_x}{2\pi pcd^2}, \\ \Delta\nu_z &= \frac{NZe^2\beta_z}{2\pi pcd^2},\end{aligned}\tag{3.50}$$

where, $\beta_{x,z}$ are the values of β -functions at PIP. Usually, the beam separation distance d is measured in units of σ (σ_x for the separation in the horizontal plane). Defining $\mathcal{M} = d/\sigma_x$ and using $\sigma_x^2 = \beta_x\epsilon_x$, we arrive to

$$\begin{aligned}\Delta\nu_x &= -\frac{NZe^2}{2\pi p\epsilon_x\mathcal{M}^2} \simeq -\frac{\xi_x}{\mathcal{M}^2}, \\ \Delta\nu_z &\simeq \frac{\beta_z}{\beta_x} \frac{\xi_x}{\mathcal{M}^2}.\end{aligned}\tag{3.51}$$

These equations show that in the case, when $\mathcal{M} \gg 1$ (which is typical), the tune shifts due to beam-beam interaction at PIP are small as compared to the tune shift of the horizontal oscillations from the main interaction point, except the case, when

$$\frac{\beta_z}{\beta_x} \sim \mathcal{M}^2.$$

The last possibility may occur for very flat colliding bunches, which is more close to the region of parameters of the future B-factories.

To conclude this section we make two notes. First, as can be seen from Fig.3.2, if $\mathcal{M} \gg 1$, the strongest nonlinearity of the beam-beam kick at PIP occurs for the amplitudes of oscillations $\sqrt{J\beta} \simeq d$, so that in some sense d defines the dynamic aperture of the interaction region. The second, if the bunches collide at PIP at some angle so that their average velocities are not antiparallel, the beam-beam interaction at PIP will be accompanied by excitations of the synchro-betatron resonances. Such resonances also occur due to a non-zero dispersion function at PIP for head-on collisions at the main IP. The effect of the parasitic crossings on the luminosity performance must be studied more carefully during design of the particular scheme of the ENC.

3.5 Conclusion

A common effect of the beam-beam interaction and of the space charge repulsions of ions results in the compensation of the tune shifts of betatron oscillations (a compensation of the resonant harmonics of the perturbing forces, generally, does not take place). If the bunch radii of the electron and ion bunches are equal, the beam-beam tune shift, or the Laslett tune shift must prevail in order to ensure the stability of the bunches. In such a case, the luminosity will be determined by the smallest threshold value of ξ , or $\Delta\nu_L$. The dependences of the tune shifts of betatron oscillations on the amplitudes are the monotonous (strictly positive, or negative) functions so that the resonant conditions in Eq.(3.42) result in unique positions of the resonant buckets. The sizes of these resonances in amplitudes of oscillations will generally exceed that, calculated for the conventional cases.

For colliding bunches of different sizes such a compensation results in a non-monotonous dependences of the tune shifts of betatron oscillations on the amplitudes. Correspondingly, the resonant condition in Eq.(3.42) may have the doubled roots. Due to a resonant coupling of the oscillations in such buckets these double-root solutions may embarrass the collective stability of the colliding electron and ion bunches. Since the widths of the buckets in the space of J is inversely proportional to $(\partial\Delta\nu/\partial J)_s$, where J_s gives the center of the bucket (a root of Eq.(3.42)), in the vicinity of the maximum value of the tune shift the widths of the buckets dramatically blow up. If the Laslett tune shift of the ion bunch prevail, the ion bunch footprint enlarges, while the space charge resonant stopbands are extended in both sides from $\nu_{x,z} = n$.

Described simplified simulations indicate that in the unstable region of the unperturbed ion tunes the incoherent beam-beam instability blow-ups the ion bunch stronger, when the emittance of the electron bunch is higher than that of the ion bunch. On the other hand, we may expect stronger suppression of the high order resonances due to the phase averaging effect (see, for example, in Ref.[10]). For that reason, a reliable choice of the electron and ion bunch emittances ratio for the case of ENC demands more careful simulations.

The described contradiction between the stability conditions of incoherent oscillations of ions and dipole coherent oscillations of the colliding ion and electron bunches eliminates a possibility for the Laslett tune shift of ion bunches to exceed the beam-beam tune shift. Moreover, to prevent abnormal blow-up of ion bunches the beam-beam tune shifts must significantly exceed the ion bunch Laslett tune shifts. Say, if the collider has two interaction points so that $\Delta\nu_{bb} = 2\xi$, it seems that a safe value for $\Delta\nu_L$ could be $\Delta\nu_L \leq \xi$. In this case, in an analogy with electron-positron colliders the working points for electron and ion rings can be places in a corner slightly above integers.

The requirement to reach in ENC the highest possible luminosity demands to maintain ξ_i as high as possible. In that case, the reachable values of the Laslett tune shifts also will be high. Since the position of the working point in the colliding beams

operational mode contradicts to the stability conditions of a single ion beam, it is very likely that there will be necessary to develop a special scenario for the initial filling up of the ion ring. An obvious possibility of the subsequent filling up of the electron and then of the ion rings will very likely suffer due to permanent beam-beam interaction of electron and injected ion bunches.

The mentioned problems are avoided in the positron-ion collider, when the beam-beam interaction decreases the tunes of colliding particles. In this case, the threshold value of the Laslett tune shift is not limited anymore by its comparison with the beam-beam tune shift. Since both tune shifts are negative, the working points of both positron and ion ring can be chosen in a corner below integers (like for proton-proton, or electron-electron collider). Both rings can be filled up more or less arbitrarily, deflecting bunches at the interaction points. Moreover, an employment of positrons as the ion partners eliminates the limitations due to accumulation by electron beam of the ions, produced by the ionization of the atoms of the residual gas by electron bunches.

Apart from direct collisions, the tails of ion bunches can be populated due to ion drifting along the beam-beam resonances. This effect occurs when the dimension of the resonance surface is higher than the dimension of the resonance. If, for example, $\Delta\nu_z(a_x, a_z) = n/m_z - \nu_z$, the cooling of radial oscillations will result in the vertical blow-up provided that $da_z/da_x < 0$. For this reason, a decrease in the dimension of the oscillations tune shifts is very desirable. For the case of the space charge predominant ion bunches, such a requirement demands careful simulations.

Chapter 4

Cooling of Ion Bunches

According to the design concepts described in Chapter 2, the high luminosity performance of ENC is possible only in the case, when ion bunches are strongly cooled. The cooling rates must be sufficient to suppress the intrabeam scattering in ion bunches and the beam-beam resonances at least of higher orders. Both these requirements together with the requirement of the collider luminosity 10^{33} 1/[cm²s] demand the ion beam cooling times in the region of several milliseconds.

For bare ions two cooling techniques have been successfully tested up to now. These are the stochastic and electron coolings. Both possibilities were examined for ENC operations.

4.1 Stochastic Cooling of High Energy Ion Beams

In this section we follow to ENC note [23].

4.1.1 Theoretical limit for the cooling time

The stochastic cooling systems cool the beam using special wideband feedback loops, detecting and correcting the deviations of particles from the reference orbit. The cooling occurs due to self-action of a particle via the feedback system. For a given particle all others produce in the cooling system the noise signals, exciting additional deviations of the particle motion from the reference orbit. The common effect of the cooling signal and of these noise signals results in a decrease of the stochastic cooling time with an increase in the number of particles in the beam, if it exceeds some threshold value. This threshold number of particles in the beam occurs in the region, where the damping decrements of coherent fluctuations of the beam become comparable to its frequency spreads. For that reason, the threshold is higher for higher bandwidth of the feedback circuit and is smaller for higher Z^2/A .

The theoretical limit for the cooling time τ that can be achieved by stochastic

cooling is given by

$$\tau_{min} = \frac{N_{eff}}{W}$$

with

N_{eff} equivalent number of ions to be cooled in coasting beam operation, and
 W bandwidth of the stochastic cooling system.

For bunched beam operation with

k_B bunches in the ring
 N_B ions per bunch, and
 B as the bunching factor,

one has

$$N_{eff} = k_B \cdot N_B \cdot 1/B$$

4.1.2 Numerical example for ENC operation

The comparison of the stochastic cooling rate $1/\tau_{min}$ with the effect of intrabeam scattering $1/\tau_{IBS}$ shows that stochastic cooling should not work for ENC operation. For the case of U^{92+} this simple estimate should be also correct, however, the required RF-voltage amplitudes have to be scaled with respect to the ion charge Z and the ion mass A .

	p	U^{92+}
N_B	$3 \cdot 10^{10}$	$3 \cdot 10^7$
k_B	200	200
$B(0.1m/5m)$	0.02	0.02
N_{eff}	$3 \cdot 10^{14}$	$3 \cdot 10^{11}$
$W(\text{GHz})$	10	10
$\tau_{min}(\text{s})$	$3 \cdot 10^4$	30
$\tau_{IBS}(\text{s})$	$2 \cdot 10^3$	0.003

4.2 Electron Cooling for the Electron-Ion Collider

The electron cooling method uses the energy exchange between hot ions and cold electrons due to their Coulomb collisions. For that purpose, the electron cooling device is placed in a special cooling straight section of the ion ring. Starting from experiments at NAP-M [12], [24] [27] this cooling method was successfully tested on many low and medium energy ion storage rings (see, for example in [28]).

Although various schemes were discussed as suitable for different energy ranges (see, for example, in Ref.[29]), traditionally, DC-electron beams are used in the operating electron cooling devices. In such a scheme the electron beam after accelerating

till the required energy is transported to the cooling region and then, to the collector, where it is decelerated till as low as possible energy. Since in the cooling region the ion and electron beam average velocities must coincide, the cooling electrons must be accelerated till the energy $\gamma_i mc^2$. For ENC that covers the region 7.5 – 16 MeV. The power consumption in such a scheme is determined by the lowest possible difference in the particle energies at the cathode and at the collector. This parameter is the most important for the majority of the electron cooling devices. In the high energy region the required power can limit the performance of the cooling device. Generally, the cooling times are sensitive to the angular divergences in electron beam so that it must be focused. Typically, such a focusing is performed using the longitudinal magnetic field accompanying electrons from the cathode till collector. For high energy cooling devices and long cooling sections the quadrupole focusing is also discussed. It seems, however, that with the quadrupole focusing it is difficult to provide as short betatron wavelength of the cooling electrons as it is enabled by the solenoidal focusing.

Radial distributions of the cooling electron velocities may result in the redistribution of decrements between transverse and longitudinal ion motions. Generally, that is accompanied by the shrinking of the cross section area of electron beam providing the ion beam cooling. In order to exclude such undesirable redistribution, the dispersion function of the ring must be vanished along the cooling region.

The operations with high intensity cooled beams have indicated phenomena, which can limit the cooling rates of the intense beam, or even result in its heating (see, for example, in Refs [30] and [31]). These phenomena are not yet well understood. Nevertheless, such possibilities should be taken into account designing the cooling device for ENC demanding additional studies.

4.2.1 Cooling force

The measurements at NAP-M have figured out a strong effect of the magnetic field of the cooling device on the efficiency of the cooling. Without magnetic field the cooling force in the beam rest frame system reads

$$\mathbf{F} = -\frac{4\pi n Z^2 e^4 L_{cool}}{m} \int \frac{\mathbf{v} - \mathbf{v}_e}{|\mathbf{v} - \mathbf{v}_e|^3} f(\mathbf{v}_e) d^3 v_e. \quad (4.1)$$

Here, L_{cool} is the so-called Coulomb logarithm

$$L_{cool} = \ln \left(\frac{\rho_{max}}{\rho_{min}} \right), \quad \rho_{max} = \min\{v/\omega_p, \tau v, a\}, \quad \rho_{min} = e^2/mv^2,$$

τ is the time of flight of a particle through the cooling electron beam, v is the ion velocity, v_e is the electron velocity, ω_p is the electron beam plasma frequency.

In general case, an effect the longitudinal magnetic field on electron-ion collisions separates three different regions of impact parameters [32].

- Small impact parameters.

$$\frac{v_A}{\omega_L} > \rho > \rho_{\min} = \frac{e^2}{mv_e^2}, \quad (4.2)$$

where $\mathbf{v}_A = \mathbf{v} - \mathbf{v}_{\parallel e}$. In this region, the magnetic field does not affect collisions. For the "flat" distribution functions in electron velocities

$$v_{\perp e} \gg v_{\parallel e} = \sqrt{2e^2 n^{1/3}/m}, \quad v_{\perp e} = \sqrt{T_{\perp}/m},$$

where T_{\perp} is the transverse temperature of the electron beam, the contribution in the cooling force from this region reads

$$\mathbf{F}_{\perp} = -\frac{4\pi n Z^2 e^4}{m} \frac{\mathbf{v}_{\perp}}{v_{\perp e}^3} \ln\left(\frac{v_a/\omega_L}{e^2/(mv^2)}\right), \quad v \ll v_e; \quad (4.3)$$

- Intermediate impact parameters. In this region, an electron during collision time makes several Larmour rotations near the ion

$$\frac{v_{\perp e}}{\omega_L} = \rho_L > \rho > \frac{v_A}{\omega_L} \quad (4.4)$$

That results in the following contribution in the cooling force

$$\mathbf{F} = -\frac{4\pi n Z^2 e^4}{m} \frac{\mathbf{v}}{v^2 v_{\perp e}} \ln(v_{\perp e}/v); \quad (4.5)$$

- Large impact parameters.

$$\rho_{\max} > \rho > \rho_L \quad (4.6)$$

In this region, an ion collides with an electron Larmour circle as a whole. The contribution of this region in the cooling force in adiabatic approximation can be estimated using

$$\mathbf{F}_{\perp} = -\frac{2\pi n Z^2 e^4}{m} \frac{\mathbf{v}_{\perp}(v_{\perp}^2 - 2v_{\parallel})}{v^5} \ln(\rho_{\max}/\rho_L), \quad v > v_{\parallel e} \quad (4.7)$$

All these expressions are calculated in the logarithmic approximation ($L_{cool} \gg 1$) and assuming pair collisions of particles. In the dense ion beam ($n_i \simeq n$), the last assumption can hold only for impact parameters obeying the following condition

$$\rho \ll \rho_{i,max} = (n_i)^{-1/3}$$

In the region $\rho \geq \rho_{i,max}$, an electron simultaneously collides with several ions and gets energy from all of them. Resulting reaction force will contain both the contribution from the cooling force of the particular ion and the forces, describing the intrabeam influence of the cooled ions on each others. Recently [33], using a simplified model

it was shown that such an influence of the cooled particles may decrease the cooling rate, or even result in the beam heating, when either ion bunch intensity increase, or the bunch momentum spread decrease. For that reason, the ion bunch density must not strongly exceed the density of the electron beam.

The cooling force reaches its maximum near $v = v_{\parallel e}$

$$F_{max} = 2Ze^2n^{2/3}. \quad (4.8)$$

At the NAP-M facility, when the magnetic field in the cooling section was about 0.1 T, the dependences of the longitudinal cooling force and of the cooling decrements fit well an assumption of a partially magnetized electron beam [34]. In that case, the cooling force grew proportionally to $1/v_{\perp e}$. The minimum transverse cooling time in these measurements was less than 50 ms. For the case of ENC, the goal for the design of the cooling device is the ensure a predominance of the adiabatic region in the cooling of ion bunches.

4.2.2 Experimental background

In order to prove the ideas of the fast cooling a single-pass installation was constructed [35]. It included an electrostatic accelerator of H^- ions (energy 830 keV), a solenoid with a very homogenous magnetic field ($\Delta B/B = 10^{-5}$) in the range 0.1 - 0.4 T, an electrostatic ion energy spectrometer. In order to study the dependence of the cooling force on the sign of the ion charge the H^- ions could be stripped using the special magnesium target, which was placed at the entrance in the solenoid. The electron beam was formed in the electron gun, which was placed in the magnetic field of the solenoid. Then, it was transported along the solenoid magnetic field to an electron collector. The interaction of ions with the electron beam resulted in variations of ion energies and transverse velocities, which were detected by the electrostatic spectrometer. The measured data showed that (Fig.4.1) the cooling force for negative ions (H^-) was several times higher than that for positive ions (H^+). With an increase in the electron current the cooling force grew up and attained its maximum value at a current of 5 mA (for $B = 0.3$ T; see in Fig.4.2). These measurements also indicate a significant increase in the maximum cooling force with an increase in the magnetic field of the cooling device (see in Fig.4.3).

The observed limitation on the cooling force occurred due to an increase in the longitudinal electron beam temperature. The last can increase during transporting the electron beam to the cooling section due to intrabeam scattering of electrons. In a strong magnetic field only fast collisions contribute in such a blow-up of electron temperature. The suppressions of the intrabeam scattering in electron beam by the magnetic field of the cooling device (see in Fig.4.4) can be described using the following empirical equation:

$$\frac{dT_s}{ds} = \frac{\pi e^3 j L_c}{W} \sqrt{\frac{m}{T_{\perp}}} \exp\left(-\frac{2.8e^2}{\rho_{\perp}(e^2 n_e^{1/3} + T_s)}\right), \quad (4.9)$$

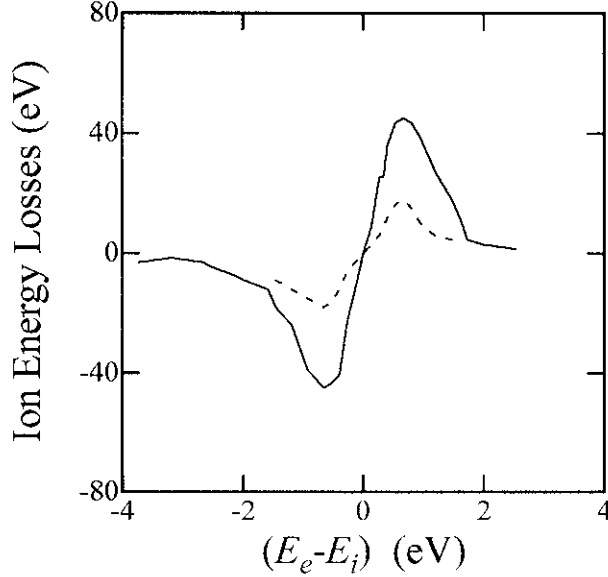


Figure 4.1: The cooling force (ion energy losses after passing of 2.4 m cooling section) versus the electron energy for H^+ and H^- . $B = 0.4$ T, $I_e = 3$ mA.

where $\rho_{\perp} = \sqrt{2T_{\perp}mc^2/(eB)}$ corresponds to the average Larmour radius of the electron beam. Initial temperature of the electron beam for such calculations was taken in the form

$$T_s = T_c^2/(2W) + 2e^2n^{1/3}.$$

Fig.4.5 shows the results of measurements of the cooling force like Fig.4.1 but in the beam rest frame system, reported in [35, 36] and in [28] (ESR). A comparison of these data shows that the cooling force, measured in [28] is about 20 times less than the value, which could be expected for the case, when the longitudinal magnetic field is high. All these data were fit using the following simple expression

$$\mathbf{F} = - \frac{4\pi n e^4 L_{cool}}{m} \frac{\mathbf{v}}{(v_e^2 + v^2)^{3/2}}, \quad (4.10)$$

The values v_e and L_{cool} were used as the fitting parameters. The found optimal value $L_{cool}=2$ presents a reasonable value for the Coulomb logarithm of the fast electron cooling.

The ion beam in ENC will have small emittances and small transverse momenta in the cooling region. Typical values of the transverse momenta ($\Delta p/p = 3 \times 10^{-6}$) correspond to $v_i = 10^6$ cm/s, which is very close to the maximum of the cooling force (see in Fig.4.5). It means that an increase in the magnetic field in the cooling section can increase the cooling rates.

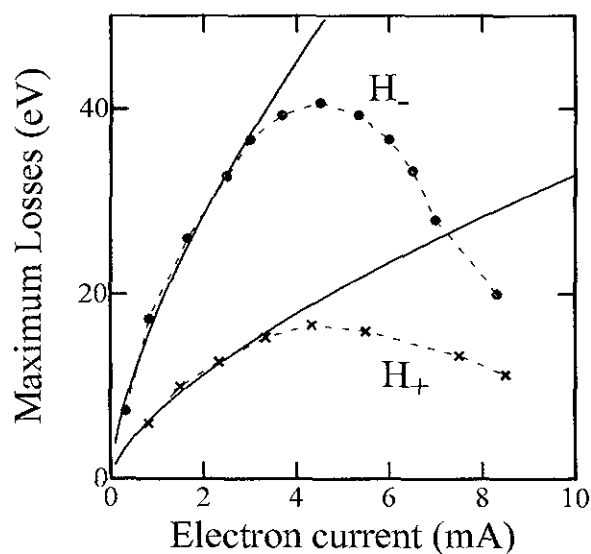


Figure 4.2: The maximum cooling force losses versus the electron current (energy losses after the cooling length of 2.4m) for H^+ and H^- ($B = 0.3$ T). The solid line refers to the results obtained using the expression $F_{max} = ke^2n_e^{2/3}$, $k=1.82$ for H^- and $k=0.72$ for H^+ .

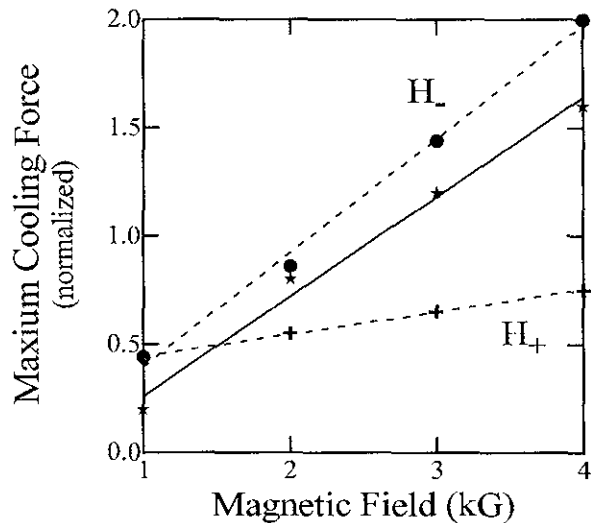


Figure 4.3: The maximum cooling force (in units of $e^2n^{1/3}$; dashed lines) and the optimum electron beam currents (solid line) versus the solenoid magnetic field.

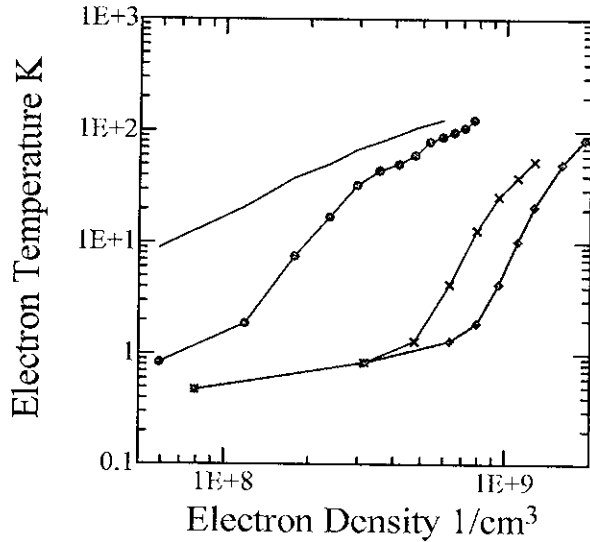


Figure 4.4: Dependence of the longitudinal temperature of electron beam after passing the cooling section on its current. Longitudinal temperature (T_s) was calculated from the energy spread using $\Delta E = \sqrt{2WT_s}$. The data for $B = 0$ were calculated using the equation $dT_s/ds = \pi e^3 j L_{cool} \sqrt{m/T_{\perp}}/W$, where j is the electron current density, W is the electron kinetic energy and s is the distance along the cooling section.

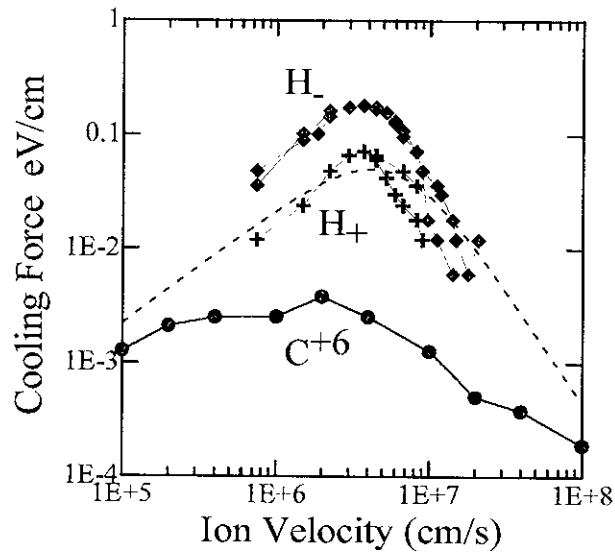


Figure 4.5: The cooling force versus the velocity for H^- (full rombs) and for H^+ (full crosses; $B = 0.4$ T, $I_e = 3$ mA). The dashed line presents the fitting cooling force for $L_{cool} = 2$ and $\Delta v_e = 1.4 \times 10^6$ cm/s. Full dots correspond to the ESR data (F/Z^2 for C^{+6} ; electron beam density $n = 4.6 \times 10^8$ 1/cm³).

4.3 Effect of the Magnetic Field on Cooling

4.3.1 Drift of the cooling electrons due to ion space charge

The electric and magnetic fields of the ion bunch, when it pass the cooling region, produce the drifting of cooling electrons and, thus, increase the relative velocities of these electrons and ions. Since the drift velocity depends on the distance of an electron from the center of the ion bunch, the spread of the drift velocities is equivalent to an increase in the temperature of electron Larmour circles. In the case of the magnetized electron cooling, dependences of the cooling rates on such temperature can be very sharp, if it exceeds the thermal velocity spread in the ion bunch.

The value of the drift velocity

$$\mathbf{v}_d = \frac{c [\mathbf{F} \times \mathbf{H}]}{e H^2} \quad (4.11)$$

is determined by the force

$$\mathbf{F} = \frac{2NZe^2}{\sqrt{2\pi}\sigma_s\gamma^2} \frac{1 - \exp(-r^2/2\sigma^2)}{r^2} \mathbf{r}. \quad (4.12)$$

Here, N is the number of ions in a bunch, Ze is their charge, σ_s is the bunch length, σ is the rms bunch radius and \mathbf{H} is the magnetic field of the cooling device. In order

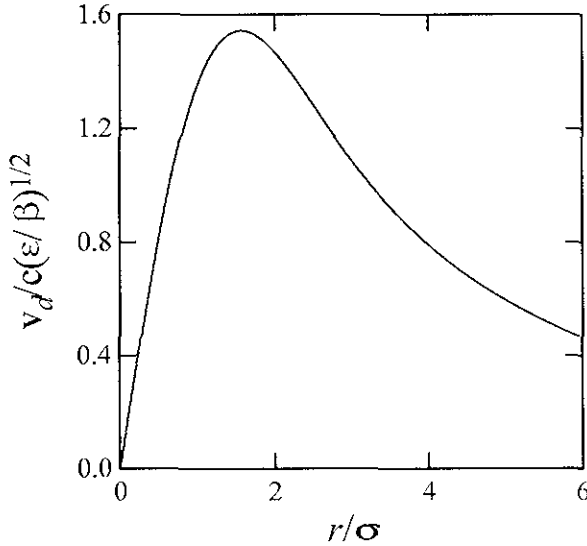


Figure 4.6: Dependence of the drift velocity (Q) due to the space charge of the U_{2238}^{90} bunch on the distance in electron beam. $N = 3.6 \times 10^7$, $\gamma = 12$, $\epsilon = 2.4 \times 10^{-7}$ cm, $\sigma_s = 10$ cm, $H = 1000$ G.

to evaluate relevant limitation, we plot the ratio

$$Q = \frac{v_d}{c\sqrt{\epsilon/\beta_{cool}}}$$

versus the radial distance inside the ion beam (r/σ). As is seen from Fig.4.6, in the displayed example the spread of the drift velocities exceeds the velocity spread in ion bunch by the factor about 1.5.

For the discussed parameters of the future ENC [8] the compensating effect of the space charge of the cooling electron beam is negligible small. As is seen from Eqs (4.11) and (4.12) this effect limits the ratio of the linear density in the ion bunch to the magnetic field in the cooling device. So that, if the bunch becomes shorter, the maintenance of the given cooling time requires relevant increase in the magnetic field of the cooling device.

4.3.2 Effect of the magnetic field on the cooling force

An enhancement of the cooling efficiency with an increase in the magnetic field of the cooling device occurs due to two reasons. First, it reduces of the Larmour radii of electrons increasing the width of the region, where adiabatic collisions dominate. Second, strong magnetic field suppresses the blow-up of the longitudinal temperature of electrons due to their intrabeam scattering. The cooling force comprises conventionally three parts: "fast" interactions with very low impact parameters, where the influence of the magnetic field is negligible; multiple interactions with impact parameters near the radius of the Larmour rotation; and "slow" interactions at distances essentially larger than the Larmour radius. The contributions of these components and the decrement at a small and a large densities of the beam are shown in Figs.4.7. As is seen, the field exceeding 0.5 T provides the cooling times in the millisecond region.

The maximum cooling decrements are very sensitive to the magnetic field at the cooling section. In order to estimate the influence of the magnetic field on the damping of final amplitude betatron oscillation damping there was made a calculation of this damping at angles $\Delta p/p = 10^{-4}, 10^{-5}, 10^{-6}$. As is seen from Fig.4.3.2, the damping at angles $\Delta p/p = 10^{-4}$ does not improve with the growth of the magnetic field, but for smaller amplitudes the damping can be essentially improved with an increase in the magnetic field.

4.4 Cooling Rates

Let us first calculate the cooling rate of, for example, vertical betatron emittance (ϵ_z) assuming that the cooling force is determined by the following simplified expression (all values are calculated in the beam rest frame system)

$$F_z = -\frac{4\pi n_e Z^2 e^4 L}{m} \frac{v_z}{(v_0^2 + v^2)^{3/2}}. \quad (4.13)$$

Such an expression for the cooling force simulates the case, when the cooling electrons are not magnetized.

We take that betatron oscillations in cooling section are described using (and similar equations for x -oscillations)

$$z = \sqrt{J_z \beta_z} c \cos \psi_z, \quad p_z = p \frac{dz}{ds} \quad (4.14)$$

so that $I_z = pJ_z/2$ is relevant action variable, while

$$J_z = \frac{\tilde{z}^2}{\beta_z} + \beta_z \left(\theta_z - \frac{\beta'_z}{2\beta_z} \tilde{z} \right)^2, \quad \theta_z = \frac{p_z}{p}. \quad (4.15)$$

If the particles are distributed in the bunch according to a Gaussian function so that the bunch distribution function reads (Δp is the deviation of the ion momentum from the synchronous value p)

$$f = \frac{e^{-\Sigma}}{(2\pi)^3 \epsilon_x \epsilon_z \sigma_s \delta}, \quad \Sigma = \frac{J_z}{2\epsilon_z} + \frac{J_x}{2\epsilon_x} + \frac{[s - ct]^2}{2\sigma_s^2} + \frac{[\Delta p/p]^2}{2\delta^2}, \quad (4.16)$$

then

$$\epsilon_z = \int d\Gamma (I_z/p) f, \quad d\Gamma = d^3\theta dx dz ds, \quad \theta_{\parallel} = \frac{\Delta p}{p},$$

while

$$\frac{d\epsilon_z}{dt} = \frac{1}{p} \int d\Gamma \frac{dI_z}{dt} f = \frac{1}{p} \int d\Gamma \frac{\partial I_z}{\partial p_z} F_z f = \frac{1}{p} \int d\Gamma \frac{\partial z}{\partial \psi_z} F_z f.$$

Now, using

$$\frac{\partial z}{\partial \psi_z} = -\sqrt{J_z \beta_z} \sin \psi_z = \beta_z \left(\theta_z - \frac{\beta'_z}{2\beta_z} \tilde{z} \right),$$

we write

$$\frac{d\epsilon_z}{dt} = \frac{1}{p} \int d\Gamma \beta_z \left(\theta_z - \frac{\beta'_z}{2\beta_z} \tilde{z} \right) F_z f. \quad (4.17)$$

To select the systematic variation of ϵ_z this expression must be averaged over the closed orbit perimeter. As we mentioned, below we simplify calculations neglecting the variations of β -functions along the cooling section ($\beta' = 0$). For more simplicity, we also assume equal vertical and horizontal β -functions in the cooling section ($\beta_z = \beta_x = \beta$) and equal vertical and horizontal bunch emittances ($\epsilon_z = \epsilon_x = \epsilon$).

Using that in the beam rest frame system $n_e \rightarrow n_e/\gamma$, $\mathbf{v}_\perp \rightarrow \gamma c(\mathbf{p}_\perp/p)$, $v_\parallel \rightarrow c\theta_\parallel$, we write

$$\dot{\epsilon}_z = -\frac{K\beta}{(2\pi)^3 \epsilon^2 \sigma_s \delta} \int d\Gamma \frac{\exp(-\Sigma)\theta_z^2}{(a^2 + \theta_\perp^2 + \theta_\parallel^2/\gamma^2)^{3/2}}. \quad (4.18)$$

Here, $a = v_0/(\gamma c)$ and

$$K = \frac{Z^2 4\pi n_e e^4 L l}{A \gamma^5 m M c^3 \Pi}.$$

The integration over coordinates (x, z, s) yields $(2\pi)^{3/2} \beta \epsilon \sigma_s$, so that

$$\dot{\epsilon}_z = -\frac{K\beta^2\gamma}{(2\pi)^{3/2} \epsilon \delta} \int \frac{d^3\theta \theta_z^2}{(a^2 + \theta^2)^{3/2}} \exp\left(-\frac{\beta\theta_\perp^2}{2\epsilon} - \frac{\gamma^2}{2\delta^2}\theta_\parallel^2\right). \quad (4.19)$$

Using the substitution

$$\frac{1}{w^{3/2}} = \frac{2}{\sqrt{\pi}} \int_0^\infty ds \sqrt{s} \exp(-sw),$$

and calculating Gaussian integrals, we find

$$\frac{\dot{\epsilon}_z}{\epsilon_z} = \frac{K}{\sqrt{2\pi}} \int_0^\infty \frac{du \sqrt{u} \exp(-a^2 u/2)}{(1 + \epsilon u/\beta)^2 \sqrt{1 + \delta^2 u/\gamma^2}}. \quad (4.20)$$

Simple expressions for the cooling rates ($\Lambda = -\dot{\epsilon}_z/\epsilon_z$) can be obtained in regions, where $a^2 \gg (\epsilon/\beta)$, (δ/γ) and hence

$$\Lambda = \frac{K}{\sqrt{2\pi}} \frac{\sqrt{\pi}}{2} \frac{2^{3/2}}{a^3} = \frac{Z^2 4\pi n_e e^4 L l}{A \gamma^2 m M v_0^3 \Pi}, \quad (4.21)$$

and in the region, where $a^2 \ll (\epsilon/\beta)$, (δ/γ) so that

$$\Lambda = \frac{K}{\sqrt{2\pi}} \int_0^\infty \frac{du \sqrt{u}}{(1 + \epsilon u/\beta)^2 \sqrt{1 + \delta^2 u/\gamma^2}}.$$

After simple transformations the integral in the r.h.s. in this formula is expressed in terms of elementary functions

$$\Lambda = \frac{\Lambda_0}{\sqrt{2\pi}} \begin{cases} \frac{\arcsin \sqrt{1-z^2}}{(1-z^2)^{3/2}} - \frac{z}{1-z^2}, & z \leq 1, \\ \frac{z}{z^2-1} - \frac{\ln[z + \sqrt{z^2-1}]}{(z^2-1)^{3/2}}, & z \geq 1, \end{cases} \quad (4.22)$$

where $z = (\delta/\gamma)\sqrt{\beta/\epsilon}$ and

$$\Lambda_0 = \frac{K}{(\epsilon/\beta)^{3/2}} = \frac{Z^2}{A} \frac{4\pi n_e e^4 L}{\gamma^5 m M c^3 (\epsilon/\beta)^{3/2} \Pi} l \quad (4.23)$$

is the emittance cooling decrement of the monochromatic bunch. It is interesting to note that in the asymptotic region $z \gg 1$ (or, $\delta \gg \gamma\sqrt{\epsilon/\beta}$) the cooling decrement in Eq.(4.22) decrease proportionally to γ/δ only

$$\Lambda \simeq \frac{K\gamma}{(\epsilon/\beta)\delta} = \frac{Z^2}{A} \frac{4\pi n_e e^4 L}{\gamma^4 m M c^3 (\epsilon/\beta)\delta \Pi} l, \quad \delta \gg \gamma\sqrt{\epsilon/\beta} \gg v_0/c. \quad (4.24)$$

4.4.1 Magnetized electron cooling

If the contributions of the adiabatic collisions in the cooling force predominate, the vertical cooling force is determined by the following expression

$$F_z = -\frac{2\pi n_e Z^2 e^4 L}{m} \frac{v_z (v_\perp^2 - 2v_\parallel^2)}{(v_\perp^2 + v_\parallel^2)^{5/2}}. \quad (4.25)$$

Here, we neglect the temperature velocities of the cooling electron Larmour circles as compared to ion velocities. Substituting this expression in Eq.(4.17) we obtain (again $\beta' = 0$)

$$\dot{\epsilon}_z = \frac{K}{2(2\pi)^{3/2}} \frac{\beta^2 \gamma}{\epsilon \delta} \int \frac{d^3 \theta \theta_z^2 [\theta_\perp^2 - 2\theta_\parallel^2]}{\theta^5} \exp\left(-\frac{\beta \theta_\perp^2}{2\epsilon} - \frac{\gamma^2 \theta_\parallel^2}{2\delta^2}\right). \quad (4.26)$$

The integral in this expression is calculated in the spherical coordinates $(\theta, \alpha, \varphi)$ with the polar axes directed along θ_\parallel , so that

$$\theta_z = \theta \sin \alpha \cos \varphi, \quad \theta_x = \theta \sin \alpha \sin \varphi, \quad \theta_\parallel = \theta \cos \alpha.$$

The integrations over φ and θ yield

$$\Lambda = -\frac{\dot{\epsilon}_z}{\epsilon_z} = -\frac{K}{2\sqrt{2\pi}} \frac{\beta \gamma}{\epsilon \delta} \int_0^1 du \frac{(1-u^2)(1-3u^2)}{1-qu^2}, \quad q = 1 - \frac{\gamma^2 \epsilon}{\beta \delta^2}. \quad (4.27)$$

Simple calculations result in

$$\Lambda = \frac{\Lambda_0}{2\sqrt{2\pi}} \Phi_x(z) \quad (4.28)$$

where

$$\Phi_x(z) = \begin{cases} \frac{1+2z^2}{(1-z^2)^{5/2}} \arcsin \sqrt{1-z^2} - \frac{3z}{(1-z^2)^2}, & z \leq 1, \\ \frac{1+2z^2}{(z^2-1)^{5/2}} \ln [z + \sqrt{z^2-1}] - \frac{3z}{(z^2-1)^2}, & z \geq 1. \end{cases} \quad (4.29)$$

Note, that although the cooling force change the sign when $v_{\perp} \leq \sqrt{2}v_{\parallel}$, the emittance cooling decrement is positive for all ratios between the betatron angular divergency (ϵ/β) and the bunch momentum spread (δ). The effect of the local instability results only in a more sharp decrease in the cooling decrement with an increase in δ

$$\Lambda \simeq \frac{\Lambda_0}{\sqrt{2\pi}} \frac{\ln(2z) - 3/2}{z^3}, \quad z \gg 1. \quad (4.30)$$

4.4.2 Magnetized momentum cooling

The magnetized momentum cooling force is determined by the following expression (in the beam rest frame system)

$$F_{\parallel} = -3 \frac{2\pi n_e Z^2 e^4 L v_{\perp}^2 v_{\parallel}}{m v^5}. \quad (4.31)$$

Then, for a Gaussian distribution in the ion bunch, the variation of the rms bunch momentum spread (δ) reads

$$\frac{d\delta^2}{dt} = \frac{2}{p} \int d\Gamma \frac{\Delta p}{p} F_{\parallel} f,$$

or

$$\begin{aligned} \frac{d\delta^2}{dt} &= -\frac{3}{(2\pi)^{3/2}} \frac{\beta}{\epsilon\delta} \frac{4\pi n_e Z^2 e^4 L}{m\gamma^4 c^2 p} \int d^3\theta \frac{\theta_{\perp}^2 \theta_{\parallel}^2}{(\theta_{\perp}^2 + \theta_{\parallel}^2/\gamma^2)^{5/2}} \exp\left(-\frac{\beta\theta_{\perp}^2}{2\epsilon} - \frac{\theta_{\parallel}^2}{2\delta^2}\right) \quad (4.32) \\ &= -\frac{3K}{(2\pi)^{3/2}} \frac{\beta}{\epsilon\delta} \gamma^3 \int d^3\theta \frac{\theta_{\perp}^2 \theta_{\parallel}^2}{\theta^5} \exp\left(-\frac{\beta\theta_{\perp}^2}{2\epsilon} - \frac{\gamma^2 \theta_{\parallel}^2}{2\delta^2}\right) \\ &= -\frac{3K}{(2\pi)^{1/2}} \frac{\gamma^3}{\delta} 2 \int_0^1 du \frac{u^2(1-u^2)}{1-qu^2}, \quad q = 1 - \frac{\gamma^2 \epsilon}{\beta\delta^2}. \end{aligned}$$

The calculation of the integral in the r.h.s. of Eq.(4.32) results in

$$\int_0^1 du \frac{u^2(1-u^2)}{1-qu^2} = \begin{cases} \frac{3-2q}{3q^2} - \frac{1-q}{q^{5/2}} \ln \frac{(1+\sqrt{q})^2}{1-q}, & q \geq 0, \\ \frac{3-2q}{3q^2} - \frac{1-q}{(-q)^{5/2}} \arcsin \frac{\sqrt{-q}}{1-q}, & q \leq 0. \end{cases}$$

Substituting this expression in Eq.(4.32), we find

$$\frac{d\delta^2}{dt} = -\frac{2K}{\sqrt{2\pi}} \gamma^2 \sqrt{\frac{\beta}{\epsilon}} z \Phi(z), \quad z = \frac{\delta}{\gamma} \sqrt{\frac{\beta}{\epsilon}}, \quad (4.33)$$

where

$$\Phi(z) = \begin{cases} \frac{2+z^2}{(1-z^2)^2} - \frac{3z \arcsin(\sqrt{1-z^2})}{(1-z^2)^{5/2}}, & z \leq 1, \\ \frac{2+z^2}{(z^2-1)^2} - \frac{3z \ln(z + \sqrt{z^2-1})}{(z^2-1)^{5/2}}, & z \geq 1. \end{cases} \quad (4.34)$$

The momentum cooling decrement is obtained dividing $\dot{\delta}^2$ by δ^2 , which yields

$$\Lambda_{\parallel} = -\frac{\dot{\delta}^2}{\delta^2} = \frac{2\Lambda_0}{\sqrt{2\pi}} \frac{\Phi(z)}{z}, \quad (4.35)$$

where Λ_0 is defined in Eq.(4.23). Since $\Phi(0) = 2$, the momentum cooling decrement in Eq.(4.35) diverges for small momentum spreads ($\delta \ll \gamma\sqrt{\epsilon/\beta}$). In the region $\delta \ll \gamma\sqrt{\epsilon/\beta}$ the momentum cooling decrements substantially exceed the betatron ones (see in Fig.4.9).

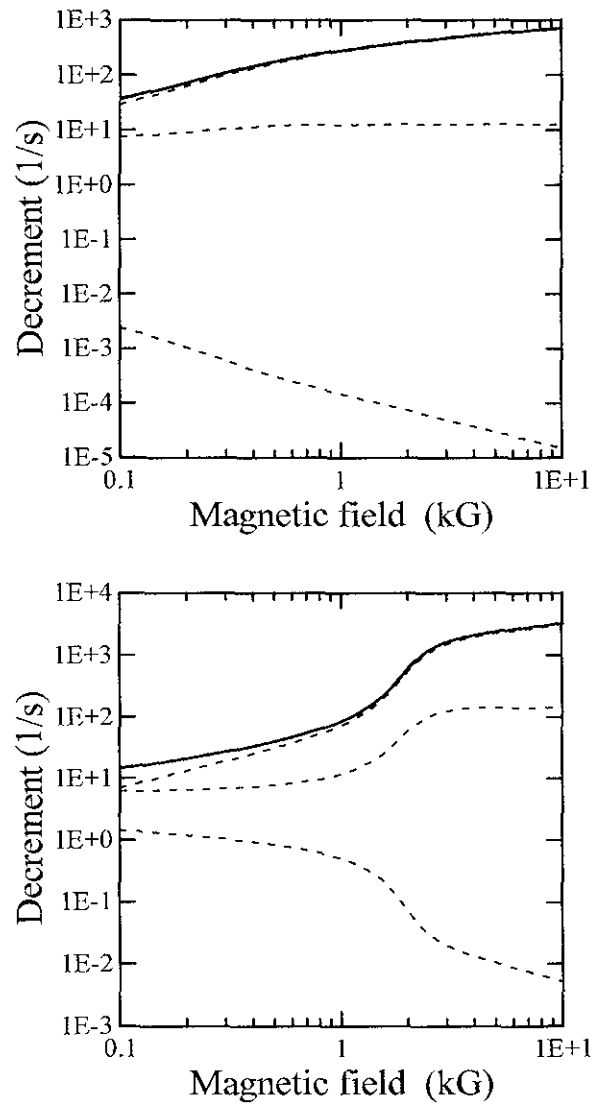


Figure 4.7: Dependences of the maximum damping decrements of protons on the magnetic field of the cooling device. From top to bottom the dashed curves show the contributions due to slow, multiple and fast collisions; the solid line presents the sum of these items; the cooling section length is 0.01 of the ring perimeter, the density of the cooling electron beam is 10^7 $1/\text{cm}^3$ (left picture) and 5×10^8 $1/\text{cm}^3$ (right picture).

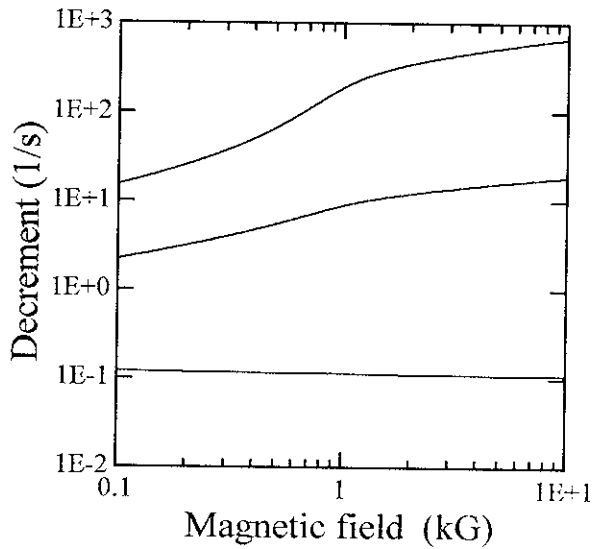


Figure 4.8: Dependences of the damping decrements of protons on the magnetic field of the cooling device. From top to bottom the angular spread in the proton beam is 10^{-6} , 10^{-5} , 10^{-4} ; the cooling section length is 0.01 of the ring perimeter, the density of the cooling electron beam is 1.0×10^8 $1/\text{cm}^3$.

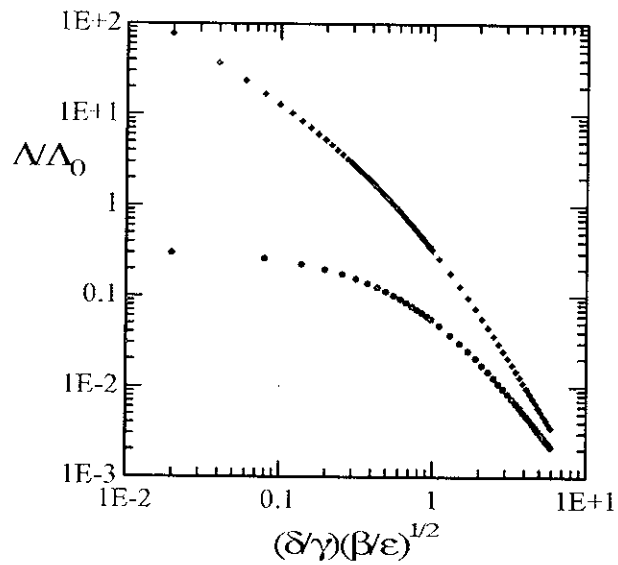


Figure 4.9: Dependence of the longitudinal (full diamonds) and of the betatron (full dots) cooling decrements on the bunch momentum spread.

Chapter 5

Intrabeam Scattering

Among other factors, the luminosity performance in the electron-nucleon collider (ENC, [8]) can be limited due to Coulomb collisions in ion bunches. Depending on the assumed operational mode these collisions may contribute to a decrease in the lifetime of the luminosity, or in a decrease of the luminosity peak value. The first possibility may occur in colliders without ion beam cooling, where high value of the luminosity is maintained due to huge beam emittances (and currents). the desired value of the luminosity.

In an alternative mode the desired high value of the luminosity is achieved due to strong electron cooling of ion bunches. Since electron cooling makes equal the temperatures of an ion and electron beam we expect strong intrabeam scattering (IBS) effect on emittances of especially heavy and highly charged ion bunch.

Another source of the bunch emittances blow-ups in a deeply cooled ion bunch, is the space charge instability. In general, the space charge instability may affect both transverse and longitudinal phase space of bunches. However, it seems that reliable predictions concerning an increase in the longitudinal bunch emittance should take into account the effects due to both the space charge and the wake-fields of ion bunches. That problem will be considered anywhere. Below, we shall neglect the effect of the bunch space charge on the longitudinal emittance, assuming that the bunch length is maintained to be equal to the β -function at the interaction point, while the bunch momentum spread is determined by IBS.

In a storage ring with an alternating gradient focusing IBS results in the bunch self-heating - i.e. in the tendency of the collisions to maintain a permanent blow-up of the bunch emittances [37, 38, 39]. As it was shown in Ref.[10], such a self-heating mechanism poses a lower border on the required value of the sum of cooling decrements to ensure that the ion beam can reach an equilibrium.

The mentioned self-heating effect occurs due to collisions of ions transferring the particle momenta from the transverse to the longitudinal motion and due to betatron modulations of the beam partial velocity spreads along the closed orbit. The first possibility can be illustrated studying a 90° -collision of a couple of ions, which had before collision the opposite-directed and, for example, horizontal momenta (see in

Fig.5.1). Let the horizontal betatron oscillations of a particle be described using

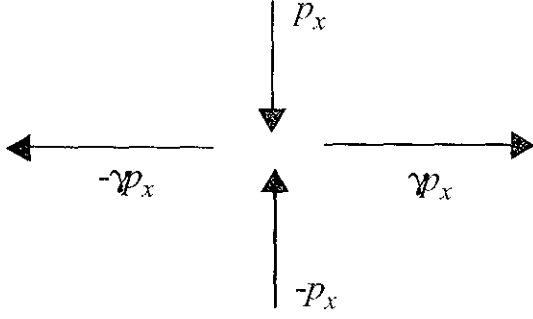


Figure 5.1: To the bunch self-heating due to IBS. In the rest frame system of the bunch before collision particles had momenta p_x and $-p_x$. After a 90° collision one particle gains and its partner loses (in the laboratory system) $\Delta p = \pm \gamma p_x$.

$$x = \sqrt{J\beta} \cos \phi + D_x \delta, \quad \frac{p_x}{p} = x' = D'_x \delta + \frac{\beta'}{2\beta} (x - D_x \delta) - \sqrt{\frac{J}{\beta}} \sin \phi, \quad (5.1)$$

where

$$J = \frac{(x - D_x \delta)^2}{\beta} + \beta \left(\frac{p_x}{p} - \frac{\beta'}{2\beta} x + \Phi \delta \right)^2 \quad (5.2)$$

is the action variable and $\phi = \nu_x \theta + \chi_x$, $\phi' = d\phi/ds = 1/\beta$ is the variable of the unperturbed oscillations, $D_x(s)$ is the dispersion function of the ring,

$$\Phi = D_x \frac{\beta'}{2\beta} - D'_x,$$

s is the path along the closed orbit. The energy of betatron oscillations is expressed in terms of the action variable

$$\mathcal{E}_x = \frac{p\omega_0 \nu_x}{2R_0} J.$$

The beam self-heating occurs, when collisions result in simultaneous increases in the beam momentum spread and in the energies of betatron oscillations of the colliding particles. For a single 90° collision we have

$$J_{in}^{(1,2)} = \frac{x^2}{\beta} + \beta \left(\pm \frac{p_x}{p} - \frac{\beta'}{2\beta} x \right)^2$$

and

$$J_f^{(1,2)} = \frac{(x \pm D_x \delta)^2}{\beta} + \beta \left(\frac{\beta'}{2\beta} x \pm \Phi \delta \right)^2, \quad \delta = \gamma \frac{p_x}{p},$$

so that

$$\begin{aligned}\Delta\mathcal{E}^{(1,2)} &= (\mathcal{E}^{(1)} + \mathcal{E}^{(2)})_f - (\mathcal{E}^{(1)} + \mathcal{E}^{(2)})_{in} \\ &= \frac{\omega_0\nu_x p_x^2}{p} \left(\gamma^2 \left[\frac{D_x^2}{\beta} + \beta\Phi^2 \right] - \beta \right).\end{aligned}\quad (5.3)$$

The average value of $\Delta\mathcal{E}^{(1,2)}$ along the closed orbit will be positive provided that

$$\gamma^2 \int_0^\Pi \frac{ds}{\Pi} \mathcal{H}(s) > \int_0^\Pi \frac{ds}{\Pi} \beta(s), \quad (5.4)$$

where

$$\mathcal{H} = \frac{D_x^2(s)}{\beta(s)} + \beta(s)\Phi^2. \quad (5.5)$$

In the smoothed focusing approximation ($\beta \simeq R_0/\nu_x$, $\Phi \simeq 0$ and $D_x \simeq R_0/\nu_x$) the last expression is reduced to $\gamma^2 > \nu_x^2 \simeq \gamma_{tr}$. It also shows that a requirement to increase the threshold value of γ demands a decrease in the average value of \mathcal{H} .

5.1 Bunch Entropy Growth Rate

In a ring with an alternating gradient focusing the Coulomb collisions of ions result in a systematic growth of the total phase space volume of the bunch (see, for example, in Refs [38, 39, 10]). The blow-up of the bunch phase space volume occurs due to collisions transferring the particle momenta from the transverse to longitudinal motion and due to the dependence of the position of the closed orbit on the particle energy.

For the bunch with a Gaussian distribution function the corresponding growth rate, which is equal to the sum of the partial increments

$$\Lambda = \frac{1}{\epsilon_x} \frac{d\epsilon_x}{dt} + \frac{1}{\epsilon_z} \frac{d\epsilon_z}{dt} + \frac{1}{\delta^2} \frac{d\delta^2}{dt}, \quad (5.6)$$

can be estimated using the following expression (see, for example, in Appendix C.1)

$$\Lambda = \frac{K_{IBS}}{\epsilon_x \epsilon_z \sigma_s \delta} \langle G \rangle, \quad K_{IBS} = \frac{N_i (Z^2/A)^2 r_p^2 c L_{IBS}}{2\pi\gamma^4}. \quad (5.7)$$

Here, N_i is the number of particles in the ion bunch, $r_p = e^2/Mc^2$, ϵ_{ix} and ϵ_{iz} are the horizontal and vertical bunch emittances, $\delta = \Delta p/p$ is the rms bunch momentum spread, Ze is the ion charge and A is its atomic number, $L_{IBS} = \ln(\rho_{\max}/\rho_{\min})$ is the Coulomb logarithm for fast collisions and

$$\langle G \rangle = \int_0^\Pi \frac{ds}{\Pi} G(s), \quad (5.8)$$

is the form factor, describing the effect of the lattice focusing on IBS. Prior to discussing the properties of $\langle G \rangle$ we note that for collisions in a focusing lattice

among the candidates for ρ_{\max} we have also to consider $\rho_{\max} = \Delta v_{\parallel}/\omega_b$, where ω_b is the frequency of betatron oscillations of particles and Δv_{\parallel} is the longitudinal relative velocity of colliding particles. Equation (5.7) holds for the so-called fast collisions, when

$$\rho_{\min} = \frac{(Ze)^2}{AM\Delta v^2} \ll \rho \ll \frac{\Delta v_{\parallel}}{\omega_b}.$$

In the case of the strong focusing lattice, the integrand in Eq.(5.8)

$$G(s) = \int_0^1 \frac{[a_z + q_+ + q_-]du}{\sqrt{[q_- + (a_z - q_-)u^2][q_+ + (a_z - q_+)u^2]}} - 3 \quad (5.9)$$

depends on the betatron functions of the ring via the angular bunch divergencies $a_{x,z} = \beta_{x,z}/\epsilon_{x,z}$ and via the eigenvalues (q_{\pm}) of the matrix

$$\mathbf{A} = \begin{bmatrix} a_x & -\gamma a_x \Phi \\ -\gamma a_x \Phi & \gamma^2 a_s \end{bmatrix}, \quad a_s = \frac{1}{\epsilon_x} \left(\frac{D_x^2}{\beta_x^2} + \Phi^2 \right) + \frac{1}{\delta^2}, \quad (5.10)$$

which read

$$q_{\pm} = \frac{a_x}{2} \left(a_x + \gamma^2 a_s \pm \sqrt{(a_x - \gamma^2 a_s)^2 + 4\gamma^2 a_x^2 \Phi^2} \right). \quad (5.11)$$

The function $G(s)$ is a non-negative function of $a_z(s)$, $q_{\pm}(s)$ with the following properties

$$G(\mu a_z, \mu q_+, \mu q_-) = G(a_z, q_+, q_-),$$

and

$$G(a_z = q_+ = q_-) = 0.$$

In a storage ring with an alternating gradient focusing the last condition never holds. Without beam cooling intrabeam scattering always results in a permanent increase in the total phase space volume, or in the entropy of a bunch. In general case, the function $G(s)$ is expressed in terms of the elliptic integrals (see, for example, in Appendix C.2).

In order to evaluate the effect of the modulation of the betatron functions on the behaviour of the IBS form factor the value $\langle G \rangle$ was plotted as a function of the bunch momentum spread. Remaining parameters of the ring and of the ion bunch were taken from Ref.[8]. We compared two possibilities: the FODO-lattice (neglecting the effect of the electron-ion bunch interaction region), and, as an alternative case, the lattice which enables $\alpha_p < 0$. The last possibility although does not eliminate the self-heating of the ion bunch, will probably a useful option against the beam-beam instability as well as against collective instabilities due to interactions of ions with their surrounding electrodes. The betatron functions for these lattices are shown in Figs 5.2 and 5.3. Although the maximum values of the modulation factors

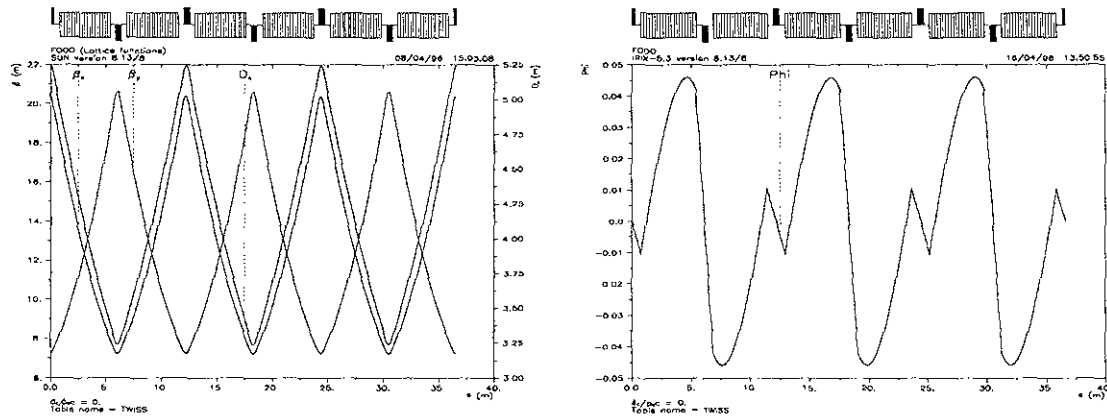


Figure 5.2: Dependences of the betatron functions (left) and of the modulation factor (Φ , right) on the distance along the closed orbit (s) for the FODO-lattice in a ring, described in the Ref.[8].

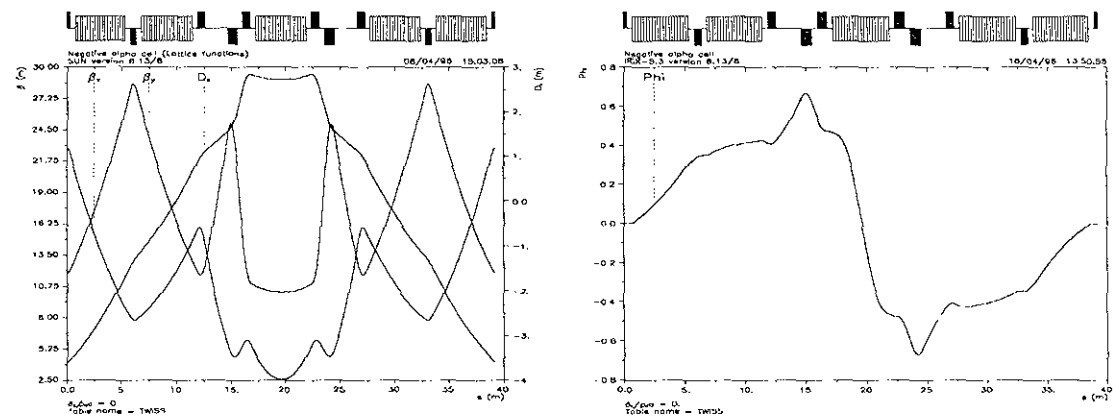


Figure 5.3: Dependences of the betatron functions (left) and of the modulation factor (Φ , right) on the distance along the closed orbit (s) for a lattice consisting of the cells with the negative momentum compaction factor.

(Φ) for these lattices differ more than one order in magnitude (see in Figs 5.2 (right) and 5.3 (right)), the difference in the corresponding values of $\langle G \rangle$ is not very high (see in Fig.5.4). Moreover, within accuracy of about 10 % the value of $\langle G \rangle$ calculated for the FODO-lattice coincides with that, calculated in the smoothed focusing approximation:

$$G(a) = \frac{2+a}{\sqrt{a-1}} \arcsin \left(\sqrt{\frac{a-1}{a}} \right) - 3, \quad a = \gamma^2 \left(\frac{\eta^2}{\beta^2} + \frac{\epsilon}{\beta\delta^2} \right) > 1.$$

Note also that for chosen parameters Fig.5.4 indicates larger deviations between the upper and lower curves for larger bunch momentum spreads and for larger bunch emittance.

We remind the reader that all these calculations hold provided that the collisions of the most particles are fast and that the IBS can be described within the framework of the logarithmic approximation. A beam cooling till very small bunch emittances and momentum spreads may break such assumptions and eliminate relevant limitations on the bunch phase space density due to IBS.

5.2 Equilibrium Emittances

Provided that the sum of the cooling decrements exceeds Λ , the bunch will reach an equilibrium. The equilibrium emittances are found using the following equations

$$\begin{aligned} \dot{\epsilon}_x &= -\lambda_x(\epsilon_x - \epsilon_{x0}) + (\dot{\epsilon}_x)_{IBS} = 0, \\ \dot{\epsilon}_z &= -\lambda_z(\epsilon_z - \epsilon_{z0}) + (\dot{\epsilon}_z)_{IBS} = 0, \\ \dot{\delta}^2 &= -\lambda_{\parallel}(\delta^2 - \delta_0^2) + (\dot{\delta}^2)_{IBS} = 0. \end{aligned} \quad (5.12)$$

Here, $\lambda_{x,z,s}$ are the cooling decrements and $\epsilon_{\alpha 0}$ are the equilibrium emittances, calculated neglecting IBS ($\alpha = x, z, s$). The values $(\dot{\epsilon}_\alpha)_{IBS}$ describe the blow-up of the bunch due to IBS. In general case, these values are determined by the following expressions (see Appendix C.1 for detail)

$$\left(\frac{d\epsilon_z}{dt} \right)_{IBS} = \frac{K_{IBS}}{\epsilon_x \epsilon_z \epsilon_s} \int_0^{\Pi} \frac{ds}{\Pi} \beta_z(s) G_z(s), \quad K_{IBS} = \frac{N(Z^2/A)^2 \gamma_p^2 c L_{IBS}}{2\pi \gamma^4}, \quad (5.13)$$

$$\left(\frac{d\delta^2}{dt} \right)_{IBS} = \frac{K_{IBS} \gamma^2}{\epsilon_x \epsilon_z \epsilon_s} \int_0^{\Pi} \frac{ds}{\Pi} G_s(s), \quad (5.14)$$

$$\left(\frac{d\epsilon_x}{dt} \right)_{IBS} = \frac{K_{IBS}}{\epsilon_x \epsilon_z \epsilon_s} \int_0^{\Pi} \frac{ds}{\Pi} \left[\beta_x(s) G_x(s) + \gamma^2 \mathcal{H}(s) G_s(s) + 2G_{xs}(s) \right], \quad (5.15)$$

where the form factors G_z , G_s and G_{xs} are determined in Eqs (C.16), (C.19) and (C.21). Since

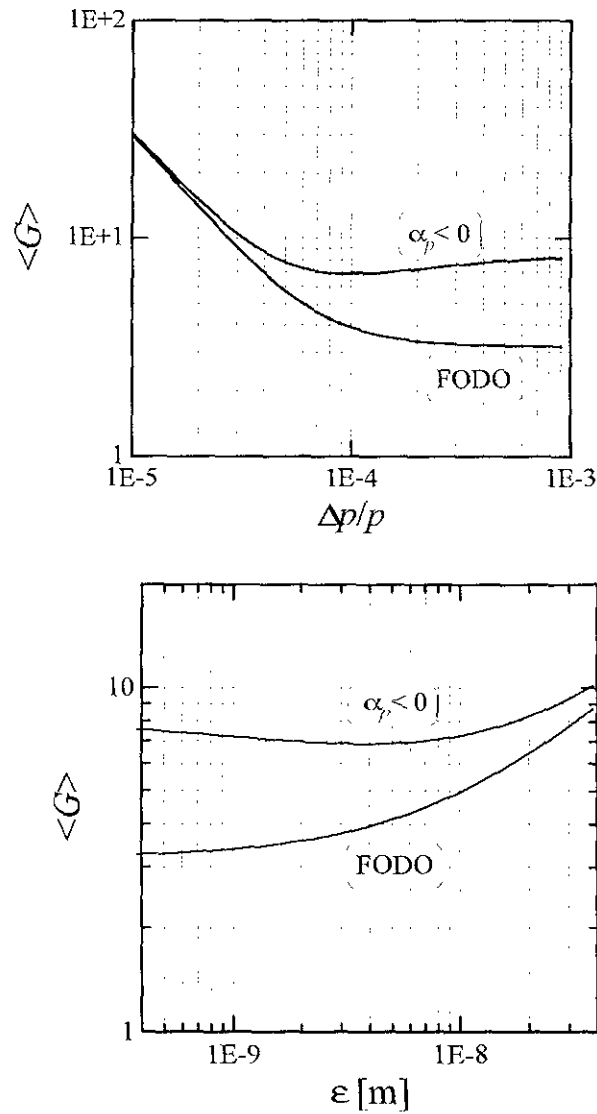


Figure 5.4: Dependence of the IBS form factor on the momentum spread of the ion bunch (left) and on the emittance of the ion bunch ($\epsilon_x = \epsilon_z = \epsilon$). Both curves are calculated for the lattices shown in Figs 5.2 and 5.3 and for the bunch of the bare uranium ions moving in a ring with $BR_i = 100 \text{ Tm}$ ($\gamma_i \simeq 12$); for the left graph the horizontal and vertical emittances are taken to be $\epsilon_x = \epsilon_z \simeq 4 \text{ nm}$; for the right - $\Delta p/p = 0.0001$.

$$\frac{1}{\epsilon_x} \left(\frac{d\epsilon_x}{dt} \right)_{IBS} + \frac{1}{\epsilon_z} \left(\frac{d\epsilon_z}{dt} \right)_{IBS} + \frac{1}{\delta^2} \left(\frac{d\delta^2}{dt} \right)_{IBS} = \langle G \rangle,$$

where the function $\langle G \rangle$ is determined in Eqs 5.7 – 5.9, we find that the equilibrium conditions in Eqs (5.12) can be rewritten in the following form

$$\lambda_x + \lambda_z + \lambda_{\parallel} - \langle G \rangle = \lambda_x \frac{\epsilon_{x0}}{\epsilon_x} + \lambda_z \frac{\epsilon_{z0}}{\epsilon_z} + \lambda_{\parallel} \frac{\delta_0^2}{\delta^2} > 0. \quad (5.16)$$

To simplify the study of equilibrium emittances on the bunch current below we consider a special case, when betatron oscillations are described in the smoothed focusing approximation:

$$\beta_{x,z} \simeq \frac{R_0}{\nu_{x,z}}, \quad D_x \simeq \frac{R_0}{\nu_x^2}, \quad \Phi = 0. \quad (5.17)$$

In this case, the form factors in Eqs (5.13) – (5.15) are reduced to

$$G_s = \int_0^1 du \frac{(1 - 3u^2)}{\sqrt{Q(a_x)Q(a_z)}}, \quad Q(a, u) = a + (\gamma^2 a_s - a)u^2 \quad (5.18)$$

and

$$G_z = -\frac{G_s + G_-}{2}, \quad G_x = -\frac{G_s - G_-}{2}. \quad (5.19)$$

Here,

$$G_-(a_+, a_-, a_s) = \frac{1}{a_-} \left[(\gamma^2 a_s - a_+) G_s + \langle G \rangle \right], \quad (5.20)$$

the function $\langle G \rangle$ is defined in Eqs (5.8) and (5.9), $a_{\pm} = (a_x \pm a_z)/2$, $a_{x,z} = \beta_{x,z}/\epsilon_{x,z}$.

It is easy to find that $G_-(a_+, a_- = 0, a_s) = 0$. The integrals in Eqs (5.18) – (5.20) can be expressed in terms of the elliptic integrals of the 1st and 2nd kind (see, for example, in Appendix C.3).

With these assumptions the stationary solutions of Eqs (5.12) ($\dot{\epsilon}_\alpha = 0$) obey the following equations

$$\begin{aligned} \lambda_x(\epsilon_x - \epsilon_{x0}) &= \frac{K_{IBS}\beta_x}{\epsilon_x\epsilon_z\epsilon_s} \left[\left(\frac{\gamma^2}{\gamma_c^2} - \frac{1}{2} \right) G_s + \frac{G_-}{2} \right], \quad \gamma_c = \frac{\beta_x}{D_x} \simeq \gamma_{tr}, \\ \lambda_z(\epsilon_z - \epsilon_{z0}) &= -\frac{K_{IBS}\beta_z}{\epsilon_x\epsilon_z\epsilon_s} \left[\frac{G_s + G_-}{2} \right], \\ \lambda_s(\delta^2 - \delta_0^2) &= \frac{K_{IBS}}{\epsilon_x\epsilon_z\epsilon_s} \gamma^2 G_s. \end{aligned} \quad (5.21)$$

Since the roots of these satisfy the known relationship

$$\delta^2 - \delta_0^2 = \frac{\gamma_c^2 \gamma^2}{\gamma^2 - \gamma_c^2} \left(\frac{\lambda_x [\epsilon_x - \epsilon_{0x}]}{\lambda_s \beta_x} + \frac{\lambda_z [\epsilon_z - \epsilon_{0z}]}{\lambda_s \beta_z} \right), \quad (5.22)$$

only two equations from Eqs(5.21) must be solved. This equation shows that the ratios between the equilibrium momentum spread and angular divergencies in the equilibrium bunch ($\sqrt{\epsilon_{x,z}/\beta_{x,z}}$) do not depend on the cooling beam current, but only on the ring focusing and on the particle energy.

Above transition energy of the ring the equilibrium between the intrabeam scattering and the beam cooling results in the flattening of the bunch in the horizontal direction ($\epsilon_x > \epsilon_z$). For initially round bunch $\epsilon_x = \epsilon_z = \epsilon$ and $\beta_x \simeq \beta_z = \beta$ we have $G_- = 0$, while

$$G_s = \frac{\epsilon}{\beta} \Phi_{IBS} \left(\frac{\gamma^2}{\gamma_c^2} - q \right), \quad q = 1 - \frac{\gamma^2 \epsilon}{\beta \delta^2},$$

$$\Phi_{IBS}(w) = \int_0^1 du \frac{1 - 3u^2}{1 + wu^2} = \frac{1}{w} \left(\frac{w+3}{\sqrt{w}} \arctan \sqrt{w} - 3 \right). \quad (5.23)$$

If $\gamma > \gamma_c$, then

$$\frac{\gamma^2}{\gamma_c^2} - q = \frac{\gamma^2}{\gamma_c^2} - 1 + \frac{\gamma^2 \epsilon}{\beta \delta^2} > 0.$$

Hence, $G_s \geq 0$. The equilibria equations in this case read ($\lambda_x = \lambda_z = \lambda$)

$$\begin{aligned} \epsilon_x &= \epsilon_{x0} + \frac{K_{IBS}}{\lambda \epsilon \epsilon_s} \left(\frac{\gamma^2}{\gamma_c^2} - \frac{1}{2} \right) \Phi_{IBS}, \\ \epsilon_z &= \epsilon_{z0} - \frac{K_{IBS}}{2\lambda \epsilon \epsilon_s} \Phi_{IBS}, \\ \delta^2 &= \delta_0^2 + \frac{K_{IBS}}{\lambda_s \epsilon \epsilon_s \beta} \gamma^2 \Phi_{IBS}. \end{aligned} \quad (5.24)$$

So that $\epsilon_x > \epsilon_{x0}$, $\delta > \delta_0$ and $\epsilon_z < \epsilon_{z0}$

5.3 Space Charge Effect

As was already mentioned in the case of ENC, the parameter sets occur in the regions, where at least the betatron bunch emittances are strongly affected by the beam-beam, or the ion bunch space charge instability. Typically, these instabilities result in much stronger bunch emittance blow-up than intrabeam scattering, which means that betatron equilibria equations in Eq.(5.12) are strongly violated. Although the blow-up of the bunch phase space due to these instabilities is a complicated phenomenon, from numerous observations and computer simulations we expect that

$$\epsilon = \epsilon_0 + \Delta\epsilon_{SP}, \quad \Delta\epsilon \gg \epsilon_0, \quad (5.25)$$

where

$$\Delta\epsilon_{SP} = \begin{cases} \frac{Z^2}{A} \frac{N_i r_p}{4\pi\gamma^3 \Delta\nu_L} \frac{\Pi}{\sqrt{2\pi}\sigma_s}, & \xi_i \ll \Delta\nu_L, \\ \frac{Z}{A} \frac{N_e r_p}{4\pi\gamma\xi_i}, & \xi_i \gg \Delta\nu_L. \end{cases} \quad (5.26)$$

For a given \sqrt{s} and in the optimum luminosity conditions the bunches and ring parameters are set to hold conditions $\xi_c = \xi_i = \Delta\nu_L$. It means that for all energies we can take

$$\epsilon_x = \epsilon_z = \left(\frac{Z^2}{A} \right) \frac{N_i r_p \Pi}{4\pi\sqrt{2\pi}\gamma^3 \sigma_s \Delta\nu_L} \quad (5.27)$$

If the longitudinal phase space of ion bunches is not in the space charge dominated region, the intrabeam scattering may define the equilibrium bunch momentum spread due to its balance with longitudinal heating. In the smoothed focusing approximation ($\beta_{x,z}(s) \rightarrow \bar{\beta}_{x,z}$; $D_x(s) \rightarrow \bar{D}$), assuming that the bunch length (σ_s) is maintained to be a constant, while $\delta_{st} \gg \delta_0$ and using Eq.(4.35), we write

$$\frac{d\delta^2}{dt} = -\frac{2K}{\sqrt{2\pi}} \gamma^2 \sqrt{\frac{\bar{\beta}}{\epsilon}} z\Phi(z) + \frac{K_{IBS}\gamma}{\sigma_s \sqrt{\bar{\beta}\epsilon^{3/2}}} \Phi_{IBS}(z\sqrt{\bar{\beta}/\beta}), \quad (5.28)$$

or

$$\frac{d\delta^2}{dt} = -Q \left[z\Phi(z) - \frac{\Delta\nu_L \gamma^3}{2n_e r_e l \sqrt{\bar{\beta}\beta}} \Phi_{IBS}(z\sqrt{\bar{\beta}/\beta}) \right]. \quad (5.29)$$

Here $z = (\delta/\gamma)\sqrt{\bar{\beta}/\epsilon}$ and ($g = \gamma^2/\gamma_c^2$)

$$\Phi_{IBS}(z) = \frac{1}{1+(g-1)z^2} \left\{ \frac{(2+g)z^2+1}{\sqrt{1+(g-1)z^2}} \arcsin \sqrt{\frac{1+(g-1)z^2}{1+gz^2}} - 3z \right\}, \quad (5.30)$$

while

$$Q = \left(\frac{Z^2}{A} \right) \sqrt{\frac{2}{\pi}} \frac{4\pi n_e r_e r_p c L}{\gamma^3 \sqrt{\epsilon/\beta}} \frac{l}{\Pi}.$$

Since $z\Phi(z) \simeq 2z$, when $z \ll 1$, and $\Phi_{IBS}(0) = \pi/2$, while $z\Phi(z) \simeq 1/z$, when $z \gg 1$, and

$$\Phi_{IBS}(z) \simeq \frac{1}{z(g-1)} \left[\frac{g+2}{\sqrt{g-1}} \arcsin \sqrt{\frac{g-1}{g}} - 3 \right],$$

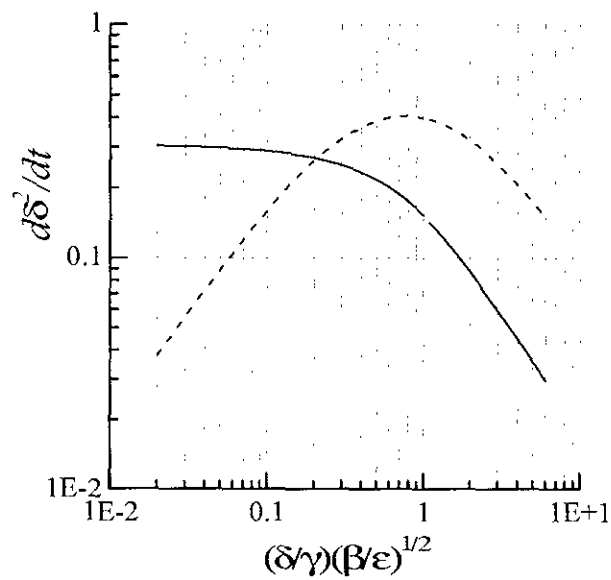


Figure 5.5: Dependence of the IBS momentum heating rate (solid line) and the momentum cooling rate (dashed line) on the relative momentum spread in the bunch $[(\delta/\gamma)\sqrt{\beta/\epsilon}]$. Electron- U_{238}^{92} ENC mode, $\sqrt{s} = 20$ GeV/u, $N_i \simeq 5.3 \times 10^7$, $n_e = 1.6 \times 10^8$ 1/cm³.

Eq.(5.29) may have a stable fixed point ($\delta = \delta_{st}$, see in Fig.5.5), if

$$n_e > (n_e)_{th} = \frac{\Delta\nu_L \gamma^3}{2r_e l \beta} \frac{1}{g-1} \left[\frac{g+2}{\sqrt{g-1}} \arcsin \sqrt{\frac{g-1}{g}} - 3 \right]. \quad (5.31)$$

A comparison of $(n_e)_{th}$ and the ion bunch density (in the cooling section), which is required to reach the necessary luminosity in ENC, shows that in the optimum luminosity conditions ($\Delta\nu_L = \xi_i$, two interaction points) the momentum heating due to intrabeam scattering of ions does not eliminate a possibility for bunches to reach an equilibrium (see in Fig.5.6). The calculation of the stationary momentum spreads (z_{st}) for the bare uranium ion bunches in ENC ($\bar{\beta} \simeq 12$ m, $\bar{D} \simeq 1.6$ m, $\beta \simeq 200$ m, $\sigma_s = 10$ cm) shows (see in Fig.5.7) that its value is about constant $z_{st} \simeq 0.2$ [$\delta_{st} \simeq 0.2\gamma\sqrt{\epsilon/\beta}$; see also in Fig.5.5] in the energy range $\sqrt{s} = 10 \div 30$ GeV/u.

In the storage ring with an alternating gradient focusing IBS increases the total phase space volumes of bunches. The blow-up of the phase space volume occurs both due to modulations of betatron functions and due to the coupling of horizontal (radial) and longitudinal oscillations, which is specific for motions along the closed orbits. At high energies of particles the diffusion with the energy transfer from betatron to the longitudinal oscillations predominates. For that reason, at higher particle energies the bunch self-heating mainly occurs due to the radial-longitudinal coupling. According to results, shown in Figs 5.4, the effect of the modulation of betatron functions on the growth rate of the total phase space volume of the bunch (Λ) is as weaker as smaller is the momentum spread of the bunch.

Without beam cooling the blow-up of the beam emittances may contribute to the lifetime of the luminosity of ENC, if initial values of emittances are small enough. We also remind the reader, that the rates of the blow-ups due to IBS decrease, when the bunch emittances increase. For that reason, the luminosity decays due to IBS slower than by an exponential law.

In the strongly cooled ion beam, IBS will affect the values of equilibrium emittances only in the case, when it overcomes the bunch blow-up due to the space charge instability. In particular, if the last mainly affects the blow-up of betatron emittances, the balance between IBS and the beam cooling results in a very weak dependence of equilibrium momentum spread on the bunch current.

An effect of the space charge instability on the longitudinal bunch emittance should take into account contributions due to the bunch wake-fields. The calculation of the equilibrium beam emittances in such a case demands additional study.

5.4 Touschek Lifetimes

IBS collisions with the longitudinal momentum transfer exceeding the separatrix width

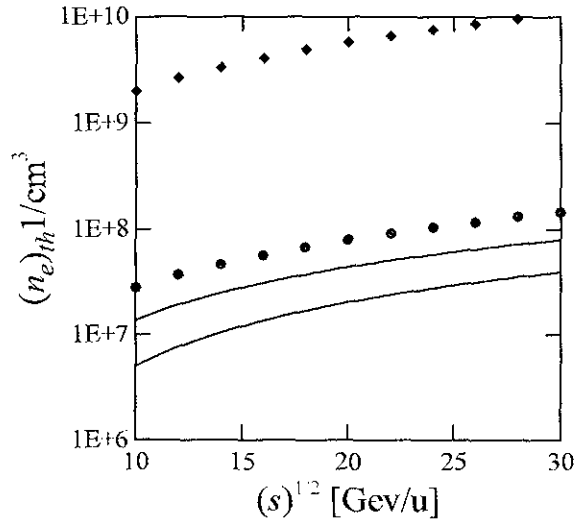


Figure 5.6: Dependence of $(n_e)_{th}$ on \sqrt{s} . Upper solid line – protons, lower – bare uranium ions; full diamonds and full dots show the densities of the proton (diamonds) and bare uranium ion bunches in the cooling section. Optimum luminosity conditions, $L = 10^{33}$ [1/cm²s].

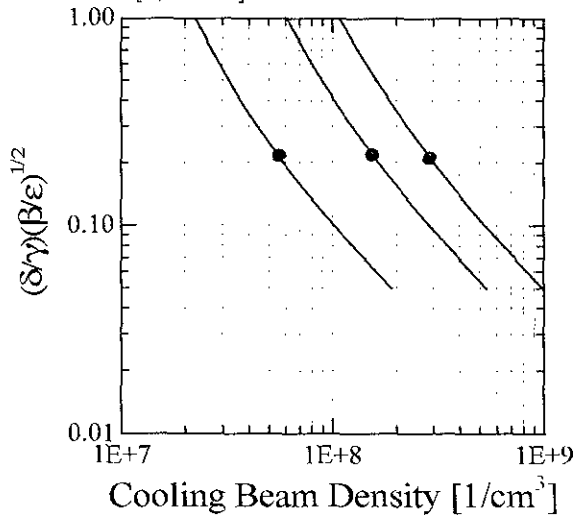


Figure 5.7: Dependence of the equilibrium bunch momentum spread on the cooling electron beam density. Optimum luminosity conditions ($L = 10^{33}$ [1/cm²s] per nucleon), from left to right $\sqrt{s} = 10, 20, 30$ GeV/u, full dots – the electron beam densities from Table 2.4.

$$\frac{\Delta p_c}{p} \simeq \sqrt{\frac{4ZeV}{2\pi pch\alpha_p}}, \quad (5.32)$$

determine the beam lifetime. This the so-called Touschek lifetime can be estimated using [40]

$$\frac{1}{\tau} \simeq \frac{Z^3}{4\sqrt{2}A} \times \frac{N_i r_p^2 ch\alpha Mc^2}{\epsilon\sqrt{\epsilon\beta}\gamma_i^2 \sigma_s eV} \Phi(\chi), \quad \chi = \frac{\Delta p_c}{p\gamma_i\sqrt{\epsilon/\beta}}, \quad (5.33)$$

where h is the RF harmonic number (in our case, it is equal to the number of bunches), α is the momentum compaction factor, V is the accelerating voltage, $r_p = e^2/Mc^2 \simeq 1.5 \times 10^{-16}$ cm and

$$\Phi(\chi) = -\frac{3}{2}e^{-\chi} + \frac{\chi}{2} \int_{\chi}^{\infty} \frac{du}{u} e^{-u} \ln u + \frac{3\chi + 2 - \chi \ln \chi}{2} \int_{\chi}^{\infty} \frac{du}{u} e^{-u}. \quad (5.34)$$

The dependence of the lifetime on the accelerating voltage and the beam emittance ($\Phi(\chi)$) is shown in Fig.5.8. Figure 5.9 shows that even for the bare uranium ion bunches the Touschek lifetime does not limit the ENC performance. This value decrease with an increase in \sqrt{s} . It occurs due to the fact that in the optimum luminosity condition the bunch density increase faster than γ_i^2 .

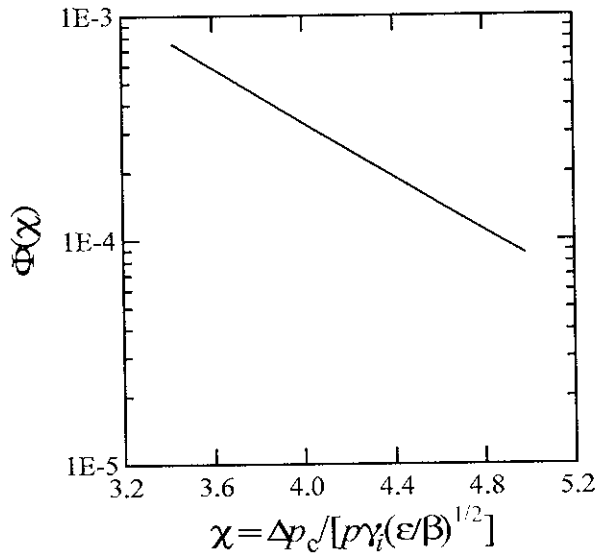


Figure 5.8: Dependence of the factor Φ in Eq.(5.33) on χ . Bare uranium ions, optimum luminosity conditions, RF-voltage 50 kV, $\alpha = 0.006$.

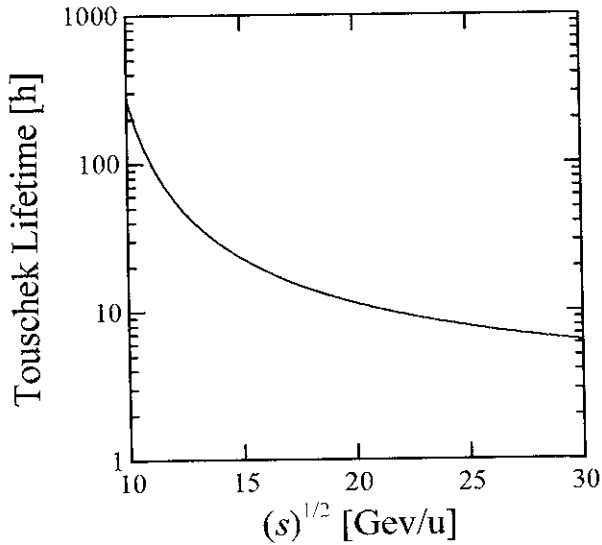


Figure 5.9: Dependence of the Touschek lifetime of the bare uranium ion bunch on \sqrt{s} . Optimum luminosity conditions, RF-voltage 50 kV, $\alpha = 0.006$.

Chapter 6

Conventional Collective Effects

The high luminosity performance is possible only in the case, when both the bunch current ($\propto N$) and the total beam current ($\propto n_b N$) are not strongly limited. Apart from other reasons, these values can be limited by conventional collective instabilities due to interaction of bunches with surrounding electrodes.

In this Chapter we estimate strengths of various collective instabilities and possible ways to avoid corresponding limitations. Specific features of the coherent instabilities in a bunched beam are determined by the ratio of the increment (decrement) of coherent oscillations to the frequency of synchrotron oscillations. If coherent rise-times ($1/\tau_{coh}$) are longer than the frequency of synchrotron oscillations ($\tau_{coh}\omega_s \gg 1$), the synchrotron modes of the bunch are uncoupled. In this case, the suppression of the instability demands a damping of particular betatron, or synchro-betatron modes. Otherwise, occur the so called mode-coupling instabilities.

6.1 Single-Bunch Effects

These issues usually provide the basis for estimating the longitudinal and transverse wideband impedance budgets of the ring. The instabilities due to single-bunch collective effects are more important for rings, where the number of bunches is not very high and, therefore, the current in a single bunch can be relatively high. Important are cases, when the single-bunch interactions with special devices result in a damping of coherent modes of a bunch. Such a damping due to interaction with the either passive, or active devices seems be useful in all cases.

6.1.1 Head-tail instability

A slow head-tail instability occurs due to excitation of coherent oscillations in the tail particles of the bunch by coherent oscillations of its head-on part. Synchrotron oscillations of particles change their position in the bunch, which provides instability of coherent oscillations of the whole bunch. The instability occurs due to wake fields, which are proportional to the average displacement of the bunch. For that reason,

the oscillations become unstable, if there is a phase advance of betatron oscillations of particles along the bunch. In storage rings, such a phase advance is provided by the ring chromaticity ($\omega_{x,z} = \omega_{x,z}(\Delta p)$), which results in

$$\psi_{x,z} = \psi_{x,z}^0 + \frac{d\omega_{x,z}}{d\omega_0} \varphi \cos \psi_s,$$

where $\psi_{x,z}^0$ is the phase of betatron oscillations of the synchronous particle, $a_s = R_0 \varphi$ is the amplitude of synchrotron oscillations of a particle, ψ_s is the phase of that oscillation,

$$\frac{d\omega_z}{d\omega_0} = \nu_z + \frac{d\nu_z}{d \ln \omega_0} = \nu_z + \frac{1}{\alpha_p} \frac{d\nu_z}{d \ln p}, \quad \alpha_p = \frac{1}{\gamma^2} - \frac{1}{\gamma_{tr}^2}.$$

Above transition energy of the ring $\alpha_p < 0$. Then, for the natural chromaticity of the ring ($d\nu_{\perp}/d \ln p < 0$) the value $d\nu_{\perp}/d \ln \omega_0$ is positive.

For the case of ENC, the strength of the head-tail instability was estimated using the following simplified expressions for increments of the unstable modes (vertical betatron oscillations)

$$\delta_m = -m_z \frac{qI_b}{2p\nu_z} \int_{-\infty}^{\infty} dn \operatorname{Im}[Z_{\perp}(n)] J_{m_s}^2(\varphi_0 n + m_z \zeta), \quad (6.1)$$

$$I_b = \frac{qN\omega_0}{2\pi}, \quad \zeta = \frac{\sigma_s}{R_0} \frac{d\nu_z}{d \ln \omega_0}.$$

Here, q is the charge of a particle, $\varphi_0 = \sigma_s/R_0$, $m_z = \pm 1$ and $Z_{\perp}(\omega)$ is the transverse coupling impedance of the vacuum chamber. Since $\operatorname{Im}Z_{\perp}$ is an odd function of its argument and since

$$\sum_{m=-\infty}^{\infty} J_m^2(x) = 1,$$

the total sum of decrements in Eq.(6.1) is equal to zero. It means that at least one (betatron [$m_s = 0$], or synchro-betatron [$m_s \neq 0$]) mode is unstable. In our estimations we used an assumption that the vacuum chamber can be described as a so-called $Q = 1$ cavity

$$Z_{\perp}(\omega) \simeq \frac{\omega_s}{\omega} \frac{Z_{\perp}^{(0)}}{1 + i \left(\frac{\omega_s}{\omega} - \frac{\omega}{\omega_s} \right)}, \quad Z_{\perp}^{(0)} \simeq \frac{Z_0}{l_{\perp}}, \quad (6.2)$$

where $\omega_s = c/l_{\perp}$ is the cutoff frequency of the vacuum chamber, l_{\perp} is its radius and Z_0 is the equivalent cavity shunt impedance. Substituting Eq.(6.2) in Eq.(6.1), we obtain ($m = m_s$)

$$\delta_m = \delta_0 \int_0^{\infty} \frac{dx x}{(1-x^2)^2 + x^2} \left[J_m^2(bx - \zeta) - J_m^2(bx + \zeta) \right], \quad b = \frac{\sigma_s}{l_{\perp}}, \quad (6.3)$$

$$\delta_0 = c \frac{q I_b (Z/n)_{av} R_0^2}{p c l_{\perp}^3}, \quad (Z/n)_{av} = Z_0 \frac{l_{\perp}}{R_0}. \quad (6.4)$$

Assuming that the ring chromaticity is determined by the lattice natural chromatic-

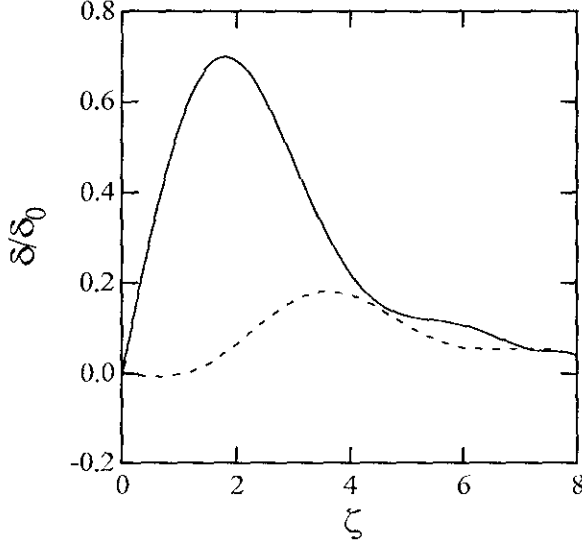


Figure 6.1: Dependence of the form-factor in the increment of the head-tail instability on the betatron phase advance on the bunch length ($\zeta = (\sigma_s d\nu/d \ln \omega_0)/R_0$). Solid line – betatron mode; dashed line – the first synchro-betatron mode.

ity

$$p \frac{\Delta \nu_{\perp}}{\Delta p} \simeq \nu_{\perp},$$

we find that in the case of ENC, the value of the phase advance of betatron oscillations on the bunch length (ξ) is about 2.5 (ions). For that reason, the integral in Eq.(6.3) was calculated numerically. The results are shown in Fig.6.1 and in the Tables 6.1 and 6.2. An inspection of the tables shows that the increments of the betatron modes exceed the beam cooling decrements. Hence, some damping mechanism must be foreseen in order to damp the instability for all energies of the particles. In particular, careful compensation of the ring chromaticity decreases the increments, which can eliminate the instability for higher energies.

The instability is the most severe for low-energy rings. As is seen from the Tables 6.1 and 6.2, in these cases, the increments of the instability can approach, or become even higher than, the frequency of synchrotron oscillations. The data in the Table 6.2 shows that for bunches of U_{238}^{92} increments of the head-tail instability are smaller than the cooling decrements. For that reason we may expect that the heavy ion

Table 6.1: Head-tail increments for betatron collective mode in electron-proton collider. Parameters in this Table are taken close to that in the Table 2.2; $(\Delta\nu_L)_{th} = \xi_i$; RF-voltage in the proton ring 10 kV and $\xi_i = 0.05$, $l_{\perp} = 5cm$ $(Z/n)_{av} = 1$ Ohm.

\sqrt{s} (GeV)	30	20	10
Proton Energy Gev	30.94	25.94	15.94
$N_i \times 10^{-10}$	1.541	1.838	2.992
Ion Bunch Current mA	0.7395	0.8818	1.434
λ_i 1/s	11.72	8.376	4.213
$(\omega_s)_i$ 1/s	377.7	412.4	525.6
δ_i 1/s	53.57	76.2	201.6
Electron energy Gev	7.5	4	1.6
$N_e \times 10^{-10}$	5.652	9.591	41.34
Electron bunch current mA	2.713	4.604	19.84
λ_e 1/s	100	15.17	0.9709
$(\omega_s)_e$ 1/s	24130	9400	2378
δ_e 1/s	810.8	2580	27800

Table 6.2: Head-tail increments for betatron collective mode in electron-U₂₃₈⁹² collider. Parameters in this Table are taken close to that in the Table 2.2; $(\Delta\nu_L)_{th} = \xi_i$; RF-voltage in the proton ring 10 kV and $\xi_i = 0.05$, $l_{\perp} = 5cm$ $(Z/n)_{av} = 1$ Ohm.

\sqrt{s} (GeV/u)	30	20	10
Ion Energy Gev	30.94	20.94	15.94
$N_i \times 10^{-7}$	2.503	3.699	4.859
Ion Bunch Current mA	0.1105	0.1632	0.2142
λ_i 1/s	16770	11040	3862
$(\omega_s)_i$ 1/s	234.8	285.3	326.8
δ_i 1/s	3.094	6.752	11.64
Electron energy Gev	7.5	5	1.6
$N_e \times 10^{-10}$	0.8446	2.725	6.177
Electron bunch current mA	0.4	1.3	2.9
λ_e 1/s	100	29.6	0.97
$(\omega_s)_e$ 1/s	24130	13140	2378
δ_e 1/s	121.1	586.2	4154

beams will suffer less due to this instability. Note also, that for a given $(Z/n)_{av}$ and a ring perimeter the increments in Eq.(6.4) increase with a decrease in the vacuum pipe radius (l_{\perp}) proportionally to $1/l_{\perp}^3$.

6.1.2 Mode-coupling instability

Since both coherent frequency shifts and increments of coherent oscillations increase with an increase in the beam current, it may occur that a coherent interaction will couple the synchrotron modes of the bunch, and the multipole number m_s will no longer classify its coherent modes. Typically, the coupling of synchrotron modes of the bunch breaks the stability of the coherent oscillations. Although careful cal-

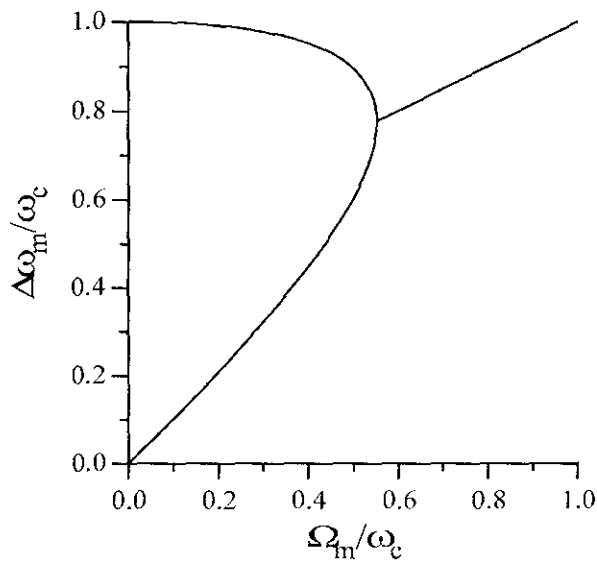


Figure 6.2: Dependences of coherent frequency shifts of the betatron and of the first synchro-betatron mode on the bunch current. The bunch becomes unstable, when these modes merge.

culations of the collective spectra in cases of practical interest requires the use of numerical methods, the lowest instability thresholds can be evaluated using a simple model, where the bunch wake is produced by a pure resistive impedance

$$Z_{\perp} = \frac{ic}{l_{\perp}^2} \cdot \frac{Z}{\omega}, \quad (6.5)$$

while all the particles in the bunch have the same amplitude of synchrotron oscillations. Such a dependence of the coupling impedance on the frequency corresponds to a step-wise dependence of the wake-fields on the distance inside the bunch. Using

such a model it is easy to show (see, for example, in [41]) that oscillations become unstable, when the betatron and the first synchrotron modes of the bunch merge (see in Fig.6.2). If we define the coherent frequency shift, calculated for the bunch with the zero length:

$$\Omega_m = -\frac{qI_b}{2p\nu_\perp} \int_{-\infty}^{\infty} dn Z_\perp(n), \quad (6.6)$$

That occurs when

$$|\Omega_m| \simeq .55\omega_s. \quad (6.7)$$

Substituting here Z_\perp from Eq.(6.5), we find the threshold value for the coupling impedance

$$\mathcal{Z} \leq \nu_s \frac{A E}{Z e I_b} \frac{l_\perp^2}{\beta_{av} R_0}. \quad (6.8)$$

Here, $2\pi R_0$ is the perimeter of the orbit, for electrons $Z = A = 1$, for ions E is the energy per nucleon, $\beta_{av} \simeq R_0/\nu_\perp$ is the typical value of β -function in a ring. This equation holds, if the bunch length (σ_s) is shorter than a typical "wake" length. If the bandwidth in frequencies is W , then $l_{wake} \simeq c/(2\pi W)$, so that Eq.(6.8) holds, if

$$\frac{c}{D_{bb}} \ll W \ll \frac{c}{\sigma_s}. \quad (6.9)$$

In the region, where $W \gg c/(\sigma_s)$, the right hand side in Eq.(6.8) gets additional factor $\simeq (2\pi\sigma_s W/c)$ so that instead of Eq.(6.8) we write

$$\mathcal{Z} \leq \nu_s \frac{A E}{Z e I_b} \frac{l_\perp^2}{\beta_{av} R_0^2} \sigma_s n_c, \quad W \gg \frac{c}{\sigma_s}. \quad (6.10)$$

Here, $n_c = 2\pi W/\omega_0$. Several examples of the threshold wideband impedances with bandwidths (W) in the range

$$\frac{c}{D_{bb}} \ll W \ll \frac{c}{\sigma_s}$$

are given in Table 6.3. In this Table we also give the value of the impedance, averaged over the harmonic band $n_c = R_0/l_\perp$

$$(Z/n)_{av} = \mathcal{Z}/n_c.$$

In spite of significant difference in the tunes of synchrotron oscillations for ions and electrons, the threshold values of impedances for electron and proton ring do not differ too much for all sets of parameters. For the region $\sqrt{s} = 30$ GeV, the proton ring is 4 times harder electromagnetically than the electron ring; for $\sqrt{s} = 20$ GeV, both rings present about same problems. In low energy region ($\sqrt{s} = 10$ GeV) the stability of bunches in electron ring requires about 30 times less threshold impedance than that for proton ring. The reason is that in such cases, the currents of electron bunches must be higher in order to achieve high luminosity.

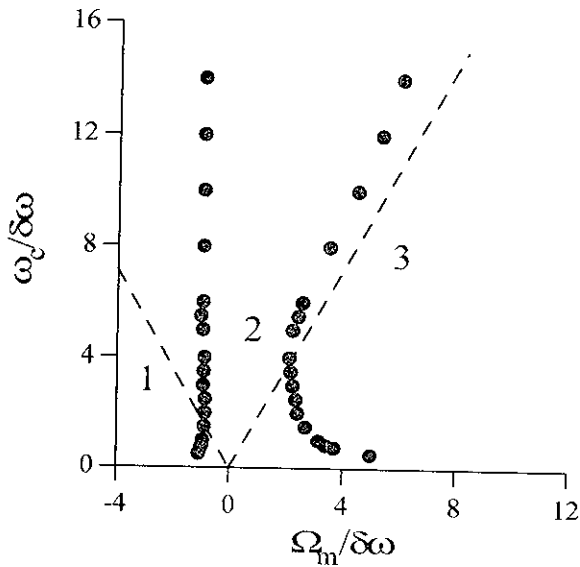


Figure 6.3: Stability diagram for the mode coupling instability due to cubic nonlinearity of betatron oscillations (full dots; $\Delta\omega_z = \kappa J_z$, $J_z \propto a_z^2$ is the action variable for vertical oscillations). Dashed lines show stability diagram for a "monochromatic beam" ($\delta\omega_z = 0$). Oscillations are unstable in the regions 1 and 3. For bunches with round cross section, when $\delta\omega_z = \kappa_z J_z - \kappa_x J_x$ with $\kappa_x \simeq \kappa_z$, the stability diagram will have more symmetrical form.

Table 6.3: Threshold values of the wideband impedances for the electron-proton mode of ENC; $(\Delta\nu_L)_{th} = \xi_i$; RF-voltage in the proton ring 10 kV and $\xi_i = 0.05$, $l_{\perp} = 5cm$.

\sqrt{s} (GeV)	30	20	10
Proton Energy (GeV)	30.9	25.9	15.9
$N_i [\times 10^{-10}]$	1.54	1.84	3
I_i (A)	0.15	0.176	0.287
$\nu_s \times 10^4$	2	2.18	2.79
Z Ohm	3294	2529	1219
$(Z/n)_{av}$	1	0.79	0.38
Electron Energy (GeV)	7.5	4	1.6
$N_e [\times 10^{-10}]$	5.6	9.6	41.3
I_e (A)	0.54	0.92	4
RF Voltage (MeV)	9.88	0.8	0.02
ν_s	0.013	0.005	0.001
Z Ohm	1.4×10^4	1702	40
$(Z/n)_{av}$	4.4	0.54	0.013

The synchro-betatron mode-coupling instability can be damped due to frequency spread of betatron oscillations, if it exceeds ω_s .¹ Such a spread can be produced by the nonlinearity of the beam-beam force, or by a special family of octupole magnets. The stability diagram for the last case is shown in Fig.6.3.

6.1.3 Longitudinal single-bunch effects

In most projects of the future (electron-positron) factories the limitations due to longitudinal single-bunch effects are addressed to the growth of the bunch length with its intensity. It implies that stability conditions for longitudinal coherent oscillations hold due to Landau damping, or due to effect of a wide-band damping system. The theory of the bunch lengthening is yet far from its completion (see, for example, in [43]), and particular designs are typically based on the half-empirical rules. Generally, the interaction of a bunch with the wideband environment results in two kinds of effects: in a distortion of the RF potential well, and in an instability of synchrotron coherent oscillations. It seems that the experimental results indicate that a flattening of the RF-well and associated bunch lengthening is observed at a lower beam current. This gives at least some basis to consider these two mechanisms of bunch lengthening separately.

A character of the potential well distortion due to bunch wakes is determined

¹The instability of the coupled synchro-betatron modes cannot be damped by the frequency spread of synchrotron oscillations [42].

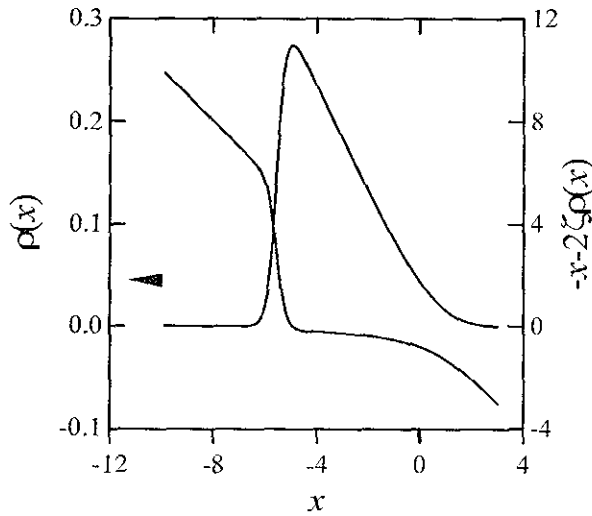


Figure 6.4: An example of the deformation of the shape of the bunch linear density with the bunch intensity and of the RF voltage of the ring due to a pure resistive wake; $N/N_0 = 9$.

by the ratio of the real and imaginary parts of the longitudinal coupling impedance. If the real part dominates, the resulting linear density of the bunch becomes very asymmetric, while the synchrotron frequency dependence on the amplitude of the synchrotron oscillations indicates a dip (see, for example, in Ref.[44] and [45] and in Fig.6.5), which may result in additional instability of both coherent and incoherent oscillations. In this case, the strength of the bunch lengthening is given by the parameter

$$\frac{N}{N_0} = \pi \frac{qI_b Z \alpha_p R_0}{v_s^2 E \sigma_s}.$$

In the asymptotic region $N/N_0 \gg 1$ the bunch length varies according to (see also in Fig.6.6)

$$\sigma_s \simeq (\sigma_s)_0 \sqrt{N/N_0}, \quad N \gg N_0. \quad (6.11)$$

For the case of ENC, when colliding bunches are long ($\sigma_s \gg l_\perp$) the inductive part of the impedance may predominate. In such a case, the selfconsistent linear density of the bunch is an even function of the distance inside the bunch, while the wake-fields result in additional defocusing of the synchrotron oscillations of particles (see, for example, in Fig.6.7). In this case, the bunch length asymptotically varies according to (see also in Fig.6.8)

$$\sigma_s \simeq (\sigma_s)_0 (N/N_0)^{1/3}, \quad N \gg N_0,$$

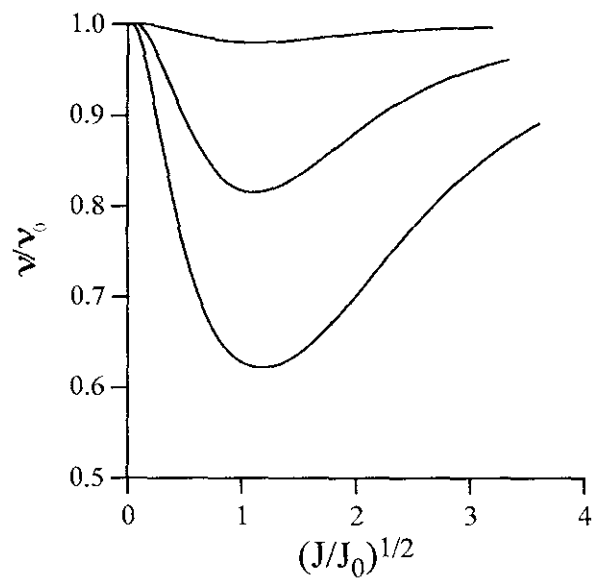


Figure 6.5: Dependence of the synchrotron tune on the amplitude of the synchrotron oscillations. From top to bottom $N/N_0 = 1, 4, 9$.

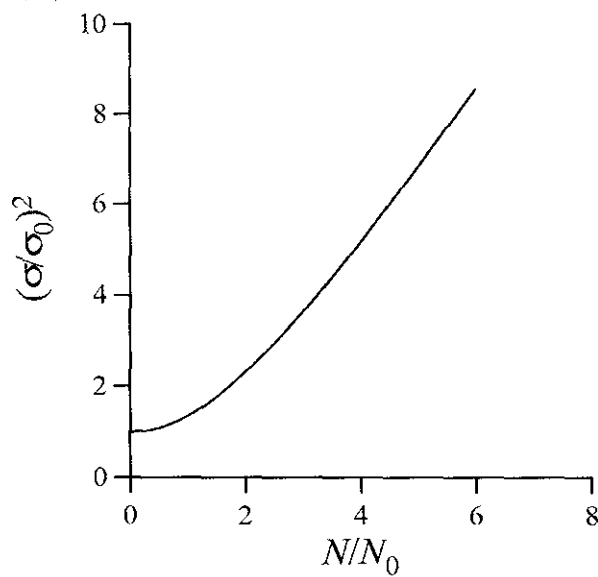


Figure 6.6: Dependence of the bunch length on N for a pure resistive wake.

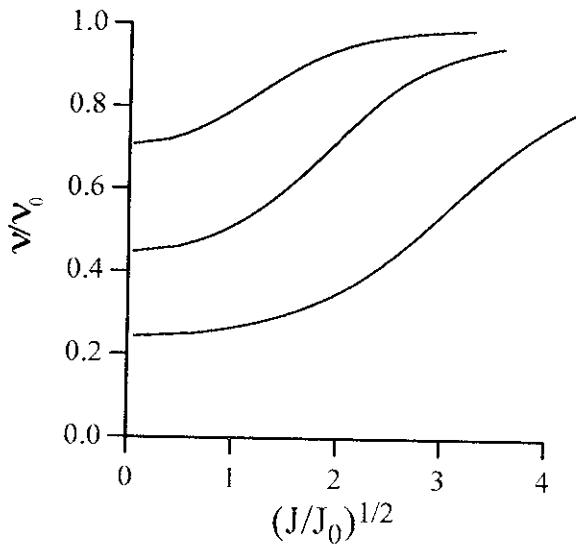


Figure 6.7: Dependences of synchrotron tunes on the amplitude of synchrotron oscillations. Pure inductive wake, from top to bottom $N/N_0 = 1, 4, 16$.

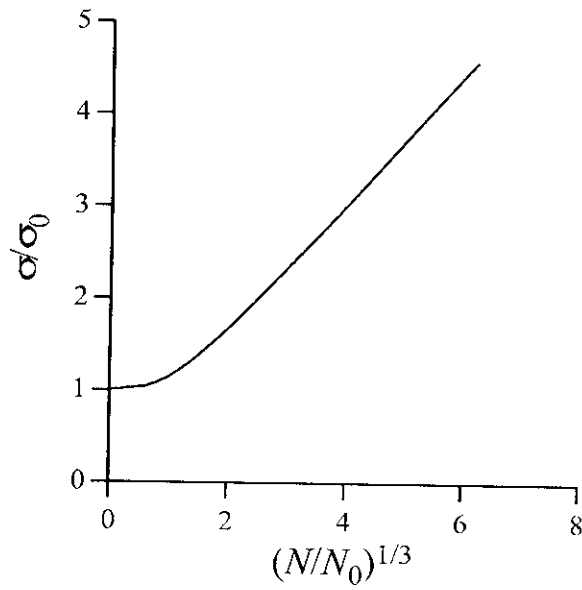


Figure 6.8: Dependence of the bunch length on its current for a pure inductive wake.

where

$$\frac{N}{N_0} = \frac{I_b(Z/n)_0 \Pi R_0^2}{\sigma_s h V \sin \phi_s l_1^2} \quad (6.12)$$

The depression of the synchrotron tunes due to interaction with an inductive element of the vacuum chamber can be described by the following formula

$$\nu_s^2 = \frac{\nu_{s0}^2}{1 + N/N_0},$$

where ν_s and ν_{s0} are relevant tunes of small synchrotron oscillations. Such a dependence of synchrotron tunes on the beam intensity decreases the thresholds of instabilities due to the coupling of the synchrotron modes. Note also, that in the case, when the synchrotron tunes are comparable to the beam-beam parameters, the distortions of the accelerating RF by the beam wakes may also affect the geometry of the beam-beam synchrotron and synchro-betatron resonances in the space of the amplitudes of the oscillations.

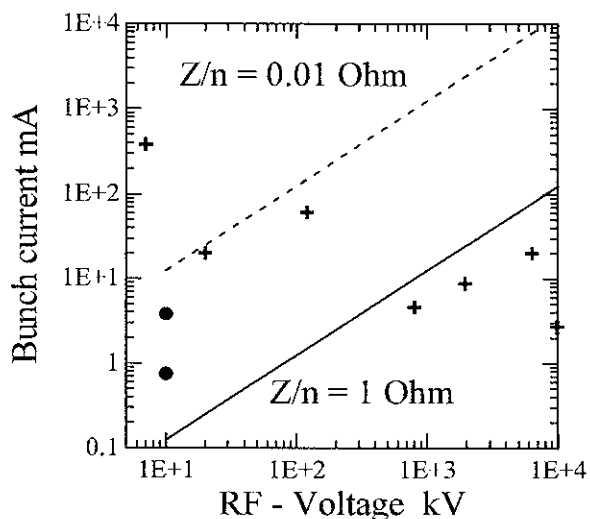


Figure 6.9: The 20 % safe margins against the bunch lengthening for the bunch current and RF-voltage in the case, when the bunch interacts with an inductive element of the chamber. Solid line corresponds to $Z/n = 1$ Ohm, dashed – $Z/n = 0.01$ Ohm; full dots show the required currents of proton bunches; full crosses – the required currents of electron bunches (see, for example, in the Table 6.3).

Safe margins for the bunch lengthening can be estimated using the formula for

σ/σ_0 obtained using the perturbation theory. It reads ²

$$\frac{\sigma_s^2}{\sigma_{s0}^2} = 1 + \sqrt{2\pi} \frac{I_b (Z/n)_0 R_0^3}{hV \sin \phi_s \sigma_s^3}, \quad \sigma_s \gg l_\perp. \quad (6.13)$$

Here, h is the harmonic number of the RF system, $V \cos \phi_s$ is the accelerating voltage and $(Z/n)_0$ is the value of the impedance below the cutoff frequency. If, for example, we demand that the bunch lengthening should not exceed 20 %, then the bunch current should be below

$$I_b \leq \frac{0.2hV \sin \phi_s}{(Z/n)_0} \left(\frac{\sigma_s}{R_0} \right)^3.$$

For low Rf-voltages that may request very low longitudinal coupling impedances (see in Fig.6.9).

6.2 Multi-Bunch Effects

If the bunch wakes last longer than the bunch-to-bunch distance the interaction of bunches couples their coherent oscillations, which can cause a multi-bunch instability of the beam. It is clear in advance that the worst stability has a beam containing n_b identical bunches. In this case, the symmetry of the stationary state relative to the rotation on the angle $2\pi/n_b$ results in the propagation along the beam of uncoupled multi-bunch modes with wave-vectors of

$$k_a = \frac{2\pi a}{n_b}, \quad a = 0, 1, \dots, n_b - 1. \quad (6.14)$$

This increase in the degrees of freedom of a multi-bunch beam makes its dynamical features more similar to the case of a coasting beam and, therefore, even more unstable when n_b increases. The main difficulty in this case is caused by the multiplication by the bunch-to bunch interaction of the multi-turn stability diagram of a single bunch. Let $\delta(\nu)$ be the multi-turn part of the decrement of a dipole mode of a single bunch. Due to the multi-turn interaction it is a periodic function of the tune ν

$$\delta(\nu + 1) = \delta(\nu). \quad (6.15)$$

Somewhere between $\nu = 0$ and $\nu = 1$ the function $\delta(\nu)$ usually changes sign, which defines the width of the stopband of the instability. As an example, we can take that this happens when ν crosses the point $\nu = 1/2$, as in the case of a resistive wall instability, or an instability due to interaction of the beam with a low-Q cavity. If, now, the beam contains n_b identical bunches, and interacts with the same system, the decrement of the a -th multi-bunch mode is defined by the same function, which, however, depends on ν and a through the following combination:

$$-\text{Im}\omega(\nu) = n_b \delta \left(\frac{\nu + a}{n_b} \right). \quad (6.16)$$

²To simplify equations in this section we write Z_n instead of $Z_{\parallel}(n)$

If, for instance, the stability condition for a single bunch is

$$0 \leq \nu \leq 1/2,$$

for n_b bunches we must simultaneously satisfy n_b stability conditions of the form

$$0 \leq \nu + a \leq n_b/2, \quad a = 0, 1, \dots, n_b - 1. \quad (6.17)$$

It means that, if some mode with a mode-number of $a < n_b/2$ is stable, its reflecting partner $n_b/2 - a$ would be unstable. Although the fact of instability seems to be independent of ν , the sum of the decrements of all multi-bunch modes

$$\sum_{a=0}^{n_b-1} \delta_a,$$

does not depend on the bunch-to-bunch coupling. Moreover, it is exactly equal to the sum of the multi-turn parts of the decrements, calculated for particular bunches while neglecting their coupling. In this sense the correct choice of ν can simplify the stabilization of unstable modes.

The multi-bunch instabilities can usually be suppressed by a relevant decrease of the Q-values; by the varying the parameters of the bunches (typically the tunes) along the beam³; and by using suitable feedback systems. The 1-st and the 3-d possibilities have been more carefully inspected to overcome the multi-bunch instability in, for example, future B-factories (see, for instance, in [2], or [1]).

In some sense, multi-bunch instabilities due to the interaction of the beam with some parasitic cavities or modes can be considered to be less dangerous. Once the parasitic element is specified, definite efforts can be spent to decrease its impedance and to cure the instability. It becomes less easy, however, for the case when the beam interacts with the fundamental mode of the accelerating RF-system. Recently [1], the instability of this kind has been reported as a serious limitation on the performance of B-factories with long rings. For short bunches ($\sigma_s \ll \lambda_{RF}$, where λ_{RF} is the wavelength of the accelerating field), the maximum increment of coherent oscillations of the beam due to its interaction with the fundamental mode of the RF-system, containing N_c accelerating cells, is defined by the parameter:

$$1/\tau_{mb} = \Omega = N_c \frac{eI(Z/Q)}{T_0 E} \frac{h^2 \alpha}{4\nu_s}, \quad h = \omega_{RF}/\omega_0. \quad (6.18)$$

These values were calculated (see in Tables 6.4 and 6.5) for parameter sets, given in the Tables 2.2 and 2.4 for $(Z/Q) = 200$ Ohm, which is typical for the normal conducting cavities. As is seen, for the proton ring the beam cooling never suppresses

³As was already mentioned, the stability of a single bunch is determined by the proper choice of the working point, and in this sense coherent oscillations of a single bunch can be done stable easily. Hence, we may conclude that a multi-bunch system can be stabilized by a suitable distribution of bunches along the orbit.

Table 6.4: Multibunch longitudinal increments in electron-proton collider; RF-voltage in the proton ring 10 kV, $(Z/Q) = 200$ Ohm.

\sqrt{s} (GeV)	30	20	10
Proton Energy Gev	30.94	25.94	15.94
Ion beam current A	0.1479	0.1764	0.2867
λ_i 1/s	11.72	8.376	4.213
$1/\tau_{mb,i}$ 1/s	230.5	472	1504
$(\omega_s)_i$ 1/s	377.7	412.4	525.6
Electron energy Gev	7.5	4	1.6
Electron beam current A	0.5426	0.9208	3.969
λ_e 1/s	100	15.17	0.9709
$1/\tau_{mb,e}$ 1/s	13.24	108.2	4608
$(\omega_s)_e$ 1/s	24130	9400	2378

Table 6.5: Multibunch longitudinal increments in electron-U₂₃₈⁹² collider; RF-voltage in the proton ring 20 kV, $(Z/Q) = 200$ Ohm.

\sqrt{s} (GeV)	30	20	10
Ion Energy Gev/u	30.94	20.94	15.94
Ion beam current A	0.022	0.0326	0.0428
λ_i 1/s	16770	11040	3862
$1/\tau_{mb,i}$ 1/s	21.42	39.03	139.7
$(\omega_s)_i$ 1/s	234.8	285.3	326.8
Electron energy Gev	7.5	5	1.6
Electron beam current A	0.081	0.261	0.593
λ_e 1/s	100	29.63	0.9709
$1/\tau_{mb,e}$ 1/s	1.979	17.59	688.5
$(\omega_s)_e$ 1/s	24130	13140	2378

this instability. For that reason, the feedback system must be foreseen to ensure the beam stability. On the contrary for the uranium beam the cooling rates always exceed the growth rates of the instability, so that such a feedback will not be necessary. In electron ring the synchrotron radiation cooling decrements are higher than $1/\tau_{mb}$ only for the energy about 7 GeV (see in the Tables 6.4) and 6.5). Hence, relevant feedback system will be necessary in this case either.

The dependences of the multi-bunch longitudinal increments on the synchrotron tune and on the mode number reads (see, for example, in [1], or [10])

$$\delta_m = m\Omega \exp\left(-\frac{\pi h}{n_b Q_L}\right) F(\nu_k, m\nu_s + a), \quad m = \pm 1, \quad (6.19)$$

$$F(x, y) = \frac{\pi}{n_b} \left\{ \frac{\cos(2\pi\alpha_-) - p}{1 - 2p \cos(2\pi\alpha_-) + p^2} - \frac{\cos(2\pi\alpha_+) - p}{1 - 2p \cos(2\pi\alpha_+) + p^2} \right\}, \quad (6.20)$$

$$\alpha_{\pm} = \frac{x \pm y}{n_b}, \quad p = \exp\left(-\frac{\pi h}{n_b Q_L}\right).$$

Here, $\nu_k = \omega_k/\omega_0$ (ω_k is the frequency of the cavity mode k), and Q_L is the loaded Q-value of the cavity. From Eqs (6.19) and (6.20) one can see that integer ratios h/n_b are the roots of the decrements (increments) of all multi-bunch modes. Therefore, tuning of the cavity in exact resonance with the beam ($\nu_k = h$) eliminates this instability. In real operation, however, to compensate for the reactance due to beam loading and to minimize the reflected power, the frequency of the fundamental mode of the cavity must be shifted down the resonant frequency ω_{RF} to

$$\frac{\Delta\omega}{\omega_{RF}} = N_c \frac{I(Z/Q)}{2V \sin \phi_s}, \quad (6.21)$$

where, $V \cos \phi_s$ is the accelerating voltage. Due to this detuning, the phase advance of the wake of the fundamental mode on the bunch spacing gets a fractional part of 2π , which increases both the increments of unstable modes and the decrements of the stable modes of the beam.

Inspections of the dependencies $\delta_m(a)$, for example, for the proton ring (see in Figs 6.10 and 6.11) indicate that except for a single mode the increments are at least 10 times small as compared to Ω . That circumstance can simplify the design of the necessary feedback system.

6.3 Instabilities Due To Captured Ions

When the beam moves along a closed orbit the collisions of particles with atoms of the residual gas produce the positively charged ions. A train of electron bunches presents for ions a sequence of focusing lenses, separated by time intervals, in which ions are defocused due to their space charge. Provided that the betatron oscillations

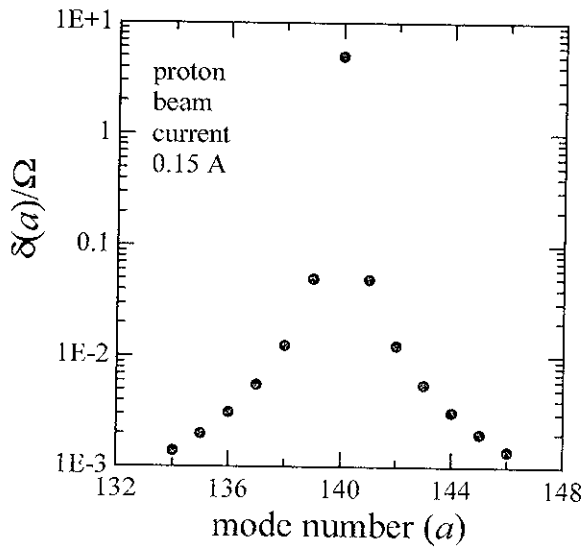


Figure 6.10: Dependence of the specific increment of the longitudinal mode coupling instability on the mode number in the proton ring. The beam current is 0.15 A, $Z/Q = 200$ $Q_L = 1000$, all remaining parameters are the same as in the Table 6.3

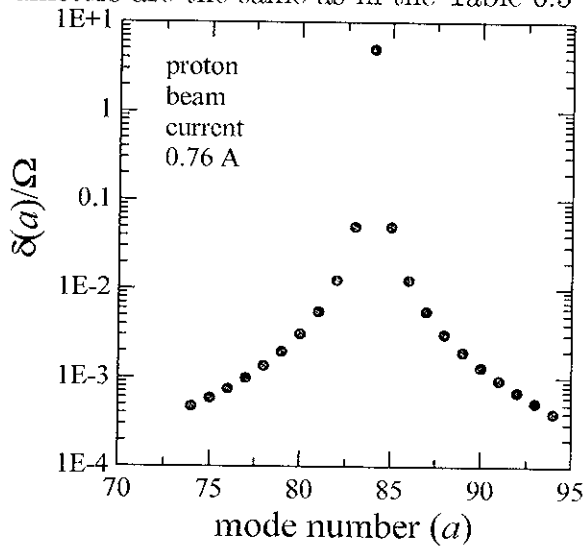


Figure 6.11: Dependence of the specific increment of the longitudinal mode coupling instability on the mode number in the proton ring. The beam current is 0.76 A, $Z/Q = 200$ $Q_L = 1000$, all remaining parameters are the same as in the Table 6.3

of the ions are stable, they can be trapped in the beam and can perturb the motion of electrons. Generally, two effects are associated with the ion-trapping. The first is a tune shift and spread due to ions, which can be estimated by (see, for instance, [46])

$$\Delta\nu = \frac{N_i r_0}{2\pi\gamma\epsilon}, \quad \epsilon = \sqrt{\epsilon_x \epsilon_z}, \quad (6.22)$$

where N_i is the number of the stored ions. For realistic parameters [46] the value of $\Delta\nu$ can reach .05. Due to the nonlinearity of the Coulomb force this effect increases the Landau damping of coherent oscillations of an electron beam and, in this sense, can be considered as being a positive one. On the other hand, since Landau damping dilutes the phase-space volume of the beam (see, for example, in [10]) it generally can limit the performance of the ring.

However, stronger limitations can be caused by the interaction of stored ions with coherent oscillations of the beam. Although the description of instabilities due to this interaction is very speculative, some of its general properties can be predicted using the analogy of this instability and the instability of colliding bunches. In particular, we may expect the unstable coherent oscillations below the resonances

$$m_z \nu_z + m_i \nu_i = n, \quad m_z m_i > 0, \quad (6.23)$$

where integers $m_{z,i}$ define the multipole numbers of collective modes of the electron and ion beams. The increments of this instability would be proportional to

$$\delta_0 \propto \omega_0 \sqrt{\Delta\nu \xi_i} \propto \omega_0 \sqrt{\frac{N N_i r_0 r_p}{A_i \gamma \epsilon^2}}, \quad (6.24)$$

and will slowly depend on the multipole numbers (m_z, m_i). Here, A_i is the atomic weight of the ion and $r_p = 1.5 \cdot 10^{-16}$ cm is the classical radius of the proton. For the reasons described in the previous section, we can expect that such an instability will be hardly suppressed by Landau damping. Since the configuration of electron and ion beams, which have different transverse sizes, is more stable [10], we may also expect the flip-flop instability of the beams.

Ions will definitely not be accumulated inside the beam if the bunch spacing is chosen to make the betatron oscillations of the ions unstable. This criterion defines the critical ratio $\mathcal{R} = N_b/n_b$ (see, for instance in [46, 47]) when the ions are swept out of the beam due to their overfocusing:

$$\mathcal{R} > \mathcal{R}_0 = \frac{2A_i \sigma_z \sigma_x (1+r)}{r_p \Pi}. \quad (6.25)$$

Here, $r = \sigma_z/\sigma_x$ is the bunch aspect ratio. If we take, for example, $A_i \simeq 30$ (CO) and $\epsilon \simeq 2 \cdot 10^{-7}$ cm, Eq.(6.25) yields $\mathcal{R}_0 = 6 \times 10^9$. This value exceeds the corresponding ratios for all realistic parameter sets (see, for example, in Table 6.3) and, without special efforts, ions definitely will be trapped in the electron ring. Additional cleaning

can be achieved by using either clearing field electrodes, or missing the necessary amount of bunches from the train. As it was found for B-factories, the missing of roughly 10% of bunches from the beam can prevent ion trapping. This method could be useful for the ENC either.

Chapter 7

Lattice Design

In order to provide the desired luminosities of ENC, the lattices of the electron and ion storage rings must enable the following operational options:

1. final focusing of the colliding bunches at two interaction points;
2. longitudinal polarization of the colliding particles at the main IP;
3. maintenance of the necessary and equal emittances of colliding bunches;
4. required cooling of the ion bunches;
5. synchronization of the revolution frequencies of electron and ion bunches;
6. required beam intensities;
7. required lifetimes of the bunches.

The simplest scheme of a storage ring, which provides these functions is a race-track with four 90° arcs and four straight sections (Fig.7.1). Two straight sections must be foreseen for the interaction regions, one – for injection and for RF-systems and another one for the emittance control of electron and ion bunches.

As it was already mentioned in Chapter 2, the operations of ENC in the energy range

$$10\text{GeV}/u \leq \sqrt{s} \leq 30\text{GeV}/u$$

and with ions from protons till U_{238}^{92} demand the magnetic rigidities for ENC rings for the electron-proton mode in the range $(BR)_i \leq 100 \text{ Tm}$, while the electron-ion modes – in the range $(BR)_i = 100 \div 200 \text{ Tm}$. Below, we describe a preliminary lattice design for ENC assuming $(BR)_i = 100 \text{ Tm}$. The main goal of these calculations is to show that desired of storage rings options can be are not too tight.

For the same reason, we do not discuss here the insertions, which equalize the horizontal and vertical emittances of electron bunches. Generally, such insertions are necessary to increase the threshold values of ξ due to round cross sections of

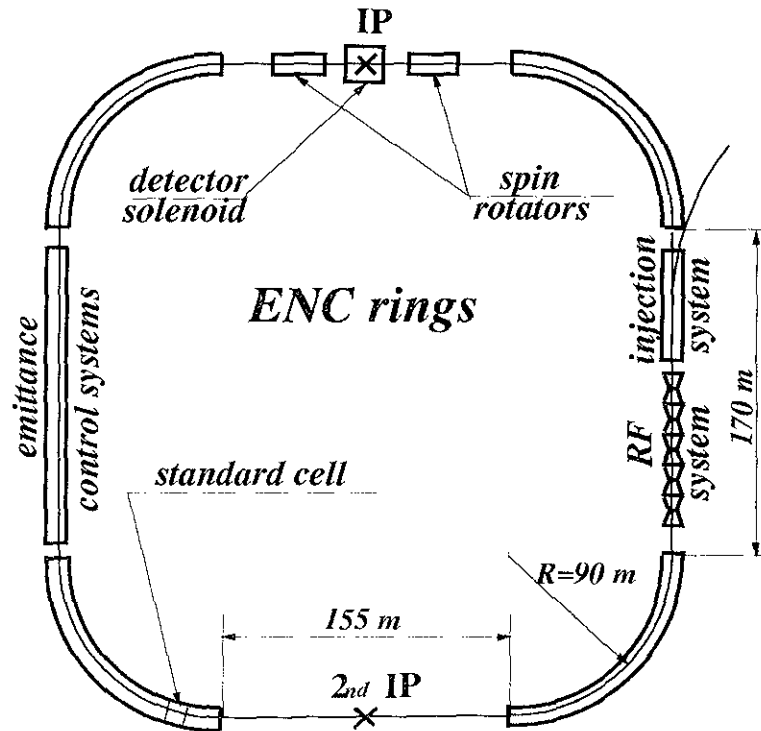


Figure 7.1: The sketch of the ENC rings.

colliding bunches. For long bunches, the expected enhancement can occur due to the described in the Chapter 3 phase averaging effect and due to decreasing of the betatron dimensions of the beam-beam resonances. It is not definitely clear, however, how important is the last point. For long bunches the beam-beam interaction still couples the betatron and synchrotron oscillations of particles. Without the phase averaging suppression it may result in significant blow-up of the bunch area. As it was mentioned in the Chapter 3, the phase averaging suppression strictly speaking demands equal horizontal and vertical β -functions at the IP only. A more reliable lattice design can be done in the future.

In this Chapter we address to the lattice design of the conventional optical functions of the rings. The polarization control and related subjects will be described in the next Chapter.

7.1 Arc Lattices

The functions of the arc optics in the ion and electron rings are different. In the ion storage ring the main goal for the arc lattice is the transporting of the beam between the straight sections, containing special insertions. In order to avoid additional blow-ups of the beam due to intrabeam scattering and due to the space charge instability, its optical functions should be as smooth as possible. As was shown in Chapter 5, that can be done using, for example, the separated functions FODO lattice.

In electron ring, the arc lattice significantly contributes to the producing of the horizontal beam emittance. The equilibrium value of the horizontal emittance of the bunch due to synchrotron radiation of electrons reads

$$\epsilon_x = 3.8 \times 10^{-4} \frac{\gamma_e^2}{G_x} \int_0^\Pi \frac{ds}{2\pi R^3} \mathcal{H} \quad [\text{nm}], \quad (7.1)$$

where R is the bending radius, $\Pi = 2\pi R_0$,

$$\mathcal{H} = \frac{D_x^2}{\beta_x} + \beta_x \left(D'_x - D_x \frac{\beta'_x}{2\beta_x} \right)^2, \quad (7.2)$$

and G_x is the so-called horizontal partition

$$G_x = \int_0^\Pi \frac{ds}{2\pi R^2} \left[1 - \frac{1-2n}{R} D_x \right], \quad (7.3)$$

n is the field index. For the lattices with the separated function magnets ($n = 0$) we have

$$G_x = \frac{1}{R} \left(1 - \frac{R_0 \alpha}{R} \right). \quad (7.4)$$

Then, if the arcs consist of N_B identical bending magnets so that $2\pi R = N_B l_B$, Eq.(7.1) yields ($\alpha \ll 1$)

$$\epsilon_x = \frac{3.8 \times 10^{-4} \gamma_e^2}{2\pi R^2} \int_0^{l_B} ds \mathcal{H}(s) \quad [\text{nm}]. \quad (7.5)$$

If the bending angle in a single dipole is small ($\phi_B = l_B/R \ll 1$), then $\mathcal{H} \propto \phi_B^2$ and Eq.(7.5) shows that the equilibrium beam emittance varies proportionally to $\gamma_e^2 \phi_B^3$ (for a given \sqrt{s} , $\epsilon_x \propto \gamma_s^3 \phi_B^3$). On the contrary, the requirement to maintain the luminosity at the level of 10^{33} $1/[\text{cm}^2\text{s}]$ per nucleon, demands a decrease in the beam emittance proportionally to $\gamma_s^{-1/2}$, which means that special tools must be foreseen in electron ring to make the bunch emittance controllable. Presently we have chosen a lattice scheme, where the arc lattices enable small emittances at higher energy of the electron ring. An increase in the beam emittance at lower electron energies must be then provided using, for example, wigglers placed in an insertion with the increased value of the dispersion function. Such an insertion can be placed in the straight section, which in ion ring is occupied by the cooling area. As we told already, the main goal of such a lattice design is to demonstrate its feasibility.

Presently, for the sake of simplicity, we design the electron and ion rings arcs as consisting of identical items (dipoles and quadrupoles). The field strengths are certainly different for both rings due to different values of the designed BR . An optimization of the arc lattice and improvements in the strategy of obtaining of the required electron beam emittances can be done during the future work.

The magnetic system of the arc lattice was designed using the MAD program [48]. The of following values

- total length of the cell (L_{cell}),
- the length of the lenses (L_{lens}),
- the length of the bending magnet (l_B) and
- total number of the elements of periodicity (N_{cell})

were used as the variable input parameters for MAD. As the output parameters we used

- the beam emittance (ϵ , for the electron ring),
- the total circumference of the arcs (L_{arc}),
- the length of the drift space (L_{drif} ; to distribute the sextupoles for the chromaticity corrections),
- the field of the bending magnet (B_{bend}) and
- the gradient field in the quadrupoles (G_{lens}).

The output parameters were required to obey the following limitations:

$$\epsilon \leq 6 \text{ [nm]}, \quad C \leq 600 \text{ [m]}, \quad L_{drif} \geq .15 \text{ [m]}, \quad G_{lens} \leq 0.215 \text{ [T/cm]}.$$

If the lengths of the bending magnets in electron and ion rings are equal, the values l_B and N_{cell} obey the additional condition. We adopt that the maximum magnetic field in the proton ring must be smaller than $B_{max} \leq 1.9 \text{ T}$ for $BR = 100 \text{ Tm}$. Then,

$$\phi_{B,max} = \frac{2\pi}{N_{cell}} = \frac{B_{max}l_B}{BR} \longrightarrow l_B \cdot N_{cell} \geq \frac{2\pi}{B_{max}/BR} \approx 330.7 \text{ [m]}.$$

After examining different schemes [49, 50] the antisymmetrical FODO structure was chosen as the standard cell (see in the Table 7.1 and in Fig. 7.2). The optical functions for both rings are shown in Fig.7.3.

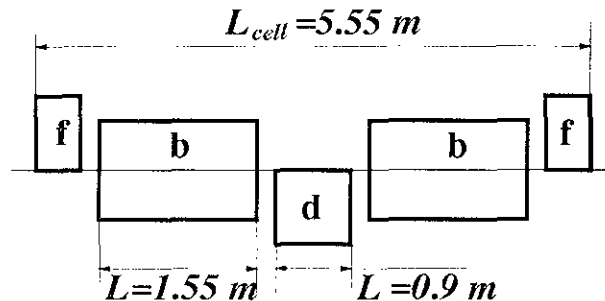


Figure 7.2: Layout of the element of periodicity for both rings.

Table 7.1: ENC standard cell for $\sqrt{s} = 30$ GeV.

parameter		electron	proton
cell	N_{cell}	108	
	L_{cell} , m	5.55	
	$N_{drift} \times L_{drift}$, m	4×0.1625	
each of 2 magnets	l_B , m	1.55	
	$\phi_B/2 = \pi/N_{cell}$	0.029088821	
	$R = 2l_B/\phi_B$, m	53.285	
	B , T	.4692	1.8767
f,d lenses	L_{lens} , m	0.9	
	G_f , T/cm	.2002	
	G_d , T/cm	-.2006	
total $L_{arcs} = 599.4$ m			

An inspection of the Table 7.2 shows that the obtained arc lattices are very rigid ($\nu_{x,y} \approx 37$ for electrons and $\nu_{x,y} \approx 8$ for protons) and are characterized by large natural chromaticities. However, we can mention as an advantage that this arc structure provides for the proton ring the transition energy below the injection energy. The Table 7.3 shows that a special devices (wigglers) must be foreseen to increase the electron beam emittance at lower energies.

7.2 Main Interaction Region

The ENC lattice should foresee two interaction regions. We remind the reader main requirements to the parameters and layout of the main interaction region. It must contain the detector solenoid ($\int Bdl = 5$ Tm, similar to TOPAZ [4]) surrounded by two spectrometer dipoles ($\int Bdl = 1.7$ Tm). The optical scheme of the main interaction region (IR) should provide the following options:

- head-on collisions;
- equal and small β -functions (≈ 10 cm) at interaction point (IP);
- electron-ion beams separation at the first parasitic IP (not less than $(5 \div 7)\sigma_{\perp}$);
- the longitudinal polarization of the bunches at IP;
- the required equipment inside detector should be placed in the cones between $\alpha = 3^{\circ}$ and $\alpha = 10^{\circ}$.

Table 7.2: Optical parameters of the ENC arc cells.

ring motion		electron		proton	
		horizontal	vertical	horizontal	vertical
Betatron tune ν	cell	.345298	.346222	.071847	.071442
	total	37.292	37.392	7.759	7.716
β_{max} ,	m	12.03	12.07	15.34	15.43
$\langle \beta \rangle$,	m	6.5	6.5	12.7	12.7
D_{xmax} ,	m	.147	0	1.781	0
Chromaticity of the arcs	cell	-.599	-.603	-.0694	-.0705
	total	-64.68	-65.106	-7.495	-7.611
Momentum compaction		.0009904		.0167982	
Energy spread		0.00088			
Transition Energy	GeV	.016		7.239	

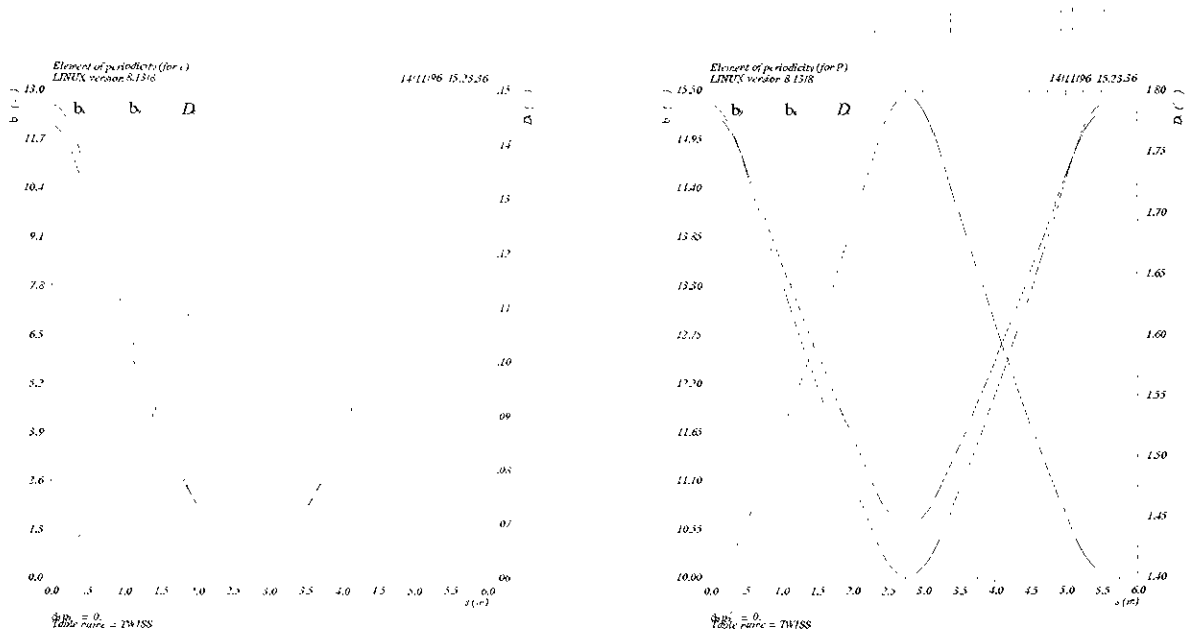


Figure 7.3: Optical functions of the element of periodicity for the electron (left) and proton (right) rings.

Table 7.3: Beam emittances for different regimes of ENC.

	\sqrt{s} , GeV	30	20	19	10
electron ring	E, GeV	7.5	4.0	3.0	1.6
	BR , Tm	25	13.33	10.0	5.33
	ϵ , nm	4.53	1.29	0.73	0.21
proton ring	E, GeV	30	25	30	16
	BR , Tm	100	83.33	100	53.3

The optical requirements for the second interaction region are not well defined yet, except for an assumption that the β -function at this interaction point can be large. For that reason, below we describe the design of the main interaction region, assuming that both interaction regions are identical [51].

Since between the final focus quadrupoles β -functions vary according to

$$\beta(s) = \beta + \frac{s^2}{\beta},$$

the first final focus quadrupoles should be placed as close as possible to the IP.

For the closed orbit perimeter $\Pi = 1000$ m and for the collision frequency 60 MHz the bunch to bunch distance is exactly equal to the length of the detector solenoid (5 m). It means that the distance between the main IP and the first parasitic IP is 2.5 m. If we want to avoid the parasitic beam-beam interactions, then the separating dipoles also should be placed inside the detector solenoid. Presently, the chosen scheme provides the beams separation in the horizontal plane.

Additional embarrassments for the final focus system occur due to the spectrometer dipoles (1 m long). It can be cured, if a spectrometer dipole is divided into two parts, while the second lens of the final focus system is placed between these dipoles (Fig.7.4). Such a scheme may also enhance the energy resolution of the spectrometer.

The separating magnet and the first lens provide a ≈ 47 mrad deflection for the electron beam which result is ≈ 60 mm beams separation at the first parasitic IP (see in Fig.7.5). These elements are placed inside the above-mentioned narrow cones. An inspection of the main parameters of the elements around IP (Table 7.4) shows that the required magnets although must be performed as superconducting, are not very tight. The figure 7.6 demonstrates the optical functions of the interaction region for both rings.

A direct matching of the optics in IR and arcs has yielded the different lengths of the IR straight sections for protons and electrons (Table 7.5). This difference is compensated by two special insertions (up- and down-stream from IP) with the length $L_{sp.ins.} = 36.74$ m, which are matched with the optics of the interaction region and arcs of the electron ring. They increase the total betatron tunes and total chromaticity of the interaction region (tunes by 2×1.0 and $2 \times .5$ and chromaticity

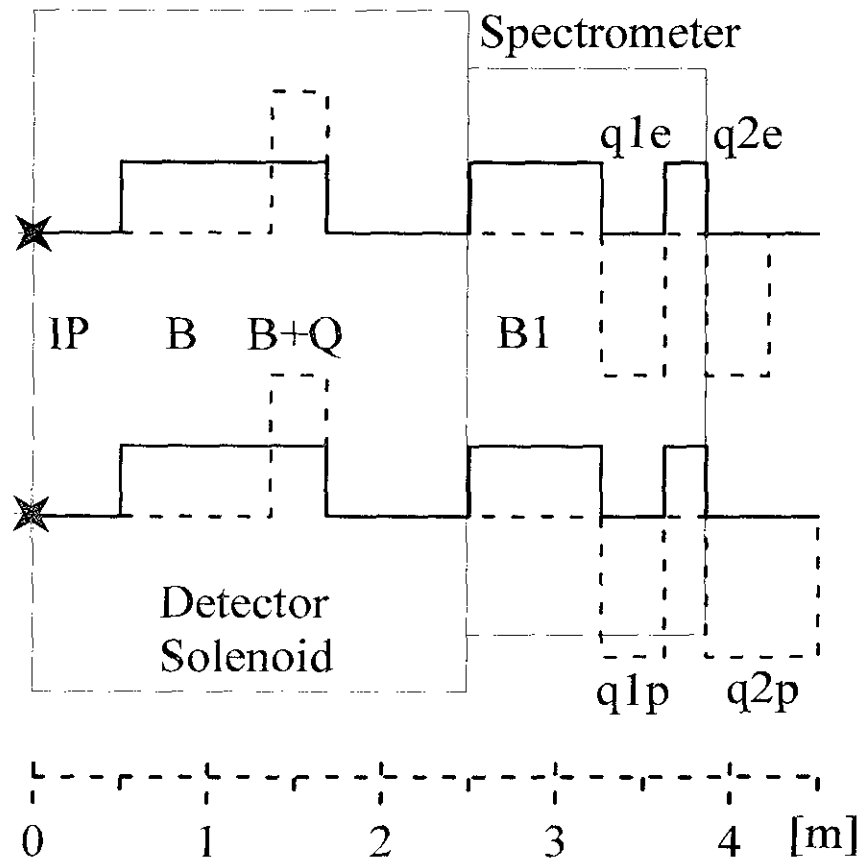


Figure 7.4: Schematic layout of the interaction region around IP for both rings; upper graph – electrons. Since the mirror symmetry is assumed, only the right half of the interaction region is shown.

Table 7.4: Parameters of the elements around IP for ENC with $\beta^* = 10$ cm.

placement	inside TOPAZ		spectrometer with $fBds = 1.7$ Tm			
element	1st magnet	1st lens	total L ,	cm	100	
dist. from IP,	cm	48.70	130.35	L_{B1} ,	cm	77.48
L ,	cm	81.64	36.49	lens L ,	cm	36.49
α (for e^-),	mrad	32.66	14.60	(inside) G , T/cm		-.2576
B ,	T	1.00		beams separation, cm		
G ,	T/cm	-	.0806	5.77 after solenoid and 10.93 after B1		

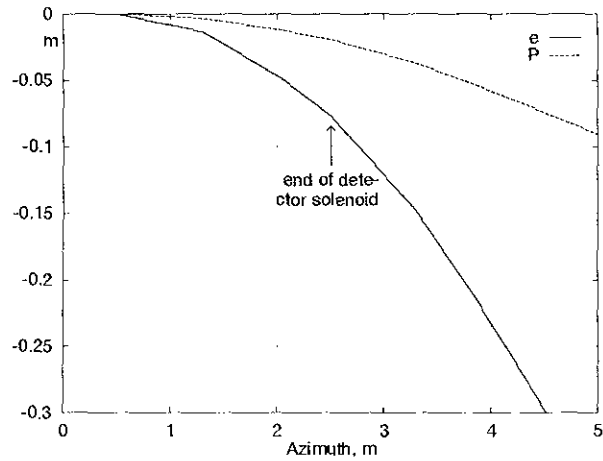


Figure 7.5: Ion (upper curve) and electron trajectories with the beam separation magnets on.

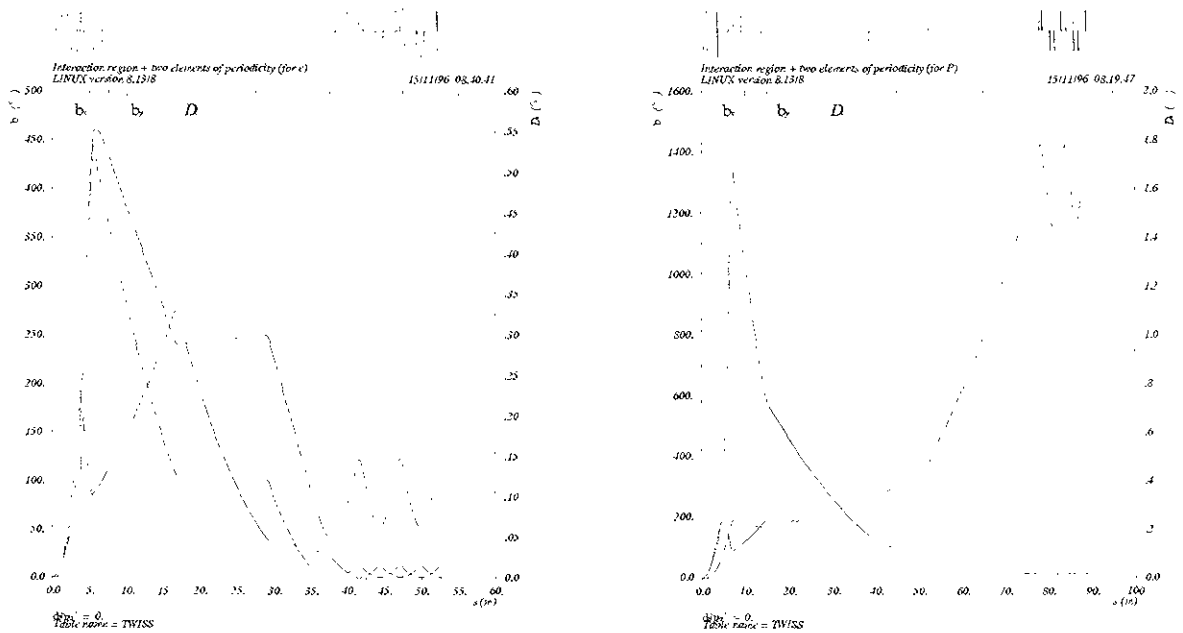


Figure 7.6: Optical functions of the interaction region + 2 arc cells for electron (left figure) and proton (right figure) rings.

Table 7.5: Main parameters of the interaction region.

ring motion		electron		proton	
		horizontal	vertical	horizontal	vertical
L_{IR} ,	m	2×41.1		2×77.8	
betatron tune ν		2×1.023184	$2 \times .856482$	$2 \times .620651$	$2 \times .510431$
β_{max} ,	m	445.6	275.0	1333.5	192.5
D_{xmax} ,	m	.55	0	1.784	0
chromaticity		-2×10.565	-2×6.600	-2×6.673	-2×4.056

by $-2 \times .451$ and $-2 \times .930$ correspondingly).

The places for the spin rotators are foreseen in the electron and proton interaction regions; besides, the places for the emittance control wigglers are foreseen in the electron ring.

7.3 Cooling Region Straight Section

The optics of the cooling straight section must provide the electron cooling area with the cooling length of about 0.02Π , zero dispersion and the β -function of about 200 m. This area must be optically matched with the adjacent arcs of the ion ring. The optical functions of the cooler insertion with a total length 60 m are presented in Fig.7.7.

7.4 Synchronization of Ion and Electron Revolution Frequencies

Colliding electron and ion bunches must have identical rotation frequencies. The required electron energies are ultra-relativistic so that for constant perimeter of the closed orbit their rotation frequency is practically constant

$$f_0 = \frac{v_e}{\Pi} \simeq \frac{c}{\Pi}.$$

On the contrary, the ion bunches in ENC are not so much relativistic. For that reason, in the energy range $\sqrt{s} = 10 \div 30$ GeV/u the rotation frequencies of ion bunches may vary significantly (see, for example, in Fig.7.8). This difference in the rotation frequencies of electron and ion bunches can be compensated varying the perimeter of the closed orbit for different energies of ions. In general, such a circumference adjustment reads

$$\frac{\Delta\Pi}{\Pi} = \Delta\beta - \frac{\Delta\omega}{\omega} = \sqrt{1 - 1/\gamma^2} - \sqrt{1 - 1/\gamma_{ref}^2} - \frac{\Delta\omega}{\omega},$$

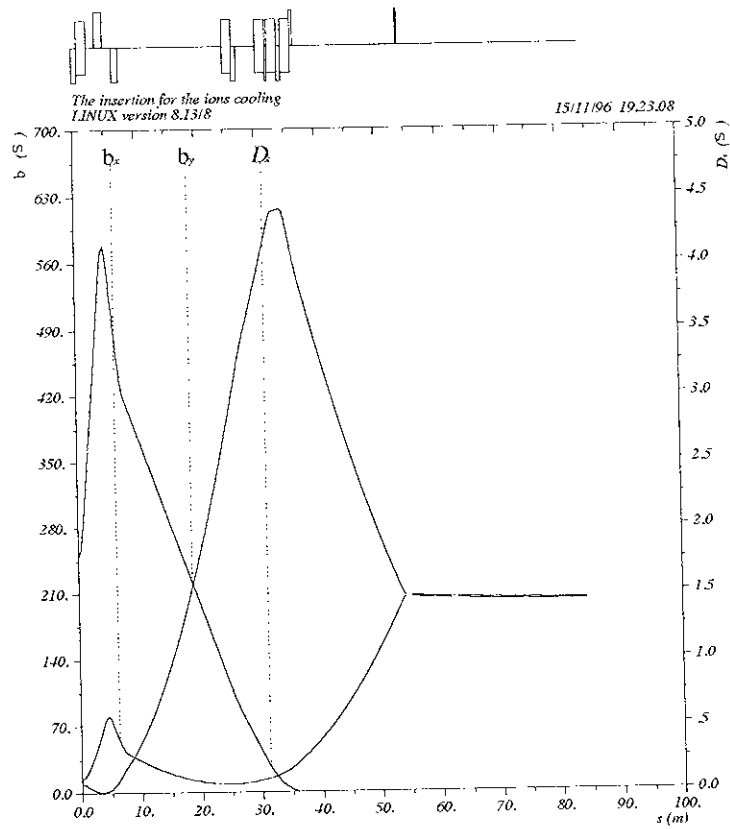


Figure 7.7: Optical functions of the cooler insertion.

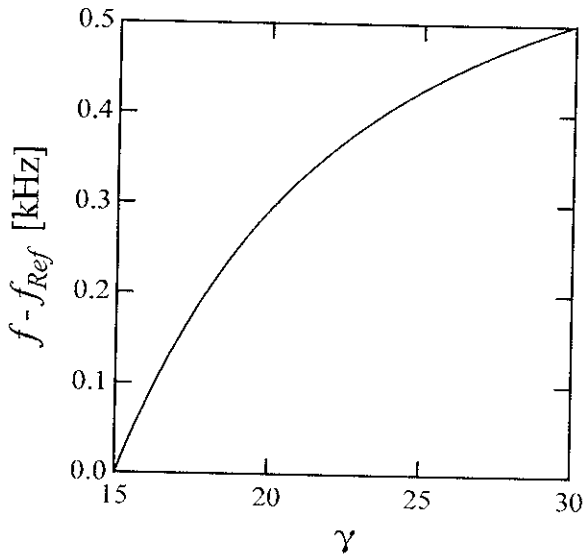


Figure 7.8: Dependence of the deviation of the rotation frequency of an ion bunch from the reference frequency on the ion energy ($\gamma = E/(Am_p c^2)$). For this figure we take as the reference point the rotation frequency for $\gamma = 15$ and $\Pi = 1$ km.

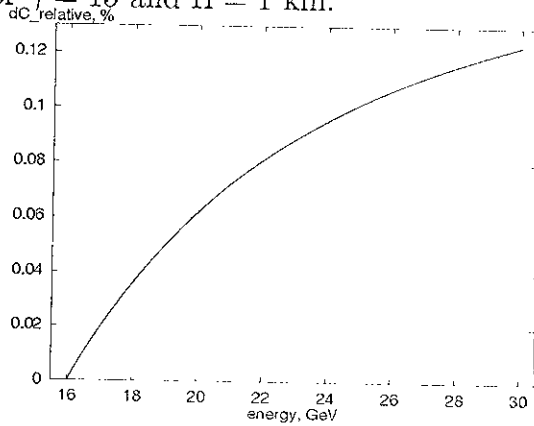


Figure 7.9: Dependence of the required adjustment on the ion energy. In this figure the reference energy is $E_{ref} = 16$ GeV/u, $\Delta\omega/\omega = 0$.

As is seen from Fig.7.9, the necessary variation of the closed orbit perimeter can be rather high.

The variation of the ion closed orbit circumference with an increase in ion energy can be done using special orbit bumps (see in Fig. 7.10). The amplitudes of the orbit bumps and values of the required fields can be considerably decreased if the total adjustment of the circumference is divided into several parts (see in Table 7.6). Each bump provides the same bending angle as the replaced arc cells. For that reason, the magnetic fields in the bump dipoles are different (correspondingly, B1 and B2 in Fig. 7.10). The betatron functions of the bump must be matched with that of adjacent arcs. Distributing these bumps in the arcs, it is possible to save the length of the technical insertions.

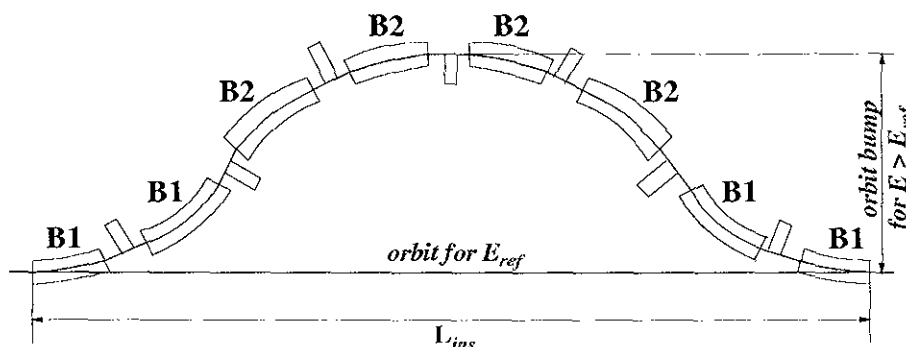


Figure 7.10: The principle scheme of the element of the adjustment system.

The Table 7.6 shows that the scheme with 8 orbit bumps (see Fig.7.11) enables the lowest (as compared to schemes with one, or four bumps) required radial displacement of the ion orbit. The operation with ion energies in the range from $E_d = 25$ GeV/u to $E_u = 30$ GeV/u can be carried out using magnets with large radial aperture (about 20 cm, see in Fig.7.12). Wider variation of the proton (ion) energies still will demand a tool enabling the radial displacement (of about 1 m, Fig.7.12) of the bump segments. The fields in the bump magnets are reasonable. The magnets do not violate the symmetry of the ring.

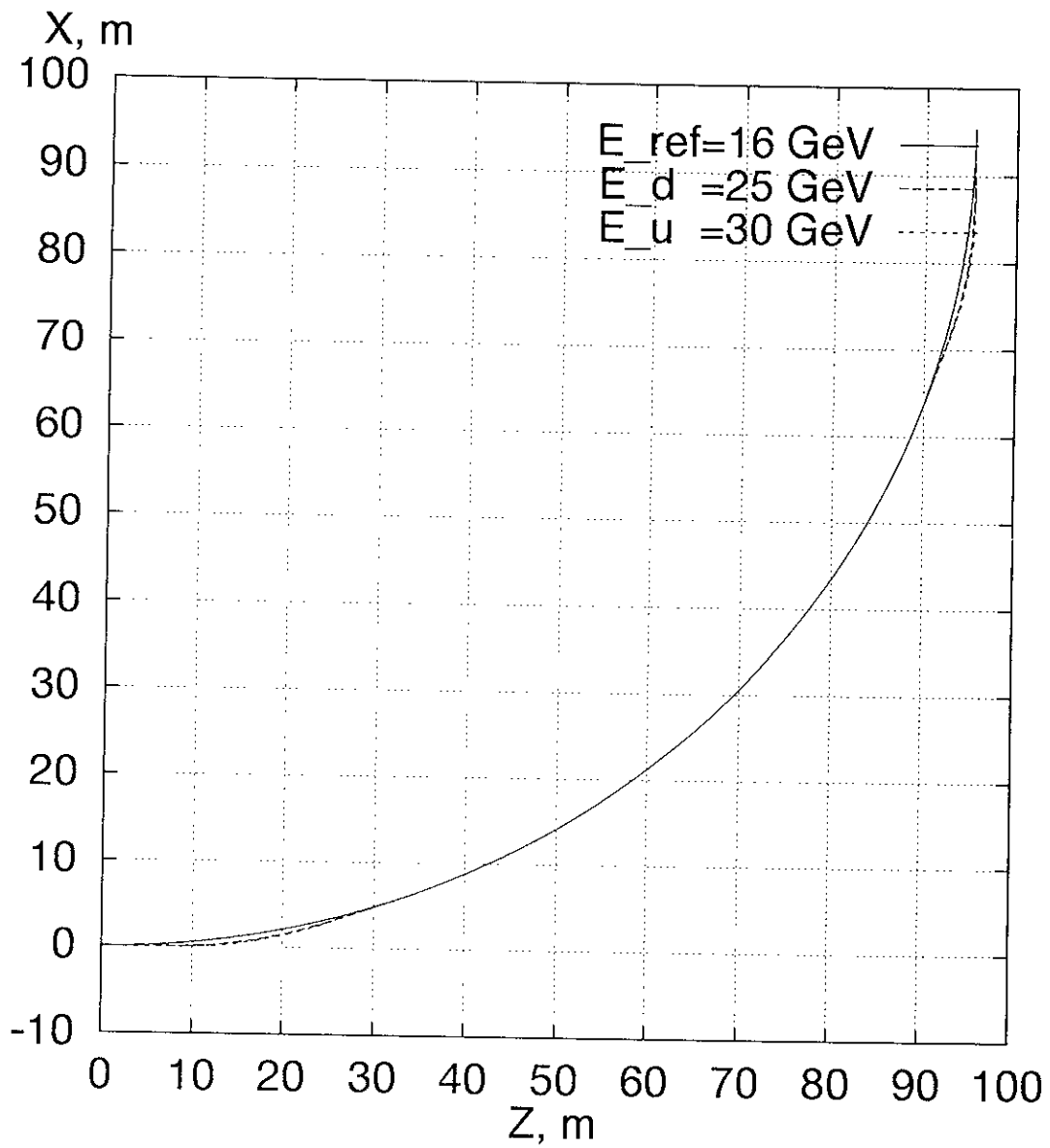


Figure 7.11: The quarter of the ring with two orbit bumps.

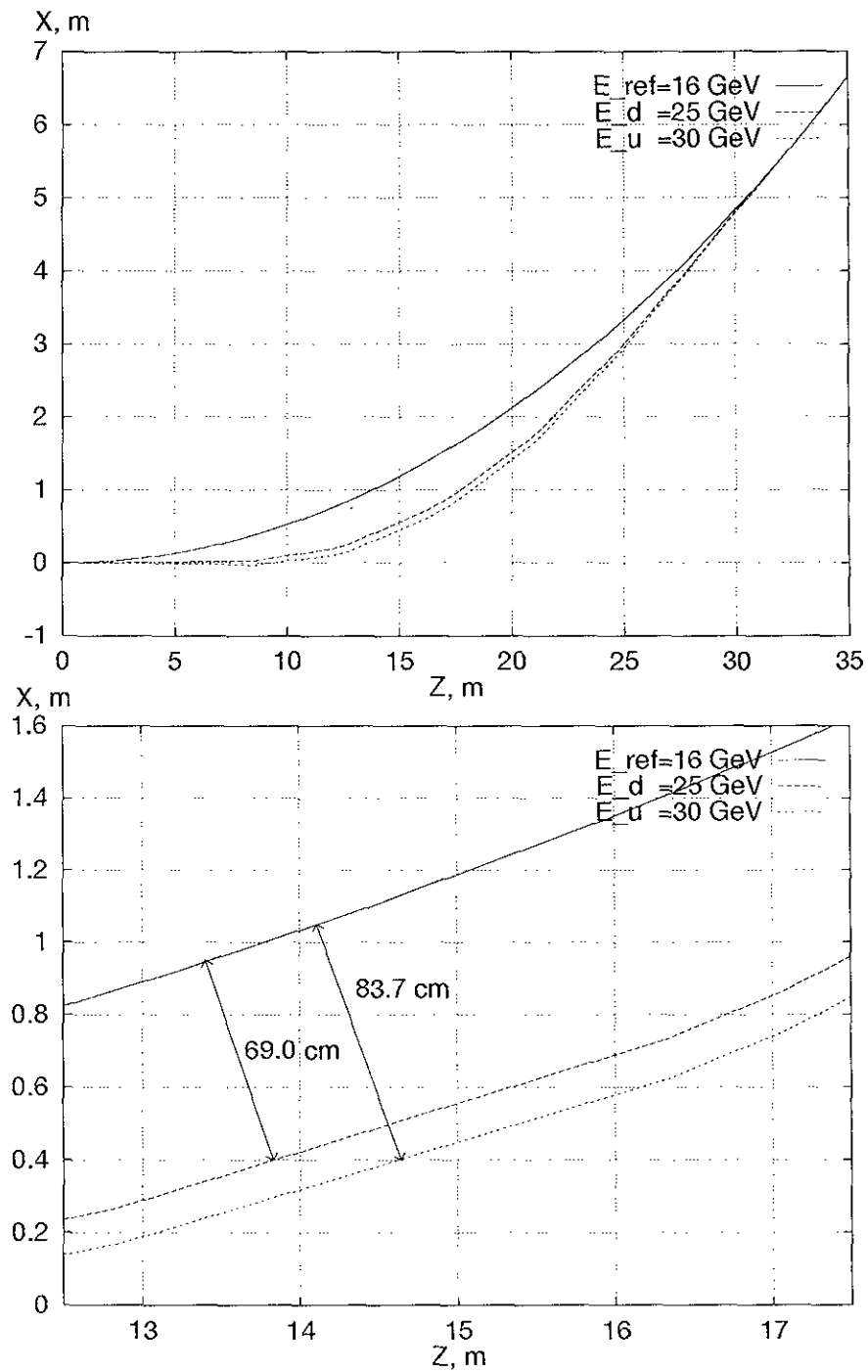


Figure 7.12: One of the two orbit bumps inside the ring quarter with different magnifications.

Table 7.6: Characteristics of the adjustment systems for
 $E_{ref} = 16$ GeV and $\Pi = 1200$ m.

GeV		$E_d = 25$			$E_u = 30$		
$\Delta\Pi$,	m	1.21965			1.47800		
Bump number		1	4	8	1	4	8
L_{B1}	m	0.35	3.5	3.5	0.35	3.5	3.5
L_{B2}	m	6.65	3.5	3.5	6.65	3.5	3.5
L_{drift} ,	m	.746	1.593	.779	.784	1.603	.784
L_{lens} ,	m	33.220	39.155	33.452	33.478	39.212	33.485
B_{B1}	T	5.3596	1.336	0.706	7.0476	4.016	0.0974
B_{B2}	T	5.3596	2.5577	2	7.0476	3.31	2.591
Total N_{bend} ,	m	8	32	64	8	32	64
Total N_{lens} ,	m	7	16	48	7	16	48
Orbit bump,	m	3.749	1.118	.690	4.127	1.277	.837
Difference of the orbit bumps ΔR for E_u and E_d							
bump number		1			4		8
ΔR ,	cm	37.8			16.9		14.7

Chapter 8

Polarization Control

8.1 Electron Bunches

The radiation polarization time of electrons (τ_p) reads

$$\tau_p[\text{sec}] \approx \frac{3440}{(E[\text{GeV}])^2 |B[\text{T}]|^3}.$$

As is seen from Fig.8.1, the values of $|B|^3$, which are necessary to reach the polarization times 10, 20, or 30 min, essentially exceed the values provided by the ring arcs. For that reason, the polarized electron bunches in ENC can be obtained either using the polarized electron source (with subsequent acceleration of particles in the injection chain accelerators), or using special wigglers (see, for example, in Table 8.1). Such a magnet was already produced in the BINP. Two such wigglers provide the required polarization time (≤ 30 min.) for $E = 7.5$ GeV, three wigglers for $E = 4$ GeV and five wigglers are necessary for $E = 3$ GeV¹. As a payment, such wigglers will decrease the equilibrium degree of polarization P_{eq} (see in the Table 8.1) and will increase energy losses of the beam due to synchrotron radiation (SR):

$$\Delta E_{SR} \simeq 3.31 \times 10^{-7} \mathcal{I}_2.$$

The contributions of these losses to the energy spread read (see also the Table 8.2)

$$\sigma_E \simeq 1.5 \times 10^{-5} \sqrt{\gamma_e \mathcal{I}_3 / \mathcal{I}_2},$$

where

$$\mathcal{I}_2 = \oint B^2 ds \quad [\text{T}^2\text{m}], \quad \mathcal{I}_3 = \oint |B|^3 ds \quad [\text{T}^3\text{m}].$$

Since after passing the IP the bunches are separated in the horizontal plane, the longitudinal polarization of particles at the IP is obtained using two spin rotations

¹For the energy 1.6 GeV the polarization time in the collider ring becomes very long. In this case, polarized electrons must be produced using a special source.

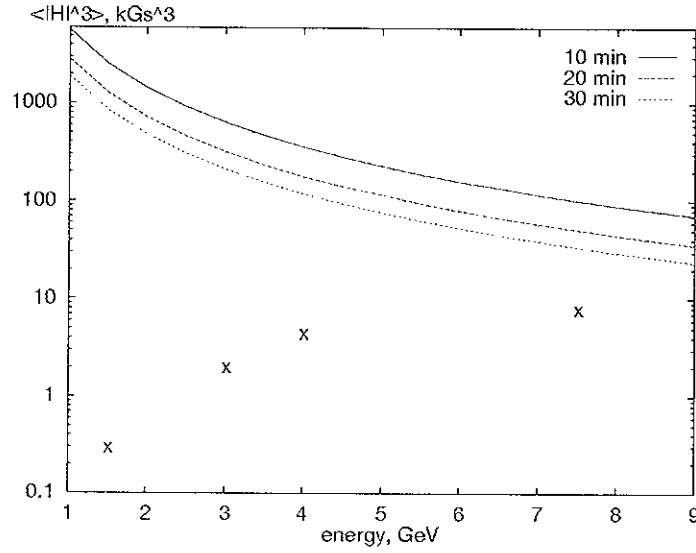


Figure 8.1: The required average cube of the field modulus for different polarization time depending on the beam energy; x — the contribution into $\langle |B|^3 \rangle$ of the arcs for $\Pi = 1.2$ km.

Table 8.1: Wiggler characteristics.

The basic pole,	T · cm	$7.097 \cdot 12$
compensating poles,	T · cm	$2 \times 1.581 \cdot 35$
Magnet length,	cm	82
$ H ^3$ ¹⁾	T ³	0.0375
$\oint B^2 ds$ ¹⁾	T ² ·cm	780
$\oint B ^3 ds$ ¹⁾	T ³ ·cm	$4.5 \cdot 10^3$
$\oint ds/R^3$ ²⁾	cm ⁻²	$1.17 \cdot 10^{-5}$
$\oint ds/ R ^3$ ²⁾	cm ⁻²	$1.33 \cdot 10^{-5}$
$P_{eq} = 92.4\% \cdot \oint ds/R^3 / [\oint ds/ R ^3]$ %		81.2

¹⁾ If one considers the variants with a different beam energy, the wiggler field B does not change.

²⁾ for $E = 3$ GeV, so that $(BR)_e = 10$ Tm.

Table 8.2: Contributions of the electron SR in arcs and wigglers to its energy loss and the bunch energy spread.

E ,	GeV	1.6	3	4	7.5
\mathcal{I}_2 for arcs,	T^2m	3.366	11.833	21.037	73.957
\mathcal{I}_3 for arcs,	T^3m	0.337	2.225	5.273	34.760
\mathcal{I}_2 for 1 wiggler,	T^2m	7.794			
\mathcal{I}_3 for 1 wiggler,	T^3m	45.611			
required wiggler number		–	5	3	1
total \mathcal{I}_2 ,	T^2m	3.336	50.80	44.42	81.75
total \mathcal{I}_3 ,	T^3m	0.337	230.28	142.11	80.4
σ_E for arcs		$2.6 \cdot 10^{-4}$	$5.4 \cdot 10^{-4}$	$6.7 \cdot 10^{-4}$	$1.2 \cdot 10^{-3}$
σ_E total		$2.6 \cdot 10^{-4}$	$2.4 \cdot 10^{-3}$	$2.4 \cdot 10^{-3}$	$1.8 \cdot 10^{-3}$
ΔE_{SR} for arcs,	keV	10.9	135.0	426.5	5273.8
ΔE_{SR} total,	MeV	.011	0.579	0.901	5.83
losses RF power (for arcs), kW		10.9	135.0	426.5	5273.8
($I_{beam}=1$ A) (total), MW		.011	0.579	0.901	5.83

[52]. First, after the arc exit the spin is rotated from the vertical into horizontal plane. This transformation is performed using the solenoidal spin rotator. Then, the spin is turned in the horizontal plane by 90° using the vertical magnetic field. For the matched particle energy and strengths of the rotating fields, the particle arrives to the IP having its spin parallel (or, antiparallel) its momentum.

It is convenient to select such a scheme of the rotator, when the vertical-horizontal coupling of the particle oscillations is localized in the rotator. In this case, the 4×4 transport matrix of the rotator will be diagonal

$$\begin{pmatrix} \mathcal{A} & 0 \\ 0 & -\mathcal{A} \end{pmatrix}.$$

It is also possible for the 2×2 matrix \mathcal{A} to have a form of the matrix of the empty space with the length (L), equal to that of the rotator

$$\mathcal{A} = \begin{pmatrix} 1 & L \\ 0 & 1 \end{pmatrix}.$$

To realize this scheme [53] the rotator solenoids must be surrounded by two lenses, which are turned in the $(x - z)$ plane on the angle $\alpha_{tilt} \simeq \pm\pi/4$ ², while a nontilted quadrupole should be placed between the solenoids (see Fig.8.2).

²More precisely, by

$$\alpha_{tilt} = \pm \frac{\pi}{4(1+a)},$$

The chosen parameters of the elements of the electron spin rotators are presented in Table 8.3, while β -functions with and without rotator are shown in Fig.8.3.

Table 8.3: Main parameters of the solenoid spin rotator (e-ring).

element	name	number	L , m	G , T/cm	$\text{sign}(\alpha_{\text{tilt}})$
lenses	q1	2	0.2	.4335	-, +
	q2	2	0.2	-.4441	-, +
	q5	1	0.4	-.3358	no
solenoid		2	3.2	$B = 6.629$ T	

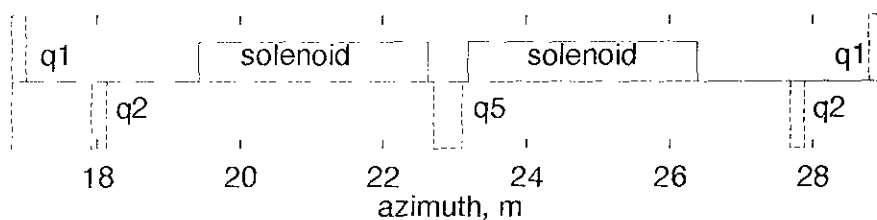


Figure 8.2: Solenoid spin rotator insertion (e-ring).

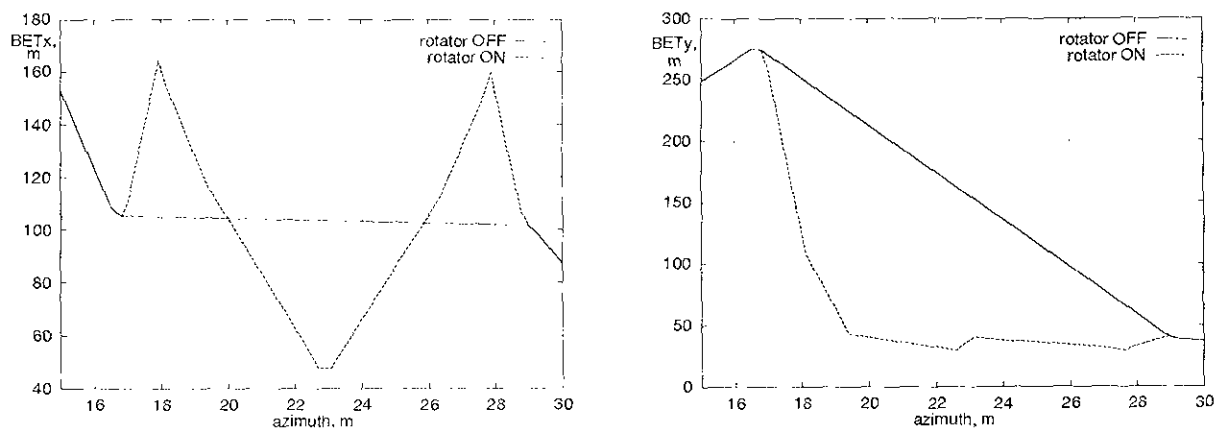


Figure 8.3: Solenoid spin rotator influence on the β -functions (e-ring).

where $a = 0.00115965\dots$ is the dimensionless part of the anomalous magnetic moment of the electron.

8.2 Ion Bunches

To work with the polarized protons it is necessary to solve two problems:

- proton acceleration without losing its polarization;
- achievement of the longitudinal polarization in the interaction point.

It is proposed to solve both problems using siberian snakes and rotators which are manufactured on the basis of spiral magnets. This decision is preferable since:

- smaller orbit disturbance than in the case of a dipole magnet snakes is achieved;
- power capacity of such snakes ($\sim \int B^2 dV$) turns to be less due to a smaller magnet aperture.

As is known, siberian snakes assure the independence of the precession frequency of the spin of the particle energy, which enable conservation of the beam polarization during its acceleration. In the last case, a correct choice of betatron frequencies permits to avoid all dangerous spin resonances.

When a particle passes the snake, its spin changes the sign. It is equivalent to a rotation of the spin on the angle π around some axes in the horizontal plane. It is convenient to define the angle between this axes and the particle velocity (ϕ). If $\phi = 0$, the snake is called as a longitudinal; if $\phi = \pi/2$ it is called as a transverse one.

The spin tune (ν) will not depend on the particle energy, if two snakes are placed on the closed orbit and are separated by the half of the orbit perimeter. In this case, the value of ν must be matched with angles ϕ_1 and ϕ_2 , which are specific for these snakes (for example, $\nu = 1/2$ for $\phi_1 - \phi_2 = \pm\pi/2$).

A "continuous" snake (with a random angle of spin rotation in it and direction of its axis in the horizontal plane) was suggested by Steffen [54]. When dipole magnets are used, its scheme takes the form [55] (see Fig.8.4):

$$S = (-H, -V, mH, 2V, -mH, -V, H),$$

where H and V are rotating magnets in horizontal and vertical planes respectively, and $m > 1$ (m is not obligatory integer!). The choice of H and V determines the spin rotation angle (180° for 100 %th snake) and the direction of its axis. The same kind of the snake can be constructed from spiral magnets. The main advantage of this choice is the achievement of a smaller orbit disturbance than in the case of a dipole magnet snake.

Though the field integral ($\int B ds$) is higher when spiral magnets are used, the power capacity of such a snake ($\sim \int B^2 dV$) turns to be, nevertheless, less, because of a smaller magnet aperture. Each magnet is characterized by the undulator factor p :

$$p = \frac{eB}{mc^2|k|},$$

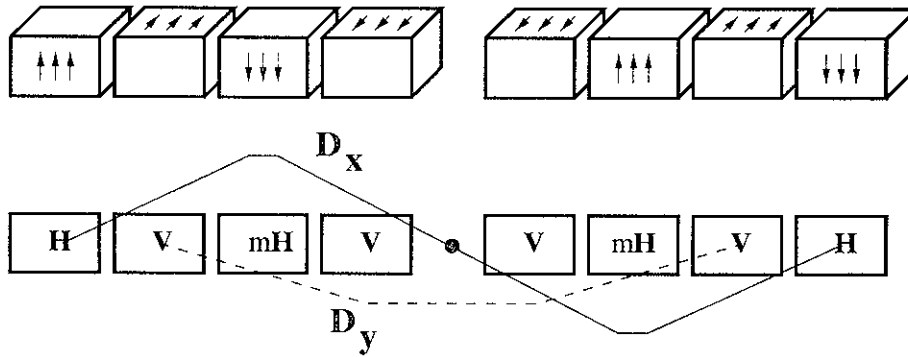


Figure 8.4: Scheme of "continuous" snake. $D_{x,y}$ are the orbit deviations.

where B is the amplitude of the undulator magnetic field. Along the undulator the magnetic field is distributed according to

$$B_x = -B \sin ks, \quad B_y = B \cos ks, \quad B_z = 0,$$

so that $k = 2\pi/\lambda$ is determined by the period λ of field transformation in the magnet; helicities of the utmost and all the central magnets coincide in pairs.

8.2.1 Acceleration of the polarized beam

In the Table 8.4 the parameters of the snakes are represented. The orbit deviation is listed for $\lambda = 2.4$ m.

Table 8.4: Parameters of the snakes.

type	number of magnets	scheme	ϕ	p_1	p_2	$f Bdl,$ Tm	orbit deviation (cm) for different energies (GeV)		
							30	25	16
A	4	$p_1 = -p_4, p_2 = -p_3$	45°	-.15	.49	25.5	2.6	3.1	4.8
B		$p_1 = -p_4, p_2 = -p_3$	0°	.27	-.35	24.5	2.0	2.4	3.8
C		$p_1 = p_4, p_2 = p_3$	90°	.26	.52	30.9	2.0	2.4	3.7

Two possible schemes can be composed from these snakes. In one scheme, two snakes of type A with opposite signs of the magnetic fields provide the acceleration of the proton beam without depolarization. In the other scheme, the snakes B and C are applied with the same result. Design of these snakes and their helicities are

shown in Fig.8.5 and 8.6. The snakes A and B use the vertical field at the entrance of the magnets, while the field orientation of the snake C is at 67° from the vertical direction.

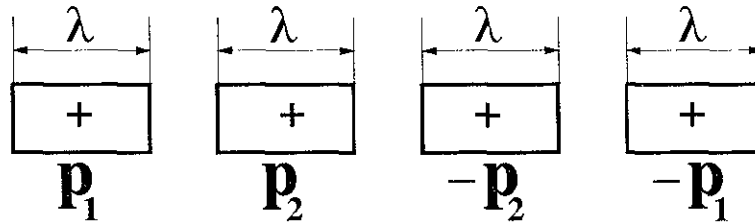


Figure 8.5: Scheme of the A-type and B-type snakes.

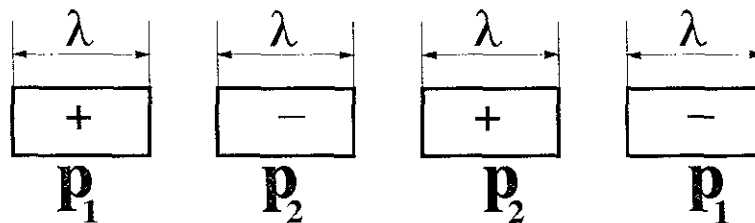


Figure 8.6: Scheme of the C-type snake.

For $\lambda = 2.4$ m the value $p = 0.5$ corresponds to the magnetic field of ≈ 4.1 T. The more precise values of the magnetic field would be obtained by direct integration spin and orbit motion along the beam trajectory, taking into account fringe fields and natural nonlinearities in helical magnets. The total length of the snake (all types) equals ≈ 10 m. The length of the snake as well as the orbit deviation are reduced proportionally to the increase of the magnetic field. Thus, the parameters are quite satisfactory.

8.2.2 Longitudinal polarization

Longitudinal polarization in the interaction point can be received using a spin rotator consisting of spiral magnets. Schemes with a different number of such magnets are possible. To separate the electrons helical magnets are used (see Fig.8.7). The snake C uses the horizontal field at the entrance of the magnets, while the field orientation of the snake D is vertical.

It necessary to note that the separation magnets used in the interaction region (with the angle ≈ 47 mrad) introduce additional small spin rotation. It will be taken into account in future.

Table 8.5: Parameters of the snakes.

type	number of magnets	scheme	p_1	p_2	p_3	$\int B dl,$ Tm	orbit deviation (cm) for different energies (GeV)		
							30	25	16
C	4	$p_1 = p_4, p_2 = p_3$.225	.357	-	22.9	1.7	2.0	3.2
D	3	-	-.209	.505	.296	19.9	2.2	2.7	4.2

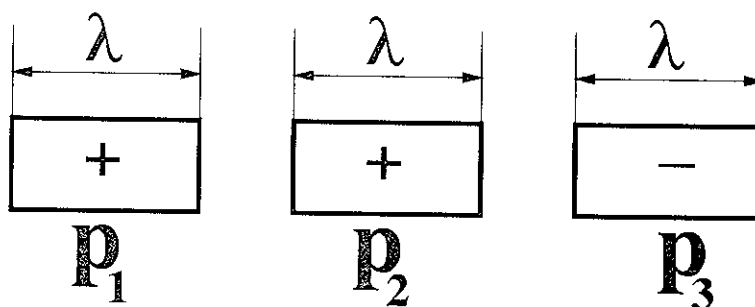


Figure 8.7: Scheme of the D-type snake.

Chapter 9

Injection Chain

9.1 General Description

The electron and ion bunches are delivered to the collider experiment energy in a sequence of accelerators providing the bunches with the parameters which are necessary for the experiments. As far as the planned experiments are going to use the polarized bunches, the accelerators in the injection chain must be capable to preserve the polarization of the accelerated bunches. Corresponding intensity requirements to injector accelerators can be found in the Tables 2.2 – 2.4 (see also in Table 9.1). These data show that lifetimes of ion bunches are long enough for all ENC modes, while the lifetimes of electron bunches can be rather short (several hundred seconds) for the heavy ion operational modes. For these modes, a requirement to maintain the average luminosity close to the level 10^{33} 1/[cm²s] per nucleon demands the full-energy injection of electron bunches in ENC. We remind the reader that the top required energy for electrons in ENC is about 9 Gev. In order to avoid huge energy losses of electrons due to their synchrotron radiation, the perimeter of such a synchrotron should be comparable to that of ENC. For that reason, with the increased level of the guiding magnetic field such a synchrotron could be used to accelerate the ion bunches either.

Additional desirable functions of the high energy ion/electron synchrotron can be figured out calculating initial cooling times for ion bunches after their injection in ENC. In these calculations we assume that the ion bunches injection chain can be based on the existing accelerators UNILAC and SIS after their relevant upgrade. Below we shall use the parameters of the SIS given in Table 9.2 (see also in [58]):

The cooling time of an ion bunch after its direct acceleration to the colliding experiment energy reads

$$\frac{1}{\tau_c} = \frac{Z^2 2\lambda_e r_e r_p c L_c \sqrt{\beta_c}}{A \gamma^5 (\epsilon')^{5/2}}. \quad (9.1)$$

Here, $\lambda_e = n_e 2\pi\beta_c \epsilon$ is the linear density of the cooling electron beam, $\sqrt{2\pi\beta_c \epsilon}$ is its rms radius, $\epsilon' = \epsilon_{inj} \gamma_{inj} / \gamma$ is the emittance of the injected beam after its acceleration

Table 9.1: Intensity and energy requirements for the electron-proton and electron- U_{238}^{92} modes of ENC.

\sqrt{s} [GeV]	10	20	30
Protons			
$N_i \times 10^{-10}$	3.656	2.585	2.111
Energy [Gev]	17.21	24.34	29.81
BR [Tm]	57.3	81	99.3
Radiat. Recombination Lifetime [h]	87	61	50
$N_e \times 10^{-10}$	43.32	15.31	8.336
Energy [GeV]	1.4	4.1	7.5
BR [Tm]	4.67	13.6	25
Bremsstrahlung Lifetime [h]	50.55	22.63	15.01
Bare uranium ions			
$N_i \times 10^{-7}$	7.5	5.32	4.35
Energy [Gev/u]	13.57	19.19	23.51
BR [Tm]	117	165	200
Radiat. Recombination Lifetime [s]	786	556	434
$N_e \times 10^{-10}$	13.2	4.668	2.541
Energy [GeV]	1.8	5.2	9.6
BR [Tm]	6	17.3	32
Bremsstrahlung Lifetime [s]	1672	766	520

Table 9.2: Short SIS Parameter List.

Perimeter [m]	216.7		
BR (injection) [Tm]	1.8		
BR (top) [Tm]	18		
Magnet bending radius [m]	10		
Straight section length [m]	5.99		
Number of bunches	4		
Beam emittance [mm]	5000		
Beam energy spread	0.001		
Cycle period [s]	3		
Ions	p	Ne ¹⁰	U ⁷³
Kinetic energy [Gev/u]	4.5	2.0	1
$(\gamma\beta)_{\max}$	5.74	2.89	1.89
Ions/cycle $\times 10^{10}$	20	10	2.0

till the final energy ($A\gamma Mc^2$).

The calculations of the cooling times with parameters given in the Table 9.2 yield the cooling times, which from protons till bare uranium ions range from about a half till several hours (see the second lines in Tables 9.3 and 9.4). These cooling times are certainly too long especially for the collider modes working with heavy ions, where the lifetimes of electron bunches are short. The required duration of the ENC injection cycle for protons can be estimated as follows. According to data from Table 9.2, the proton beam in ENC containing about 3.6×10^{12} protons using relevant rebunching of the extracted from SIS beam can be obtained during 18 SIS cycles (about 1 minute). After subsequent acceleration, the cooling of these bunches depending on the experiment energy will take from 0.7 till about 5 hours. These numbers estimate the required injection cycle periods of ENC, if the bunches are cooled at the top energies. In this case, the low-energy beam intensity in the high energy synchrotron can coincide with the extraction beam intensity from SIS.

Table 9.3: Cooling times of proton bunches in electron-proton collider; precooling energy 4.5 GeV, the density of the cooling electron beam $n_e = 3 \times 10^8$ 1/cm³, energy of the cooling beam 2.89 MeV.

\sqrt{s} GeV	10	20	30
High energy cooling time (without precooling) [h]	0.7	2.3	4.7
Injection precooling time [s]	273	273	273
Injection energy Laslett tune shift	0.018	0.013	0.010
High energy cooling time [s]	35	49	60
Precooled emittance [nm]	908.3	642.3	524.4

Table 9.4: Cooling times of bare uranium bunches in ENC; precooling energy 1 GeV/u, $n_e = 3 \times 10^8$ 1/cm³, energy of the cooling beam 1 MeV, the recombination lifetime at SIS extraction energy is about 700 s.

\sqrt{s} GeV	10	20	30
High energy cooling time (without precooling) [s]	1411	4746	9650
Injection precooling time [s]	0.044	0.044	0.044
Injection energy Laslett tune shift	0.03	0.020	0.017
High energy cooling time [s]	0.27	0.27	0.27
Precooled emittance [nm]	1470	1039	848.7

The injection cycle periods can be made significantly shorter, if prior to acceleration the bunches are precooled at the extraction energy of SIS, or at some intermediate energies. The bunch emittance after precooling is determined by the threshold

value of the Laslett tune shift at the precooling energy. The precooling electron beam density especially in the electron-proton mode cannot be as high as that in the main cooling system. Taking as a reasonable value $n_e = 3 \times 10^8 \text{ 1/cm}^3$ within the radius 0.5 cm (the cooling beam current about 1 A), we find the numbers, given in Tables 9.3 and 9.4. The gain is strong for the heavy ion modes of ENC, where the required cooling times decrease from thousands seconds to 0.27 s. In the electron-proton mode the precooling will result in significant benefit in the injection cycle periods only in the case, if the full ENC intensity injection in the high energy synchrotron is possible.

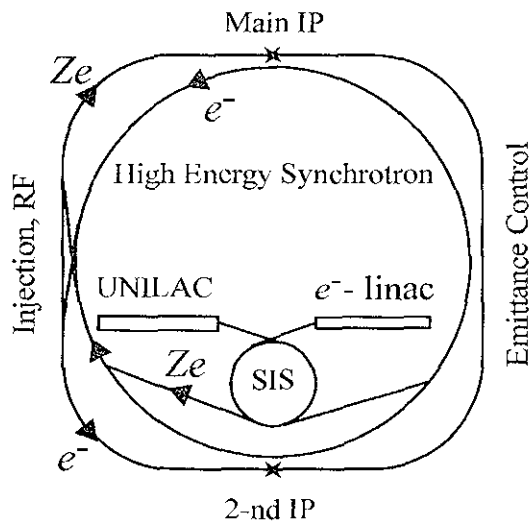


Figure 9.1: ENC injection scheme using SIS as an electron booster

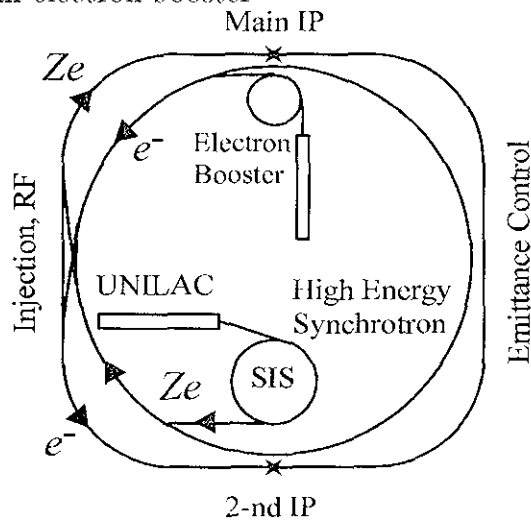


Figure 9.2: ENC injection scheme using additional electron booster

Two examples of the ENC injection schemes with the full-energy injection in the ENC are shown in Figs 9.1 and 9.2. The first one employs SIS either as the booster synchrotron for electrons. Since the injection magnetic rigidity of SIS is 1.8 Tm, the final energy of electron linac should be 540 MeV. The top magnetic rigidity of SIS corresponds to electron energy 5.4 GeV. If the closed orbit radius is held 10 m, an electron will lose the energy 7.65 MeV per turn. The perimeter of SIS may contain up to 43 electron bunches, which is 1/5-th of the electron ring ENC current. So that the required power of the RF-system can be estimated as 4.6 MW. These figures are maybe a little bit high for the booster synchrotron. A decrease in the extraction electron energy from SIS twice reduces the required accelerating voltage and the RF-power 8 times. Remaining acceleration of electrons can be done, if necessary, in the high energy synchrotron.

If an employment of SIS as an electron booster is not desirable, the electron injection chain must be supplied with the electron booster synchrotron. The extraction energy from this synchrotron could range from the lowest required electron energy for ENC (1.4 GeV) till, say, 3 GeV ($BR = 10$ Tm). In that case, the required variation of the magnetic field in the high energy synchrotron will be not too wide (10 - 200 Tm).

9.2 Electron Linac

9.2.1 General scheme of the electron linac

A list of the possible main injector parameters is given in Table 9.5.

Table 9.5: Main injector parameters.

Final energy	500 MeV
Number of electrons per bunch	$5 \cdot 10^{10}$
Repetition rate up to	120 Hz
Energy spread: electron bunch	$\pm 1\%$
RF frequency	2856 MHz
Klystron pulse power	~ 63 MW
Number of klystrons	3

The main components of the injector are shown in Fig. 9.3. The injector comprises a thermionic electron gun, a buncher, and 500 MeV electron linac [59, 60]. All parts of this accelerator enable to provide a single bunch regime at the repetition rate up to 120 Hz.

The thermionic 200 kV triode gun delivers 2 ns pulse current of 10 A. The emittance of the beam is less than 10^{-2} cm. This bunch passes the subharmonic buncher

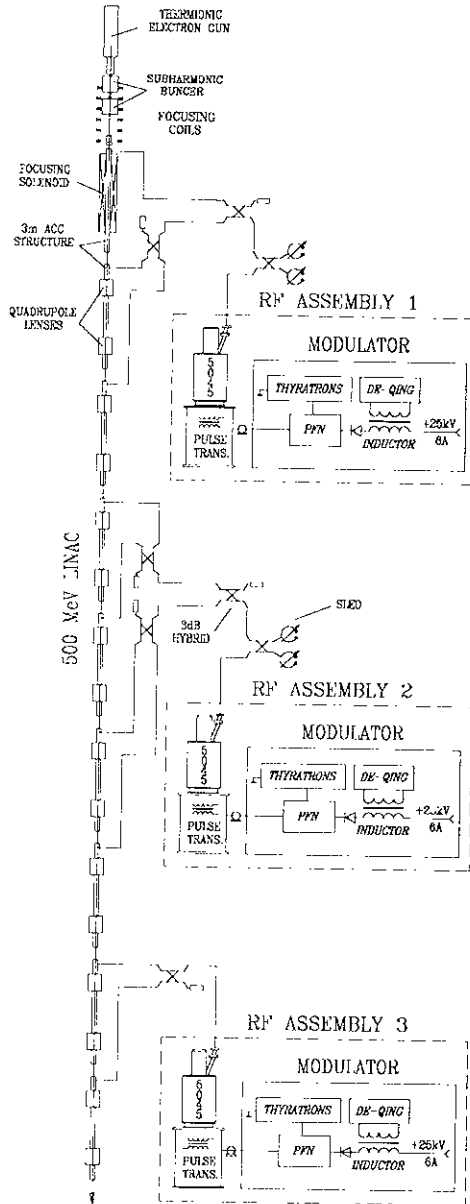


Figure 9.3: General scheme of the injector.

operated at the 16-th subharmonic of the basic frequency of 2856 MHz. The buncher contains two quarter-wavelength cavities with drift gaps. The transverse focusing of the beam is made using the longitudinal magnetic field, which is produced by current coils, placed around the cavities. Such a bunching system provides a 200 ps bunch on the exit of the S-band bunching section. S-band buncher operates at the back travelling wave with exponentially increasing accelerating field and provides a 20 ps electron bunch at the entrance of the first accelerating structure [62]. The short bunch length is needed to provide a small energy spread ($\pm 1\%$) during a further acceleration.

The 500 MeV linac consists of 9 accelerating sections which are 3 m long and have a constant impedance structure operating at a travelling wave ($2\pi/3$). The transverse focusing of the bunch along the linac is realized by the solenoid field at the first section of linac and two quadrupoles in each of the other sections. The accelerating gradient in the first section is 25 MeV/m, and in the other sections it is up to 18 MeV/m.

The 9 accelerating sections are powered by 3 RF modules which can base on S-band klystrons 5045 (SLAC, USA). This klystrons provides 63 MW, 4 μ s RF pulse at 2856 MHz. A SLED power compression system permits to obtain the necessary gradients of accelerating fields. The output power of SLED is fed to three or four accelerating sections. In order to maintain the reliable capturing, the first section of linac have higher accelerating rate. It is attained by applying half of the RF power from the power compression system of the first klystron to these section, then the second half of this power is divided equally between two regular sections. The power of the second klystron is divided half-and-half between four regular sections (the power is divided by 3 dB hybrids). The third klystron feed two last sections without any power compression system.

9.2.2 RF module

The RF module for example consists of a 5045 klystron and a high voltage pulse modulator. The high voltage pulse for the klystron is produced by the modulator. The modulator is a conventional line type modulator with an oscillatory charge of a pulse forming network (PFN). It consists of a high voltage power supply, a charging choke, PFN and a thyatron switch [61].

9.2.3 Beam diagnostic.

The beam diagnostic system of linac can be divided by two parts. The first one provides a single bunch diagnostic at maximum repetition rate and has no significant influence on the beam. This system includes a wall current monitor placed just after the gun, and 9 Beam Position Monitors (BPM) mounted at the entrance of each section. The second system includes 4 movable beam profile monitors and magnetic spectrometer with Faraday cup placed at the end of accelerator. This system destroy

the beam, but give us information about transverse bunch size, energy, energy spread and total bunch charge.

9.2.4 RF control system.

RF control system includes the low power RF driving system, the RF measurement system, the subharmonic buncher RF system and the system for sections and SLED thermostabilising.

9.2.5 A rough cost estimation.

The S-band RF system forms the main part of linac cost. Including all expenses comes from another systems of linac, the rough evaluation of the linacs cost should be near 1000 k\$ /100 MeV. Note, that this number will not be valid for the energy range below 200 MeV.

9.3 The Full-Energy ENC Filling-up Scenario

Let us briefly discuss the ENC filing-up scenario for the case, when the full-energy injection is realized. The sequences of the required operations with electron and ion beams for the first ENC filling-up procedure is listed below. With full energy injection subsequent injections demand smaller amounts of particles and can be done during a single injector cycle. Such further injections could be done for electron – light ion modes once per 3 hours, or once per 10 hours depending on the experiment energy. The electron-heavy ion modes of ENC demand more frequent (once 500 s – 1 hour) additional injections of electron and ion bunches. If the polarization of electron bunches is made in ENC using the wigglers, the item 4 can be skipped. In such a case, the ENC filling time with electron beam is reduced to a single cycle polarization time (10 – 20 min).

- Filling-up of ENC with electron bunches (about 10 min per cycle, total about 50 min):
 1. extraction from electron linac ($E_f = 0.54$ Gev) and filling-up of the electron booster synchrotron (about 40 bunches, during 1 s);
 2. preacceleration in electron booster synchrotron 0.54 Gev \rightarrow 3 GeV;
 3. injection in the high energy synchrotron and acceleration till top energy;
 4. waiting for the beam polarization (about 10 min or so);
 5. deceleration till required energy;
 6. injection in ENC;
 7. bunch shaping (longitudinal and transverse);

8. repeat injection cycle 5 times.
- Filling-up of ENC with proton bunches (about 25 min per cycle);
 1. rebunching of the SIS beam (4 → 20 bunches);
 2. injection of 2×20 proton bunches in the high energy synchrotron (6 s);
 3. precooling (about 5 min);
 4. acceleration till desired energy;
 5. injection in ENC;
 6. repeat injection cycle 5 times;
 7. final cooling in ENC (about 1 min);
 8. switch off the bunch separation at the interaction points.
 - Run.

In the electron – heavy ion ENC modes the filling-up of ENC with ion bunches takes several seconds. The electron bunches must be changed, or must get additional deposits about each 1–2 min. These time intervals are very short for the bunch polarization and may demand the generation of electron bunches using the source of the polarized electrons. According to data from Tables 9.2 and 9.5 the filling time of ENC can be then reduced to several seconds.

Since the positions, width and, generally, the shape of the ion bunch footprints essentially depend on the intensity of electron bunches (two interaction points)

$$\Delta\nu_i = 2\xi_i - \Delta\nu_L, \quad \xi_i \propto \frac{N_e}{\epsilon_e},$$

without special efforts short lifetimes of electron bunches may result in the decreases in the lifetimes of ion bunches due to, for example, crossing of resonances by ion oscillation tunes. For that reason, the working point of ion beam must be corrected

Chapter 10

Basic Technical Systems

As could be seen from previous Chapters, the required ENC beam parameters can be obtained using the storage rings employing technical systems, which are more or less ordinary for electron and ion storage rings of this size and working in the desired energy ranges. Detailed design of these ordinary systems is out of scope of this study and can be done in a reliable way in the future. In this Chapter we focus on the discussion of the technical systems, which can limit the ENC high luminosity performance.

10.1 Main Interaction Region Magnets

One of the severe ENC design demands is a requirement to leave free of the optical elements the small and the large collision angle cones. For that reasons, the optical elements in the interaction region, which are necessary to squeeze the beam at IP and to separate the bunches at the parasitic IP must be placed within the equipment cones ($3^\circ \leq \alpha \leq 10^\circ$, see also in Fig. 10.1). For the magnets placed close to the interaction point the embarrassments occur due to small available transverse distances. Outside the detector solenoid the required parameters of the quadrupoles become too tight. For these reasons, the ENC magnets in the main interaction region (see in Chapter 7 for their parameters) should be performed as superconducting ones. Examples of such dipole and quadrupole magnets are shown in Figs. 10.2 and 10.3.

10.2 RF-systems

Since the required RF-voltage in the ion storage ring is only 50 kV, the designing of the RF-system of this ring should not present any difficulty for light ion modes. For the heavy ion operation modes relevant feedback systems must be foreseen to compensate the cavity detuning due to their beam loading.

RF-systems of the high energy synchrotron (or of the upgraded SIS) should enable the ion beam rebunching.

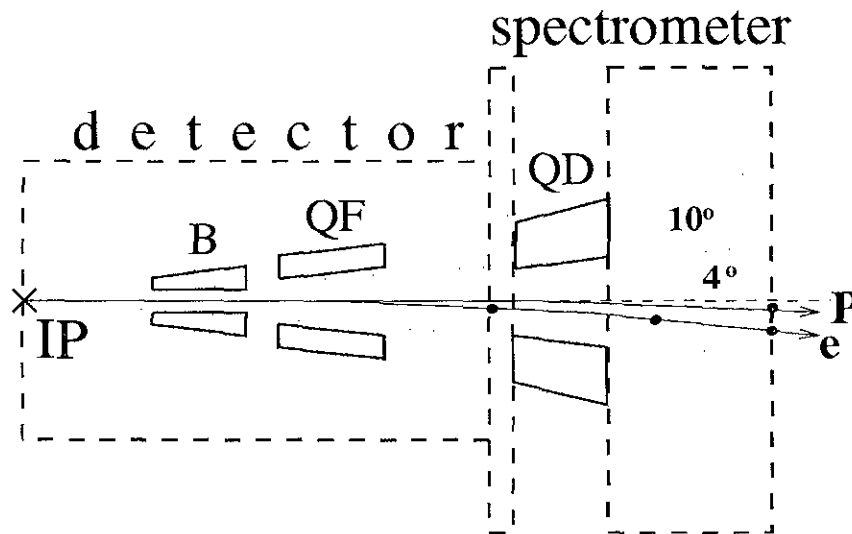


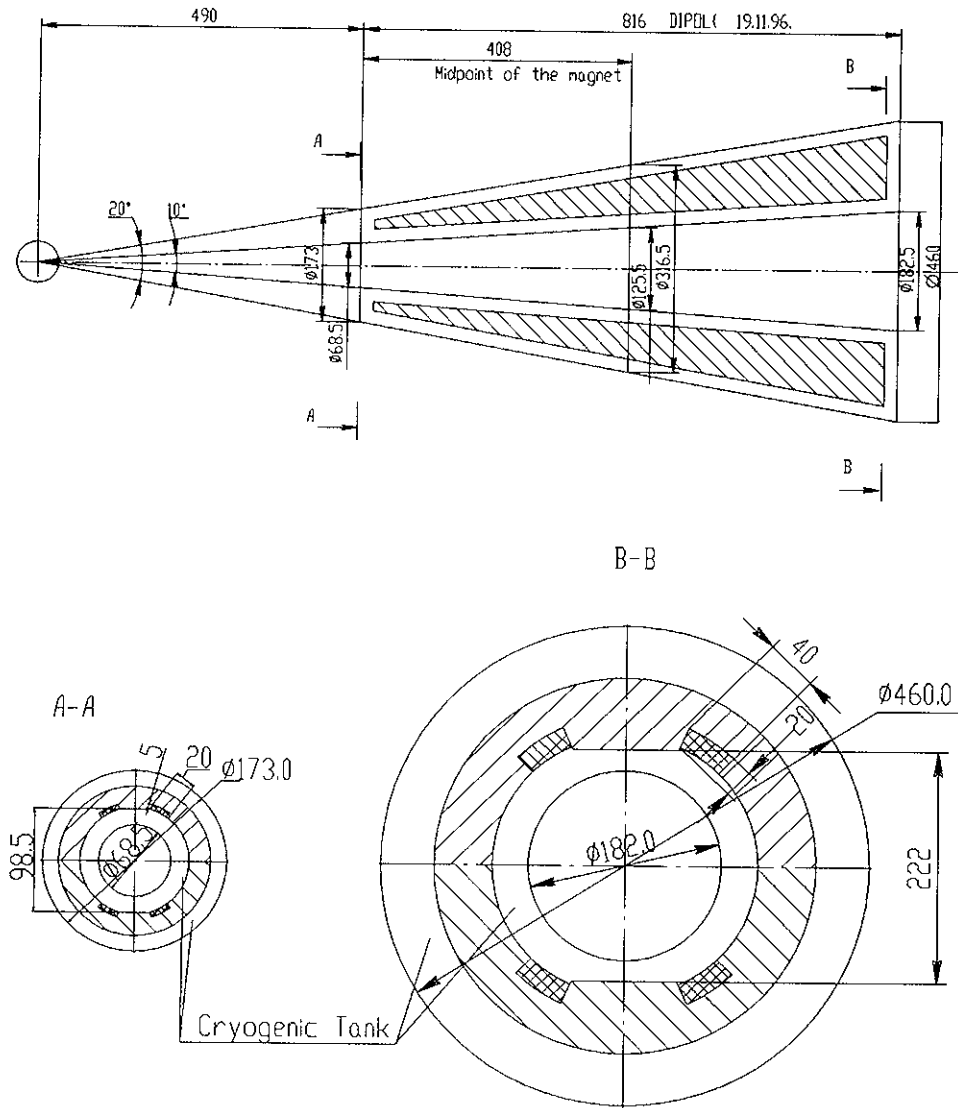
Figure 10.1: Schematic layout of the optical elements in the main interaction region; D - dipole, Q - quadrupole.

The RF-voltage in the electron ring must be sufficient to compensate their synchrotron radiation losses. As is seen from the Tables 2.2 - 2.4, in the high energy operational modes the required RF-voltages should be several MeV per turn, while the RF-system power should reach 4 MW. These parameters are close to the RF-system demands for the future B-factories. Examples of relevant RF-system designs can be found, for instance, in Refs.[1] and [2]. Definite precautions should also be taken to decrease the higher order modes impedances of the cavities. Designing of the RF-system for electron ring should take into account rather high cavity detuning in the low energy light ion operational modes.

10.3 Technical Design Study of the Cooling Device

10.3.1 Cooling region solenoid

As far as an employment of strong electron cooling is one of the main requirements for the high luminosity performance, the optical system of the cooling region must ensure small disturbances of both ion and electron motions. In Chapter 4 it was shown that the required damping times are feasible, if the strength of the solenoidal field will be close to 0.5 T. Since the angular divergence of the magnetic force lines simulate additional electron velocity spread, it must be sufficiently small. A typical angular divergence in the ion beam $\sqrt{\epsilon/\beta_{cool}} \simeq 3 \times 10^{-6}$, determines the required divergence of the magnetic force lines. Although such a level of the transverse magnetic field



Position A-A: 100 kAtrns

Position B-B: 200 kAtrns

Figure 10.2: Sketch of the first superconducting separating dipole inside the detector solenoid.

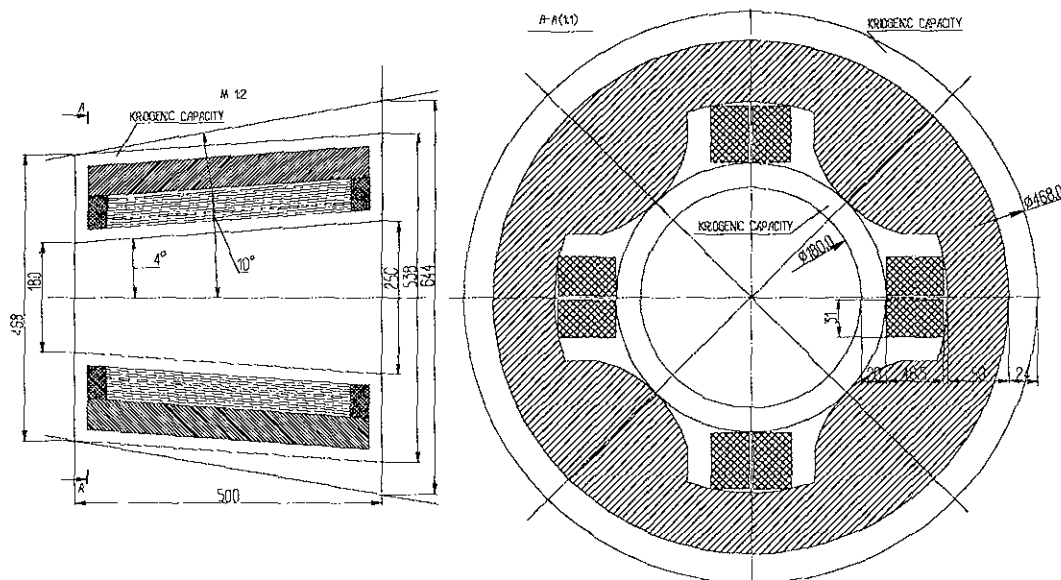


Figure 10.3: Sketch of the superconducting quadrupole inside detector solenoid.

in the cooling region is a tight, an installation with close requirements was already manufactured in BINP for SIS ion synchrotron [63].

In this Chapter we discuss an employment of the traditional DC-current device for electron cooling of ion bunches in ENC [64]. The proposed recently scheme employing the bunched electron beam from a linac, or another source still demands additional study and testing.

10.3.2 High voltage accelerator

Configuration diagram of the proposed accelerator is shown in Fig. 10.4. Main elements of the accelerator are the following: a high-voltage rectifier, accelerating tubes, recuperation device rectifier. They are placed inside a tank filled with elegas under a pressure of 12 bar. For the accelerator with the energy higher than 7 MeV an additional electrode is supposed to be used to reduce its overall dimensions. Fig. 10.5 shows a sectional view of the accelerating tubes and a high-voltage terminal. The tubes are located in a solenoid which creates magnetic field up to 0.1 T. Power consumed by the solenoid is 8 kW/m. The high-voltage rectifier and solenoid are transformer supplied. The recuperation rectifier, ion pumps with power supplies, injector control unit, collector cooling system are located in the high-voltage terminal. Power of the recuperation rectifier is 10 kW.

Alternative designs of accelerators for an energy of 5, 7, 10, and 15 MeV were examined. Main parameters of the variants considered are presented in the Tabl. 10.1:

The accelerator tank overall dimensions were determined meeting a condition of providing the electric strength. When choosing a configuration the following consid-

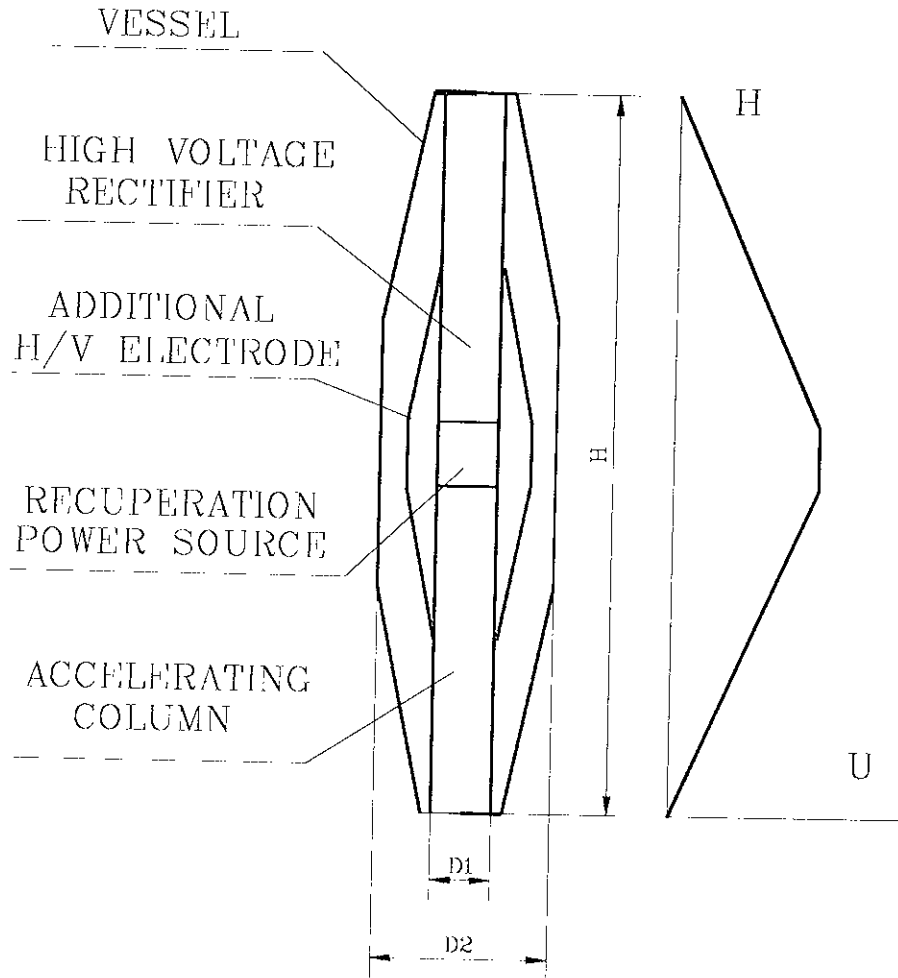


Figure 10.4: Configuration of the accelerator.

Table 10.1: Main parameters of accelerators.

Energy of electrons,	MeV	5	7	10	15
Height of tank H ,	m	11	15	21	31
Diameter of column D_1 ,	m	0.9			
Maximal diameter of tank D_2 ,	m	2.5	2.5	3	4
Mass of tank,	tonnes	6	7.5	17	38
Mass of solenoid,	tonnes	5	7	10	15
Volume of tank,	m^3	50	65	125	310
SF6 Mass,	tonnes	4	5.2	10	25
Power consumed,	kW	65	90	130	200

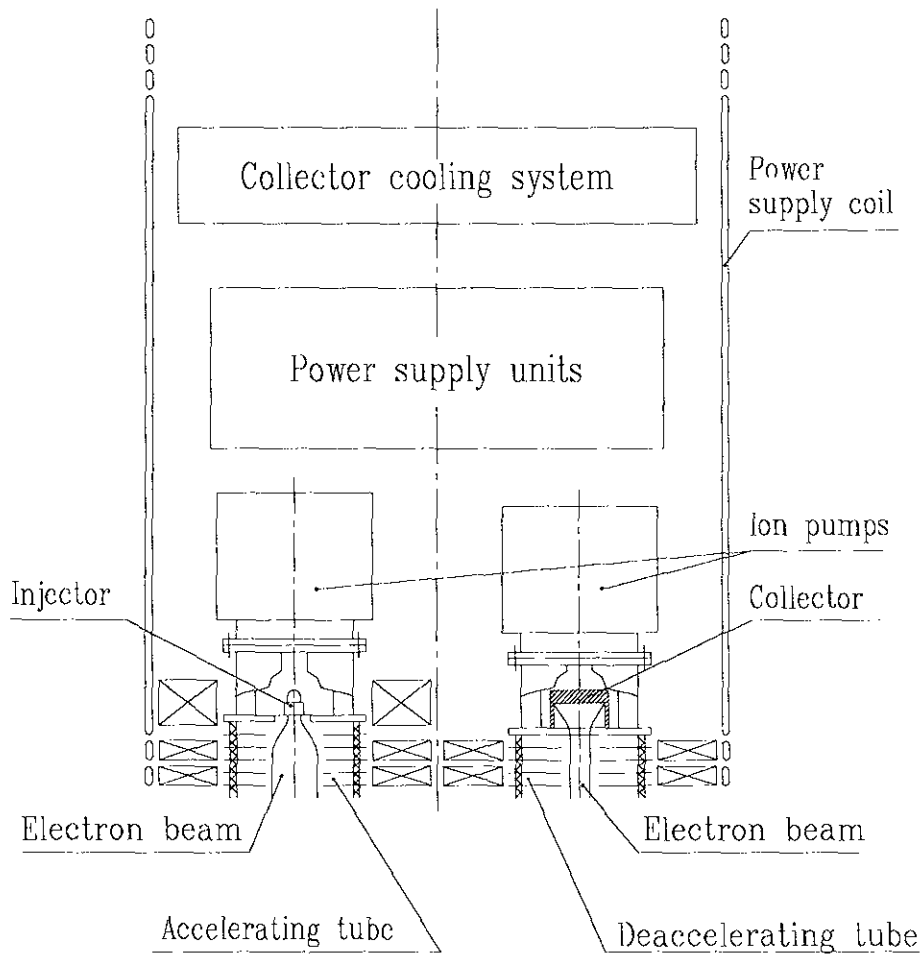


Figure 10.5: A sectional view of the accelerating tubes and a high-voltage terminal.

erations were taken into account. In a case when the accelerator column ends with a sphere electrode, the electric field intensity at the electrode surface is determined from the relation $E = 2U/r_1 = 4U/r_2$, where r_1 and r_2 are radiuses of inner and outer electros, U is a voltage of a high-voltage gap. Hereinafter the equations for the electric field intensity are given at an optimal relation of the electrodes radiuses. In a case when a tandem arrangement is used, the high-voltage electrode is of a cylinder form, and the electric field intensity $E = U/r_1 = 2.718U/r_2$. In the latter case, the tank radius is 1.47 times less and the area is 2.17 times less than in the variant with a sphere electrode. As far as the accelerator lengths differs more than twice, the tank volume at the tandem arrangement is slightly smaller. Besides, in this case the rectifier and solenoid are spaced apart through the length, it allows to provide their separate supplying and independence of energy and magnetic field adjustment.

As the practice shows the long accelerating tubes operate reliably at an acceleration rate no more than 1 MeV/m. The same gradient is close to a maximal one for a high-voltage cascade generator. So the accelerator total length is determined on this basis. The tank diameter is determined from a gas insulation electric strength of about 200 kV/cm. Presence of gaps between the high-voltage rectifier sections and accelerating column leads to 20 - 30 % increase of the maximal electric field intensity as compared to the case with a smooth cilinder. Thus, the tank and column diameters should be choosen meeting the condition of 150 - 160 kV/cm intensity at a surface of the smaller cylinder. At a voltage of more than 7 MV it is advantageous to use an additional electrode at an intermediate potential. In this case the intensity is determined from the formula $E = 0.423U/R_1 = 1.917U/R_2$, and it is 1.4 times less than that of the variant without an electrode at the same outer radius.

The following data were used to estimate the solenoid power consumption. The solenoid sectional view is shown in Fig. 10.6. Diameter of the accelerating tube in

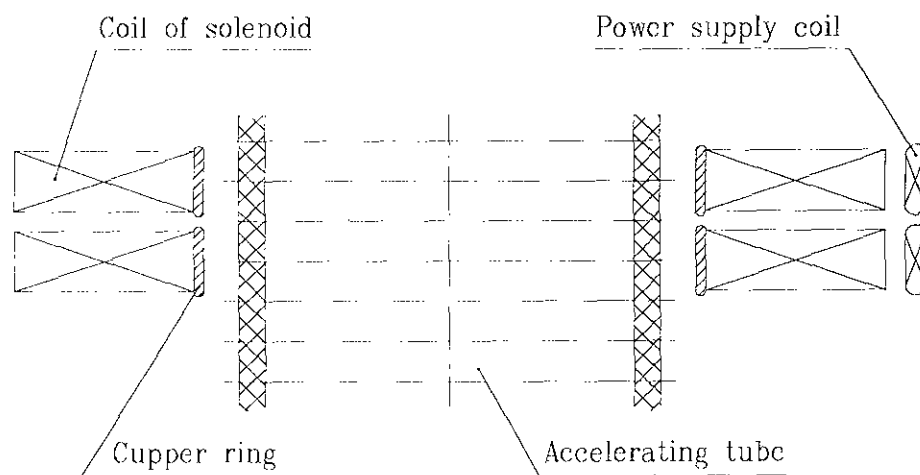


Figure 10.6: The solenoid sectional view.

an outer edge of the electrodes is 220 mm. Considering that a potential difference

between the electrode and coil is up to 20 kV and that it is necessary to locate a shielding ring protecting the tube from an alternating magnetic field component, the coil inner diameter should be no less than 250 mm. The outer diameter is determined from the column dimensions, it is 425 mm. The section step is 40 mm, the coil height is 30 mm. To obtain the magnetic field of 0.1 T it is necessary to provide 3200 A·turn for every coil. At a filling factor of 0.7, the power in a coil will be 103 W at 20°C, and 136 W at a maximal operation temperature of 100°C. Considering losses in the shielding rings and rectifier, the power given off in the solenoid is 8 kW per meter (for two accelerating tubes).

The solenoid is supposed to be cooled by an elegas flow. A diagram of the cooling system is presented in Fig. 10.7. The output at 10°C heating of the gas should be

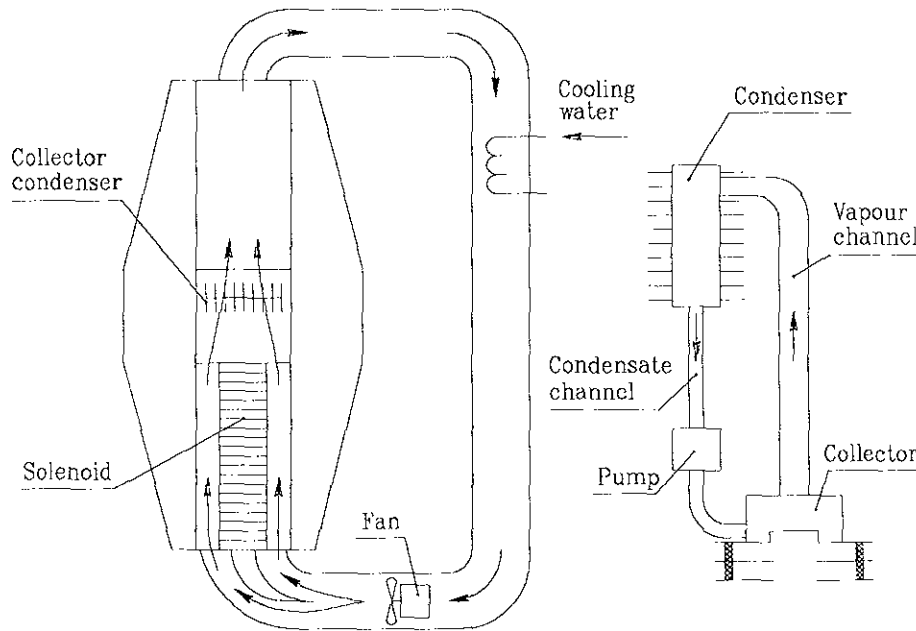


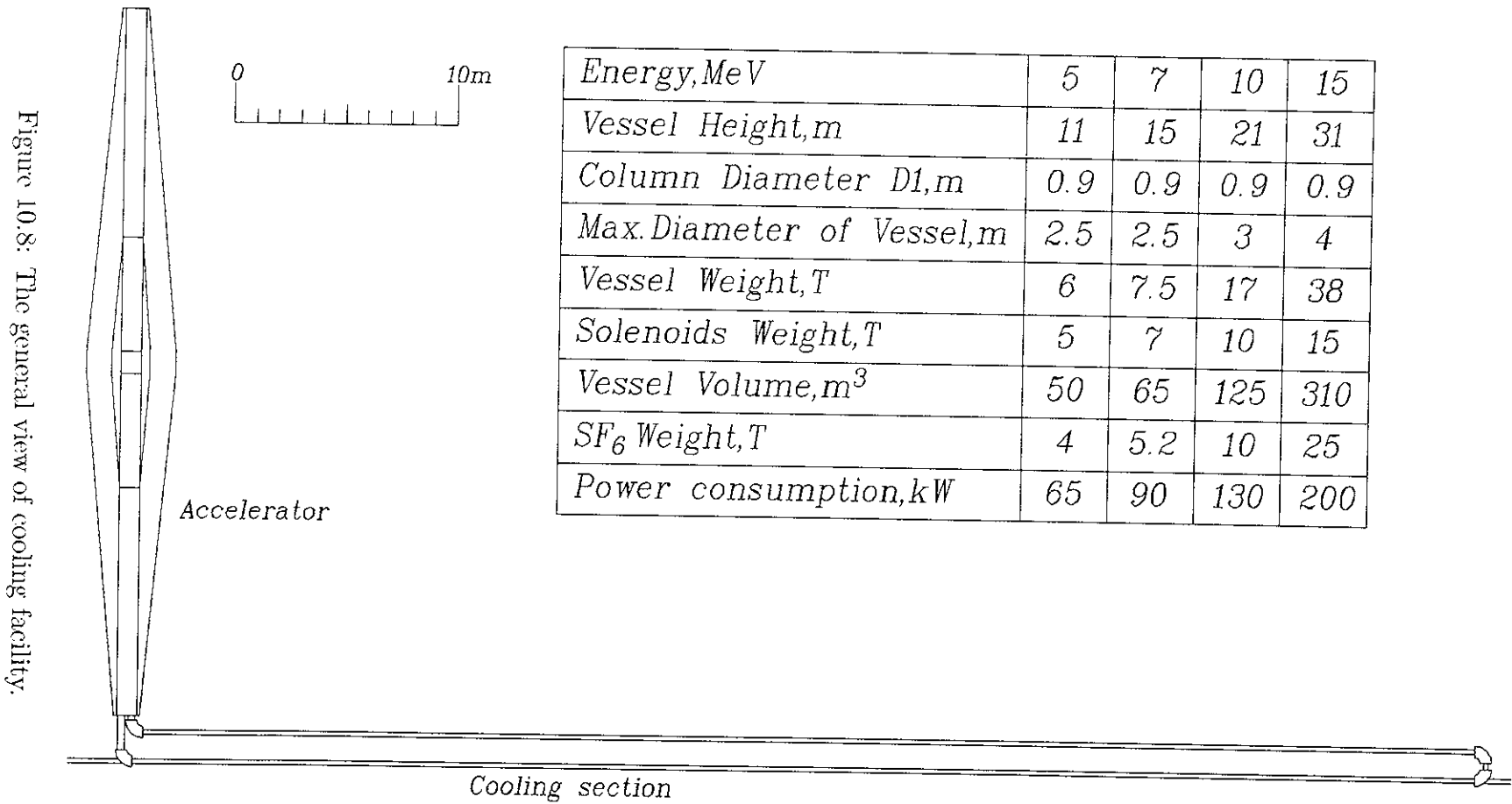
Figure 10.7: Cooling system of the solenoid.

1500 m³/hour for the 15 MeV accelerator. At the gas flow rate of 1.5 m/s, a convective heat transfer factor is about 80 W/(m²·°C), this is enough for heat removing from the solenoid side surface. The collector is cooled by an additional cooling loop on the heat tube principle.

When estimating the power consumption we took into account consumptions of the solenoid, recuperation rectifier, high-voltage rectifier and 85 % efficiency of the facility.

The total view of cooling facility is presented at Fig.10.8.

These data are the estimation parameters, they should be improved at a more detailed consideration.



Chapter 11

First Cost Estimations

Preliminary cost estimation for ENC is given in Tables 11.1, 11.2 and 11.3. These costs include only technical equipment. The building costs have to be estimated separately.

Table 11.1: First cost estimations for electron accelerators of ENC.

Collider Ring (1.5 – 7.5 GeV)	200	MDM
Special Equipment:		
Final focusing systems		
Spin Rotators	35	MDM
Emittance Control		
Injector synchrotron (2 GeV)	20	MDM
Injector linac (540 MeV)	10	MDM
Total	265	MDM

Table 11.2: First cost estimations for proton/ion accelerators of ENC.

Collider Ring (15 -- 30 GeV) Either NC-Magnets, or Low field SC-Magnets	200	MDM
Electron Cooler (15 MeV, 1 A)	60	MDM
Special Equipment: Final focusing systems Spin Rotators Emittance Control	35	MDM
Injector synchrotron According to estimations of WG VII	344	MDM
Total	639	MDM

Table 11.3: Totals from Tables 11.1 and 11.2.

Electron accelerators	265	MDM
Proton/ion accelerators	639	MDM
TOTAL COST	904	MDM

Chapter 12

Time Schedule

As it was shown in previous Chapters, a creation of the electron-nucleon collider for the energy range $\sqrt{s} = 10 \div 30$ GeV/u and with the luminosity 10^{33} 1/[cm²s] is feasible provided that electron cooling device will ensure the required small ion beam emittances. A possibility to reach necessary damping times was demonstrated in the experiments at the installations NAP-M and MODSOL (BINP) as well as at other electron cooling storage rings in US and in the Western Europe. However, an extrapolation of data obtained in the energy range of hundred MeV to that of several tens of GeV still leaves some concern. For that reason, the experiments on ion and proton cooling in a range of 1-5 GeV could be very useful. In our opinion, one should move in this direction by two ways.

The first way is the creation of the electron cooling device with an electron energy of 2 MeV. The principal feasibility to obtain the electron source with an energy of 1 MeV and 1A current with the recuperation of electron energy was demonstrated at INP in 1988, that is why going from 1 MeV energy to 2 MeV energy is an ordinary design problem requiring the proper qualification of designers.

The untrivial part of this work is the provision of electron beam magnetizing mode and of magnetic line collinearity at a cooling section with an accuracy better than $3 - 5 \times 10^{-6}$. With the availability of finances (a rough price of the 2 MeV installation with a 3 m long cooling section is 7-8 MDM) INP can create such the installation in a period of 2.5 years. The experiments on cooling could be carried out at the synchrotron SIS in Darmstadt. With the SIS extracted beam intensity, such measurements could also be useful to prove the ion beam intensity limitations on the electron cooling performance.

The second way is the creation of the bunched beam electron cooling device based on a longwavelength linear accelerator. This variant requires a detailed theoretical comprehension taking no less than a year. If it turns out that there are no principal limitations, it will be possible to create the prototype with an electron energy of 2 MeV and carry out the experiments also at the synchrotron SIS in a matter of 3 years.

Both for the first and the second cases the result of the model experiment can

be reached in 2001-2002 years, after which it is possible to manufacture a full-scale version of the electron cooler.

If the decision to realize the electron-ion collider is taken in 2002, under the proper financing the Project ENC can be completed by 2007.

Appendix A

A.1 To the Calculation of the Luminosity

Equation (2.1) calculated using a general definition of the luminosity in the following form

$$L = 2cn_b f_0 \int dx dz ds dt \rho_i(x, z, s + ct) \rho_e(x, z, s - ct). \quad (\text{A.1})$$

Here, x, z are transverse and s is the longitudinal coordinate of a particle, n_b is the number of the colliding bunches, f_0 is the revolution frequency. For the sake of simplicity, we neglect the deviation of the particle velocities from the speed of light (c). We take Gaussian distributions in colliding bunches so that

$$\rho(x, z, s) = \frac{N}{(2\pi)^{3/2} \sigma_{\perp}^2(s) \sigma_s} \exp \left[-\frac{x^2 + z^2}{2\sigma_{\perp}^2(s)} - \frac{s^2}{2\sigma_s^2} \right], \quad \sigma_{\perp}^2(s) = \sigma_{\perp}^2 \left(1 + \frac{s^2}{\beta^2} \right). \quad (\text{A.2})$$

Here, σ_{\perp} and β are the rms bunch radius and β -function at the interaction point. We also assume that the bunches have round cross sections at the interaction point and equal β -functions for ions and electrons. Transverse emittances for these particles (and bunch radii of the colliding ion and electron bunches) still can be different. Then, the integral over transverse coordinates (x, z) reads

$$\begin{aligned} I_{\perp}(s) &= \frac{N_i N_e}{(2\pi)^3 \sigma_{1e}^2(s) \sigma_{1i}^2(s)} \int dx dz \exp \left[-\frac{x^2 + z^2}{2(1 + s^2/\beta^2)} \left(\frac{1}{\sigma_{1i}^2} + \frac{1}{\sigma_{1e}^2} \right) \right] \\ &= \frac{N_i N_e}{(2\pi)^3 \sigma_{1e}^2(s) \sigma_{1i}^2(s)} \times \frac{2\pi(1 + s^2/\beta^2) \sigma_{1e}^2 \sigma_{1i}^2}{(\sigma_{1e}^2 + \sigma_{1i}^2)} \\ &= \frac{N_i N_e}{(2\pi)^2 (\sigma_{1e}^2 + \sigma_{1i}^2)} \times \frac{1}{1 + s^2/\beta^2}. \end{aligned}$$

Substituting $I_{\perp}(s)$ in Eq.(A.1), we obtain

$$\begin{aligned}
 L &= n_b f_0 \int ds d(2ct) I_{\perp}(s) \exp\left(-\frac{s^2 + (ct)^2}{\sigma_s^2}\right) \\
 &= \frac{n_b f_0 N_i N_e}{(2\pi)(\sigma_{\perp e}^2 + \sigma_{\perp i}^2)} \int_{-\infty}^{\infty} \frac{ds}{1 + s^2/\beta^2} \int_{-\infty}^{\infty} \frac{d(ct)}{\pi} \exp\left(-\frac{s^2 + (ct)^2}{\sigma_s^2}\right) \\
 &= \frac{n_b f_0 N_i N_e}{(2\pi)(\sigma_{\perp e}^2 + \sigma_{\perp i}^2)} \int_{-\infty}^{\infty} \frac{ds}{\sqrt{\pi}} \frac{\exp(-s^2/2\sigma_s^2)}{1 + s^2/\beta^2}.
 \end{aligned}$$

If we multiply L by the ion atomic number A (to calculate the electron - nucleon luminosity), define $\zeta = \sigma_s/\beta$ and

$$L_0 = \frac{A n_b f_0 N_i N_e}{(2\pi)(\sigma_{\perp e}^2 + \sigma_{\perp i}^2)},$$

we arrive to Eq.(2.1):

$$L = L_0 \frac{2}{\sqrt{\pi}} \int_0^{\infty} \frac{ds e^{-s^2}}{1 + \zeta^2 s^2}.$$

If we take $\sigma_{\perp e} = \sigma_{\perp i}$, L_0 decreases by the factor of 2. If we can decrease $\sigma_{\perp i}$ to have $\sigma_{\perp e} \gg \sigma_{\perp i}$ without decrease in the bunch intensities (N_i , N_e), we gain this factor 2 back.

Appendix B

B.1 Calculation of the Beam-Beam Kick

The perturbation of the betatron oscillations of a particle, when it moves across the interaction point, is described by the following equation

$$\frac{d\mathbf{p}_\perp}{dt} = \mathbf{F}_\perp = e_1(\mathbf{E} + \frac{1}{c}[\mathbf{v}_1 \times \mathbf{H}])_\perp. \quad (\text{B.1})$$

Here, e_1 is the charge of a particle from the bunch 1, \mathbf{v}_1 is its velocity, \mathbf{E} and \mathbf{H} are the electric and magnetic fields of the counter-moving bunch 2 and c is the speed of light. The beam-beam instability occurs due to the perturbations from the quasistatic fields of the counter-moving bunch. For relativistic energies ($\gamma \gg 1$) these quasistatic fields of a bunch are almost transverse relative to its average velocity. If \mathbf{v}_2 is the average velocity of the bunch 2, we write

$$\mathbf{H} = [\frac{\mathbf{v}_2}{c} \times \mathbf{E}],$$

so that

$$\begin{aligned} \mathbf{F} &= e_1(\mathbf{E} + \frac{1}{c}[\mathbf{v}_1 \times \mathbf{H}]) \\ &= e_1(\mathbf{E} + \frac{1}{c^2}[\mathbf{v}_1 \times [\mathbf{v}_2 \times \mathbf{E}]]) \\ &= e_1 \left(\mathbf{E} \left(1 - \frac{\mathbf{v}_1 \mathbf{v}_2}{c^2} \right) + \frac{\mathbf{v}_2}{c^2} (\mathbf{v}_1 \mathbf{E}) \right), \end{aligned}$$

and ($\mathbf{v}_1 = -\mathbf{v}_2$), for example

$$\begin{aligned} \frac{dp_z}{dt} &= e_1 E_z \left(1 + \frac{v_1 v_2}{c^2} \right) \\ &\simeq 2e_1 E_z = -2e_1 \frac{\partial A_0}{\partial z}, \end{aligned} \quad (\text{B.2})$$

where $A_0 = A_0(\mathbf{r}_\perp, s + v_2 t)$ is the scalar potential of the field E_z . The function A_0 obeys the following equation ($y = s + v_2 t$)

$$\left(\Delta_\perp + \frac{1}{\gamma^2} \frac{\partial^2}{\partial y^2} \right) A_0 = -4\pi e \rho(\mathbf{r}_\perp, y), \quad (\text{B.3})$$

where ρ is the density of the counter-moving bunch. Since $\rho(\mathbf{r}_\perp, y)$ is a periodic function of s

$$\rho(\mathbf{r}_\perp, y) = \sum_{n=-\infty}^{\infty} \rho_n(\mathbf{r}_\perp) e^{ik_n y}, \quad k_n = n/R_0, \quad (\text{B.4})$$

we shall find the solution of Eq.(B.3) in the form

$$A_0(\mathbf{r}_\perp, y) = \sum_n A_n(\mathbf{r}_\perp) e^{ik_n y}.$$

Then, the amplitudes $A_n(\mathbf{r}_\perp)$ satisfy the equation

$$\Delta_\perp A_n - \frac{k_n^2}{\gamma^2} A_n = -4\pi e \rho_n(\mathbf{r}_\perp). \quad (\text{B.5})$$

Taking into account that

$$\Delta_\perp A_0 \propto k_\perp^2 A_0 > A_0/l_\perp^2,$$

where l_\perp is the typical transverse size of the vacuum chamber at the IP, for the harmonics $|n| \leq \gamma R_0/l_\perp$ the second term in the left-hand side in Eq.(B.5) is negligible small as compared to the first one and, thus, can be omitted. As shall be seen below, the main contribution to the bunch fields yields the region $k_\perp a \geq 1$ (a is the bunch radius), where we can neglect the effect of the walls of the vacuum chamber on the bunch fields and, therefore, where we can write

$$A_0(\mathbf{r}_\perp, y) = 4\pi N e \int \frac{d^2 k_\perp}{(2\pi)^2 k_\perp^2} \exp(i\mathbf{k}_\perp \mathbf{r}_\perp) \rho(\mathbf{k}_\perp, y), \quad (\text{B.6})$$

$$\rho(\mathbf{k}_\perp, y) = \int d^2 r_\perp \exp(-i\mathbf{k}_\perp \mathbf{r}_\perp) \rho(\mathbf{r}_\perp, y). \quad (\text{B.7})$$

If we also write $\rho(\mathbf{r}_\perp, y) = \rho(\mathbf{r}_\perp) \lambda(y)$, where $\lambda(y)$ is the linear density of the bunch, we can rewrite Eq.(B.6) in the final form

$$A_0(\mathbf{r}_\perp, y) = N_2 e_2 \lambda(s + v_2 t) \int \frac{dk_x dk_z}{\pi k_\perp^2} \exp(i\mathbf{k}_\perp \mathbf{r}_\perp) \rho(k_x, k_z). \quad (\text{B.8})$$

In order to calculate the transverse beam-beam kick in the linear approximation we take

$$\rho(x, z) = \frac{1}{2\pi\sigma_x\sigma_z} \exp\left(-\frac{x^2}{2\sigma_x^2} - \frac{z^2}{2\sigma_z^2}\right),$$

so that

$$\rho(k_x, k_z) = \exp\left(-\frac{k_x^2 \sigma_x^2 + k_z^2 \sigma_z^2}{2}\right)$$

and use the expansion

$$\exp(i\mathbf{k}_\perp \mathbf{r}_\perp) \simeq 1 + i\mathbf{k}_\perp \mathbf{r}_\perp - \frac{(\mathbf{k}_\perp \mathbf{r}_\perp)^2}{2} + \dots$$

Then, we write

$$A_0(\mathbf{r}_\perp, y) \simeq N_2 e_2 \lambda(s + v_2 t) \int \frac{dk_x dk_z}{2\pi k_\perp^2} (k_x^2 x^2 + k_z^2 z^2) \exp\left(-\frac{k_x^2 \sigma_x^2 + k_z^2 \sigma_z^2}{2}\right).$$

Substituting this expression in Eq.(B.2), we obtain

$$\frac{dp_z}{dt} = -\kappa_z z, \tag{B.9}$$

where ($e_1 e_2 = -Ze^2$)

$$\kappa_z = 2N_2 Z e^2 \lambda(s + v_2 t) \int \frac{dk_x dk_z}{\pi k_\perp^2} k_x^2 \exp\left(-\frac{k_x^2 \sigma_x^2 + k_z^2 \sigma_z^2}{2}\right).$$

The integrals in this expression can be calculated using, for example, the substitution

$$\frac{1}{k_\perp^2} = \int_0^\infty ds e^{-sk_\perp^2},$$

which yields

$$\kappa_z = -2N_2 Z e^2 \lambda(s + v_2 t) \int_0^\infty \frac{ds}{\pi} I_x(s) \frac{d}{ds} I_z(s), \tag{B.10}$$

where

$$I_\alpha(s) = \int_{-\infty}^\infty dk_\alpha \exp[-k_\alpha^2(\sigma_\alpha^2/2 + s)] = \left(\frac{2\pi}{\sigma_\alpha^2 + 2s}\right)^{1/2}, \quad \alpha = x, z.$$

Now, we have to calculate

$$\begin{aligned} J_z &= \int_0^\infty \frac{ds}{\pi} I_x(s) \frac{d}{ds} I_z(s) \\ &= -\frac{1}{2} \int_0^\infty \frac{ds}{(\sigma_x^2/2 + s)^{1/2} (\sigma_z^2/2 + s)^{3/2}} \\ &= -\sigma_x \int_0^1 \frac{dt}{(\sigma_x^2 + [\sigma_z^2 - \sigma_x^2]t)^{3/2}} \\ &= -\frac{2}{\sigma_z(\sigma_x + \sigma_z)}. \end{aligned}$$

Hence, we obtain

$$\kappa_z = \frac{4N_2 Z e^2}{\sigma_z(\sigma_x + \sigma_z)} \lambda(s + v_2 t), \quad (\text{B.11})$$

and

$$\frac{dp_z}{ds} = -\frac{4N_2 Z e^2}{c\sigma_z(\sigma_x + \sigma_z)} \lambda(s + v_2 t) z. \quad (\text{B.12})$$

B.2 Coulomb Tune Shifts

Let us, for example, calculate the tune shift of the horizontal ion betatron oscillations due to the ion bunch space charge in the first approximation of the perturbation theory. We write

$$\begin{aligned} \Delta\nu_x &= \frac{1}{\omega_0} \left\langle \frac{d\psi_x}{dt} \right\rangle = \frac{1}{\omega_0} \left\langle \frac{\partial\psi_x}{\partial p_x} F_x^{(i)} \right\rangle \\ &= -\frac{2R_0}{pc} \int_0^\Pi ds \int_0^{2\pi} \frac{d\psi_x d\psi_z}{(2\pi)^2} \frac{\partial x}{\partial J_x} F_x^{(i)}. \end{aligned} \quad (\text{B.13})$$

Using that for relativistic ions ($\gamma_i \gg 1$, $v_i \simeq c$) $F_x^{(i)} = ZeE_r x / (\gamma_i^2 r_\perp)$, where $r_\perp^2 = x^2 + z^2$ and E_r is the radial component of the electric field of the ion bunch, we rewrite Eq.(B.13) in the following form

$$\Delta\nu_x = -\frac{2R_0}{p_i c \gamma_i^2} \int_0^\Pi ds \int_0^{2\pi} \frac{d\psi_x d\psi_z}{(2\pi)^2} \frac{\partial x}{\partial J_x} \frac{x}{r} ZeE_r(\mathbf{r}_\perp, s = ct). \quad (\text{B.14})$$

For the bunch with a round cross section we have

$$\begin{aligned} E_r(\mathbf{r}_\perp, s = ct) &= \frac{2N_i Ze \lambda_i(0)}{r_\perp \sigma_i^2} \int_0^{r_\perp} dx x \exp\left(-\frac{x^2}{2\sigma_i^2}\right) \\ &= \frac{N_i Ze \lambda_i(0) r_\perp}{\sigma_i^2} \int_0^1 dt \exp\left(-t \frac{r_\perp^2}{2\sigma_i^2}\right), \end{aligned}$$

or

$$\begin{aligned} \Delta\nu_x &= -\frac{N_i (Ze)^2 \lambda_i(0) 2R_0}{p_i c \gamma_i^2} \int_0^\Pi ds \int_0^{2\pi} \frac{d\psi_x d\psi_z}{(2\pi)^2} x \frac{\partial x}{\partial J_x} \int_0^1 dt \exp\left(-t \frac{r_\perp^2}{2\sigma_i^2}\right) \\ &= -\Delta\nu_L Q_x(J_x, J_z). \end{aligned} \quad (\text{B.15})$$

Here,

$$\Delta\nu_L = \frac{N_i (Ze)^2 \lambda_i(0) \Pi}{4\pi p_i c \gamma_i^2 \epsilon} \quad (\text{B.16})$$

is the Laslett tune shift, and

$$Q_x = 2 \int_0^\Pi \frac{ds}{\Pi} \frac{\beta_x(s)}{(\sigma_i^2/\epsilon)} \int_0^{2\pi} \frac{d\psi_x d\psi_z}{(2\pi)^2} \cos^2(\psi_x) \int_0^1 dt \exp\left(-t \frac{r_1^2}{2\sigma_i^2}\right). \quad (\text{B.17})$$

If the modulations of the β -functions along the closed orbit are not very deep, we can replace in integrands in Eq.(B.17) the expressions $\beta_{x,z}\epsilon/\sigma_i^2$ for 1. That results in

$$\begin{aligned} Q_x &= 2 \int_0^{2\pi} \frac{d\psi_x d\psi_z}{(2\pi)^2} \cos^2(\psi_x) \int_0^1 dt \exp\left(-t \frac{J_x \cos^2(\psi_x) + J_z \cos^2(\psi_z)}{2\epsilon}\right) (\text{B.18}) \\ &= \int_0^1 dt \exp\left(-t \frac{J_x + J_z}{4\epsilon}\right) I_0\left(\frac{tJ_z}{4\epsilon}\right) \left[I_0\left(\frac{tJ_x}{4\epsilon}\right) - I_1\left(\frac{tJ_x}{4\epsilon}\right) \right]. \end{aligned}$$

Appendix C

C.1 IBS Diffusion Coefficients

The blow-up of the bunch emittances due to intrabeam scattering (IBS) is described by the Landau kinetic equation

$$\frac{\partial f}{\partial t} = - \frac{\partial}{\partial p_{1\alpha}} N \int d^3 p_2 w_{\alpha\beta}(u) \left(f_1 \frac{\partial f_2}{\partial p_{2\beta}} - \frac{\partial f_1}{\partial p_{1\beta}} f_2 \right). \quad (\text{C.1})$$

Here, N is the number of particles in the bunch, $f(\mathbf{p}, \mathbf{r}, t)$ is the distribution function of the bunch, $w_{\alpha\beta}(u)$ is the collision tensor, u is the relative velocity of the colliding particles and we use a convention that repeated subscripts mean the summation:

$$A_\alpha B_\alpha = \sum_{\alpha=x,z,s} A_\alpha B_\alpha.$$

We assume that without collisions the bunch distribution function is a Gaussian

$$f(\mathbf{p}, \mathbf{r}, t) = \frac{1}{(2\pi)^3 p^3 \epsilon_x \epsilon_z \epsilon_s} \exp\left(-\frac{J_x}{2\epsilon_x} - \frac{J_z}{2\epsilon_z} - \frac{J_s}{2\epsilon_s}\right). \quad (\text{C.2})$$

Here, ϵ_α ($\alpha = x, z, s$) are the bunch emittances, $I_\alpha = pJ_\alpha/2$ are the action-variables of the unperturbed oscillations

$$\begin{aligned} J_z &= \frac{\tilde{z}^2}{\beta_z} + \beta_z \left(\frac{p_z}{p} - \frac{\beta'_z}{2\beta_z} \tilde{z} \right)^2, \\ J_x &= \frac{1}{\beta_x} \left(x - D_x \frac{\Delta p}{p} \right)^2 + \beta_x \left(\frac{p_x}{p} - \frac{\beta'_x}{2\beta_x} x - \Phi \frac{\Delta p}{p} \right)^2, \\ \frac{J_s}{R_0} &= \frac{\nu_s}{|\eta|} \phi^2 + \frac{|\eta|}{\nu_s} \left(\frac{\Delta p}{p} \right)^2, \end{aligned} \quad (\text{C.3})$$

the values $\beta_{x,z}$ are the β functions of betatron oscillations, $\beta' = d\beta/ds$ (s is the path along the orbit), ϕ and $\Delta p/p$ describe the synchrotron oscillations of ions, ν_s is the

synchrotron tune, $\eta = 1/\gamma^2 - 1/\gamma_{tr}^2$, $\Pi = 2\pi R_0$ is the perimeter of the orbit. For synchrotron oscillations we also shall use $\epsilon_s = \sigma_s \delta$, where σ_s is the r.m.s. bunch length and δ is the r.m.s. relative momentum spread of the bunch. The bunch distribution function in Eq.(C.2) is normalized according to

$$\int d^3p d^3r f = \int d\Gamma f = 1. \quad (C.4)$$

Let us find, for example, the equation describing the variation of the vertical emittance of the bunch

$$\epsilon_z = \frac{1}{2} \int d\Gamma J_z f.$$

Using Eq.(C.1), we obtain

$$\frac{d\epsilon_z}{dt} = \frac{1}{2} \int d^3r d^3p_1 d^3p_2 \frac{\partial J_z}{\partial p_z} w_{z\beta} \left(f_1 \frac{\partial f_2}{\partial p_{2\beta}} - \frac{\partial f_1}{\partial p_{1\beta}} f_2 \right). \quad (C.5)$$

According to Eqs (C.2) and (C.3) we can write

$$-\ln f = \frac{1}{2} A_{\alpha\beta} p_\alpha p_\beta + \frac{1}{2} B_{\alpha\beta} p_\alpha r_\beta + \frac{1}{2} C_{\alpha\beta} r_\alpha r_\beta$$

and, therefore,

$$f_1 \frac{\partial f_2}{\partial p_{2\beta}} - \frac{\partial f_1}{\partial p_{1\beta}} f_2 = A_{\alpha\beta} (p_1 - p_2)_\beta f_1 f_2. \quad (C.6)$$

Using also

$$\frac{\partial J_z}{\partial p_z} = \frac{2\beta_z}{p} \left(\frac{p_z}{p} - \frac{\beta'_z}{2\beta_z} z \right),$$

we rewrite Eq.(C.5) in the following form

$$\frac{d\epsilon_z}{dt} = \int d^3r d^3p_1 d^3p_2 \frac{\beta_z}{p^2} q_z w_{z\beta} A_{\beta\lambda} q_\lambda f_1 f_2, \quad \mathbf{q} = \mathbf{p}_1 - \mathbf{p}_2. \quad (C.7)$$

The calculation of these integrals is simplified substituting $\mathbf{p}_1 = \mathbf{P} + \mathbf{q}/2$ and $\mathbf{p}_2 = \mathbf{P} - \mathbf{q}/2$, when $f_1 f_2 \propto \exp[-\Sigma(\mathbf{P}, \mathbf{r}) - Q(\mathbf{q})]$ and

$$\begin{aligned} \Sigma &= A_{\alpha\beta} P_\alpha P_\beta + B_{\alpha\beta} P_\alpha r_\beta + C_{\alpha\beta} r_\alpha r_\beta \\ Q &= \frac{1}{4} A_{\alpha\beta} q_\alpha q_\beta. \end{aligned} \quad (C.8)$$

Since $d^3P d^3q = d^3p_1 d^3p_2$, Eq.(C.7) reads

$$\frac{d\epsilon_z}{dt} = \int_0^\Pi ds \int \frac{dx dz d^3P}{(2\pi)^3 p^3 \epsilon_x \epsilon_z \epsilon_s} e^{-\Sigma} E_z(s), \quad (C.9)$$

$$E_z(s) = N \frac{\beta_z(s)}{p^2} \int \frac{d^3q}{(2\pi)^3 p^3 \epsilon_x \epsilon_z \epsilon_s} q_z w_{z\beta} A_{\beta\lambda} q_\lambda e^{-Q} \quad (C.10)$$

Now, we note that $\exp(-\Sigma) \propto \exp[-(s - ct)^2/(2\sigma_s^2)]$. For that reason, the variation of ϵ_z during the rotation period $T_0 = \Pi/c$ is equal to

$$\Delta\epsilon_z = \int_0^{T_0} dt \frac{d\epsilon_z}{dt},$$

which yields the average growth rate of ϵ_z in the following form

$$\begin{aligned} \dot{\epsilon}_z &= \frac{\Delta\epsilon_z}{T_0} = \frac{c}{\Pi} \int_0^{T_0} dt \frac{d\epsilon_z}{dt} \\ &= \int_0^\Pi \frac{ds}{\Pi} E_z(s) \int \frac{d(ct) dx dz d^3P}{(2\pi)^3 p^3 \epsilon_x \epsilon_z \epsilon_s} e^{-\Sigma}. \end{aligned}$$

Since the function $e^{-\Sigma}/(8\pi^3 p^3 \epsilon_x \epsilon_z \epsilon_s)$ is exactly equal to $f(\sqrt{2}\mathbf{p}, \sqrt{2}\mathbf{r}, \sqrt{2}t)$, we find

$$\int \frac{d(ct) dx dz d^3P}{(2\pi)^3 p^3 \epsilon_x \epsilon_z \epsilon_s} e^{-\Sigma} = \frac{1}{8}$$

and

$$\dot{\epsilon}_z = \frac{N}{(4\pi)^3 p^2 \epsilon_x \epsilon_z \epsilon_s} \int_0^\Pi \frac{ds}{\Pi} \beta_z(s) \int \frac{d^3q}{p^3} q_z w_{z\beta} A_{\beta\lambda} q_\lambda e^{-Q}. \quad (\text{C.11})$$

To calculate $E_z(s)$ we note that

$$A_{\alpha\beta} q_\beta e^{-Q} = -2 \frac{\partial}{\partial q_\beta} \exp\left(-\frac{1}{4} A_{\alpha\beta} q_\alpha q_\beta\right).$$

Hence,

$$\begin{aligned} \dot{\epsilon}_z &= \frac{2N}{(4\pi)^3 p^2 \epsilon_x \epsilon_z \epsilon_s} \int_0^\Pi \frac{ds}{\Pi} \beta_z \int \frac{d^3q}{p^3} q_z w_{z\beta} \frac{\partial}{\partial q_\beta} e^{-Q} \\ &= \frac{2N}{(4\pi)^3 p^2 \epsilon_x \epsilon_z \epsilon_s} \int_0^\Pi \frac{ds}{\Pi} \beta_z \int \frac{d^3q}{p^3} e^{-Q} \left(w_{zz} + q_z \frac{\partial w_{z\beta}}{\partial q_\beta} \right) \end{aligned} \quad (\text{C.12})$$

The integral over q is calculated in the rest frame system of the bunch, where (Ze is the ion charge)

$$w_{\alpha\beta}(u) = 2\pi(Ze)^4 L_{IBS} \frac{\delta_{\alpha\beta} u^2 - u_\alpha u_\beta}{u^3} \quad (\text{C.13})$$

$$= \frac{2\pi(Ze)^4 L_{IBS}}{\gamma c} \left(\frac{\delta_{\alpha\beta}}{\theta} - \frac{\theta_\alpha \theta_\beta}{\theta^3} \right), \quad \theta_\alpha = \frac{q_\alpha}{p}. \quad (\text{C.14})$$

Substituting this expression in Eq.(C.12), we obtain

$$\dot{\epsilon}_z = \frac{N(Ze)^4 L_{IBS}}{(4\pi)^2 \gamma^2 p^2 c \epsilon_x \epsilon_z \epsilon_s} \int_0^\Pi \frac{ds}{\Pi} \beta_z \int d^3\theta \frac{\theta^2 - 3\theta_z^2}{\theta^3} e^{-Q},$$

or, using $d^3\theta = \theta^2 d\theta d\Omega$, $n_\alpha = \theta_\alpha/\theta$, $\exp(-Q) = \exp(-\theta^2 a_{\alpha\beta} n_\alpha n_\beta/4)$ and

$$\int_0^\infty d\theta \theta \exp\left(-\theta^2 \frac{a_{\alpha\beta} n_\alpha n_\beta}{4}\right) = \frac{2}{a_{\alpha\beta} n_\alpha n_\beta},$$

we finally find ($p = A\gamma Mc$, A is the ion atomic number and M is the proton mass)

$$\dot{\epsilon}_z = \frac{K}{\epsilon_x \epsilon_z \epsilon_s} \int_0^\Pi \frac{ds}{\Pi} \beta_z(s) G_z(s), \quad K = \frac{N(Z^2/A)^2 r_p^2 c L_{IBS}}{2\pi \gamma^4}, \quad r_p = \frac{e^2}{Mc^2}. \quad (\text{C.15})$$

Here,

$$G_z(s) = \int \frac{d\Omega}{4\pi} \frac{1 - 3n_z^2}{a_{\alpha\beta} n_\alpha n_\beta}. \quad (\text{C.16})$$

The matrix $a_{\alpha\beta}$ in this equation is obtained from Eqs(C.3). In the rest frame system of the beam it reads

$$\mathbf{a} = \begin{bmatrix} a_z & 0 & 0 \\ 0 & a_x & -\gamma\Phi a_x \\ 0 & -\gamma\Phi a_x & \gamma^2 a_s \end{bmatrix}, \quad (\text{C.17})$$

where

$$a_z = \frac{\beta_z}{\epsilon_z}, \quad a_x = \frac{\beta_x}{\epsilon_x}, \quad a_s = \frac{1}{\epsilon_x} \left(\frac{D_x^2}{\beta_x} + \beta_x \Phi^2 \right) + \frac{1}{\delta^2}. \quad (\text{C.18})$$

Similar calculations result in ($n_s = \theta_s/\theta$)

$$\frac{d\delta^2}{dt} = \frac{K\gamma^2}{\epsilon_x \epsilon_z \epsilon_s} \int_0^\Pi \frac{ds}{\Pi} G_s(s), \quad G_s = \int \frac{d\Omega}{4\pi} \frac{1 - 3n_s^2}{a_{\alpha\beta} n_\alpha n_\beta}, \quad (\text{C.19})$$

and in

$$\frac{d\epsilon_x}{dt} = \frac{K}{\epsilon_x \epsilon_z \epsilon_s} \int_0^\Pi \frac{ds}{\Pi} \left[\beta_x(s) G_x(s) + \gamma^2 \left(\frac{D_x^2}{\beta_x} + \beta_x \Phi^2 \right) G_s(s) + 2G_{xs}(s) \right], \quad (\text{C.20})$$

where

$$G_{xs}(s) = \gamma \beta_x \Phi \int \frac{d\Omega}{4\pi} \frac{3n_s n_x}{a_{\alpha\beta} n_\alpha n_\beta}. \quad (\text{C.21})$$

Using Eqs (C.15)–(C.20) we can, for example, directly calculate the growth rate of the total phase space volume of the bunch

$$\Lambda = \frac{1}{\epsilon_x} \frac{d\epsilon_x}{dt} + \frac{1}{\epsilon_z} \frac{d\epsilon_z}{dt} + \frac{1}{\delta^2} \frac{d\delta^2}{dt}.$$

Since

$$\begin{aligned} & \frac{G_z}{\epsilon_z} + \frac{1}{\epsilon_x} \left[G_x(s) + \left(\frac{D_x^2}{\beta_x} + \beta_x \Phi^2 \right) G_s(s) + 2G_{xs}(s) \right] + \frac{G_s}{\delta^2} \\ &= \int \frac{d\Omega}{4\pi} \frac{a_z(1-3n_z^2) + a_x(1-3n_x^2) + 2a_x\gamma\Phi n_x n_s + \gamma^2 a_s(1-n_s^2)}{\mathbf{a}_{\alpha\beta} n_\alpha n_\beta} \\ &= \int \frac{d\Omega}{4\pi} \frac{\text{Sp}(\mathbf{a})}{\mathbf{a}_{\alpha\beta} n_\alpha n_\beta} - 3, \end{aligned}$$

we find

$$\Lambda = \frac{K}{\epsilon_x \epsilon_z \epsilon_s} \left[\int_0^\Pi \frac{ds}{\Pi} \int \frac{d\Omega}{4\pi} \frac{\text{Sp}(\mathbf{a})}{\mathbf{a}_{\alpha\beta} n_\alpha n_\beta} - 3 \right]. \quad (\text{C.22})$$

C.2 Calculation of $G(s)$

As we told the function $G(s)$ in Eq.(5.9) can be expressed in terms of the elliptic integrals. If, for example, we have

1. $q_+ > q_- > a_z$, then a substitution

$$u = \sqrt{\frac{q_+}{q_+ - a_z}} \sin \varphi$$

transforms this integral into the following

$$G(s) = \frac{[a_z + q_+ + q_-]}{\sqrt{q_-(q_+ - a_z)}} F(\varphi_1, k_1) - 3, \quad (\text{C.23})$$

where $F(\varphi, k)$ is the elliptic integral of the first kind:

$$F(\varphi, k) = \int_0^\varphi \frac{d\alpha}{\sqrt{1 - k^2 \sin^2 \alpha}},$$

and

$$\varphi_1 = \arcsin \sqrt{1 - \frac{a_z}{q_+}}, \quad k_1^2 = \frac{q_+(q_- - a_z)}{q_-(q_+ - a_z)}. \quad (\text{C.24})$$

Two others possibilities are given by the following expressions

2. $q_+ > a_z > q_-$

$$G(s) = \frac{[a_z + q_+ + q_-]}{\sqrt{a_z(q_+ - q_-)}} \left[\mathbf{K}(k_2) - F\left(\frac{\pi}{2} - \varphi_1, k_2\right) \right] - 3, \quad (\text{C.25})$$

where $\mathbf{K}(k) = F(\pi/2, k)$ is the complete elliptic integral of the first kind and

$$k_2^2 = \frac{q_+(a_z - q_-)}{a_z(q_+ - q_-)};$$

3. $a_z > q_+ > q_-$

$$G(s) = \frac{[a_z + q_+ + q_-]}{\sqrt{a_z(q_+ - q_-)}} [\mathbf{K}(k_3) - F(\varphi_3, k_3)] - 3, \quad (\text{C.26})$$

where

$$\varphi_3 = \arcsin \sqrt{1 - \frac{q_+}{a_z}}, \quad k_3^2 = \frac{a_z(q_+ - q_-)}{q_+(a_z - q_-)}. \quad (\text{C.27})$$

C.3 IBS Integrals

Let us calculate the integrals in Eqs (C.15) through (C.20). For example, to find an analytic expression for the form factor G_z in Eq.(C.15) we have to calculate the integral

$$G_z(s) = \int \frac{d\Omega}{4\pi} \frac{1 - 3n_z^2}{a_{\alpha\beta} n_\alpha n_\beta}. \quad (\text{C.28})$$

We choose as the polar axes n_z , so that $n_z = \cos(\theta)$, $n_x = \sin \theta \cos \varphi$, $n_s = \sin \theta \sin \varphi$ and substitute in Eq.(C.28) $\cos \theta = u$. Then, we can write

$$G_z = \int_0^1 du (1 - 3u^2) I_z(u), \quad (\text{C.29})$$

$$I_z(u) = \int_0^{2\pi} \frac{d\varphi/2\pi}{a_z u^2 + (1 - u^2)[a_x \cos^2 \varphi + \gamma^2 a_s \sin^2 \varphi - 2\gamma \Phi a_x \sin \varphi \cos \varphi]} \quad (\text{C.30})$$

Using here $\cos^2 \varphi = (1 + \cos 2\varphi)/2$, $\sin^2 \varphi = (1 - \cos 2\varphi)/2$ and $a_\pm = (a_x \pm \gamma^2 a_s)/2$, we transform I_z to the following form

$$I_z(u) = \int_0^{2\pi} \frac{d\varphi/2\pi}{a_z u^2 + (1 - u^2)[a_+ + a_- \cos \varphi - \gamma \Phi a_x \sin \varphi]},$$

or

$$I_z(u) = \int_0^{2\pi} \frac{d\varphi/2\pi}{a_z u^2 + (1-u^2)a_+ + (1-u^2)\sqrt{a_-^2 + (\gamma\Phi a_x)^2} \cos(\varphi + \alpha)}, \quad (\text{C.31})$$

where

$$\sin \alpha = \frac{\gamma\Phi a_x}{\sqrt{a_-^2 + (\gamma\Phi a_x)^2}}, \quad \cos \alpha = \frac{a_-}{\sqrt{a_-^2 + (\gamma\Phi a_x)^2}}.$$

Now, the function $I_z(u)$ is reduced to the integral

$$\int_0^{2\pi} \frac{d\varphi}{2\pi} \frac{1}{a + b \cos \varphi} = \frac{1}{\sqrt{a^2 - b^2}}.$$

After simple transformations that results in

$$I_z = \frac{1}{\sqrt{[q_+ - (q_+ - a_z)u^2][q_- - (q_- - a_z)u^2]}}, \quad (\text{C.32})$$

where

$$q_{\pm} = a_{\pm} \pm \sqrt{a_-^2 + (\gamma\Phi a_x)^2} \quad (\text{C.33})$$

are the eigenvalues of the matrix

$$\mathbf{a}_{rs} = \begin{bmatrix} a_x & -\gamma\Phi a_x \\ -\gamma\Phi a_x & \gamma^2 a_s \end{bmatrix}.$$

Substituting I_z in Eq.(C.29) we obtain

$$G_z = \int_0^1 du \frac{(1-3u^2)}{\sqrt{[q_+ - (q_+ - a_z)u^2][q_- - (q_- - a_z)u^2]}},$$

or ($y_{\pm} = q_{\pm}/a_z$)

$$G_z = \frac{1}{a_z} \int_0^1 du \frac{(1-3u^2)}{\sqrt{[y_+ - (y_+ - 1)u^2][y_- - (y_- - 1)u^2]}}. \quad (\text{C.34})$$

In general case, such an integral is expressed in terms of the elliptic integrals. If, for example, $y_+ > 1$ and $y_- > 1$, simple transformations yield

$$G_z = \frac{\epsilon_z/\beta_z}{\sqrt{y_-(y_+ - 1)}} \left[\frac{3y_-}{y_- - 1} E(\varphi_0, k) - \frac{2y_- + 1}{y_- - 1} F(\varphi_0, k) \right]. \quad (\text{C.35})$$

Here,

$$\varphi_0 = \arcsin \sqrt{\frac{y_+ - 1}{y_+}}, \quad k^2 = \frac{y_+}{y_-} \times \frac{y_- - 1}{y_+ - 1}. \quad (\text{C.36})$$

Similarly, we write

$$\begin{aligned} G_s &= \int \frac{d\Omega}{4\pi} \frac{1 - 3n_s^2}{a_{\alpha\beta} n_\alpha n_\beta} \\ &= -\frac{1}{2} \int_0^1 du \int_0^{2\pi} d\varphi \frac{(1 - 3u^2) - 3(1 - u^2) \cos \alpha \cos \varphi}{2\pi a_z u^2 + (1 - u^2)a_+ + (1 - u^2)\sqrt{a_-^2 + (\gamma\Phi a_x)^2} \cos \varphi} \\ &= \frac{1}{2} \left[-G_z + 3 \frac{a_-}{a_-^2 + (\gamma\Phi a_x)^2} I_s \right]. \end{aligned} \quad (\text{C.37})$$

Here,

$$\begin{aligned} I_s &= \int_0^1 du \frac{a_+ - (a_+ - a_z)u^2}{a_z \sqrt{[q_+ - (q_+ - a_z)u^2][q_- - (q_- - a_z)u^2]}} \\ &= \int_0^1 du \left\{ \sqrt{\frac{[y_+ - (y_+ - 1)u^2]}{[y_- - (y_- - 1)u^2]}} + \sqrt{\frac{[y_- - (y_- - 1)u^2]}{[y_+ - (y_+ - 1)u^2]}} \right\}. \end{aligned} \quad (\text{C.38})$$

These integrals expressed in terms of the elliptic integral of the second kind. If, for example, $y_+ > 1$ and $y_- > 1$, we find

$$I_s = \sqrt{\frac{y_+}{y_- - 1}} E(\varphi_+, k_+) + \sqrt{\frac{y_-}{y_+ - 1}} E(\varphi_-, k_-), \quad (\text{C.39})$$

where

$$\varphi_\pm = \arcsin \sqrt{\frac{y_\pm - 1}{y_\pm}}, \quad k_\pm^2 = \frac{y_\mp (y_\pm - 1)}{y_\pm (y_\mp - 1)}. \quad (\text{C.40})$$

As far as we know similar expression for the sum of increments (Λ), a direct calculation of G_x is not necessary.

Bibliography

- [1] Accelerator Design of the KEK B-factory. Ed. by S. Kurokawa, K. Satoh and E. Kikutani. KEK Report 90-24, 1991.
- [2] An Asymmetric B-Factory Based on PEP. Conceptual Design Report. LBL PUB-5303, SLAC-372, CALT-68-1715, UCRL-ID-106426, UC-IIRPA-91-01, 1991.
- [3] Minutes of the Meeting with the Convencers of the Accelerator Study Group. GSI, February 1996.
- [4] A. Yamamoto et al., Jpn. J. Appl. Phys. Lett., Pt.2, **25**, L440 (1986).
- [5] D.V. Pestrikov. Self-consistent β -functions in Asymmetric Colliders. ENC 190696, BINP, Novosibirsk, <http://www.gsi.de>, 1996.
- [6] D.V. Pestrikov. Ion Tune Shifts and the Beam-Beam Instability in Electron-Nucleon Colliders ENC 110796, BINP, Novosibirsk, <http://www.gsi.de>, 1996.
- [7] D.V. Pestrikov. Threshold Values of Laslett Tune Shifts in Electron-Nucleon Colliders. ENC 200896, Gesellschaft für Schwerionenforschung (GSI), Darmstadt, <http://www.gsi.de>, 1996.
- [8] N.S. Dikansky, V.V. Parkhomchuk, D.V. Pestrikov, A.N. Skrinsky, V.E. Yakimenko. Physics Aspects of Electron-Ion Collider ENC 220396, BINP, Novosibirsk, <http://www.gsi.de>, 1996.
- [9] D.V. Pestrikov, V.E. Yakimenko. To Intrabeam Scattering in Electron-Nucleon Collider. ENC 200696, BINP, Novosibirsk, <http://www.gsi.de>, 1996.
- [10] N.S. Dikansky, D.V. Pestrikov. Physics of Intense Beams and Storage Rings. AIP PRESS, New York, 1994.
- [11] V. Katkov and V. Strakhovenko. JETPh, **75**, p. 1269, 1978.
- [12] G. Budker, A. Bulushev et. al. In Proceedings of the 10-th Intern. Conf on High Energy Acc. Serpukhov (1977), v1, p. 498, 1977.

- [13] K.Beckert, F. Bosch, H. Eikhoff, B. Franzke et al. Recombination rate measurements at the ESR. GSI 95-1., p.246, 1995; see also in T. Winkler. Untersuchungen zur Elektronenkühlung hochgeladener sccwreter Ionen. Inaugural-Dissertation zur Erlangung der Doktorwürde. Ruprecht-Karls-Universität, Heidelberg, 1996;
- [14] D.V. Pestrikov, Beam Loading in a Long Electron-Nucleon Collider. ENC 150896, GSI, Darmstadt, <http://www.gsi.de>, 1996.
- [15] Ya.S. Derbenev, A.N. Skrinsky. In Proc. of the 3rd All Union PAC. Moscow. v.1, p.386, 1972.
- [16] K. Hirata. Phys. Rev. D **37**, 1307, 1988.
- [17] M. Furman. In Proc. of the 3rd Advanced ICFA Beam Dynamics Workshop On Beam-Beam Effects in Circular Colliders. p. 52, Novosibirsk, 1989.
- [18] S. Krishnagopal, R. Siemann. Phys.Rev. D **41**, 2312, 1990.
- [19] A. Piwinski. In Proc. of the 8th Intern. Conf. on High Energy Accel., CERN, Geneva, p.357, 1971.
- [20] D. Pestrikov. SLAC-PUB-5575. SLAC, 1991.
- [21] D. Pestrikov. KEK Preprint 92-208. KEK 1993.
- [22] K. Hirata, F. Ruggiero. LEP Note 611, 1988.
- [23] K. Blasche. Stochastic Cooling of High Energy Ion Beams. ENC 200696, Gesellschaft für Schwerionenforschung (GSI), Darmstadt, <http://www.gsi.de>, 1996.
- [24] Budker G.I. Efficient method for damping particle oscillation in a proton and antiproton storage ring. Atomnaya Ehergiya **22**, p. 346-348, 1967.
- [25] Budker G.I., Derbenev Ya.S., Dikansky N.S., Kudelainen V.I., Meshkov I.N., Parkhomchuk V.V., Pestrikov D.V., Sukhina B.N., Skrinsky A.N. Experiment on electron cooling,IEEE Trans. Nucl. Sci. **NS-22**, p. 2093-7, 1975.
- [26] Budker G.I, Dikansky N.S, Kudelainen V.I, Meshkov I.N, Parkhomchuk V.V, Pestrikov D.V, Skrinsky A.N, Sukhina B.N. Experimental study of electron cooling.Particle Accelerators **7** p. 197-211, 1976.
- [27] Dikansky N.S, Kononov V.I, Kudelainen V.I, Meshkov I.N, Parkhomchuk V.V, Pestrikov D.V, Skrinsky A.N, Sukhina B.N. Study of fast electron cooling. Poc. 6 ALL-Union Meeting on Acceleration of Charged Particles (Dubna,1978)(Moscow, Nauka), 1978.

- [28] K. Beckert, H. Eickhoff, B. Frazke, F. Nolden, H. Reich, B. Schlitt, P. Spadtke, M. Steck, T. Winkler. Electron Cooling at the ESR, Essentials of Five Years' Operation. Report at Workshop Crystalline beam and Related Issues, Erice, 11-21 Nov. 1995.
- [29] G.I. Budker, A.N. Skrinsky. *Uspekhi Phys. Nauk*, **124**, p. 561, 1978.
- [30] D. Anderson, M.S. Ball, V. Dremenchuk et al. In Proc. of the Workshop on beam cooling and related topics. Montreux 4-5 October 1993, CERN 94-03, p.377, 1994.
- [31] D. Reistad, L. Hermansson, T. Bergmark, et al. *ibid*, p.183.
- [32] Derbenev Ya.S. and Skrinsky A.N. Magnetization effect in electron cooling Proc. 10 Int. Conf. on High-Energy Accelerators of Charged Particles, 1979, Protvino, v2 p516-521, *Fizika Plasmy* 4,p.492-500, 1978.
- [33] V.V. Parkhomchuk. Limitation of Intensities of Ion Beams at Electron Cooling Devices. ENC 240997, <http://www.gsi.de>, 1996.
- [34] Parkhomchuk V.V. 1984. Physics of fast electron cooling. Proc. Workshop on Electron cooling and Related Applications, 1984 ed. H.Poth (Karlsruhe:KfK).
- [35] Dikansky N.S., Kudelainen V.I, Lebedev V.A, Meshkov I.N, Parkhomchuk V.V, Sery A.A, Skrinsky A.N., Sukhina B.N. Ultimate possibilities of electron cooling. Preprint INP 88-61 1988.
- [36] Parkhomchuk V.V. and Skrinsky A.N. Electron cooling: physics and prospective applications. Reports on progress in Physics **54**, 7 , p. 919, 1991.
- [37] A. Piwinski. In Proc. of the 9th Intern. Conf. on High Energy Accel., p. 405, Stanford, 1974.
- [38] J.D Bjorken, S.K. Mtingwa. *Part. Accel.* **13**, p. 115, 1983.
- [39] N.S. Dikansky, D.V. Pestrikov. In Proc. of the 1984 Linear Accel. Conf., GSI 84-11, p. 253, Darmstadt, GSI, 1984.
- [40] H. Bruck. *Accelérateurs Circulaires de Particules*. Presses Universitaires de France, Paris, 1966.
- [41] R.D. Kohaupt. DESY Report 80/22, 1980.
- [42] D.Pestrikov. *NIM A-373*, p. 179, 1996.
- [43] K.Bane. Bunch Lengthening in the SLC Damping Rings. SLAC-PUB-5177, SLAC 1990.

- [44] K. Oide. Part. Acc. **51**, p.43, 1995.
- [45] D. Pestrikov. NIM **A 376**, p. 124, 1996.
- [46] R. Capi In the Beam Dynamics Issues of High-Luminosity Asymmetric Collider Rings. AIP Conf. Proc. 214. Ed. by A.M. Sessler, Berkeley, Ca. 1990. p. 419.
- [47] J. Le Duff. NIM, **A239**, 83, 1985.
- [48] H. Grote, F.C. Iselin. The MAD Program. User's Reference Manual. CERN/SL/90-13 (AP), (Rev. 5), 1996.
- [49] Yu. Eidelman. Preliminary Lattice Design of the Electron-Nucleon Collider. ENC 220896, Gesellschaft für Schwerionenforschung (GSI), Darmstadt, <http://www.gsi.de>, 1996.
- [50] Yu. Eidelman. Two topics concerning ENC lattice design. <http://www.gsi.de>, Gesellschaft für Schwerionenforschung (GSI), Darmstadt, 1996.
- [51] Yu. Eidelman. Design of the Interaction Region. ENC 130896, Gesellschaft für Schwerionenforschung (GSI), Darmstadt, <http://www.gsi.de>, 1996.
- [52] Yu. Eidelman. Beam polarization and related questions. ENC 080696, Gesellschaft für Schwerionenforschung (GSI), Darmstadt, <http://www.gsi.de>, 1996.
- [53] A.A. Zholentz, V.N. Litvinenko. To compensation of the solenoid field influence by quadrupole lens. Preprint BINP 81-80, Novosibirsk, 1980.
- [54] K. Steffen. DESY Report, DESY 83-124 (1983).
- [55] S.Y. Lee. Snakes and spin rotators for high energy accelerators. NIM, **A306** (1991) 1.
- [56] V.I. Ptitsin, Yu.M. Shatunov. Helical spin rotators and snakes. Third Workshop on Siberian Snakes and Spin Rotators, Sept. 13-13, 1994. Brookhaven National Laboratory, BNL-52453, 1994.
- [57] V.I. Ptitsin. Symmetric designs for helical spin rotators at RHIC. Preprint RHIC/AP/49, 1994.
- [58] B. Franczak, GSI-SIS-TN 87-13
- [59] A.V. Novokhatski et al., "Electron-positron Preinjector Complex at Novosibirsk". Proc. 1994 Int. Workshop SOURCES'94, Schwerin, Germany, Sept.29-Oct.4.
- [60] A.V. Alexandrov et al., "Preinjector for electron-positron factories". Proc. 1994 XIV Conf. on Charge Part. Acc., Protvino, Russia.

- [61] N.S. Dikansky et al., "Modulator for Klystron 5045". Proc. 1995 Part. Acc. Conf. on High-Energy Acc., Dallas, Texas, USA, May 1-5.
- [62] M.S. Avilov, A.V. Novokhatski, "A Single Bunch Compression in the Exponential Field". Proc. 1994 Fourth European Part. Acc. Conf., London, June 27, p971.
- [63] N.S. Dikansky, S.A. Labutsky, V.I. Kudelainen et al. Technical analysis and specification for electron cooling system of SIS ion synchrotron. BINP, 1995.
- [64] R.A. Salimov, N.K. Kuksanov, A.V. Malinin. Estimation of some Parameters of the ENC Electron Cooling Facility. ENC, 300996, BINP, Novosibirsk, <http://www.gsi.de>, 1996.